DESIGN, EXPRESSION AND PURIFICATION OF FUNCTIONAL HUMAN CANNABINOID RECEPTOR 2

By

Mohammed H. Alqarni

Bachelor of Science in Pharmacy, King Saud University, 2005

Submitted to the Graduate Faculty of

The School of Pharmacy in partial fulfillment

of the requirements for the degree of

Doctor of Philosophy

University of Pittsburgh
2016

UNIVERSITY OF PITTSBURGH

SCHOOL OF PHARMACY

This dissertation was presented

by

Mohammed H. Alqarni

It was defended on

February 2, 2016

and approved by

Dr. **Paul A. Johnston,** Research Associate Professor, Pharmaceutical Sciences

Dr. Al-Walid A. Mohsen, Research Associate Professor, school of medicine

Dr. Paul Schiff, Professor, Pharmaceutical Sciences

Dr. LiRong Wang, Research Assistant Professor, Pharmaceutical Sciences

Thesis /Dissertation Advisor: **Dr. Xiang-Qun (Sean) Xie**, Professor, Pharmaceutical Sciences

DESIGN, EXPRESSION AND PURIFICATION OF FUNCTIONAL HUMAN CANNABINOID RECEPTOR 2

Mohammed H. Alqarni, PhD

University of Pittsburgh, 2016

DESIGN, EXPRESSION AND PURIFICATION OF FUNCTIONAL HUMAN CANNABINOID RECEPTOR 2

Mohammed H. Alqarni, PhD

University of Pittsburgh, 2016

Cannabinoid receptors (CB1 and CB2) are GPCRs that belong to the rhodopsin-like family. Recent studies have demonstrated a role for CB2 in attenuating bone cancer-induced pain, reducing microglial activation in Alzheimer's disease, and regulating bone mass in osteoporosis. As such, there is an urgent need for the development of new therapeutic agents targeting CB2. However, structure- or fragment-based *in silico* drug design is hampered by the absence of 3D structural information on CB2, because of its inherent structural complexity.

Recently, it has been shown that specific residues of CB2 (in transmembrane helices III, V, VII and extracellular loop 2) play crucial roles in the binding of the vast majority of cannabinoid ligands. In this report, we performed computer modeling along with site-directed mutagenesis studies and the results suggest that four residues that lie within these regions have a novel importance for receptor recognition of compound XIE95-26, a discovered CB2 inverse agonist in our lab, and known cannabinoid ligands CP-55940 (agonist) and SR144528 (inverse agonist). These mutant CB2 receptors were characterized by western blot, and ligand binding studies. Moreover, functional assays were performed for some mutant CB2 receptor to illustrate the role of altered residues in downstream signaling. Next, we've taken further steps to provide a genetically modified functional CB2 for biophysical and biochemical studies with the goal of improving the current purification methodology for the production of chimeric CB2 fusion proteins from the baculovirus system. By introducing a fusion protein and rational modifications

to the chimeric receptor, investigators endeavoring to purify other GPCRs have overcome the challenge of obtaining sufficient stable protein for structural studies. Thus, different generations of truncated CB2 receptor were obtained to assess any improvements in receptor expression. Receptor expression and ligand binding capacity were assessed as criteria for pilot scale purification and for detergent selection. The best constructs were subjected to the optimal purification scheme using immobilized metal affinity, anti-M2 affinity, and size exclusion chromatography steps.

Collectively, results from this study will provide insights into the structure and functional mechanisms of CB2 and facilitate the design of small molecules that influence CB2 signaling behavior.

TABLE OF CONTENTS

LIST OF TABLES

LIST OF FIGURES

PREFACE

I dedicate this work to the numerous people I have interacted with throughout my PhD experience. I thank each and everyone for the significant support I have received.

First, I would like to express my deepest and sincere appreciation to my research advisor Dr. Xiang Qun (Sean) Xie for allowing me to join his laboratory, as well as, for his professional support, and valuable instruction during my graduate studies at the University of Pittsburgh. Dr. Xie gave me an enormous opportunity to learn, develop and grow, into an independent scientist. Dr. Xie provided immense guidance and encouragement, which proved fruitful inside and outside the lab.

Secondly, I dedicate this work to my father, Hamed and mother Zarah for their patience, unwavering support and many sacrifices. I would like to thank my wife, Ayesha, for her infinite patience, sacrifice, vast encouragement, as well as, providing the best home environment to utilize my time efficiently and productivity. My sincere love and prayers go out to my daughters Sadeem, and Leen, and my son Faris for supporting me through my long hours at work, and making my life beautiful. I wish them a great and successful future.

I would like to also to extend my sincerest gratitude to my thesis committee members, Drs. Paul A. Johnston, Al-Walid A. Mohsen, Paul Schiff, and LiRong Wang, for their valuable suggestions, continued guidance, and support during my dissertation work. Additionally, I thank all my co-workers and friends in Dr. Xie's lab. Special thanks to Drs. Peng Yang, Patrick Bartlow, Peng Zhang, Zhiwei Feng, and Shoucheng Du for their beneficial discussions. Thank you to Qin Tong for being both a great lab manager and teacher. My sincere and heartfelt thanks to former lab

colleagues Drs. Abdulrahman A. Almehizia, Ananda Chowdhury, and Kyaw Myint for energetic discussions, a lifetime of laughs and for their helpful and generous advice.

Furthermore, thank you to the faculty, staff, and students in the Department of Pharmaceutical Sciences at the University of Pittsburgh, School of Pharmacy. Special thanks go to Dr. Maggie Folan, Lori Schmotzer and Hornick, Dolores M for their help and support over my five year here.

To our collaborator at Stanford University, Dr. Brian Kobilka and Dr. Sun Bingfa, thank you. for your expert insights. I would like also to thank the UPCI (center Biomarkers Facility that is supported in part by award P30CA047904) for providing analysis of LC-MS/MS results.

Lastly, I would like to express a special thank you and regards to Prince Sattam bin Abdulaziz University, Saudi Arabia for their financial support throughout my PhD study.

ABBREVIATIONS

Å	Ångström
AC	Adenyl cyclase or adenylate cyclase
AMP	Adenosine monophosphate
AEA	N-arachidonoylethanolamide or Anandamide
A2aR	Human adenosine 2a receptor
ATP	Adenosine triphosphate
AMP	Adenosine monophosphate
2-AG	2-arachidonoylglycerol
3D	Three Dimensional
Arg	Arginine
Asp	Aspartic acid
AcMNPV	*Autographa californica's* multiple nuclear polyhedrosis virus
BEVS	baculovirus expression vector system
BCA	Bicinchoninic acid
B_{max}	Maximum binding capacity
BSA	Bovine serum albumin
β2-AR	β2-Adrenergic Receptor
BLT	Leukotriene receptors
cGMP	cyclicguanlyl cyclases
cAMP	Cyclic adenosine mono phosphate
CB1/2	Cannabinoid receptor 1 or 2
C'	Carboxy terminal
cDNA	Complementary DNA
^{o}C	Degree Celsius
CNS	Central nervous system
CPM	Counts per minute
CPS	Cleavage processes at site

CHO	Chinese hamster ovary cell
COS-1	fibroblast-like cell line derived from monkey kidney tissue
CBB	Coomassie brilliant blue
CV	Column Volume
CRD	Cysteine-rich domain
CHAPS	3[(3cholamidopropyl)dimethylammonio]-1-propanesulfonate hydrate
CHS	Cholesteryl hemisuccinate
CMC	Critical micelle concentration
CTAB	Cyltrimethylammonium bromide
DAG	1,2-diacylglycerol
DMPC	1,2-Dimyristoyl-sn-Glycero-3-Phosphocholine
DNA	Deoxyribonucleic acid
DMSO	Dimethyl sulfoxide
DTT	Dithiothreitol
DPBS	Dulbecco's Phosphate-Buffered Saline
DDM	Dodecyl-beta-D-maltoside
ECL	Extracellular loop
EDTA	Ethylene diaminetetraacetic acid
EGTA	Ethylene glycol tetraacetic acid
ERK	Extracellular signal-regulated kinase
E.coli	*Escherichia coli*
EL	Extracellular loop
EC_{50}	Half maximal effective concentration
Flag	epitope, octapeptide protein tag
FBS	Fetal bovine serum
FAAH	Fatty acid amide hydrolase
g	Gram
GTP	Guanosine 5'-triphosphate
Gαi	G alpha subunit inhibitory
Gαs	G alpha subunit stimulatory
Gα/βγ	G protein (Gα and Gβγ subunits)

GDP	Guanosine 5'-diphosphate
GPCR	G protein coupled receptor
GPR55	G-protein coupled receptor-55
× g	Centrifugal force
Glu	Glutamic acid
h or Hrs.	Hours
hCB1/2	Human cannabinoid receptors 1 or 2
High five	*Trichoplusia ni (*insect cell)
HA	Hemagglutinin
His	Histidine
HEK	Human Embryonic Kidney cells
HEPES	4-(2-hydroxyethyl)-1-piperazineethanesulfonic acid
IB	Inclusion Body
IL or ICL	Intracellular loop
IMAC	Immobilized Metal Affinity Chromatography
IA	2-Iodoacetamide
IPTG	Isopropyl β-D-1-thiogalactopyranoside
Ile	Isoleucine
K_d	Dissociation constant
K_i	Binding Affinity of the inhibitor
K_{ir}	Inwardly rectifying potassium currents
kDa	Kilodalton
LB	Luria-Bertani
L	Liter
Lys	Lysine
Leu	Leucine
MAPK	Mitogen-activated protein kinase
MEK	MAP kinase kinase
Met	Methionine
mins	Minutes
Mis	Mistic

ml	Milliliter
mM or mmol	Millimolar
M	Molar
MNG	Lauryl maltose neopentyl glycol
MBP	Maltose binding protein
MW	Molecular weight
MWCO	Molecular weight cut-off
ND	Binding not detected
N'	Amino terminal
nM	Nanomolar
Nts1	Neurotensin
NMR	Nuclear Magnetic Resonance
OG	Octyl ß- D-glucoside
POPC	1-palmitoyl-2-oleoyl-sn-glycero-3-phospho choline
Phe	Phenylalanine
PKA	Protein kinase A
PI3K	phosphatidylinositol-3-kinas
pH	-log10 [H+]
PNGase F	Peptide -*N*-Glycosidase F
PKB	Protein kinase B (Akt)
PCR	Polymerase chain reaction
P1 ,P2 and P3	Virus passage
PLC	Phospholipase C
Pro	Proline
PBS-T	Phosphate Buffered Saline- Tween
rpm	Parts per million
RT	Room temperature
R*	Active form of the receptor
R	Inactive form of the receptor
RTS	Rotamer toggle switch
Rev	Reverse

Ser	Serine
Sf21 and Sf9	*Spodoptera frugiperda* (insect cell)
S.E.M	Standard Error of Mean
SDS	Sodium dodecyl sulfate
SDS-PAGE	Sodium dodecyl sulphate polyacrylamide gel electrophoresis
SEC	Size exclusion chromatography
TarCF	Bacterial Chemosensory Aspartate Receptor (C terminal fragment)
TCEP	*tris*(2-carboxyethyl)phosphine
TR-FRET	time-resolved fluorescent resonant energy transfer
TM	Transmembrane
Tris	Tris (hydroxymethyl) aminomethane
Tris-HCl	Tris - hydrogen chloride
THC	Tetrahydrocannabinol
Trp	Tryptophan
Tyr	Tyrosine
TrxA	Thioredoxin
Val	Valine
w/v	weight per volume
WB	Western blot
WT	Wild type
μM	Micromolar
μg	Microgram

1.0 INTRODUCTION AND LITERATURE REVIEW

1.1 INSIGHTS INTO STRUCTURE OF GPCRs

G protein-coupled receptors (GPCRs) comprise a large family of integral membrane, cell-surface receptor proteins characterized by seven hydrophobic transmembrane helices that are connected by three intracellular and extracellular loops [1]. Although they share a common feature (i.e.α-helical transmembrane helices), the N-terminal is considered a highly diverse region among GPCR superfamilies [2]. GPCRs are expressed in all types of tissue throughout the human body and are involved in different physiological and pathological functions. They act as mediators responding to a huge array of stimuli, from protons to polypeptides, including extracellular and intracellular ligands, proteins, hormones and lipid derivatives. Upon receptor stimulation, serial ligand-receptor conformational changes occur, causing the receptor to change and initiate signal-transduction activities.

The GPCR superfamily accounts for nearly 800 different human genes, or approximately 4% of the entire protein-coding genome [3]. The specificity and diversity of these receptors in diseases has made GPCRs some of the most popular therapeutic targets, accounting for more than 40% of marketed drugs, nearly 200 [4]. With mapping of the human genome, most of the non-olfactory GPCRs have been cloned to date, some of which are named because they involved in heterodimeric G proteins coupling like other known GPCRs. Others are only recognized by their α-helical transmembrane signature and remain as orphan receptors, awaiting the identification of their ligands [5].

1.1.1 GPCR superfamilies

Despite the diversity of GPCR functions in the human body, most classes of GPCRs share a high degree of homology in their seven transmembrane α-helical structures [6]. The receptors consist of three regions. The extracellular region includes extracellular loops responsible for ligand recognition/binding and the N-terminal, intracellular regains, relatively short unstructured regions involved in protein-protein interactions [5, 6]. The third region is the transmembrane region, which is divided into two parts. The upper part, usually the location of the ligand-binding pocket, is considered the most structurally diverse among GPCRs. The lower part of the transmembrane region is responsible for downstream signaling and has the most conserved residues involved in the conformational changes of the receptor, as shown in (**Figure** 1-1**).**

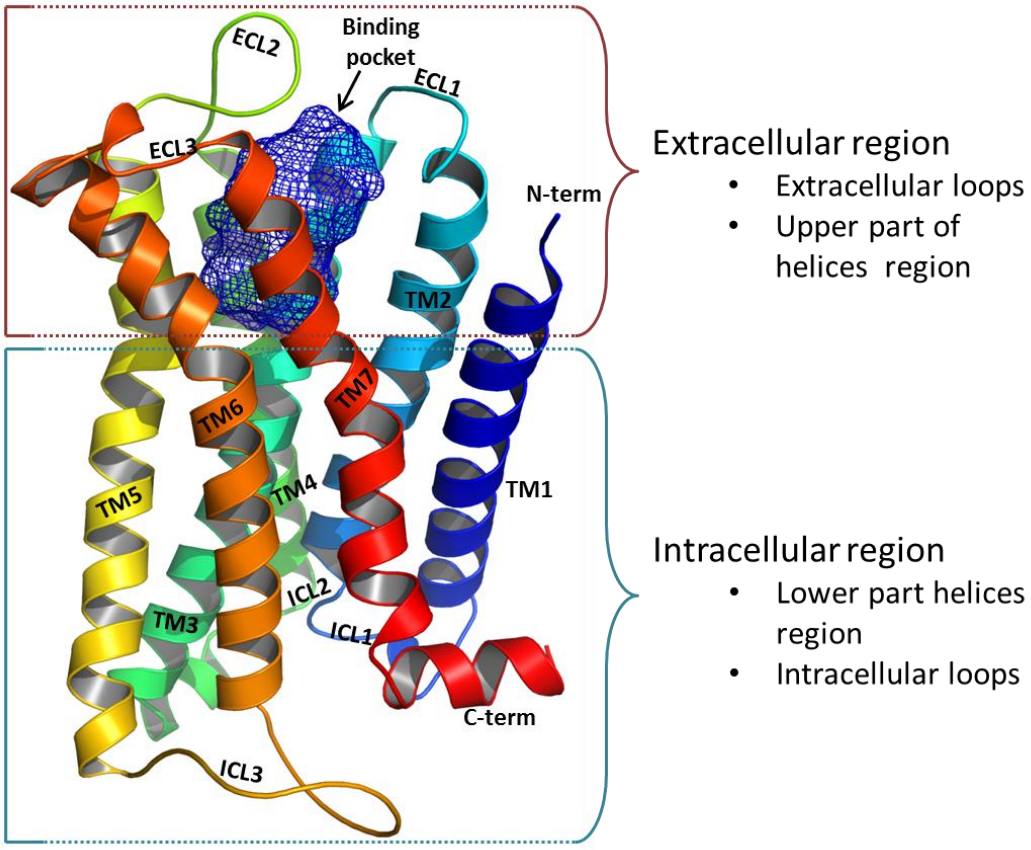

Figure 1-1. General structure of GPCRs.

Extracellular (EC) and transmembrane-extracellular (TM-EC) regions are responsible for ligand-binding and show higher diversity regions among GPCRs and less conformational changes. Whereas, intracellular (IC) and transmembrane-intracellular (TM-IC) regions are responsible for cellular signaling, have high conformational change regions, and less diversity between GPCRs [7].

Several GPCR phylogenetic classification methods have been used to differentiate between the superfamilies [8]. One classification is based on common structural features of the seven transmembrane helices, such as sequence homology and functional similarity. Other classifications are based on ligand binding. The mostly frequently system is annotated by A (rhodopsin-like receptors), B (secretin/adhesion), C (metabotropic glutamate), D (fungal mating pheromone receptors), E (cAMP receptors), and F (frizzled/smoothened receptors), plus a Roman numeral for the sub-class [9]. However, because some of these classes are not found in vertebral GPCRs, particularly in the human genome, overall GPCRs are divided into four classes, all of which bind to G proteins; rhodopsin (family A), secretin and adhesion (family B), glutamate (family C), and frizzled/taste2 (family C). **Figure** 1-2 represents the prototypical GPCR subfamilies (class A, B, and C) [9].

Family A, or rhodopsin, is considered large and diverse within the 7-TM regions. However, the members share a high percentage of amino acid sequences and conserved motifs. More than 85% of identified GPCRs are Class A/rhodopsin-like receptors, approximately 670 full-length human receptors [10]. The rhodopsin family is divided into subgroups: α, β, γ, and δ.

- The Rhodopsin family α-group represents the highly targeted druggable group (approximately 18 targets) among this class. Nevertheless, major cardiovascular side effects are noted for amine receptors, which is less frequently found in other members of α-group.
- The rhodopsin family β-group is the second drug target subgroup. It mainly comprises the peptide ligands. Like the α-group, the ligand binding of β-group is within the 7TM pocket but also involves the N-terminus and extracellular loops.

- The rhodopsin γ-group contains both peptides and lipid-like compounds. Targeting this group with drugs has shown potential for treating drug abuse for opioids and alcohol and for treatment of acute and chronic pain, inflammation, and hypertension. One of the best examples of marketed drugs for this group is maraviroc (CCR5 receptor antagonist). It is approved as an antiretroviral drug for treatment of HIV infection.
- The δ group is targeted by peptides. It is mainly composed of glycoprotein-binding receptors, PARs, and olfactory receptors, P2Y12, and leukotriene receptor 1.

A common feature of the class A GPCR is a relatively short N-terminus and the ligand binding pocket site for the endogenous ligand (or orthosteric binding site) which is located within the seven transmembrane domains (TM 1-7). This family includes the most targeted receptors among all other families. This class also contains conserved residues that are essential for structural, conformational, and signaling transduction: 1- DRY (lower part of third helix and intracellular loop), 2- CWxP (at sixth transmembrane), and 3- NPxxY (at the seventh transmembrane). Examples of class A receptors include purinergic, adrenergic, 5-hydroxytryptamine, neuropeptide, muscarinic acetylcholine, dopamine, galanin, eicosanoid, cannabinoid, chemokine, kinin, endothelin, histamine, melanocortin, lysophospholipid, vasopressin, GPR30, somatostatin, and olfactory GPCRs.

Family B GPCRs contains two subgroups, secretin and adhesion receptors. Secretin GPCRs have similar topology features to the rhodopsin family without significant sequence homology [11]. In addition, they contain large extracellular and N-terminal domains, which have the ability to bind large molecules such as peptides and hormones due to the presence of disulphide bonds. Moreover, the N-terminal has conserved residues such as rxCxxxGxw.

Adhesion receptors make up the other subgroup of family B. Adhesion receptors are known for their structural and genomic complexity compared to other families [12]. The adhesion GPCRs account for more than 30 of the receptors in vertebral genomes available in the GPCR data bank. Like secretin receptors, adhesion receptors are connected to large N-terminal domains. Moreover, they undergo proteolytic cleavage processes at site (CPS) motifs to separate the non-covalently attached complexes between transmembrane and N-terminals. These processes are responsible for the constitutively active receptors which drive signaling [13]. The binding pocket of class B receptors is located in the juxtamembrane region of the N-terminal and the extracellular loops together with TM6. The challenge among these groups is that only a few ligands have been identified due to the morphological complexity of these receptors. Examples of family B GPCRs class are Cadherin EGF LAG (CELS), calcitonin, corticotropin-releasing hormone, glucagon, latrophilin, brain-specific angiogenesis EGF-like module-containing mucin-like, and vasoactive intestinal polypeptide receptors.

Metabotropic glutamate receptors (Family C) act as modulators for synaptic and central nervous system transition [14]. Unlike family A, family C is recognized by the massive extracellular N-terminal domain that have a clamshell-like morphology, and the Venus flytrap module (VFM) which contains the endogenous ligand-binding site [15]. Similar to family B, the N-terminal demines of family C contain a cysteine-rich domain (CRD) and VFM domains consisting of two lobes dimerized together, that mediate binding to small ligands such as glutamate or Ca^{2+}. Upon ligand-VFM binding, a series of conformational changes at the cysteine-rich domains leads to the heptahelical domain C-terminal. Like other GPCRs, the C-terminal of glutamate receptors are also important in G-protein receptor coupling, which is subjected to splicing and phosphorylation [14]. Family C is sub-classified into three subgroups, all of which are expressed mainly in the CNS. The

first group includes Metabotropic glutamate receptor (mGluRs 1) (a,b,c,d,e and f) and 5. The second group includes mGluRs 2 and 3, and the third group includes mGluRs, 4, 6, 7, and 8.

The last family of GPCRs is the frizzled (FZD) and smoothened (SMO) receptor family [16]. They are known to be involved in embryonic development, cancer, and central nervous and cardiovascular system diseases treatment due to their ability to modulate cell proliferation and tissue homeostasis. Smoothened receptors have also shown to play a major role in embryogenesis through the canonical hedgehog-signaling pathway [16]. Both FZD and SMO receptors share high sequence homology and are involved in the WNT signaling pathway leading to activation of proteins in the cytosol [16]. Like family C, FZD GPCRs contains large N-terminals with a cysteine-rich domain that is involved in ligand binding [17]. Examples of ligands for FZD are WNTs, Norrins, FRPs, R-spondin, and CTGF [17].

Due to the important role of GPCRs acting as responders to signals, it has been observed that GPCRs are expressed in almost all organs and are responsible for different physiological processes such as vision, smell, taste, mood, behavior, immune modulation, and maintenance of other homeostatic processes [13, 14]. Moreover, targeting GPCRs with small molecule drugs has revealed therapeutic potential for treating pain, inflammation, cardiovascular, and metabolic diseases, as well as cancer [18].

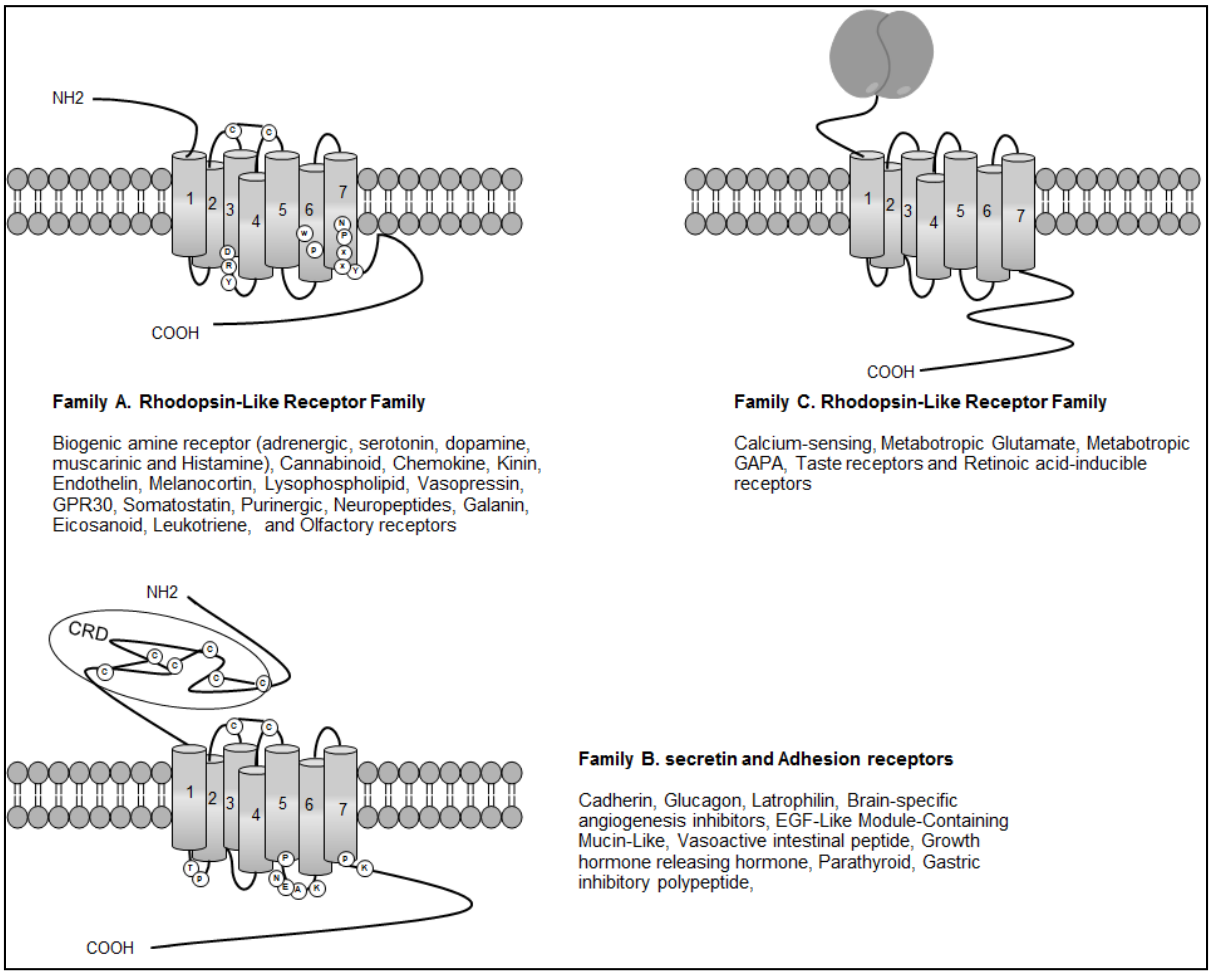

Figure 1-2. Schematic view of the 7TM model of GPCRs superfamily.

Three major class of GPCRs based on sequential similarities, ligands, and function of the receptor. Class A is the large, well-known class. The ligand binding pocket is located within 7-TM for both orthosteric and allosteric ligands. The N-terminal of family B and C contain conserved cysteine-rich domains (CRD) that form three cysteine bridges, which are important for orthosteric ligand interactions. In addition, family C has a Venus flytrap module (VFM) which contains a ligand-binding pocket at N-terminals, which have a clamshell-like configuration. adapted from [12, 17, 19] [20].

1.1.2 GPCRs activation and signaling

Despite the diversity in the biophysical and biochemical structures of GPCRs, they are mostly represented by active (R*) and inactive (R) states that are in a dynamic equilibration. Upon the ligands-receptor binding, different helical conformation and conserved residuals interactions disruption are obtained to shift the receptor towards one of these states. In addition, ligand involvement has shown to be part of this equation. For example, agonist binding to the receptor causes the receptor to strongly shift to the active state (R*) while a partial agonist will lead to a less effective active state characterized by huge receptor conformational changes [21]. On the other hand, the inverse agonist preferentially stabilizes and shifts the receptor to the inactive state (R) and reduces basal activity [21].

Solving rhodopsin, A2A adenosine receptor and β adrenergic receptor co-crystal structures, molecular modeling and dynamic simulations of GPCRs have provided preliminary data for understanding the activation and signaling of GPCRs [22, 23]. Typically, the receptor undergoes different rearrangements of its transmembrane core as well as extra- and intracellular loops. Binding of agonists will initiate these changes starting from the binding pocket to transmembrane cores. The kink-forming residue (Pro at 5.5) in TM5 undergoes a small change that leads to distortion and rotation of this helix. TM3 and 7 are then moved and rearranged. Ultimately changes these cause the extracellular side of the receptor to pull out, offering space for the G protein to bind. In addition, the hydrophobic conserved residues clustering at the bottom of the pocket will rearrange, leading to contact between TM3, TM5, and TM6 interface [24].

Studies have found that ligand induced receptor activation and signal transduction takes place by the disruption of non-covalent, intermolecular interactions which stabilize the receptor in its

inactive state (R) [25]. Family A GPCRs are held in their inactive state by a couple of slat-bridge interactions that stabilize the receptor transmembrane (TM) domains in a specific basal arrangement [26]. The transmembrane helices have a more significant role in stabilizing the receptor than the extra- and intracellular loops [27]. For example, in rhodopsin, the receptor is stabilized by interaction between Glu 134, Arg 135 in TM3, and Glu 247 and Thr 251 in the cytoplasmic end of TM6 [27]. These interactions between the cytoplasmic end of TM3 and TM6 are known as the "ionic lock" as shown in (**Figure** 1-3**)**. Disruption of the ionic lock, referred to as Ionic Lock Disruption (ILD), leads to receptor activation [25]. Amino acids, which constitute the ionic lock, are highly conserved throughout rhodopsin Family A. Mutation of these key amino acid residues, which stabilize the receptor in the inactive state, results in the generation of Constitutively Active Mutants (CAMs). The best characterized are mutations of the highly conserved (D/E)R(Y/W) motif the members of the rhodopsin GPCR family. This has also been demonstrated in the beta-2-adrenergic receptor (β2 AR), adenosine A2A receptor (A2 AR [24], cannabinoid receptor 1 [28], histamine receptor [29], and D3 dopamine receptor [30] .

Rotamer Toggle Switch (RTS) is another molecular switch commonly found in the activation of amine and opsin family GPCRs [31, 32]. This activation process was initially reported for rhodopsin [20]. This is mediated around the conserved proline residue in TM6 of these receptors. For example, the β2 AR mutation of Leu 272 to alanine at the cytoplasmic end of TM6 results in a marked increase in receptor basal activity and instability [33]. Monte Carlo simulation studies have suggested that the β2 AR amino acid residues Cys 285, Trp 286, and Phe 290 constitute the aromatic triad, and ligand interaction in this region can couple to and modulate the bend angle kink at Pro 288, leading to receptor activation [34]. Rotational toggle of conserved residues have also been reported to initiate agonist activation in the histamine H1 receptor [35], D2 dopamine receptor

[36], and the Trace Amine Associated Receptor [37]. In a recent and very elegant study with the CB1 receptor, Monte Carlo simulations were used to determine the ligand induced structural changes around the "aromatic microdomain" of CB1, which refers to the microdomain composed of aromatic residues from TM 3-4-5-6 [38]. Residues Phe 201 and Trp 357 act as the toggle pair switch to maintain the receptor in the inactive state [39]. Results from this and related studies indicate that the F201/W357 interaction leads to receptor stability and can be disrupted by several subclasses of ligands leading to CB1 receptor activation. Such detailed molecular dynamic simulation studies have also been performed with CB2[26]. Comparing the conformational changes for the cannabinoid receptor 2 helices during receptor activation by CP55940 (full agonist) revealed that CB2 endures larger conformational changes. TM3, extracellular loop (ECL2), TM6, and TM7 are all subject to a deviation of approximately 4.5 Å compared to the inactive state of the CB2 receptor. Second, the ionic lock residues of CB2 (Arg3.5, E/DRY, and Glu/Asp6.30) are more stable during binding to the inverse agonist (SR144528) compared to binding with CP55940 [40, 41]. Similarly, Trp258, which is part of the CPxY motif at TM6, showed a significant role in CB2 function [26]. The space between CPxY and the agonist is significantly smaller when compared to the inverse agonist. Upon activation of the receptor, cysteine and proline residues moved toward the intracellular side. On the other hand, Trp258 moved towards the extracellular side leaving space around 5 Å from when bounded to SR144528. Try299 of the NPxxY motif also showed subtle changes when engaged into movement at TM7 by the activation [40].

The classical model of "an activated G protein-coupled receptor" consists of 1) receptor, 2) heterotrimeric G proteins made up of Gα and Gβγ complex domains, and 3) effectors such as transporters, ion channels, and other enzymes [19]. G proteins are heterotrimeric non-transmembrane proteins attached to the cytoplasmic side of membranes by one or two lipid

moieties. The Gα subunit contains the region for GTP-GDP exchange. Additionally, there are four main sub-families of Gα: Gs, Gi/o, G12, and Gq. The subsequent role of the individual Gα subunit depends on the cognate GPCR, which also determines the downstream signaling pathway. The basal activity of the receptor includes Gα binding to GDP, and the whole heterotrimeric G is formed. Upon receptor activation by external ligands, endogenous molecules, or other proteins, Gα recruits GTP and exchanges it for GDP triggering dissociation of the Gα and the Gβγ subunits. These subunits are responsible for independent downstream signaling events (**Figure** 1-3**)**.

The second messenger can be initiated by many elements such as ion channels (calcium and potassium), guanylyl cyclases (cGMP), adenylyl cyclase (AC) and phospholipase C [42]. Gαi inhibits adenylate cyclase and leads to decreases in cyclic Adenosine Monophosphate (cAMP) levels while Gαs leads to the stimulation of adenylase cyclase activity causing increased cAMP levels in the cell which then activates protein kinase A (PKA) and phosphodiesterase proteins (PDEs) [43, 44]. In addition, receptor activation leads to phosphorylation of the C-terminal and intracellular loops by G protein-coupled receptor kinase (GRK), which can then couple to arrestin. Arrestin is a regulatory and signaling protein that is involved in extracellular signal-regulated kinase (ERK) pathways, which prevent the coupling of the G protein and regulates desensitization and internalization of the phosphorylated receptor via clathrin-mediated endocytosis [33].

Recently, the concept of GPCR activation and signaling has changed [25]. Structurally dissimilar ligands are believed to disrupt different structural motifs of the GPCRs resulting in disruption of distinct molecular stabilization motifs, which eventually leads to activation of different signal transduction events (biased ligands) [25]. New ligands that bind to β2 AR are grouped into several subclasses based on their functionality, which can be correlated to their structure. For example, the agonist, salbutamol (a catecholamine ligand), can lead to quenching of

the fluorescent probe of monobromobimane (MBB) fluorophore, whereas catechol cannot [45, 46]. Utilizing mutations at the site of activation and increased fluorescence quenching at this site will indicate disruption of ionic lock or other activation mechanisms in response to ligand binding. However, catechol does have detectable effects on the fluorescent change in fluorophore and tetramethylrhodamine methylester (TMRM) when placed at IL3. More potent (full agonist/strong partial agonist) β2 AR ligands can activate the receptor by disruption of both ionic lock disruption (ILD) and rotamer toggle switch (RTS) stabilizing interactions. However, ligands with lesser potency (partial agonist) would selectively activate the receptor by disruption of only either one of the molecular switches. Computational simulation studies involving Monte Carlo simulations suggest that the aromatic catechol ring is able to interact with the aromatic stacking present between Trp 286 and Phe 290, leading to receptor activation by rotational toggle switch, which is concerned with the movement of the Pro 288 and leads to the movement of TM6. However, the addition of the aliphatic chain bearing an amine group would allow it to access the ionic lock and thereby increase ligand potency, as was observed for catecholamines, e.g. isopreterenol, epinephrine, and norepinephrine [45, 46]. These seminal studies have indicated that ligands with diverse structural features can activate GPCRs by the disruption of distinct stabilizing interactions.

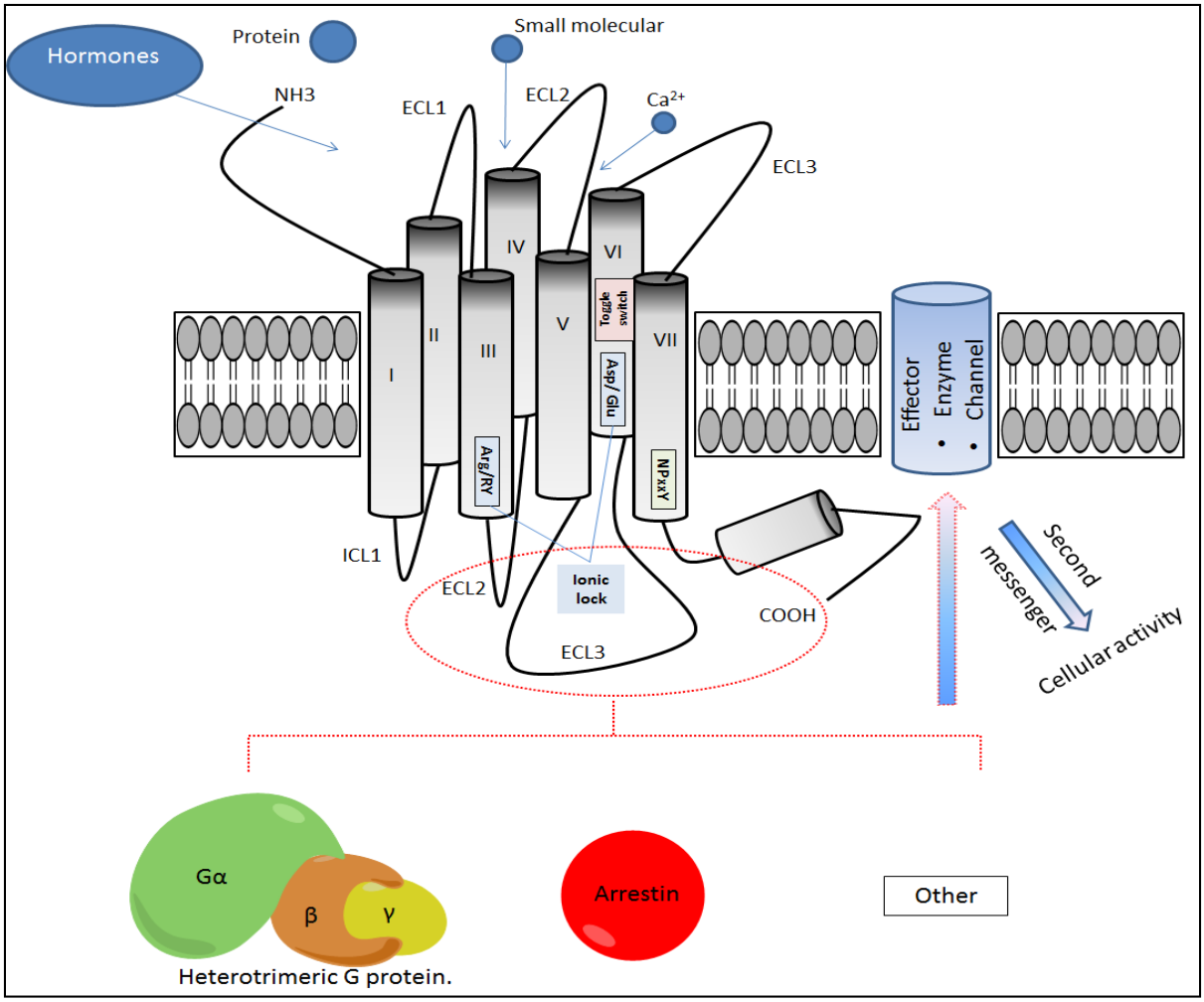

Figure 1-3. G-protein-coupled receptors and classical signal transduction.

Topological illustration of GPCRs showing different conserved motifs and molecular switches (DRY, NPXXY motifs, ionic lock, and toggle switches). Upon binding of the internal and external molecule, the receptor is subjected to helical conformational changes, which are required for activation, coupling with either the G protein or the arrestin protein. Different instigators, such as adenylate cyclase, channels, or other enzymes, are activated and produce a second messenger, such as cAMP and Ca^{2+}. The activated receptors then lead to signal transduction [33, 201]. Adapted from [19].

1.1.3 Significance, challenges for stabilization and crystallization of G protein-coupled receptors

In recent years, significant progress has been made in the study of the structure of GPCRs. For example, the past decade has witnessed remarkable progress in the study of the in the molecular biology of GPCRs after the first three dimensional (3D) crystal structure of rhodopsin was reported in 2000 [27]. Twenty-nine GPCR crystal structures have been solved, nine of which were in 2012 alone [47]. Scientists were able to gain insight into the general topology of the GPCRs for the first time. Moreover, high-resolution 3D structures of GPCRs have provided a detailed understanding of ligand binding sites, receptor-ligand interactions, and receptor conformations and functions. Despite the significant success in GPCR crystallization, heterologous GPCR production is still challenging due to difficulties in functional expression, purification, and inherent structural instability. Moreover, structural information for GPCRs remains elusive is part due to their dynamic character and versatile functionality. GPCRs bind a variety of different ligands, resulting in varying modes and degrees of signal transduction. Obtaining high quality diffraction of GPCRs is also difficult due to the presence of detergents, inherent receptor flexibility, and a lack of hydrophilic regions that can form crystal lattice contacts [48-50]. Therefore, creative efforts are necessary to design modified receptors or receptor complexes with an enhanced ability to sustain lattice-forming interactions. These include building chimeric receptors with high expression and stability levels and fewer post-translational modifications [51]. For example, the unstructured, flexible regions of the N- and/or C-terminals can be truncated to remove the N-glycosylation region and eradicate the proteolysis frequently observed in N-terminals [52]. In addition, site-directed mutagenesis can be implemented to stabilize the receptor, improve protein expression

levels, and increase the melting temperature of the receptor [52]. Different strategies have been proposed recently to overcome the lack of polar regions and receptor flexibility [51]. The GPCR's third intracellular loop, (IL3/ICL3) which links the cytoplasmic ends of TM 5 and 6, is highly flexible and plays an active role in receptor G protein interaction, activation, and signal transduction [53]. In rhodopsin family GPCRs, the IL3 residue(s) interact within the conserved DRY (Asp-Arg-Tyr) motif and comprise the ionic lock which generates the active and inactive conformations of the receptor [25], [54, 55]. The dynamic IL3 region contributes to a heterogeneous population of GPCRs with varying conformations and the structural flexibility of the protein, that prevent the growth and formation of diffraction quality crystals [43, 53]. It is now understood that structural modification of IL3 can be done to arrest receptorconformational flexibility and provide greater polar surface area (**Figure** 1-4) [56]. Increased polar surface area allows the formation of crystal lattice contacts [56]. Most of the high resolution GPCR structures solved so far require the GPCR to be locked in one of the conformational states, preferentially the inactive state [57, 58]. The inactive state is characterized by reduced conformational flexibility and has been achieved by co-crystallizing the receptor with saturating amounts of inverse agonist ligands (high affinity and low off-rate) [59]. Inverse agonists at saturating concentrations reduce the conformational heterogeneity of the receptor population by driving most of the receptor to the inactive conformation. Recently, however, the active form structure of the β2 AR was solved by co-crystallizing the receptor with saturating amounts of agonist and structural stabilization with a camelid antibody [60]. Previously, two methods have been used to stabilize this region. In one method, TM 5 and 6 regions were stabilized through binding to a Fab5 antibody, and the antibody-protein complex was used to generate a structurally stabilized receptor [61]. However, crystal structure resolution was low due to the size of the protein packing at extracellular domains [62].

In order to improve crystal structure resolution, different soluble fusion proteins can be used to replace the third intracellular loop in addition to C-terminal truncations [51]. Different criteria are used to choose the best fusion partners for insertion [51]. For example, the distance between the N- and C-terminals of the fusion protein needs to be optimized to be similar to the distance between helices 5 and 6 of the receptor. In addition, the molecular weight of the fusion protein must not exceed 20 kDa to avoid disruption of the overall integrity of the receptor. Additionally, the overall charge and origin of the protein should be considered as a factor for choosing the fusion protein. Ultimately, among hundreds of fusion proteins present in the protein data bank (PDB), only five have been previously selected: T4 lysozyme (T4L), apocytochrome b562RIL (BRIL), xylanase, rubredoxin, and flavodoxin [51]. The success of the TM5-(T4L)-TM6 fusion method has allowed for the determination of more than sixteen GPCR structures, including human β2-adrenergic receptor (β2AR) [63], adenosine A2A receptor [58], histamine receptor 1 [64], sphingosine 1-phosphate receptor 1 [65], D(3)-dopamine receptor [30], chemokine receptor type 4 (CXCR4) [57], muscarinic acetylcholine receptor M2 [66], delta-type opioid receptor [67], neurotensin receptor [68], human protease-activated receptor 1 [69], corticotropin-releasing factor receptor 1 [70], M3 muscarinic, acetylcholine receptor [71], μ-opioid receptor [72], and serotonin receptors [73]. In addition, the insertion of another fusion protein, such as apocytochrome b or rubredoxin to the third intracellular loop, led to the identification of GPCRs structures such as the human P2Y12 receptor [61, 62] and the CCR5 chemokine receptor [74], respectively. The insertion of fusion protein into the N-terminal of GPCRs led to successful crystal structure for δ-opioid receptor [75], nociceptin/orphanin FQ (N/OFQ) peptide receptor [76], and glutamate receptor 1 [77]. Additionally, antibodies that recognized one state of the receptor conformation were also used for obtaining GPCR co-crystal structures in the case of the β2 adrenoceptor [48, 67] and

muscarinic acetylcholine receptor [78]. Finally, the GPCR crystal structures with no chimeric modifications were obtained via point mutations to increase the thermostability or by deletions of the unnecessary parts of the receptor that hamper crystallization, such as in the case of the neurotensin receptor [79] and other GPCRs [80, 81].

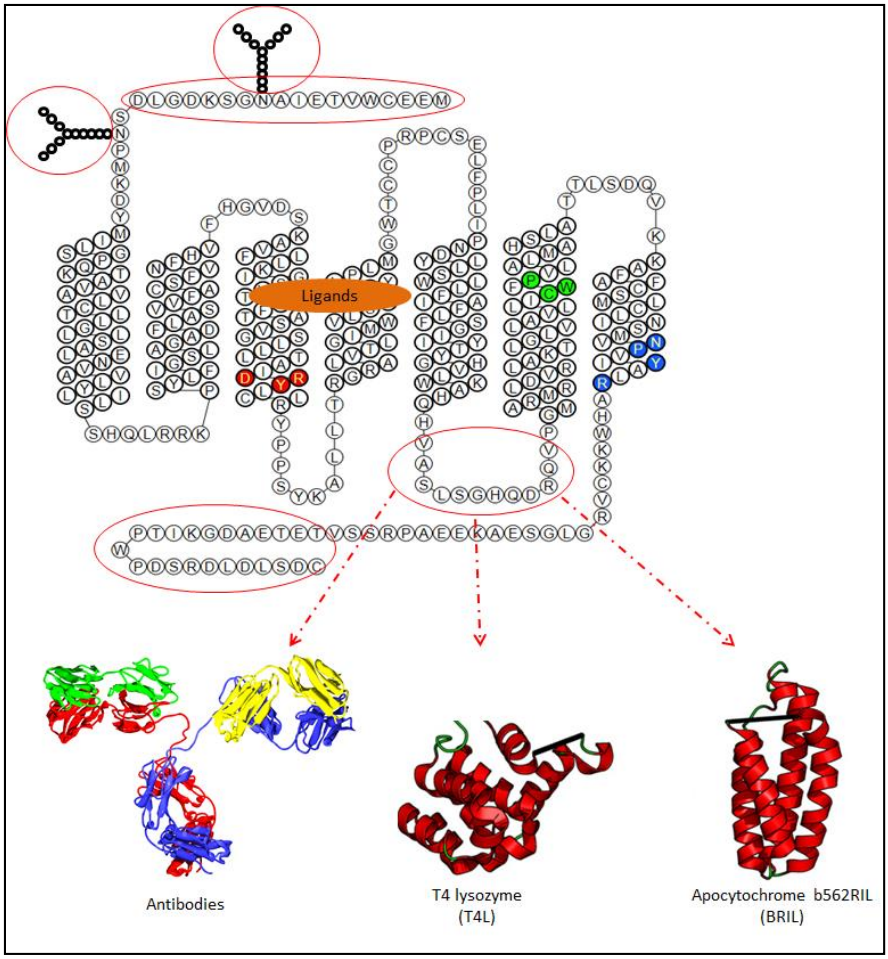

Figure 1-4. General requirements for co-crystal studies of GPCRs.

Different pre-structure/function studies on GPCRs are required to obtain crystal structure:

1. Stabilization of the third intracellular loop is required using fusion proteins or monoclonal antibodies; T4 lysozyme and apocytochrome b526 are the most used fusion proteins for co-crystallization of GPCRs; **2.** N- And/or C-terminal truncation to remove N-linked glycosylation and proteolysis (indicated by red circles); and **3.** Point mutations to increase thermal stability and functional expression and the presence of high affinity/low of rate ligands. Adapted from [43].

1.2 CURRENT METHODS FOR RECOMBINANT GPCR EXPRESSION AND PURIFICATION

Despite the recent progress in the structural and molecular determination of GPCRs over the last decade, the overexpression of membrane proteins for structural and biophysical studies remains challenging. Due to the intrinsic lipophilic properties of the seven transmembrane helices, which often results in low protein yields due to the toxic effect of overproduction of foreign transmembrane proteins, and the ineffectiveness of conventional protein purification techniques, solving the crystal structures of most GPCR structures remains a daunting task.

Purified GPCRs can be utilized for a variety of applications in drug design and development. For example, purified GPCRs protein can be used in the high throughput screening of chemical libraries in binding assays to find hits and improve the affinity and selectivity of compounds. Moreover, purified GPCRs protein can be used in used in biochemical and biophysical studies, such as nuclear magnetic resonance and mass spectrometry, X-ray crystallography, or in studies of downstream signaling using florescent probes [35, 37]. A large number of potential expression systems have been utilized and/or evaluated for producing GPCRs. The choice of expression system depends on the specific requirements for the different GPCRs and investigative purposes. Several hosts have been used previously, such as *Escherichia coli* lysates (cell-free translation), bacteria *H. salinarium*, L and lactis systems, yeasts species such as of *S. cerevesiae* and *S. pombe*, and eukaryotic expression in insects (like Sf9, Sf21, and Hi5) and mammalian cells, are illustrated in (**Figure** 1-5**)**. The use of different expression systems not only provided tools for studying GPCR structure, but also provided solid knowledge for expression strategies in general, as shown in **Table** 1.

1.2.1 Yeast

Saccharomyces cerevisiae (baker's yeast) and P. pastoris are the most widely used yeast heterologous protein expression systems [82]. They also have the first completed genomic sequence of a eukaryotic organism. Unlike most expensive and intractable higher eukaryotic microorganisms, yeast represents a unicellular microorganism that is an alternative for high-level expression of recombinant protein for both commercial and research purposes [83]. The yeast system has the advantage over the mammalian system for isotopic labeling with most of the protein folding capabilities. However, mammalian GPCRs often been proven to be toxic to yeast host cells [84]. Thus, their expression is usually controlled with an inducible promoter to maximize cell health. *Saccharomyces cerevisiae* (baker's yeast) is commonly regulated by the GAL promoter upon galactose induction. In addition, this yeast has been used for the expression and determination of transmembrane proteins and GPCR structures, including crystal structures of the human H1 histamine receptor [85] and human adenosine A2 receptor [61]. Alpha factor Ste2p was expressed and purified previously using the C-terminal Flag and His6 tags with yields up to 1 mg [86]. The human dopamine D1A receptor, mouse serotonin 5HT5A receptor, and human β2 AR are other examples of successful expression and purification of GPCRs using *Saccharomyces cerevisiae* yeast as a host system for expression and utilization [87].

Schizosaccharomyces pombe is a yeast representing another strain that was recruited for recombinant protein expression [88]. These strains are less commonly used compared to other yeast strains. Nevertheless, it has been utilized for expressing highly complex proteins. Moreover, it is different from *Saccharomyces cerevisiae* in the glycosylation process where the vector is designed for both stable and transient expression. This strain has been previously used to produce

a mammalian-like signal transduction system for human dopamine D2 receptor overexpressed in the plasma membrane [89].

Marked success was achieved for investigating the pharmacological functions of about 100 GPCRs utilizing another strain of methylotrophic yeast, *Pichia pastoris* [89]. Since *P. pastoris* is capable of maintaining most of the post-translational modifications such as glycosylation, proteolytic and disulfide bond processing, and is easily used and cultured in bioreactors, it has become one of the most attractive systems for studying GPCR pharmacological function. Recombinant protein expression in *P. pastoris* is controlled by the alcohol (methanol-regulated) oxidase promoter I (AOX1) in the presence of glucose or glycerol. A DNA vector integrates with the host genome. Although the overall total yields of GPCRs expressed in yeast are not high in some cases, functional proteins were obtained, including the human dopamine D2 and mouse OPRK receptors [89]. Cannabinoid receptors have also been expressed and characterized using *P. pastoris* [90]. Cannabinoid receptor CB1 and CB2 gene expression was engineered through a c-myc epitope and a hexa-histidine tag at the C-terminal of the receptors. The results showed that the functionality and pharmacological profiles were similar to those obtained from mammalian systems [91, 92]. Other low-producing GPCR yeast strains, namely, *Hansenula polymorpha*, were also utilized for evaluating GPCRs, such as CCR5 and CXCR4 expression [89].

Yeast systems have also been used as a tool for screening and for the optimization of functional GPCR fusion proteins for crystallography (T4 Lysozyme) [93]. A library of variant receptor forms was created in which T4L was inserted into different positions of the third intracellular (IC3) loop by replacing a number of amino acid residues in the loop [93]. By expressing receptors in *Saccharomyces cerevisiae* yeast, different criteria were taken into consideration for choosing the

best initial construct for scaling up, such as overall expression levels at the cell surface analyzed by green fluorescent protein (GFP), agonist binding and signal transduction via G protein [93].

1.2.2 Cell-free expression

Cell-free translation expression systems are another powerful technique that have been applied to producing many soluble recombinant proteins in relatively ample quantities in the presence of detergents or membrane mimetics [94]. This system is based on crude lysates of prokaryotic (mainly, *E. coli*) or eukaryotic cells (wheat germ embryos or rabbit reticulocytes) which contain all the necessary ingredients, such as amino acids and nucleotides, all of which are essential components for transcription, translation, protein folding, and energy metabolism [94]. Cell-free expression can provide isotopically labeled proteins for nuclear magnetic resonance (NMR) and X-ray crystallography. Much attention has been devoted to using this system after the NMR structure of the bacteria *proteorhodopsin* [95] and the X-ray crystal structure of eukaryotic *Acetabularia* rhodopsin II from marine alga was discovered [96]. Nevertheless, there are no NMR or X-ray crystal structure available for GPCRs using this method to date.

1.2.3 Mammalian Cells

The expression of GPCRs in mammalian cells has several advantages over other expression systems. It produces native refolding and maintains modified GPCRs during expression, enabling G protein downstream signaling [97]. The mammalian expression system is also the best way to examine the effects of modification on the receptor, such as site-directed mutagenesis and screening various compounds for a specific receptor [98]. Although there are high costs for

handling and producing GPCRs using this system, the receptor can be processed and maintained for a long time under selective conditions. Usage of mammalian cells is always advisable and recommended over insect cells in cases where low-yield functional protein and/or large quantities of misfolded protein are produced. There are two main expression processes of the membrane protein using mammalian cells, including the transient and stable expression process shown in **(Figure** 1-5**)**. Transient expression systems allow the membrane protein to be expressed in the presence of cationic lipids or recombinant non-replicative viruses for a short time compared to a stable system. In both systems, either an inducible promoter or a constitutive promoter is required to produce the protein. For non-replicative viruses used only for gene therapy and cell biological studies–the Semliki Forest Virus (SFV) expression system has been used extensively for expression of 101 G protein-coupled receptors in three mammalian cell lines [90, 91]. Although, the SFV system is successful at expression GPCRs, a high proportion of the receptors were misfolded, as indicated by their loss of functionality, e.g. bradykinin B2 receptor [99], alpha 2B adrenergic receptor [100], and angiotensin II receptor [101]. The disadvantage of SFV is the high cost and technical challenges for scaling up due to biosafety and handling restrictions. Other methods for the transient expression for incorporate DNA into the host cell though the use of chemical agents like cationic lipid compounds or electroporation. These methods are also not feasible for large scale production due to the high cost and requirement for optimization requirements, such as plasmid specification, amount of plasmids and reagents, and the optimum time for expression. Bovine rhodopsin (Opsin A) is an example of the first GPCR crystal structure solved using transient transfection of monkey kidney fibroblast cells, COS-1.The recombinant protein was mutated and designed to be more thermally stable through the generation of a disulfide bond between the N-terminal and loop E3. This mutant receptor was expressed in Cos cells.

Utilizing a constitutive adenovirus promoter and DEAE dextran, about 2.5 mg of purified protein was produced, and the structure of the receptor was determined (3.4 Å) [102].

On the other hand, stable transfections are able to integrate the gene of interest into the host cellular genome. Thus, the GPCR gene of interest contains an antibiotic resistance site for stable cell line selection. Moreover, the inducible promoter is preferable for reducing cell toxicity [103]. The advantage of using stable over transient transfection is the ability to produce the recombinant protein without needing to re-transfect the gene. Among different stable cell lines available on the market, Chinese hamster ovary cells (CHO), baby hamster kidney cells (BHK-21), and human embryonic kidney cells are the most predominantly used cells for generation of GPCR stable expression [89]. In addition, to the tetracycline inducible system ,the crystal structure for the constitutively active rhodopsin mutant Glu113Gln in complex with a peptide was also obtained by stable transfection of HEK 293S (TetR)GnTI at a resolution of 3Å [104]. Another crystal structure of the constitutively active rhodopsin mutant at M 257Y6.40 in complex with the C-terminal end of the G protein α-subunit was submitted by Standfuss and his colleagues [105]. Activation and binding was assayed with the amount of radioactivity and GTP γ35S bound to G protein transductions. Finally, the crystal structures of constitutively activated G90D rhodopsin were also obtained and utilized for their desensitization capabilities [106].

1.2.4 Escherichia coli (*E.coli*) expression

Both *E. coli* and yeast cells have provided minor advantages over other heterologous expression systems. Due to low cost, the capacity for scaling up, short doubling time, and easy handling in the laboratory, the bacterial system is usually the first choice among expression systems [59, 84]. In addition, both cell-free translation and *E. coli's* purified protein are eligible for NMR and

crystallography studies. However, the lack of post-translational modifications, absence of necessary interacting proteins for the production of fully functional receptors such as G-proteins, and the inability to translocate proteins to their subcellular destinations (for example, the transport of membrane proteins to the plasma membrane) are considered drawbacks of this system. It has been shown previously that some GPCR cases such as rhodopsin, somatostatin, follicle-stimulating hormone receptors, and β2 adrenergic receptors require this post-translational modification not only to produce folded protein but also to preserve the receptor affinity to ligand binding and/or G-protein coupling as well as insertion into the plasma membrane [107-109]. Non-relevant membrane environment for GPCR expression in bacterial systems is also very different from other eukaryotic cells. Missing are the reductive environment, required to form disulfide bonds and the lipid composition (mainly cholesterol) is another disadvantage of using *E. coli*. Nevertheless, successful examples of GPCR expression in the inner membrane of *E. coli* have been obtained, such as human β2-adrenergic receptor [108] and human CB2 receptor [110]. There are two different site used to date of recombinant GPCR expression, the plasma membrane or in bacterial inclusion bodies (IBs). Each of these approaches is subject to many requirements for success. Fusing a signaling peptide protein to the N-terminal sequence of GPCRs, like β-galactosidase or maltose binding protein (MBP), and inducing the expression with isopropyl-β-D-thiogalactoside (IPTG) in the presence of a weaker promoter has produced many functional GPCRs in the inner membrane of the bacteria, including β2-adrenergic receptors [111], A2a adenosine receptor [112], rat neurotensin NTS1 receptor [48, 113], human serotonin 5-HT1A [114], and M1/M2 muscarinic acetylcholine receptor [115, 116]. Mistic, is another integral membrane protein enhancer that can be fused to the N-terminal sequence for expression of GPCRs. It has been used in combination with the TarCF transducer to facilitate expression and produce

purified human CB2 receptor [110]. The purified CB2 protein exhibits functional binding activities comparable to the binding of membrane fractions.

In some cases, where the bacteria is incapable of handling and processing the expressed recombinant protein to the membrane, they are formed and localized in inclusion bodies as dis functional proteins. Thus, additional procedures are required to extract and refold the protein, to some extent, to the native condition. The advantages of inclusion bodies including: 1) less toxicity to the host compared to membrane expression, 2) the protein expressed levels is considerably higher than other approaches [117], and 3) inclusion bodies are resistant to proteolysis digestion and severe purification conditions [118]. In addition, the protein expressed in these inclusion bodies can be with or without fusion protein. The major drawback of using these inclusion bodies is the need for a refolding process, starting from IB enrichment from the cell preparations by centrifugation, and ending at reconstitution of the purified protein in a lipid mimetic environment and folded to its native state [119, 120]. Glutathione S-transferase (GST), ketosteroid isomerase, human α5 integrin (α5I), and thioredoxin (TRX) tag have been used previously to express GPCRs in inclusion bodies with different variations of protein yield. An example for using of (GST) for the purification and characterization olfactory receptors [121].The ketosteroid isomerase also used for expressing the serotonin 5-HT4a receptor [122] and leukotriene BLT2 for expressing human α5 integrin (α5I) [123]. NusA, TRX, and GST tags were used extensively by Michalke *et al*. to screen IBS expression, purification conditions for 100 GPCRs in Escherichia coli [117]. However, among these GPCRs, human parathyroid hormone receptor 1 and mouse cannabinoid receptor 1 were expressed without the need for fusion protein, and instead used an artificial, chaperone-assisted, purification and refolding procedure [124]. In other studies, the TrpΔLE fusion protein was used for IB-directed expression. This fused polypeptide is derived from a leader sequence

TrpL, which is composed of 17 amino acids [125]. This fused polypeptide, TrpΔLE fusion was used in our laboratory previously for construction of the pMMHb-TrpΔLE-9His–Xa vector for studying expression of cannabinoid receptor CB2 transmembrane fragments [126-129].

1.2.5 Insect cell / baculovirus

The baculovirus expression vector system (BEVS) is now widely used in GPCR research and scientific industrial communities [130]. This method of producing heterologous genes is attractive for many researchers due to the presence of a powerful polyhedrin promoter derived from the baculovirus *Autographa californica's* multiple nuclear polyhedrosis virus (AcMNPV). BEVS is based on facilitating the introduction of a foreign gene into the viral replication genome by homologous recombination of a transfer vector (polyhedrin) containing the target gene and viral DNA. Recently, scientists developed different generations of BEVS that overcame the need for the plaque assay in previous systems. The Bac-to-Bac® (Invitrogen) baculovirus expression system has the advantages of the site-specific transposition properties of the Tn7 transposon. This system comprises a pFastBac™ vector harboring the expression gene and is controlled by the polyhedrin promoter in DH10Bac™ *E. coli*-competent cells. These competent cells contain a shuttle vector (bacmid) which has a mini-attTn7 replicon, antibiotics selection, and a helper plasmid. Insertion of the expression gene of interest into DH10Bac™ *E. coli* disrupts the lacZ sequence in the bacmid, which allows isolation of the recombinant bacmid by blue/white selection. Once the bacmid DNA is isolated, the recombinant bacmid DNA is used to infect insect cells. It is necessary to quantify the virus concentration before infecting the cell in order to know the measure of PFU (plaque-forming units). The number of PFUs can be determined in either a plaque assay or by surface immune staining with gp64-PE antibody and flow cytometry analysis. After obtaining number of

(PFUs), this value is used to calculate the multiplicity of infection (MOI) using the following equation to get the correct amplification and expression of the recombinant protein:

$$\text{Inoculum required (ml)} = \frac{(\text{MOI X number of the cells})}{\text{titer of viral stock (pfu/ml)}}$$

The multiplicity of infection (MOI) usually ranges from 0.05 to 0.1 for producing the second virus titration (1×10^7 to 1×10^8) and from 1 to 5 for protein expression. Different cell lines can be substituted for insect cells such as *Trichoplusia ni* (High Five cells) and *Spodoptera frugiperda* (Sf9 and Sf21 cells). Both Sf9 and Sf21 cells are preferable over High Five cells in the production of baculovirus due to their high transfection efficiency. **Table 1** summarizes the differences between all insect cell lines. The high levels of gene expression, solubility, post-translational modification, and safe handling procedures are features that make the BEVS attractive to use [131]. Protein expression is utilized throughout the unique characterization of the virus' life cycle. In the first stage (10-24 hours, post-infection), the virus is replicated through budding of the cellular membrane, forming virus particles that infect the nearby cells. In this stage, the insect cell will increase in diameter and cell nuclei. It is unlikely that enough protein will be produced in this stage, so the cell needs to be maintained to for the next stage, which is the late stage (24-72 hours). The late of stage, enveloped nucleocapsids are occluded in the nucleus with polyhedrin. This is responsible for producing the protein and generates viral occlusion bodies. At this late stage, cell growth has stopped, and the cell develops a granular appearance. Due to the difference between mammalian and insect cell membrane composition, it might be required to add different membrane supporting materials into the media. For example, insect cells are known to lack phosphatidyl serine, cholesterol, and contain high phosphatidyl inositol content, which is required for the proper refolding of GPCRs in the membrane [94]. To mimic the expression conditions of the mammalian membrane, lipids can be added into growth media, such as in the case of the turkey β1-

adrenoceptor [132] and human D3 receptor [30]. Moreover, addition of ligands to the growth media have been shown to increase expression levels of the protein.

To date, 119 GPCR structures, representing 22 different subtypes of GPCRs, from a total of 826 GPCRs are listed in the GPCR network (http://zhanglab.ccmb.med.umich.edu/GPCR-EXP/). About 85% of the revealed structures have utilized the baculovirus system for protein expression. The majority of the GPCR structures determined used *Spodoptera frugiperda* (sf9) over other cell lines. Nevertheless, High Five ™ cells have been used to determine some GPCR crystal structures such as β1-adrenoceptor [133, 134], A2A receptor [135], and rat neurotensin A [68], and human corticotropin-releasing factor B [70]. This also showed advantages for expression of the truncated receptor. Thus, cell-line production screening is required before large-scale production.

The cost of using this system is high due to the expensive growth medium. Special growth conditions at 27°C are also required for co-transfection agents. Moreover, it takes up to month to produce enough baculovirus for large-scale expression. On the other hand, using the insect cell/baculoviros system has major advantages over other systems. It can provide the desirable GPCR recombinant protein with correct folding, as well as form disulfide bonds and post-translational modifications, which are required for many GPCR functions. However, some of the expressed proteins have non-homogeneous glycosylation, resulting in different forms of the protein, which can eventually affect the quality of the protein's crystal form [136]. In addition, *Spodoptera frugiperda* (sf9) has been used to express Gα subunits such as Gsα, Goα, and Gqα, which will make valuable resources for studying downstream signaling [137].

Table 1. Comparison of Baculovirus Expression Host Systems.

Cells	Origin	Doubling time	Cell appearance	Initial medium	Use
Sf9	Spodoptera frugiperda (Pupal ovarian tissue)	24–30 hours	Spherical with granular appearance	Complete TNM-FH or Sf-900 II/III SFM	Recombinant baculovirus production Intracellular, GPCR protein expression Plaque assay
Sf21	Spodoptera frugiperda (Pupal ovarian tissue)	24–30 hours	Spherical with granular appearance.		Intracellular protein production Secretion of recombinant protein
High Five™	Trichoplusia ni (Ovarian cells)	18–24 hours	Spherical with granular appearance.	Express Five. SFM or Express Five SFM	Secretion of recombinant protein

Adapted from [138], [130].

1.2.6 Other expression systems

Rhodobacter spheroids are examples of other prokaryotic systems which were previously used for GPCRs expression. Their success has remained limited as expression systems [59]. They have been used previously to functionally express human bradykinin B2 receptor (B2R), human adenosine A2a receptor (A2aR), and the human angiotensin AT1a receptor (AT1aR) [139]. In addition, *Halobacterium salinarum* has been used to express and identify bacteriorhodopsin. *Haloferax volcanii* and *Lactococcus lactis*, with other hosts, have shown their potential for expressing some GPCRs. However, there has been limited success with obtaining GPCRs crystal structures from these systems.

Utilizing the abundance of rhodopsin receptors in eye retina, rhodopsin was isolated from its natural source in a sufficient amount for crystal structure studies. Rhodopsin receptors were isolated in high amounts in 1998 from outer rod segment membranes using detergents [140]. This remarkable purification allowed for crystallization trials to take place. Two years later in 2000, the first GPCR structure solved by X-ray crystallography was bovine rhodopsin with a resolution of 2.8 Å [27]. Similarly, squid rhodopsin's crystal structure was defined and revealed [141, 142]. Due to the unique abundance and stability of the receptor, rhodopsin was extensively utilized for GPCR x-ray studies, leading to twenty-nine different crystal structures of with different resolution in the protein data bank.

Other eukaryotic systems have been utilized to produce GPCRs, such as transgenic animals. *Caenorhabditis elegans* is an example. Bovine and human adenosine A2A are expressed in neurons or muscles of this worm. They are able to produce native, functional GPCRs in milligram amounts. Moreover, the adenovirus encoding for CXCR1 was used to infect mice liver *in vivo* to

produce functional expression of recombinant GPCRs comparable to expressed protein in neutrophils [143]. An estimated 20 mice livers were enough to produce 1 mg of the functional protein, which is the same amount that can be produced from 5 L of cell culture media [144]. Retinal rod cells of transgenic *Xenopus laevis* have also been used to produce 20 homogeneously glycosylated GPCRs [145]. Ligand binding and functional assays of $5HT_{1A}$ and EDG_1 are performed to confirm that the function as well as the refolding of these receptors was preserved. The authors conclude that similar results could be universal and generalized to other GPCRs [145].

1.2.7 Comparisons of expression systems

There is no ideal expression system for GPCR production, taking into the account the cost, time consumed for vector production and protein expression, culturing difficulties, and scaling up as shown in (**Figure** 1-5**)**. In addition, isotope labeling for NMR is also a major factor in choosing the system. The less attractive system is the cell-free expression system due to a poor expression levels compared with other systems. No crystal structures have been solved using this system. With simplicity and low cultivation costs, *Escherichia coli* is considered the most popular host for the overproduction of membrane proteins. The ability to scale up and NMR labeling are other advantages of using the *E.coli* system. However, the lack of glycosylation, limited post-translational modifications for producing membrane protein, as well as the refolding process for some GPCRs expressed in inclusion bodies are considered major limitations of this system. The expression of recombinant GPCRs in mammalian and yeast cells is quite successful compared to cell-free translation due to the presence of post-translational modifications. However, glycosylation and hyper-glycosylation are different in yeast compared with mammalian cells. Also, the yeast cell membrane has a different lipid composition than that of mammalian cells. The

insect cell/baculovirus expression system is robust. It has mammalian-like post-translational modifications. The membrane compositions of the insect cell are different from those of mammalian cells. Insect membrane are composed of high phosphatidyl inositol content, low cholesterol content, and contain no phosphatidyl serine, indicating that additional lipid or cholesterol may need to be supplemented in the media [94]. Most of the co-crystal structures utilizing these efficient systems are shown in **Table 2.**

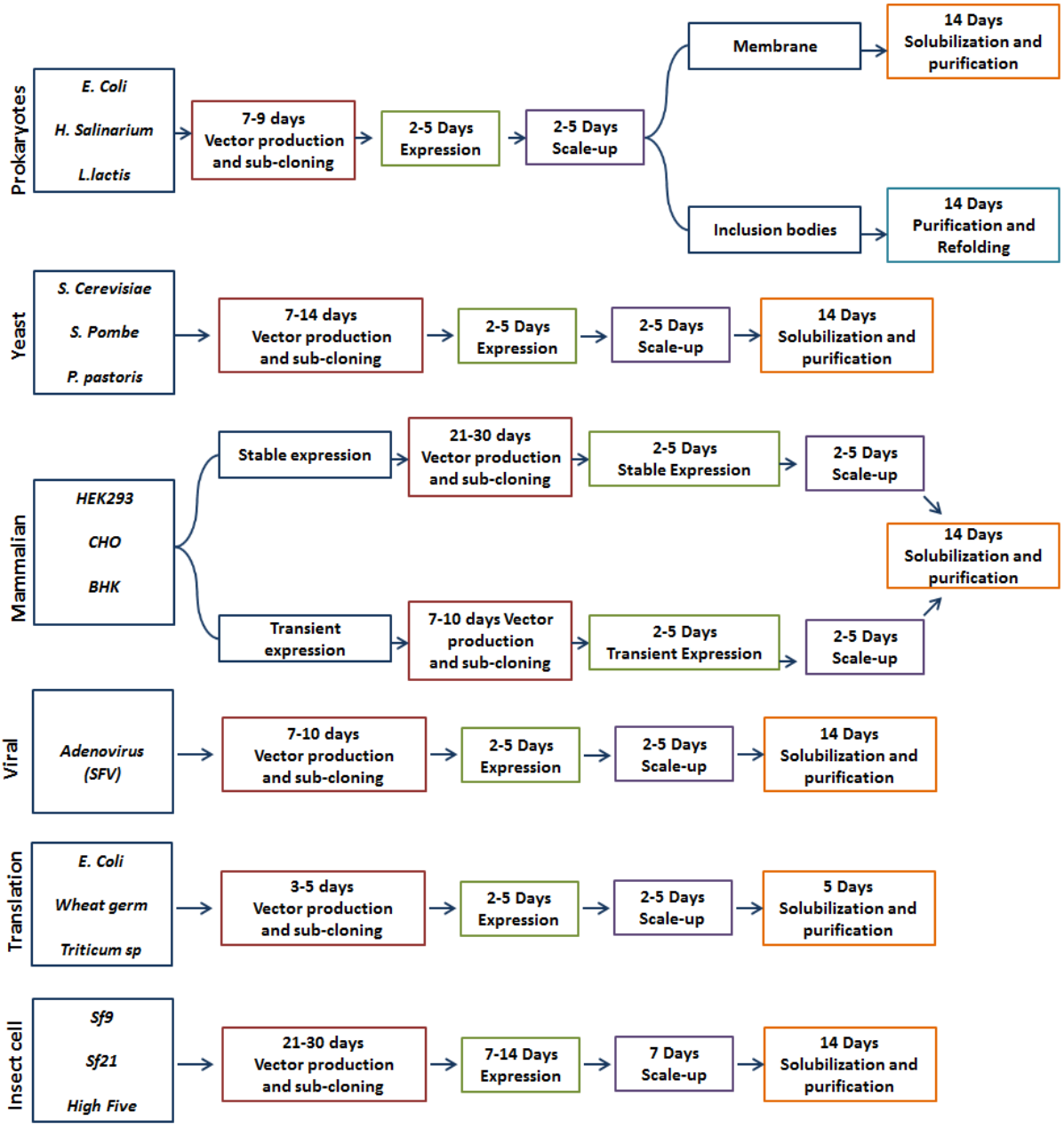

Figure 1-5. Comparison of GPCRs expression systems.

Time and procedures required for cloning, expression, and purification of recombinant GPCRs in different expression systems [77, 78].

Table 2. Updated list of GPCR crystal structures subtypes released from different expression systems.

Expression system	Advantages	Disadvantages	GPCRs name	Class	PDB-ID	Resolution	Ref
Bacterial	• Ease of handling and scaling up; inexpensive • Produced pharmacologically active receptor in the case of membrane-targeted E.coli	• No post-translational modifications • The receptor is inactive in the case of inclusion bodies, which require refolding	Human Chemokine 1R	A	2LNL	NMR	[146]
			Neurotensin receptor 1	A	3ZEV	3.00 Å	[79]
Yeast	• Can be used for scaling up; easy to use • The ability to perform post-translational modifications, including those with a high number of disulfide bonds	• Hyper-glycosylation may occur • Cell membrane differs (lipid components) from mammalian membrane	Human histamine H1R	A	3RZE	3.1 Å	[64]
			Human Adenosine A2 R	A	3VG9	2.7 Å	[61]
Retina (Natural)	• Abundance in the receptor	• Restricted to a few GPCRs • Expensive to use in the case of transgenic animals	Rhodopsin (Bovine)	A	1F88	2.8 Å	[27]
			Rhodopsin (Squid)	A	2Z73	2.5 Å	[141]
mammalian cells	• Produced functional receptor for pharmacological and signaling studies • Performing post-translational modifications	• High cost and time-consuming • Expensive to culture same as insect/baculovirus system	Rhodopsin (Bovine)	A	2J4Y	3.4 Å	[102]
Cell free translation	• Toxic protein can be expressed	• High cost • Non suitable for large scale.	None	A	---	---	---

Expression system	Advantages	Disadvantages	GPCRs name	Class	PDB-ID	Resolution	Ref
Insect cell	• Performs more complex post-translational modifications and processes disulfide bonds properly • Relatively high expression levels	• Work complexity • Producing virus and expressing protein is time consuming • High cost • Membrane composition different than mammalian cells	Human β2- adrenoceptor	A	2RH1	2.4 Å	[63]
			Turkey β1 Adrenoceptors	A	2VT4	2.7 Å	[147]
			Human Adenosine	A	3EML	2.6 Å	[58]
			Human muscarinic (M2)	A	3UON	3.0 Å	[66]
			Human Dopamine (D3)	A	3PBL	2.89 Å	[30]
			Human Chemokine (CXCR4)	A	2K05	2.5 - 3.2 Å	[57]
			Human muscarinic (M3)	A	4DAJ	3.4 Å	[71]
			Human Lysophospholipid (S1P)	A	3V2W 3V2Y	3.35 Å	[65]
			Human 5-Hydroxytryptamine (1B and 2B)	A	4IB4 4IAR	2.7 Å	[73, 148]
			Human Chemokine (CCR5)	A	3MBS	2.71 Å	[74]
			Mouse δ and μ opioid receptor	A	4EJ4 4DKL	3.4 and 2.8 Å	[67, 72]
			Human κ and δ opioid receptor	A	4DJH 4N6H	1.8 and 2.9 Å	[75, 149]
			Human NOP opioid receptor	A	4EA3	3.01 Å	[76]
			Human purinoceptor 12 receptor	A	4NTJ	2.62Å	[150]
			Rat Neurotensin 1 receptor	A	4GRV	2.8 Å	[68]

			Human Proteinase-activated 1	A	3VW7	2.2 Å	[69]
Insect cell Continued			Human Orexin 2	A	4S0V	2.5 Å	[151]
			Human Corticotropin-releasing factor 1	B	4K5Y	2.98 Å	[70]
			Human Free fatty acid 1 receptor	A	4PHU	2.33 Å	[152]
			Human Glucagon receptor	B	4L6R	3.30 Å	[153]
			Human Metabotropic glutamate 1 and 5	C	4OR2 4OO9	2.8 and 2.6 Å	[77, 154]
			Human Frizzled (SMO)	F	4QIM 4QIN 4N4W	2.6 – 2.8 Å	[155]

2.0 ENDOCANNABINOID SYSTEM

The endocannabinoid system is composed of cannabinoid receptors and endogenous ligands, as well as, lipids or enzymes that synthesize and degrade such ligands [156]. This system controls complex physiological processes that involve the endocrine and neurological systems, such as, mood regulation, immune modulation, pain, and memory and food intake [157, 158]. Currently, there are two known endogenous ligands, Anandamide also known as N-arachidonoylethanolamine or (AEA), and 2-arachidonoylglycerol (2-AG). Additionally, there have been several mediators recognized for the endocannabinoid system, such as, *N*-arachidonoyl dopamine (NADA), *N*-palmitoylethanolamine (PEA) and 2-arachidonoyl glycerol ether (noladin ether). It is also widely known that enzymes of the endocannabinoid system include fatty acid amide hydrolase and the monoacylglecerol lipase. Also the selective anandamide reuptake transporter SART.

Anandamide was obtained from porcine brain extracts and consists of poly-carbon (20) fatty acids connected to ethanolamine by an amide linkage [159]. In addition, both AEA and 2-AG are derivatives of arachidonic acid that bind with different affinities to endocannabinoid receptors. 2-AG exhibits a higher binding efficacy when compared to AEA. [160, 161]. When binding of endo- or exogenous cannabinoids to their cognate receptors (CB1 and CB2) occurs, adenylase cyclase is inhibited thereby triggering further intracellular downstream signaling. furthermore, the endocannabinoid system acts on other downstream signaling pathways which results in activation of receptor kinase, mitogen-activated protein kinase (MAPK), and c-Jun N-terminal kinases (JNK) [158] [162].

Cannabinoid ligands are often classified into three groups classical cannabinoids, such as [Δ^9-THC, Δ^8- THC-dimethylheptyl (HU210)], non-classical cannabinoids, such as [CP55,940], eicosanoids derivatives [anandamide, 2-arachidonoylglycerol], carbimimetic indols [WIN 55,212-2], and pyrazole derivatives [SR141716A, SR145528]. THC, one of the major active compounds of *Cannabis sativa*, has therapeutic uses including anti-inflammatory, immunosuppressant, analgesic [163] and anti-obesity effects [164]. However, it also produces major psychoactive effects such as catalepsia, hypothermic, and addiction [165, 166]. THC was isolated and structurally characterized in 1964 and cis considered to be a paradigm of synthesized analogs [167]. In 1971, the same researchers isolated multiple compounds of *Cannabis sativa*. These included, cannabinol, cannabichromene, and cannabicyclol **(Figure** 2-1**)** [168]**.**

A. Plant cannabinoids

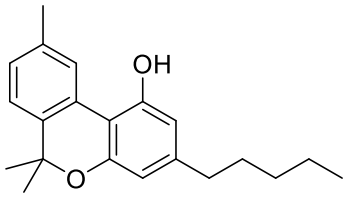

Cannabinol

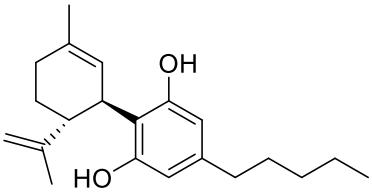

Cannabidiol

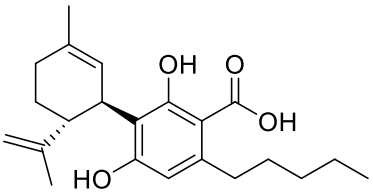

Cannabidiolic acid

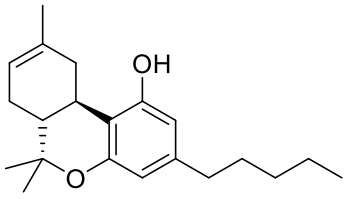

Δ^8-THC

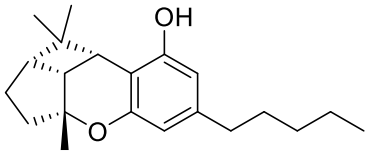

Cannabicyclol

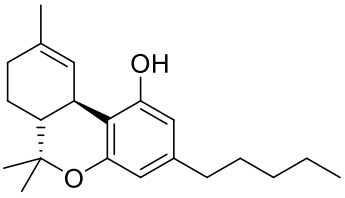

Δ^9-THC

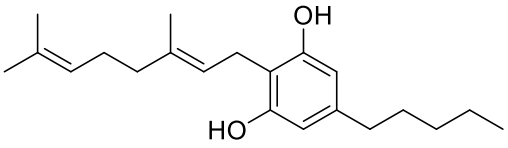

Cannabigerol

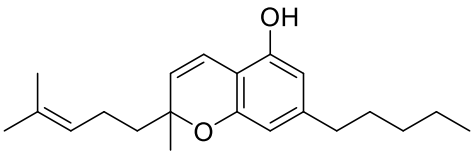

Cannabichromene

B. Classical cannabinoid

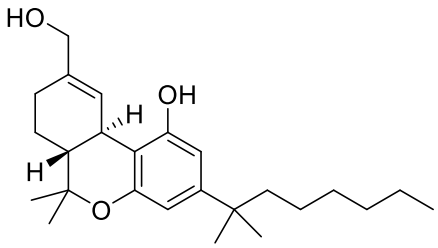

HU-210

C. Non classical cannabinoids

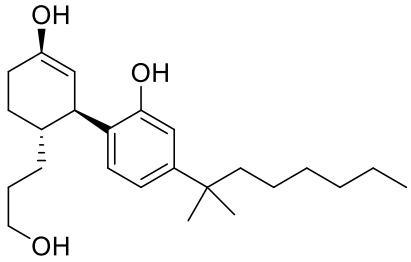

CP55,940

D. Indoles

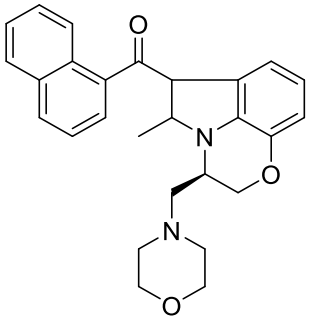

***R*-(+)-WIN55212-2**

E. Eicosanoids derivatives (Endocannabinoids)

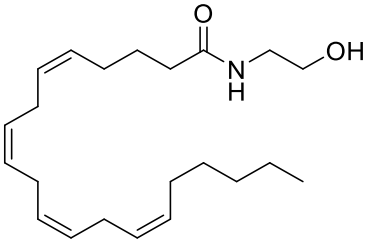

Anandamide
(AEA)

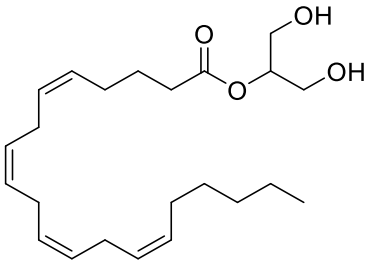

2-Arachidonyl glyceryl
(2-AG)

F.Pyrazole derivatives

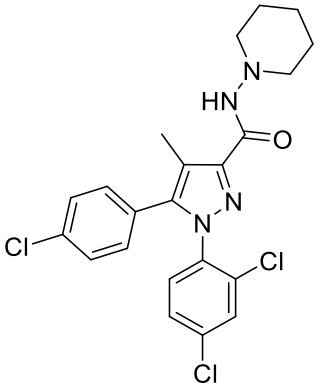

SR141716
(Rimonabant)

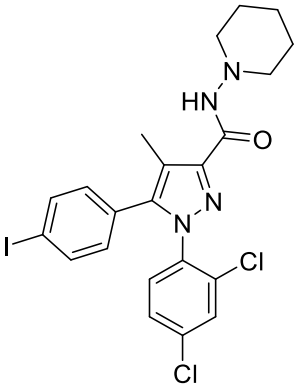

AM251

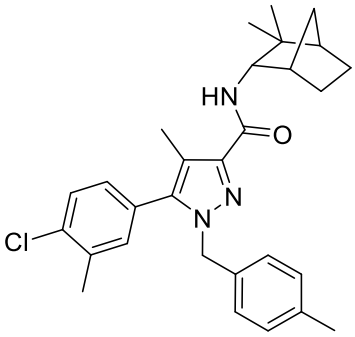

SR144528

Figure 2-1. Chemical structure, classes of cannabinoids and their examples.

Different classes for both cannabinoid receptors CB1 and CB2 with examples.

2.1 CANNABINOID RECEPTORS

2.1.1 Cannabinoid receptor CB1

The cannabinoid receptor 1 (CB1) was discovered and isolated from the cerebral cortex of the rat brain in 1990 by Matsuda and colleagues [168]. Extensive cloning studies later led to the discovery of CB1 receptors from human brain and testes [169]. Previously considered an orphan receptor until CP55,940 and Δ^9-THC were shown to inhibit adenylyl cyclase as their mechanism of action. Cannabinoid receptors CB1 only share 44% overall amino acid identity with the receptor CB2. However, within the transmembrane domains, this percentage increases to 68% [170]. CB1 is predominantly expressed in the central nervous system, but can also be located in peripheral tissues such as the heart, lung, adrenal glands, tonsils, and spleen at low levels [170, 171]. The CB1 receptor consists of 472 amino acids, with a molecular weight of approximately ~ 52.8 kDa. CB1 receptors as a therapeutic target has been recently studied. Rimonabant, a CB1 inverse agonist drug for example, was a marketed in Europe drug for the treatment of obesity, smoking cessation, and associated metabolic disorders. However, due to potential psychiatric side-effects, such as severe depression and suicide, the drug was withdrawn from the European market in 2008 [172].

2.1.2 Cannabinoid receptor CB2

Cannabinoid receptor 2 (CB2) was cloned and isolated in 1993 using a PCR-based approach along with structural homology to other GPCRs [170]. Unlike CB1, which is primarily expressed in the central nervous system and it believed to be responsible for modulating N-type Ca^{2+} and K^+ channels [173], the CB2 receptor is predominantly expressed in the spleen and other tissues with

immunological functions [170, 174-176]. CB2 does not exhibit ion channel effects [6]. CB2 mediates cannabinoid signaling via multiple signaling pathways and has been implicated in inflammatory pain [137], autoimmune and immunological disorders such as, multiple sclerosis [177], and immune system related cancers [178]. Both CB1 and CB2 fall within the general structural pattern of Rhodopsin family GPCRs. Moreover, they are classified under family A which has a glycosylated N'-terminal external domains, seven transmembrane domains, and an intracellular C'-terminal tail [174]. The expression pattern for CB2 suggests the involvement of these receptors in many clinical manifestations and may serve as a platform for disease targets with limited CNS side effects [179].

GPR55 has emerged as a novel orphan receptor that was identified and cloned as a GPCR [180]. GPR55 couples through $G\alpha_{13}$ subunit. It is a class-A, rhodopsin-like GPCR with low sequence similarity to CB1 (13.5%) and CB2 (14.4%) receptors [181]. It is mainly expressed in the CNS, similar to CB1. In addition, it has been shown to regulate osteoblasts and osteoclasts in bone remodeling [182]. Endocannabinoids such as AEA, and CB ligands such as virodhamine and CP55,940 bind and activate the GPR55 receptor. Due to the lack of the information regarding the role and mechanism of the receptor and its endogenous ligands, GPR55 remains an orphan receptor that is not classified as an endocannabinoid receptor.

2.2 CANNABINOID RECEPTOR SIGNALING

CB1 and CB2, couple to the $G_{\alpha i/o}$ G-protein [183]. Activation of these receptors through agonist triggers replacement of GDP, which is bound to the Gα subunit, by GTP, then causing dissociation of the G protein. $G_{\alpha i/o}$ effectors inhibit adenylate cyclase causing cyclic adenosine

monophosphate (cAMP) reduction inside the cell. These effects on adenylate cyclase can be used to distinguish between antagonists/inverse agonists and agonists. Binding cannabinoid receptors to inverse agonist leads to stimulate the adenylyl cyclase and thus cause enhancement of the cAMP levels in the cells. Lastly, antagonist binding to CB receptor have no effect on inhibition or stimulation of the adenylyl cyclase. Therefore, no change on the cAMP levels will be observed [184]. The βγ dimer complex serves as a scaffold protein in the MAPK activation cascade. Moreover, the phosphatidylinositol-3-kinase (PI3K) inhibitors and subsequent recruitment of protein kinase B (PKB) are blocked, as illustrated in **(Figure** 2-2**)**.

Cannabinoid receptors also can interact with different effectors (Ceramide) [185]. This lipid second messenger plays a critical role in cell cycle differentiation, proliferation, and programmed cell death [186]. In glioma and primary astrocytes, CB1 induces the hydrolysis of sphingomyelin by sphingomyelinases [187]. This increase in hydrolysis leads to an increase in the levels of ceramide which, in turn activates the ERK 1/2 pathway. Non-selective cannabinoid agonists, such as, Aanandamide, HU-210 and Δ^9 –THC increase the metabolism and expenditure of glucose due to a transient increase of ceramide levels in the cell [188]. In rat C6 glioma, both CB receptors have been linked to an increase in levels of ceramide and subsequent activation of the Raf-1/MAPK cascade [189]. These increases in ceramide levels activate the MAPK pathway, which leads to apoptosis [189]. In rat primary neonatal microglia cells expressing CB2, 2-AG has been shown to activate the MAPK signaling pathway and promote cell proliferation [190]. Activation of MAPK can also induce the expression of genes such as, Krox 24 and Fos, which have been shown to be involved in growth, differentiation, and proliferation of cells [191, 192].

Targeting the CB1 receptor has been shown to inhibit Ca^{2+} influx by ion channels [193]. CB1 receptor agonists, including CP55,940 and anandamide, inhibit calcium channels causing a

decrease in Ca^{2+} levels via a cAMP-independent pathway [194]. Additionally, the CB1 agonist inhibited the Q-type Ca^{2+} currents in pertussis toxin (PTX) sensitive tumor for the cell [195]. In neuroblastoma-glioma hybrid and neuroblastoma cells expressing CB1 receptors, calcium concentration levels inside the cell were increased using CB1 agonists such as, 2-AG and WIN55212-2 [196, 197]. An alternative experiment using pulmonary endothelial cells demonstrated anandamide increased the intracellular calcium concentration due to the activation of phospholipase C [198].

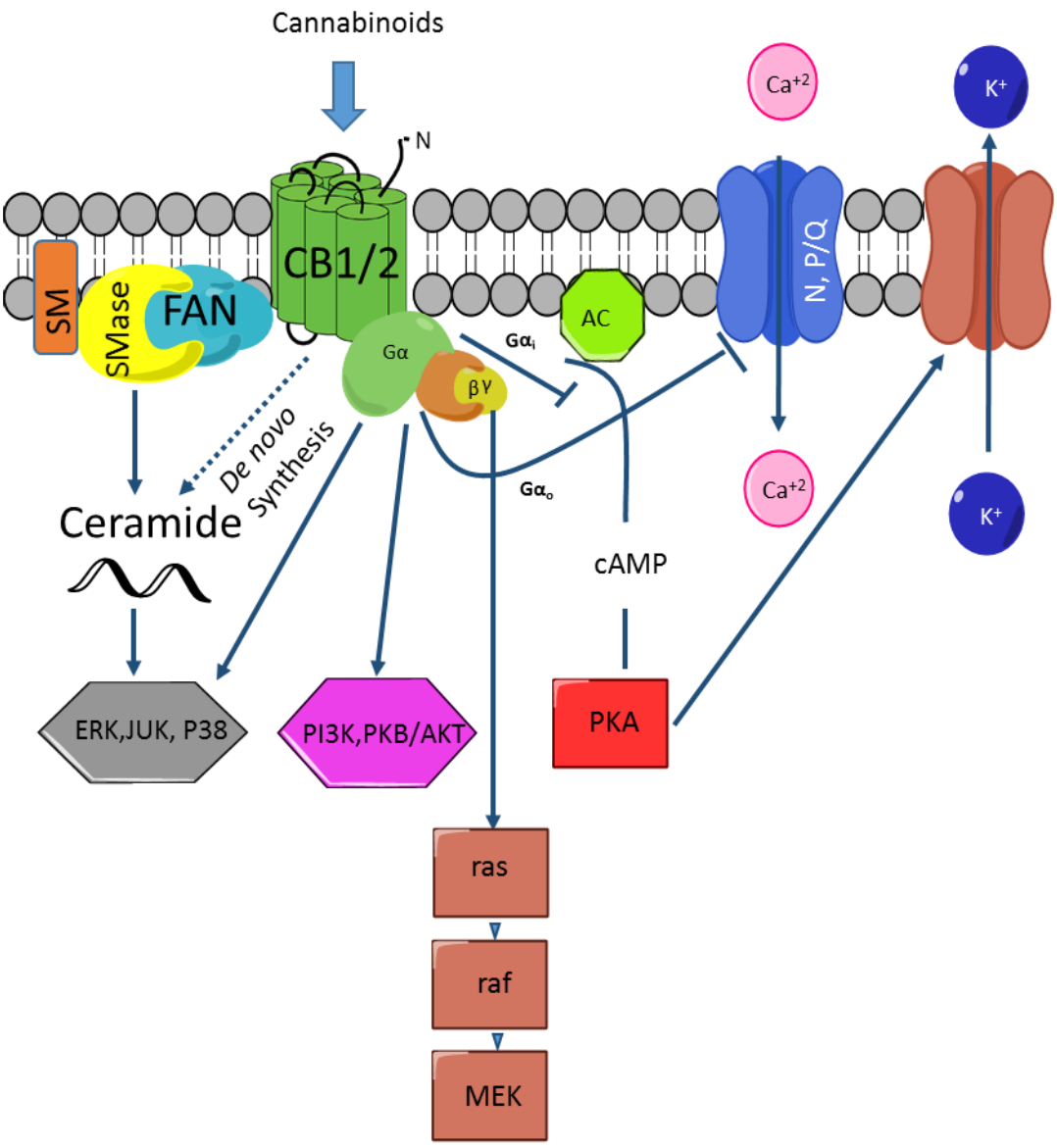

Figure 2-2. Cannabinoid receptor CB1 and CB2 signaling.

The cannabinoid receptor couples to G proteins. The coupling leads to a decrease in cAMP, activates of PKA , AKT and MPK, which all control the cell fate. Activation of the CB1 receptor leads also to produce of ceramide though sphingomyelin (SM) hydrolysis via sphingomyelinase (SMase) activation possibly through the adaptor protein FAN rectifying potassium currents. Adapted from [199, 200] and [201].

2.3 PHYSIOLOGICAL ROLE AND THERAPEUTIC SIGNIFICANCE OF ENDOCANNABINOID RECEPTORS

Endocannabinoids have proven their involvement in multiple regulatory functions which include, energy metabolism, cardiovascular tone, immune system, and reproductive roles [188]. Throughout the past three decades, there have been many drugs on the market for the treatment of various disease states. For example, Δ^9-THC (Marinol®), which has psychotropic effects, has been used as an anti-emetic drug for cancer patients as well as an appetite stimulant [202, 203]. Cesamet®, a synthetic analog for dronabinol, has been utilized by chemotherapeutic patients to treat nausea and vomiting. In Canada, Sativex® is used to treat pain management in multiple sclerosis patients. [204, 205]. The location of CB1 and CB2 determines the need for therapeutic uses. For example, CB1 receptors are primarily expressed in the CNS allowing them to be a potential target by inverse agonists. This would be significant for appetite suppression and weight loss. CB2 is expressed in the peripheral tissue and modulates immunological activity and inflammatory responses in leukocytes [206]. Several studies have demonstrated a role for CB2 in bone mass regulation [207-210] and osteoporosis. CB2 knockout mice (CB2($^{-/-}$)) exhibit a dramatic reduction in bone nodule formation when compared to WT littermates [211]. Furthermore, CB2 receptor modulation leads to various immune responses [212] which range from inflammation to neuroprotection[213]. Examples of these responses are proliferation, cell death and inhibition of antibodies that are mediated by T and B-lymphocytes. Cannabidiol, a natural constituent of Cannabis extract, [214] attenuates pathogenic T cells and reduces spinal microglial activation thereby, demonstrating improvement of multiple sclerosis symptoms in mice [215]. These studies provide compelling evidence to support that CB2 receptor agonists would be promising

therapeutics to treat neuropathies [216]. The CB2 agonist HU-910/30 has been demonstrated to reduce oxidative stress markers, inflammation and cell death following hepatic ischemia reperfusion injury in a mouse [217, 218]. Literature also supports the notion that CB2 has the potential to be a target for a myriad of other diseases such as, sepsis [219] chronic pain, anxiety, ataxia and catalepsy [220].

There has been strong evidence to support that there is upregulation of cannabinoid receptors in bone, breast, prostate lung and blood related cancers when compared to normal tissues [221] , [222, 223]. Treatment with THC led to a significant reduction in lung adenocarcinoma [224] and blood related cancer [225]. Moreover, throughout the tumor progression, an upregulation of endocannabinoid-degrading enzymes has been documented. Attempts to diminish the enzyme levels resulted in tumor size suppression [226]. Speculatively, the mechanism of action is shown in **(Figure** 2-2**)**. Briefly, cannabinoid receptors produce ceramides which leads to activated ERK and p38-MAPK signaling pathways, this in turn leads to considerable cell cycle arrest and apoptosis. Additionally, the inhibition of protein kinase A (PKA) caused by inhibition in cAMP leads to apoptosis [227, 228].

Δ^9-THC and endocannabinoid ligands have been proven to be potential inhibitors of cell proliferation, angiogenesis, and metastasis of breast cancer cell-lines [229]. In addition, selective CB2 agonists, such as JWH-133, inhibit cancer migration and angiogenesis *in-vitro* by triggering caspase activation leading to apoptosis. Prostate cancer cell-lines along with human prostate cancer tissues, were previously evaluated for overexpression of cannabinoid receptors [230-233]. Furthermore, *in-vivo* studies have indicated that Methanandamide and JWH-015, both selective agonists to CB2, have anti-proliferative and pro-apoptotic effects that reduce tumor growth in athymic mice injected with PC-3 cells [234].

The presence of CB2 receptors in brain microglia suggests possible therapeutic targets in treating CNS-related diseases. In recent studies on Alzheimer's disease JWH 015 activated the CB2 receptor, which in turn led to the removal of β-amyloid plaques by stimulation of macrophages [235]. This proof-of-concept was confirmed by treating with SR144528, a selective CB2 antagonist, to prevent JWH-015 from inducing plaque removal *in situ*. Cell cultures treated with CB2 ligand, AEA, 2-AG, and noladin led to increased viability of neurons after exposure to different Aβ species toxins [236].

However, the most significant therapeutic target endocannabinoid receptors is for bone remodeling and homeostasis [208]. It has been demonstrated that osteoclasts, osteoblasts, stromal cells and osteocytes express large amounts of endocannabinoid metabolizing enzymes, NAPE-phospholipase D, FAAH, and DAGLs α and β. Studies have shown that Estrogen-deficiency mice are associated with osteoclastogenesis and both CB1 and CB2 are highly expressed in bone-marrow precursor cells. Inhibition of both CB receptors by selective inverse agonists led to a downregulating in osteoclast formation [237]. In contrast, other studies have shown that cannabinoid receptor agonists such as HU308, JWH133 and CP55,940 increased osteoclast size, number, and stimulated bone resorption [207, 209, 237].

Therapeutic interventions targeted at CB2 receptors displays immense potential to patients suffering from neuropathic, inflammation and pain, bone related disease and cancers.

2.4 OVERALL GOALS AND APPROACHES TO THE STUDY OF CB2 RECEPTOR STRUCTURE AND FUNCTION OF CB2 RECEPTOR

Design and synthesis of CB2 selective ligands is necessary to attain pharmacological end-points [238, 239]. To design selective ligand structures, the activity of known ligands must be studied to further enhance potency and selectivity [239-241]. High resolution, three-dimensional structures of CB2 have provided a detailed understanding of form and function of the proteins and provided knowledge of ligand binding sites and receptor ligand interactions [58, 62, 63, 242]. These structures open doors to a large number of drug discovery techniques. [243]. These techniques include, but are not limited to structure-based drug design, virtual and fragment screening [244-246]. Solving the high-resolution 3D crystal structure of the CB2 receptor will contribute largely to the CB2 structure and function studies. However, heterologous GPCR expression and production is problematic due to their inefficient transport and insertion into the plasma membrane, the potential to induce toxicity to host cells, and inherent structural instability of the receptors [62]. Detergents used in the purification process negatively impact GPCR stability and yield. Crystallization of purified GPCRs are troublesome due to the presence of detergents, inherent receptors flexibility, and small hydrophilic regions [48-50]. Many technical barriers, therefore, need to be overcome in order to generate diffraction quality crystals of GPCRs.

Our goals for studying the structure of the CB2 receptor in this project are two-fold. Firstly, we utilized homology models and site directed mutagenesis to gain insight into the effects of the amino acid substitution on the binding and function of the receptors. It has been shown that some amino acid mutations aid in the purification of the receptor due to an increase in the thermal

stability of the protein [247]. The end goal would be a highly selective CB2 modulator with diminished unwanted effects.

Secondly, we will attempt to purify the functional CB2 receptor. Our goal is to develop a method for producing purified and functionally active CB2 receptor using detergents. To achieve this we selected an insect cell expression system. This system is advantages because it can produce functional receptors without the need for refolding. To stabilize the receptor during the purification, a fusion protein was inserted at the third intracellular loop of the receptor. This protein will be able to analyzed using X-ray crystallography methods to study the CB2 structure and dynamics with or without ligand activation. To accomplish this goal, we plan to carry out CB2 receptor expression, and purification studies using different fusion protein, structurally distinct ligands and different detergents. Ligand binding and western blot analysis will be used to identify the best construct for CB2 expression that also preserves the structure integrity of the CB2 receptors after insertion.

3.0 IMPORTANT BINDING RESIDUES OF CB2 RECEPTOR DETERMINED BY *IN SILICO* MODELING, MOLECULAR DYNAMIC SIMULATION, AND SITE-DIRECTED MUTAGENESIS USING MAMMALIAN CELLS

1. **Alqarni MH**, Myint KZ, Tong Q, Yang P, Bartlow P, Wang L, Feng R, and **Xie X-Q**. Examining the critical roles of human CB2 receptor residues, valine 3.32 (113) and leucine 5.41 (192), in ligand recognition and downstream signaling activities. *Biochemical* and *Biophysical* Research *Communications*, 2014; 452(3):334-339.

2. Feng Z, **Alqarni MH**, Yang P, Tong Q, Chowdhury A, Wang L, and **Xie X-Q**. Modeling, molecular dynamics simulation, and mutation validation for structure of cannabinoid receptor 2 based on known crystal structures of GPCRs. *Journal of chemical information and modeling*, 2014; 54(9):2483-2499.

3.1 INTRODUCTON

Cannabinoid receptors are in the rhodopsin-like family of G protein-coupled receptors (GPCRs) with seven characteristic hydrophobic transmembrane helices attached by three intracellular and three extracellular loops [248]. Two types of cannabinoid receptors, CB1 and CB2, were characterized and cloned in 1990 and 1993, respectively [249, 250]. Differentiation between cannabinoid receptors can be based on the variations of amino acids making up the receptor, tissue abundance, selectivity and specificity to some ligands, signaling mechanisms, and phosphorylation pathways [251]. The CB1 receptor, for example, is expressed in the central nervous system (CNS) and is less predominant in peripheral organs and tissues such as the heart, lung, adrenal gland, tonsils, and spleen [171]. Unlike the CB1 receptor, the CB2 receptor is predominantly expressed in the peripheral immune system, such as the spleen and lymph nodes, where it is expressed in low amounts [250]. The distribution patterns of the CB2 receptor in peripheral organs suggest that the CB2 receptor may plays a crucial role in the regulation of the immune response [252]. Therefore, CB2-selective ligands may likely hold promise for the treatment of diseases with an immune origin, e.g. chronic pain [253], osteoporosis [254], and various cancers such as lung, bladder [255], pancreas [256], breast [257], and prostate [230] without CNS-mediated psychoactive effects. Cannabinoid binding induces a series of conformational changes among the transmembrane helices that shift the equilibrium toward the active receptor state [258]. Consequently, $G\alpha_i$, a family of G proteins, binds to the third intracellular loop and C-terminus of CB2 to inhibit forskolin-stimulated adenylyl cyclase (causing a reduction in cAMP levels), activating the mitogen-activated protein kinase (MAPK) cascade and regulates protein kinase A (PKA) phosphorylation, all of which are important in maintaining cell

functional integrity [259]. Moreover, activation of the CB2 receptor results in a transient elevation of Ca^{2+} signaling in endothelial cells exposed to the endocannabinoid anandamide [198]. Due to the difficulties in GPCR functional expression and purification, as well as their inherent flexibility, only a limited number of GPCR crystal structures have been elucidated to date [53]. Given the scarcity of GPCR crystal structures, generating 3D models derived from previously reported GPCR structures and complementary site-directed mutagenesis experiments are considered to be a feasible alternative for studying ligand binding and receptor activation [260]. Different amino acids present in the binding pocket have been confirmed for their importance in both agonist and antagonist binding [261-268].

In this chapter, we will provide a literature review as well as case studies for the residues that have shown important roles in both structure and function of the cannabinoid receptor CB2. Molecular modeling, docking, and site-directed mutagenesis studies, suggest that some residues of TM3, ECL2, TM 5, TM6, and TM7 are responsible for the large conformational changes observed during ligand binding. The results also imply important roles of these residues in ligand binding and downstream signal transduction of the CB2 receptor. We investigated the possible roles of V113 of TM3 (position 3.32) and L192 of TM5 (position 5.41) in binding with three structurally diverse CB2 ligands: CP-55,940, a non-classical cannabinoid agonist; SR144528, a diarylpyrazole inverse agonist; and XIE95-26, a biamide derivative inverse agonist [269]. We also illustrated the role of aromatic amino acids (Phe183) in the second extracellular loop and (P281) in the seventh transmembrane helix domain in ligand-biding recognition. These aromatic amino acids tend to form π−π interactions to modify the conformational binding pocket of SR144528 and CP55940.

3.1.1 Understanding the role of binding in functional residues of the cannabinoid CB2 receptor by mutational studies

Solving the GPCR co-crystal structure for rhodopsin in 2000 expanded the horizons for understanding the activation mechanism of the receptors and differentiating the role of amino acids in both ligand binding and signaling transduction. The lower part of the receptor is known for high conformational changes and G protein coupling. The upper part of GPCR is responsible for ligand recognition by the receptor and triggering the related signaling transduction. Site-directed are applied to understand the effect of changing or removing one or more amino acids on ligand binding and receptor stabilization by thermostabilizing mutations. Thermostabilizing mutations are considered one of the most effective strategies for increasing the thermal melting point of the receptor. Different methods of thermostabilizing the mutation in the transmembrane regions have been used previously, such as creating disulfide bonds (i.e. cysteine mutation) between helix 1 and the C-terminal of the receptor to reduce their potential movement. Engineering a Zn^{2+} bridge by replacing amino acids at the end of the cytoplasmic region with histidine that can binding to Zn^{2+} to reduces conformational changes and consequently locks the receptor in the inactive state (R) [270]. On the other hand, mutations to the residues in the extracellular domains have shown some advantage over mutation in transmembrane regions by forming a salt bridge through linking extracellular loop 2 to the upper part of helix 7 (hydrogen bonding and electrostatic interactions) and by alanine or leucine scanning mutagenesis [270].

Several amino acids present in the binding pocket have been validated for their importance in agonist and antagonist binding, such as S112, W172, Y190, W194, F197, W258, and S285 [261-

268]. Moreover, the third and fifth transmembrane regions of the CB2 receptors play critical roles in the binding of the vast majority of cannabinoid ligands and subsequent signal transduction [261, 271]. The following mutation data describes the current state of knowledge about amino acid residues, including the most important findings prior to 2008, which were reviewed previously [272, 273]. **Figure** 3-1 shows all mutation conducted for the CB2 receptor also in **Table 3.**

Residues in the second helix:

Aspartate 163 in CB1 and aspartate 80 in CB2 were each mutated to asparagine or Glutamate. There was no disruption in the high affinity agonist binding (CP-55,940, THC, anandamide) [266]. However, the affinity of WIN-55,212–2 was changed significantly in CB1 mutant but not in CB2. In the case of the inverse agonist (SR141716A), mutant Aspartate 163 have been tested for the CB1 and the results show that there is no significant reduction in binding compared to wild type. Interestingly, the Aspartate-to-asparagine mutation abolished signaling responses to WIN 55,212–2, or CP-55,940, whereas the Aspartate-to-Glutamate mutants showed significant reduction in coupling [266].

Mutations in the second transmembrane domain of CB2, cysteine (89) was performed by substituted cysteine accessibility method (SCAM) [274]. This assay based on the mutation the cysteine residues in the receptor that are not responsible for ligand binding to serine. While the residues that are responsible for ligand binding (in the binding pocket) mutated to cysteine .Therefore, the sulfhydryl groups of the mutant cysteine residue were reacted with methanethiosulfonate reagents (MTS) and then the mutated receptor was tested. The study revealed that cysteine (89) is located in the boundary binding cavity of the water accessible surface [274]. The mutation showed that cysteine (89) was required for binding pocket of CB2.

Residues in the third helix:

In a chimeric receptor studies of the third transmembrane domains of CB1 and CB2, the third helix of CB1 was replaced by the third helix of CB2 in order to elucidate the role of the corresponding region to receptor binding for several types of ligands. There was a notable enhancement in the binding of amino alkylindoles AAI such as WIN 55,212-2, JWH 015, and JWH 018 to chimeric CB1 receptors compared to wild type CB1 receptors. Moreover, the data illustrated that amino acids in TM3 is important for the selectivity of several compounds to both CB1 and CB2. They concluded that after mutating glycine 195 in CB1 to the corresponding serine in CB2, both amino acids play a critical role in the binding to the mutant receptor to AAI [275].

The lysine 192 residue in the TM3 domain of the CB2 receptor is conserved between the CB1 and CB2 receptor. In CB1, lysine 192 is considered to be an important residue for the binding recognition of several agonists except WIN 55,212-2 [276]. However, a single mutation of the corresponding to lysine 109 in CB2 for alanine or arginine shows no significant effect on the binding of CP55,940, WIN 55,212-2, or THC. In contrast, JWH-015, exhibited a 10-fold reduction in binding [261]. The agonists exhibited comparable functional coupling to G proteins. Based on modeling studies, serine 112 provides a critical hydrogen bonding interactions in the K109A mutant. The CB2 double mutant of K109A/S112G lost the ability to bind to CP55940, Δ^9-THC, and anandamide, but retained affinity for Win55,212-2 and JWH015. The receptor function was abrogated for CP55,940 and drastically reduced with Win55,212-2 [261]. In a different study of aromatic CB2's micro-domain, by mutating the phenylalanine at 3.36 to alanine or tryptophan had no effect on the binding affinity for CP55,940, HU210, WIN55,212-2, anandamide, or SR144528. The F117A was an exception and produced increases in the affinity for SR144528 [277].

DRY motif (Asp-Arg-Try) at the end of TM3 is a highly conserved residue among GPCR family A. On other member of GPCRs receptors of this class, glutamic acid is found instead of aspartic

acid. This motif is the connection between the third transmembrane helix and the intracellular loop [41]. It is believed that the DRY motif is responsible for receptor activation of class A GPCRs and play a crucial role in keeping GPCRs in an inactive conformation [243], ligand binding, and downstream signaling [41]. Rhee *et al*. carried out a mutation study for all amino acids of the DRY motif (DRY130-132AAA) and D130A. Their data indicated that DRY130-132AAA and D130A markedly reduced the binding of cannabinoid agonist [^{3}H] HU-243 compared to wild type CB2 receptors, whereas R131 and Y132 were not involved in the binding function. Moreover, the effect of the R131A mutant for inhibiting cAMP was weak using HU-210 and WIN55,212-2. On the other hand, the Y132A mutant showed partial but not complete reduction of downstream signaling.

Song *et al*. [278] tested the role of R131 in single transduction of CB2 receptor .They elucidated the importance of D130 in the DRY motif, together with A244 in TM 6 to maintain the receptor in an inactive conformation (R form). Their data was comparable to previously reported data for effect of the R3.50A mutation on receptor binding affinity for HU-210, WIN55212-2, and anandamide. In contrast, the R131A mutation resulted in the abrogated functioning of G-protein signaling. In addition, the D130A and A244E mutations led to the complete loss of ligand binding, which may be due to changing of receptor conformations. Additionally, the results also indicated that both mutants abolished G-protein signaling by HU210, WIN55212-2, and AEA, and led to the loss of the constitutive activity. The data demonstrated that the D130A and A244E mutations had nothing to do with restraining the receptor in an inactive form which is contrary to the current hypothesis [278].

<u>Mutations of fourth helix, second extracellular loop, and fifth helixes:</u>

A series of chimeric studies between CB1 and CB2 were carried out to identify the domains that are responsible for binding SR141716A in CB1and SR144928 in CB2 [271, 279]. The studies

demonstrated that fourth and fifth helixes of CB1 are important for binding recognition of the antagonist. Furthermore, exchanges of the fourth transmembrane, second extracellular loop, and fifth transmembrane between both receptors led to the loss of binding of CP 55,940 for cells expressed in CB2 receptors but not CB1. The same regions of CB2 were shown responsibility for the binding affinity of SR144928 and WIN 55,212-2. In addition, having the entire second extracellular loop of CB1 placed by CB2 receptors caused elimination of binding of the agonist CP55940. Unlike CB1, mutations to cysteine 174 and cysteine 179 to serine in the E2 loop of CB2 abolished the binding of CP55,940. The same mutations in CB1 prevent the receptor from being expressed at the cell surface [271, 279].

GPCR studies of have shown that among the fourth transmembrane domains, tryptophan is a highly conserved residue [280-282]. Rhee *et al*. studied the effect of the mutations Trp at positions 158 and 172 with several different side chains on binding and signal transduction. Different aromatic amino acids residues at TM4 in also had been subjected to the mutations including W172 and W158. The study elucidated the importance of the aromatic side chain, with or without a hydroxyl group. They found that W158A and W158Y mutation receptors expressed in the COS-7 cell line led to loss of binding activity for [^{3}H] HU-243. Morover, both mutations showed subtle agonist-induced inhibition of cAMP by HU-210 or WIN55,212-2. On the other hand, W158F retained binding activity for HU-243 and the same signaling activity as wild type. In the case of mutating Trp172L, the mutant does not bind to [^{3}H] HU-243, and in W172A mutants, slightly binds to [^{3}H] HU-243, compared to the wild receptor. In addition, no inhibition of cAMP was observed for W172L, and little but insignificant for W172A, consistent with binding results. In contrast, W172F and W172Y mutants showed almost the same binding pattern and similar signaling capacity as wild type using different agonists, such as HU-210, WIN55,212-2, or 2-

arachidonoylglycerol [262].

In chimeric studies of CB1 and CB2, it has been proposed that TM5-2EL-TM5 are involved in agonist and inverse agonist binding. In addition, mutational and molecular modeling analysis carried out in these regions aim to discover the binding pocket of the inverse agonist, SR 144528 [283]. Mutating S161 and S165 to alanine, and C175 to serine led to the elimination of SR144528 binding activity. However, the binding activity of S161A and S165A mutants remains unaffected for CP 55,940 and WIN 55,212-2. The C175S mutation, on the other hand, did not alter the binding of CP55,940 but exhibited a significant reduction in binding affinity for WIN 55,212-2. The author suggests that S161 and S165 have direct hydrogen bonding with SR144528, and Cys175 may dip down toward the pocket to make direct π-π interactions with the inverse agonist. Other residue mutations have also been investigated in this study including V164I in 4TM, R177S in 2EL, and S193G in TM5. The results showed no significant effect on the binding affinity of agonists (CP 55,940 or WIN 55,212-2) or inverse agonists (SR144528) [283].

Residues in the fifth helix:

McAllister *et al.* performed mutation studies to test the role of conceived tyrosine residues in both CB1 and CB2. Using the Monte Carlo/Stochastic dynamics mixed methods that they concluded the presence of the aromatic ring at position 275 in CB1 and 190 in CB2 was crucial for maintain ligand affinity. Tyrosine was mutated to phenylalanine or isoleucine, resulting in comparable results for saturation binding to the Y190F mutants, but no specific binding of [^{3}H] CP55,940 to the Y190F. Using different ligands, such as THC, anandamide, JWH 015, JWH 051, and WIN 55,212-2 revealed that mutant Y190F led to an approximate 24-fold reduction in binding affinity of anandamide to the CB2 receptor. Thus, reduction may be attributed to lose H-bonding interactions with the cannabinoid ligand. However, the same mutants did not significantly change

the binding affinity of other ligands nor do they impacted signaling transduction. In contrast to Y190F, mutating tyrosine 190 to isoleucine led to a loss of binding affinity and abolished functional activity [263].

Based on computer modeling and mutagenesis studies, Zhang *et al*. postulate that both aromatic and hydrogen bond interactions of these residue to W194 are important for ligand binding of both WIN55212 and SR144528 as well as for signal transduction. Therefore, W194 was substituted with tyrosine, phenylalanine, or alanine. The W194Y mutant retained of the binding affinity of CP55940, whereas it caused an eight-fold and five-fold reduction in binding capacity for both WIN55212-and the inverse agonist, SR144528, respectively. In addition, the W194Y mutation also caused a significant reduction in signal transduction i.e., agonist-induced inhibition of cAMP. Other mutations, namely the W194A and W194F mutations abolished the binding affinity for all ligands as well as disrupted of downstream signaling. Together these results suggest that W194 is crucial for activation of the CB2 receptor [284].

It has been reported that WIN55212-2 has higher binding affinity to CB2 receptors than CB1 [265, 285]. In the fifth transmembrane region, molecular modeling was carried out to clarify the potential interaction site between WIN55212-2 and resides at position 5.46 in both CB1 and CB2. Based on the amino acid numbering system[286] , the amino acid with aliphatic side chain, valine, that was replaced by phenylalanine in CB1, whereas CB2, aromatic residue phenylalanine was mutated to valine. Such a mutation will disrupt the aromatic stacking of CB2 with WIN55212-2. The CB2 F197V mutant caused a 14-fold decrease in WIN 55,212-2 binding affinity and it exhibited an approximate a 15-fold decrease in cAMP accumulation. In contrast, the CB1 the V282F mutation increased the affinity of WIN55212-2 by ~12-fold and a 13-fold enhancement of signal transduction. In both mutations, no change was observed in the binding affinities of HU-

210, CP55940, or AEA [265].

Unlike the vast majority of GPCRs, cannabinoid receptors have leucine at position 5.50 instead of Proline. Since conserved tyrosine 209 is located near the third transmembrane helix, which has been shown to have a potential role in downstream signaling, Song *et al*. speculated that this is important for the function and conformation of the receptor. Y209A mutant receptors show little reduction in binding affinity for WIN-55,212-2, HU-210, and anandamide, and that was attributed to a change in structure conformation. On the other hand, mutant L201P eliminated the binding of agonists. Moreover, both L201P and Y209A mutants led to a complete loss of the ability of cannabinoid agonists to inhibit forskolin-induced cAMP. The results suggest that 5TM, lacking proline and tyrosine 5.58, are important for CB2 function [287].

Residues in the sixth helix:

Using the substituted-cysteine accessibility method (SCAM), Nebane *et al*. were able to identify key binding site residues in the sixth transmembrane domain [267]. SCAM is based on the interactions between ionized cysteine and methanethiosulfonate reagents. These reagents react more strongly with ionized cysteine in the water accessible regions than with un-ionized cysteine located in TM domains. Some mutant residues lost their ability to bind to CP55940. D630 (240)N and D630(240)C mutant CB2 receptor led to disruption of the interaction with R3.50(131) in the third helix, causing complete loss of the binding and functional activity of the receptor. Highly conserved tryptophan W6.48 (258) shows that it is crucial for receptor activation through the CWXP motif in rhodopsin-like GPCRs. Previously, this residue in CB1 was important for WIN55212-2 and SR141716A binding affinity [38]. Mutating this residue to alanine or phenylalanine leads to failure to bind to ligands and downstream signal elimination [277]. It is believed that P6.50 (260) is responsible for keeping the receptor shape. Mutation of this residue to

cysteine abolished of the ligand binding affinity and abrogated of signaling by changing helix 6 topology. Given that serine 6.58(268) is involved in interacting with the third extracellular loop, the S6.58 (268) C mutant eliminated binding affinity. The study not only demonstrates the important residues in ligand binding and receptor functional activity but also identified the water accessible amino acids in the binding crevice. Among 34 consecutive residues in TMH6, V6.51 (261), L6.52 (262), L6.54 (264), M6.55 (265), L6.59 (269), and T6.62 (272) mutant residues show significant reduction in binding affinity compared to C2.59(89)S, a background mutant that is not sensitive to the methanethiosulfonate ethylammonium reagent. [267].

The same group also investigated the effect of mutating aspartic acid at position 6.30 on the binding affinity and signaling of both CB1 and CB2 receptor [288]. The study also speculated the participation of these residues in activation of the receptors through "ionic lock". Neutralizing the negative charge by asparagine mutation D6.30 (240)N had comparable binding affinity for CP55,940 to the wild type and also maintained the inhibition of cAMP accumulation.. This study concluded that D240 does not maintain a salt bridge and thus may not be critical for maintaining the receptor in the inactive form [288].

Another studies of the DRY motif and alanine at position of 244 demonstrated their importance to signal transduction and its possible involvement in maintenance of the receptor in the inactive phase. Feng and Song showed that the A244E mutant CB2 receptors lost the binding of [^{3}H] HU-243, [^{3}H] WIN55212-2, or [^{3}H] CP55940. Signaling was significantly reduced using WIN55212-2 and HU-210 and eliminated for anandamide. These results suggest that D130A and A244E mutants are not involved in constitutive activation of the receptor [278].

Residues in the seventh helix:

Serine 285 and S292 at helix 7 had been tested for their ability to make H-bonds with a

hydroxyl group of the classical cannabinoid agonists, HU-210 and CP55940, in binding and signaling assays. The study conducted by Rhee et al. showed that mutation S285 and S292 to alanine caused about 12-fold reduction in the binding affinity of S285A and a 3-fold decrease in the binding affinity of S292A for [3H] Hu-243. The functional activity assay for the S285A mutant has similar inhibition of adenylyl cyclase activity as the wild type using HU-210 and CP55940 for agonist-induced inhibition of AC activity. However, this was not the case for S282A, where signal transduction was eliminated using HU-210 and revealed less affinity for the reduction in AC activity compared to wild type using CP55940. Interestingly, no changes have been reported in AC activity when using aminoalkylindoles (WIN55,212-2) [268].

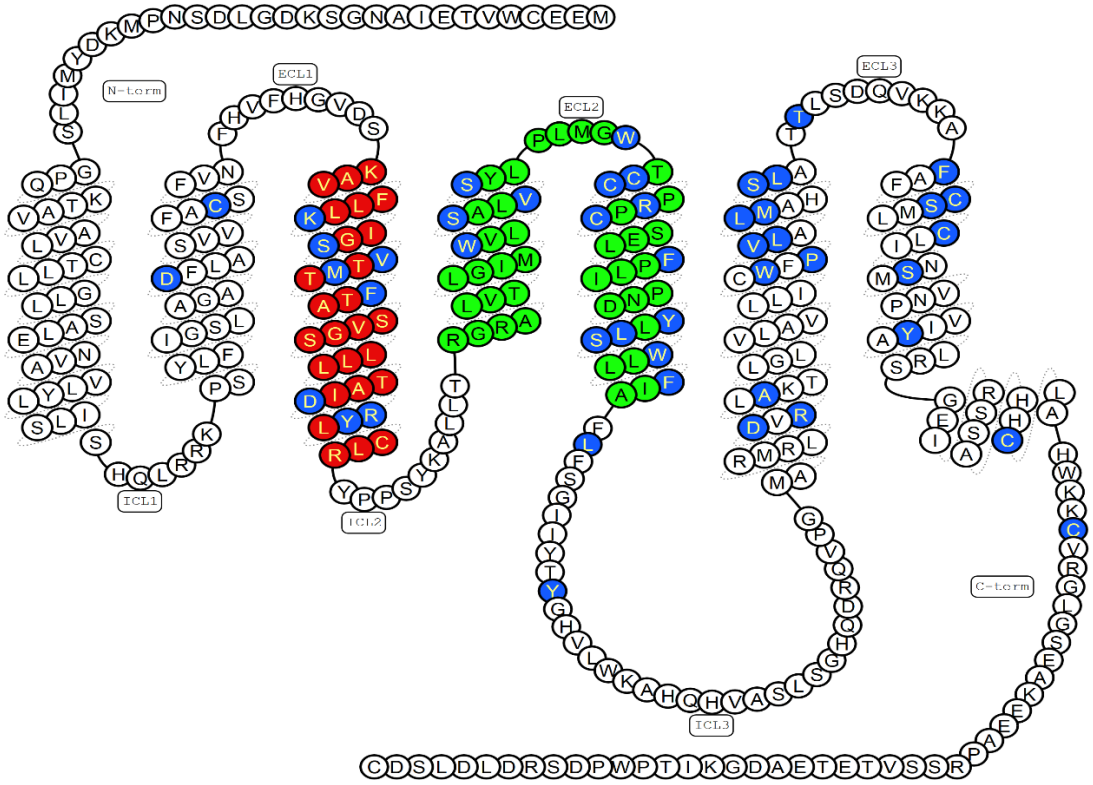

Figure 3-1. 2D diagram for mutations and receptor chimera studies of CB2.

Previse literature CB2 amino acid mutations. Blue circles- single mutated amino acids of CB2 receptor. Red circles-chimeric CB2 receptor, purpose of replacing TMH3 of CB2 receptor with THM3 of CB1 receptor [275]. Green circles, replacing TMH4-ECL2-TMH5 of CB2 with that of CB1 [271, 279]. All mutation adapted from [272, 273]. The figure generated using: http://www.gpcrdb.org/ [289, 290].

Table 3. Updated list for the mutations studies in CB2. The list shows the important residues for their ligands binding, recognition, and signaling transduction.

Domain(s)	Residue(s)	Ligands used	Effect on CB2	Type of residue	Ref
Second TM	D80	Agonists: CP-55,940, Δ9-THC, anandamide	CB2: No change (CP-55,940, $^{\Delta}$9-THC, anandamide, WIN 55,212–2) in binding affinity. Effect on signaling D80N mutation signaling abolished by WIN 55,212–2 and CP-55,940. D80E signaling significantly reduced by WIN 55,212–2 and CP-55,940.	D80 of (CB2) is required for signal transduction.	[266]
	C89	Agonists: HU-243 for (pre-incubation CB2 with MTS derivatives)	The sensitivity to MTSEA, HU-243 binding affinity was reduced significantly, whereas no detectable binding for C89S, C257S, C284S, C288S	C89 is required for binding pocket of CB2.	[274]
Third TM	Replace TM3 of CB2 with TM3 of CB1	Agonists: AAI (WIN 55,212-2, JWH 015, and JWH 018)	CB1/2(TM3) G195 to S enhancement WIN 55,212-2 binding compared to wild-type CB1 receptor. CB1/2(TM3) A198 M no effect on WIN 55,212-2	Replacement of TM3 of CB1 with TM3 of CB2 enhances binding to AAI.	[275]
	K109	Agonists: Δ9-THC, Cannabinol, CP-55,940, JWH015, WIN 55,212-2, anandamide	K109A: No effect on binding to $^{\Delta}$9-THC, CP-55,940, WIN 55,212-2, and anandamide. Reduction in binding affinity for JWH015 but no effect on signaling. K109R: No effect on binding or signaling. K109A/S112G: Loss of ability to bind to CP55940, Δ9-THC, and anandamide, but retained affinity for Win55212-2, JWH015. Signaling abrogated using CP55940 and drastically reduced in function using WIN 55,212-2.	K109 important for binding to JWH-015. K109/S112: important for binding and signal transduction of CP55940, $^{\Delta}$9-THC, and anandamide.	[261]

Third TM	V113	Agonist: CP55940 Inverse agonist: SR144528	V113E and V113L: Mutation led to loss of binding affinity and signal transduction.	V113: In this position, needs to be a hydrophobic side chain to recognize ligands.	[291] [40]
	F117	Agonists: CP55,940, HU210, WIN55,212-2, anandamide Inverse agonists: SR144528	F117A, Y: Binding remains unchanged for all ligands compared to wild type. However, F117A mutation increased the affinity of SR144528.	F117: Not important for binding of all ligands.	[277]
	DRY130-132 and R131, Y132	Agonists: HU-243 WIN 55,212-2	DRY130-132AAA and D130A: Binding is significantly decreased, and impairment of signaling function activation by HU-243 and WIN 55,212-2. R131A: No effect in binding to both HU-243 and WIN 55,212-2. Inhibition of adenyl cyclase was slightly affected more in the case of HU-210 and less for WIN 55,212-2. Y132A: No effect in agonist binding; signaling was notably affected.	D130: Important for binding activity and signal transduction. R131: Slightly affected downstream signaling. Y132: Important for signal transduction.	[41]
		Agonists: HU-210, WIN55212-2, and anandamide	R131A: No change in binding to agonist compared to wild type; signaling abolished using same agonists. D130A and A244E: Loss of binding and signaling for agonists. Also does not contribute to activation of receptor. D130A, R131A, and A244E: Leads to lost signal transduction. In addition, does not restrain receptor to inactive state.	R131: Plays role in signal transduction and constitutive activity. D130 and A244: Important for receptor conformation. Not involved in ligand–receptor interactions. D130, R131, A244: Important for constitutive activity of CB2 receptor.	[278]

TM4-2El-TM5	TM4-2El-TM5 and 2El	Agonists: CP55,940, WIN 55,212-2 Inverse agonist: SR144528	CB2/1(TM4-2EL-TM5) and CB2/1(2El): The exchange leads to loss of binding for CP55,940 and change in ligand affinity for WIN 55,212-2, SR144928.	2El: Important for CP55,940 binding.	[271, 279]
Fourth TM	W158	Agonists: HU-210, WIN55,212-2 or CP55,940	W158A/Y: Loss of binding to agonist (HU-210) and signaling was abolished using HU-210, WIN55,212-2. W158F: No effect on the binding and signal transduction using HU-210 and WIN55,212-2.	W158: Important for binding and signaling.	[262]
	S161 and S165	Agonists: CP 55,940, WIN 55,212-2 Inverse agonist: SR144528	S161A and S165A: Loss of binding activity of SR144528 and no effect on binding for CP 55,940 and WIN 55,212-2. V164I: No effect on binding for CP 55,940, WIN 55,212-2, and SR144528.	S161 and S165: Important residues for binding of inverse agonist.	[283]
	W172	Agonists: HU-210, WIN55,212-2, or 2-arachidonoylglycerol	W172L/A: Lost binding for Leu mutant; 10% of the binding was eliminated in the case of Ala mutation signaling. W172F/Y: Same binding capacity as wild type and same adenyl cyclase inhibition using HU-210, WIN55,212-2, or 2-arachidonoylglycerol.	W172: Important for binding and signaling.	[262]
Second extracellular loop	C174, C175, R177, and C179	Agonists: Δ9-THC, CP55,940, WIN 55,212-2, anandamide Inverse agonist: SR144528	C174S and C179S: Failed to bind to WIN55212-2, $^{\Delta}$9-THC, and anandamide. C175S: Loss of SR 144528 binding; no change in CP 55,940 binding and 8-fold reduced binding capacity of WIN 55,212-2. R177S: No effect on binding for CP 55,940, WIN 55,212-2, and SR144528.	C174 and C179: Important for agonist binding (CP55,940, WIN 55,212-2, anandamide, Δ9-THC C175: Important for SR144528 binding.	[279, 283]

Second extracellular loop	F183	Agonist: CP55940 Inverse agonist: SR144528	F183Q/V: Mutation led to loss of binding and signal transduction using cAMP assay.	ECL aromatic ring required for ligand recognition.	[40]
Fifth TM	Y190	Agonists: CP 55,940, WIN 55212-2, Δ9-THC, anandamide, JWH 015, JWH 051	Y190F: Leads to about 24-fold reduction in binding of anandamide whereas no change in binding to other ligands (CP 55,940, WIN 55,212-2 $^{\Delta}$9-THC, anandamide, JWH 015, JWH 051) and no effect on signals. Y190I: Lost binding for ligands and signaling was eliminated.	Y190: Important for anandamide binding through H-bond. Y190: Aromatic residue in this position is required for binding and signaling.	[263]
	L192	Agonist: CP55940 Inverse agonist: SR144528	L192A and L192S: mutation to polar side chain led to loss the receptor binding and function ability. Whereas hydrophobic side chain mutation retained the receptor binding and functionality.	L192 : At this position need to hydrophobic side chain to recognize the ligands	
	S193	Agonists: CP 55,940, WIN 55,212-2 Inverse agonist: SR144528	S193G: No effect on binding for CP 55,940, WIN 55,212-2, and SR144528.	S193: Not involved in binding pocket.	[283]
	W194	Agonists: CP 55,940, WIN 55212-2 Inverse agonist: SR144528	W194Y: No effect on CP 55,940 binding affinity; 8-fold reduction in WIN 55,212-2 and 5-fold reduction in SR144528 binding affinity. Signaling is reduced using agonists. W194F and W194A: Binding not detected for all ligands. Complete elimination of signaling.	W194: plays role in ligand binding and receptor activation.	[284]

	F197	Agonists: CP 55,940, HU-210, WIN 55,212-2, anandamide	F197V: No change in the binding affinities of HU-210, CP55940, and AEA; decreased affinity of WIN55212-2 for CB2 by 15-fold and 15-fold decrease in signaling.	F197: Important for aromatic stacking with WIN55212-2.	[265]
	L201 and Y209	Agonists: HU-210, WIN 55,212-2, anandamide	L201P: Binding affinity was lost for ligands and signaling was eliminated. Y209A: Little effect on binding affinity for HU-210, WIN 55,212-2, anandamide; the signaling was abolished.	L201: Important for receptor functions. Y209: Mutation Y209 causes conformational change leading to indirect change in the binding pocket.	[287]
Sixth TM	D240	Agonist CP55940	D240N: Neutralizing the charge shows neither reduction in binding affinity or alteration of signaling. However, it is important for activation of the receptor. D240C: Disrupts the interaction with R131 in third helix causing complete loss of binding and function of the receptor.	D240: Importent for receptor activation. Mutation of this residue causes conformational change and changes G protein receptor interaction. D240: Mutation to Cyc leads to loss of H-bond but not in the case of Asn.	[288] [267]
	A244	Agonists: HU-210, WIN55212-2, and anandamide	A244E: Loss of binding affinity for HU-243, WIN55212-2, or CP55940; significant reduction in signal transduction using WIN55212-2 and HU-210 and completely abolished signaling using anandamide.	A244: Leads to change in receptor conformation.	[278]
	W258	Agonist CP55940	W258C, F, A: All mutations led to lost binding affinity. These indicate that the aromaticity at position 5.43 is critical for ligand binding.	Trp258 is part of CWXP motif which is crucial for receptor activation.	[267, 277]

	P260 S268	Agonist CP55940	P260C: Loss of binding due to change in 6TMH structure. S268C: Loss of binding due to destabilization of receptor.	P260: Produces kink in the helix; mutation will make change in the helix geometry. S268: Making H-bond with ECL3 to stabilize the receptor.	[267]
	V261, L262, L264, M265, L269, and T272	Agonist CP55940	V261C, L262C, L264C, M265C, L269C, and T272C: Using substituted-cysteine accessibility method leads to significant inhibition in binding affinity of CP-55,940.	V261, L262, L264, M265, L269, and T272 are on the water-accessible surface of the binding-site crevice.	[267]
Seventh TM	F281	Agonist: CP55940 Inverse agonist: SR144528	F281K: Mutation led to loss of binding and function of the receptor detected by cAMP assay.	F281 making strong π–π interaction with SR144528, and formed a hydrophobic interaction with CP55940.	[40]
	C284 and C288	Inverse agonist: AM1336 and AM6720	Single mutant C284A, C284S, C288A, and C288S shows significantly low binding of AM 1336 and AM6720 compared to wild type binding. Double mutant (C284A.C 288A) or (C284S C C288S) will abolish covalent binding of AM 1336 compared to wild type binding. Only C288A or C288s but not C284A or C284s show abrogated binding with AM6720.	C284 and C288 important for binding of AM1336 and function. C288 important for binding of AM6720 and receptor function.	[292]
	S285	Agonists HU-210, CP55940 and WIN55,212-2	S285A: Important for binding of HU-243; mutation causes about 13-fold decrease in the binding affinity; not crucial residue for AC activity using HU-210, CP55940, and WIN55,212-2.	S285: Important for binding of classical cannabinoids.	[159]

	S292	Agonists HU-210, CP55940, and WIN55,212-2	S292A: Important for binding of HU-243; mutation causes about 3-fold decrease in the binding affinity; important for AC activity of classical cannabinoids (HU-210 and CP55940) but not WIN55,212-2.	S292: Important for binding and signal transduction of classical cannabinoids.	[268]
	Y299	Agonists HU-210, WIN55,212-2, AEA, and HU-243	Y7.53A: loss of binding for HU-210, WIN55,212-2, AEA, and HU-243; loss of downstream signaling by HU-210 and WIN55,212-2. Reduced signaling using AEA.	Y299: Part of Y299 within the NP(X) Y motif motif, which is important for ligand binding and signaling.	[293]
C terminal	C313 and C320	Agonists HU-210, WIN55,212-2, and AEA	C313A and C320A: No effect on binding; significantly reduces signaling for WIN55,212-2 and HU-210. No signal transduction detection using AEA.	C313 and C320 mutations markedly reduce functional coupling to adenylate cyclase.	[293]

3.2 CASE STUDY: *IN SILICO* MODELING AND SITE-DIRECTED MUTAGENESIS VALIDATION FOR ROLE VALINE 3.32 (113), PHENYLALANINE 182, 281 AND LEUCINE (192) IN LIGAND RECOGNITION AND DOWNSTREAM SIGNALING ACTIVITIES

We performed molecular modeling and docking studies to predict a putative binding pocket and associated ligand-receptor interactions for human cannabinoid receptor 2 (CB2). **Figure** 3-2 shows a schematic flow diagram of the steps for testing the important residues from 3D models and ending with a study of the binding and function of the receptor CB2 receptor. Our data demonstrated that two hydrophobic residues came in close contact with three structurally distinct CB2 ligands: CP-55,940, SR144528 and XIE95-26 [291] (**Figure** 3-3**)**. In addition, modeling and molecular dynamics simulation results predicted two new residues, Phe183 in extracellular loop 2 and Phe281 in the seventh transmembrane domain, that were important for SR144528 and CP55940 binding to CB2 [40]. Site-directed mutagenesis experiments and subsequent functional assays further implicated the roles of these residues in the ligand binding and downstream signaling activities of the CB2 receptor [40, 291]. Seven different point mutations were introduced to the wild type CB2 receptor: V113E, V113L, F183Q, F183V, F281K L192S and L192A. Our results demonstrated that mutation of Val113 to a glutamic acid and Leu192 to a serine led to the complete loss of CB2 ligand binding as well as downstream signaling activities. Substitution of these residues with those that have similar hydrophobic side chains such as leucine (V113L) and alanine (L192A), however, allowed CB2 to retain both its ligand binding and signaling functions. Moreover, disrupting the aromatic

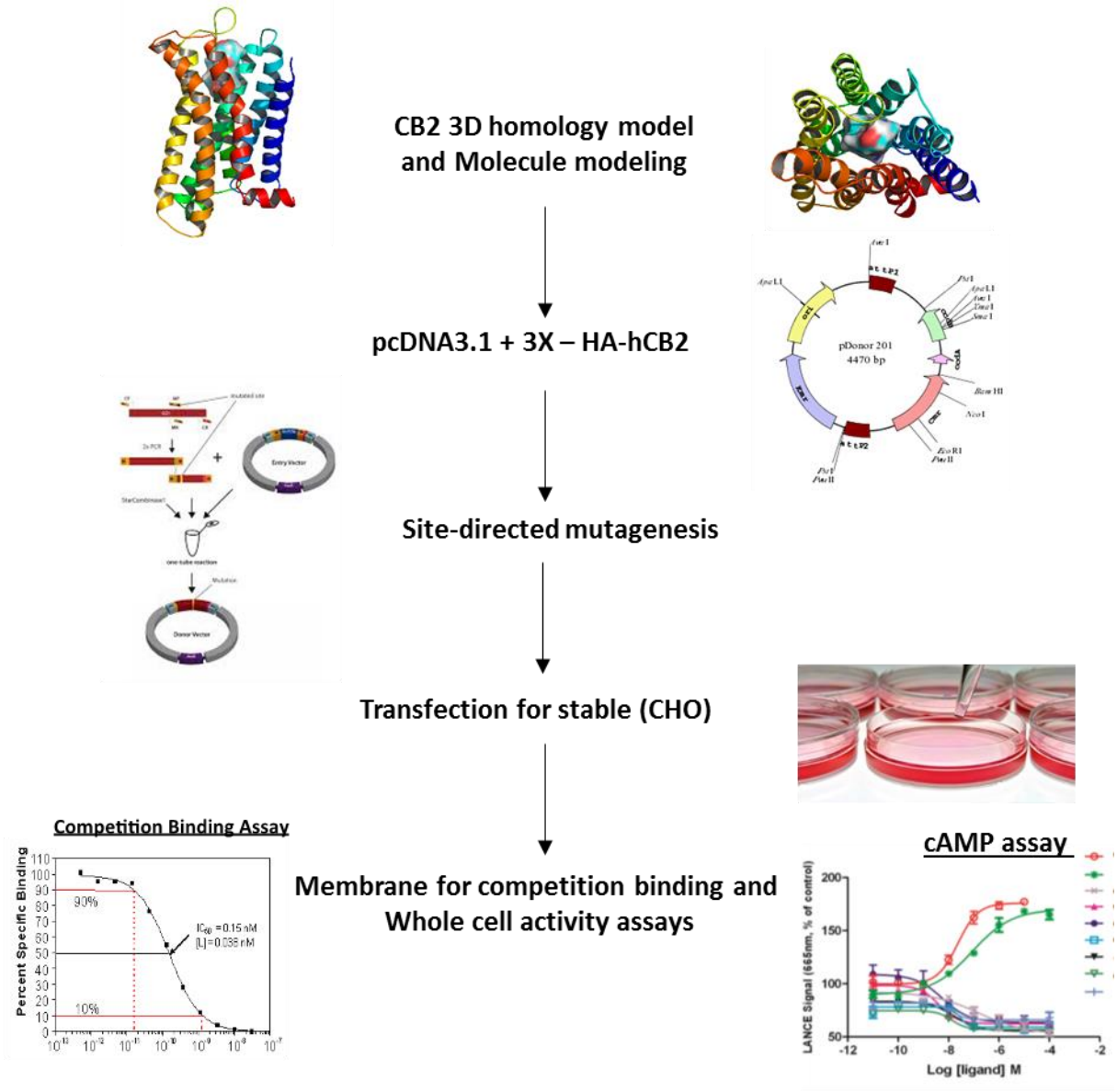

Figure 3-2. Steps involved in the prediction and validation of the important CB2's residues for the binding affinity and functionality of the receptor.

properties for F183 in 2ECL using a polar amino acid such as glutamine at 281 in at the 7TM loop using valine and lysine, led to loss of binding affinity. Our modeling results validated by competition binding and site-directed mutagenesis experiments also suggest that residues V113, F183, L192 and F281 play important roles in ligand binding and downstream signaling transduction of the CB2 receptor [40, 291].

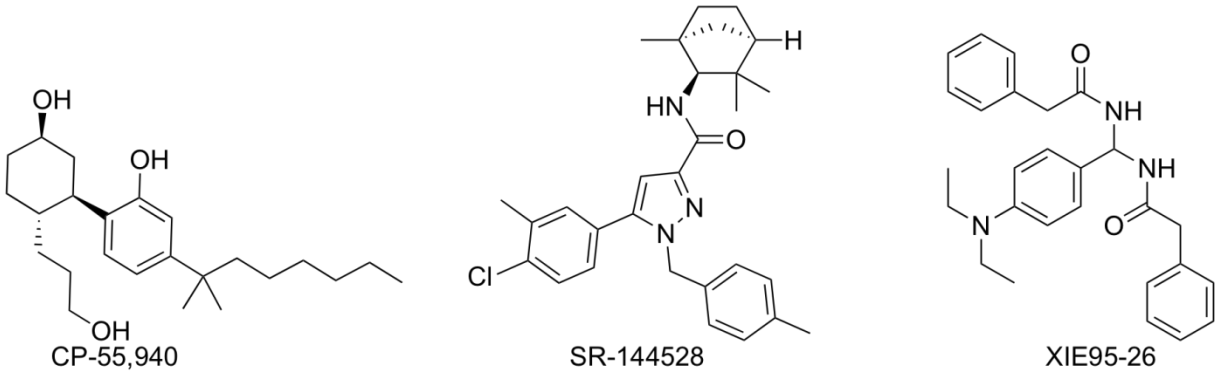

Figure 3-3 .Structures of Cannabinoid ligands.

Agonist (CP-55,940) and inverse agonists (SR144528 and XIE95-26) used in the present work.

3.2.1 Materials and Methods

3.2.1.1 Molecular modeling using I-TASSER protein structure prediction server

A CB2 homology model was constructed from the antagonist-bound A2A receptor (3EML.pdb) [294], human dopamine D3 receptor (3PBL.pdb) [295], bovine rhodopsin (1L9H.pdb and 1F88.pdb) [296, 297], human beta2-adrenergic receptor (2RH1.pdb) [63], and the turkey beta1-adrenergic receptor (2Y00.pdb and 2VT4.pdb) [298, 299] using the I-TASSER protein structure prediction server [300, 301]. Five models were obtained using the I-TASSER prediction server,

and the model (model 1) with the highest confidence score (C-score) -0.96 was selected as the optimal model. It was further minimized using a conjugate gradient method with the AMBER force field (AMBER7 FF99) defined in the Tripos Sybyl software [302]. The minimization was run for 500 iterations and the maximum derivative of energy was set to 0.05 kcal · mol^{-1} · $Å^{-1}$. Further molecular modeling studies were then carried out on the minimized CB2 homology model to predict a putative binding pocket and potential ligand-receptor interactions such as hydrophobic interactions, hydrogen-bonding and pi-pi interactions via a flexible docking protocol previously reported [264, 303]. Briefly, in order to predict a putative binding pocket, MOLCAD analysis [302] was performed on the 3D homology model to find a solvent-accessible cavity around important binding residues including SER112, TRP172, TYR190, TRP194, PHE197, TRP258, and SER285 reported in the literature [261-268]. Once a pocket was defined, flexible docking simulations were performed using the Surflex-Dock module [302]. CB2 ligands CP-55,940, SR144528 and XIE95-26 were docked into the putative pocket. During the flexible docking, the receptor structure was fixed while ligands were allowed to rotate on single bonds and move flexibly within the tentative binding pocket. The docking mode was GeomX and other default docking parameters defined in the Surflex-Dock module [302] were as follows: additional starting conformations per molecule and angstroms to expand the search grid were set to 6, the maximum conformations per fragment were set to 20, maximum number of routable bonds per molecule was 100, the maximum number of poses per ligand was set to 20, and the minimum RMSD between final poses was 0.50. Pre-dock minimization, post-dock minimization, molecule fragmentation, ring flexibility, and soft grid treatment were turned on. The binding interaction energy was calculated to include van der Waals, electrostatic, and torsional energy terms defined in the Tripos force field [302] .

3.2.1.2 Modeling, molecular dynamics simulation based on based on ten known crystal structures of GPCRs

The second approach for building CB2 models was the 3D molding method developed in different studies conducted in our lab [40]. This model is based on ten known GPCRs crystal structures (including Class A and Class B) that were used to build the new CB2 modules namely (bovine rhodopsin, SMO,CXCR4, β1AR, β2AR, A2AAR, H1R, M2MAR, S1P, D3R) for more details see (**Table 16, Appendix A**). The structure of the CB2 receptor was truncated from both N, C terminal and 3ICL before alignment with other GPCRs. Then manual alignment for the receptor from 2ECL to TM5 was conducted to insure that there would be no gaps within the helix sequences. We used Sybyl-x1.3 for generating the 3D moles and energy minimization. Then in order to choose the most reasonable conformation for all these CB2 models, we utilized molecular dynamics. The lowest energy 3D models were chosen for more energy minimization and validation. Using the Surflex-Dock program in SYBYL, we made a training set for the validation of the 3D models. 1000 compounds (17 active in house compounds, 3 known ligands and 980 randomly chosen compounds from National Cancer Institute (NCI) Database) were used and docked into the receptor. The MOLCAD program was used to determine the binding pocket for the models. For more detailed information about the methods please see [40].

3.2.1.3 Amino acid numbering scheme

Ballesteros and Weinstein have suggested a numbering system, which was adapted in the study [304]. In short, each amino acid is indexed by its helix number followed by a two-digit number. The high conserved residues in a transmembrane domain are given the value of "0.50". Then the amino acids positions are assigned relative to this reference amino acid in the helix. For example,

Pro7.50 (296) is the highly conserved residue in transmembrane helix7 of human cannabinoid receptor 2 and therefore the residues follow it is Val7.51 (297).

3.2.1.4 Mutagenesis experiments

Mutations of the CB2 receptor were carried out using the QuikChange site-directed mutagenesis kit (QuikChange; Stratagene, CA) according to the manufacturer's recommendations. A point mutation was performed individually to the human CB2 expression plasmid pcDNA3.1+3X – HA-hCB2 (Missouri S&T cDNA Resources Center), which was used as a template. Three PCR steps were used to introduce the mutations. Firstly, Oligonucleotide primers encoding the desired amino acids were annealed to the denatured DNA template and nicks were repaired with PfuTurbo DNA polymerase with high fidelity. The list of the primers used in these studies are shown in **Table 15**. Secondly, the PCR products were treated with restriction enzyme DpnI endonuclease to digest methylated and hemi-methylated DNA (the parental DNA template). Finally, the mixture was transformed into XL10-Gold ultra-competent cells (QuikChange; Stratagene, CA) to convert ssDNA to double stranded plasmid DNA. The mutant CB2 plasmids were subsequently confirmed by DNA sequencing.

3.2.1.5 Transfection and cell culture

Chinese hamster ovary (CHO) cells were maintained in RPMI-1640 (Gibco Laboratories, Grand Island, NY) containing 10% fetal bovine serum (FBS, GICBO) in a 5% CO2 humidified incubator at 37 °C. The transfection was performed when the CHO cells reached 90% confluence in 60-mm culture plates. According to manufacturer's protocol (Invitrogen), 8.0 μg of mutated human CB2 receptor cDNA plasmid and 20 μL of the transfection agent lipofectamine 2000 were separately diluted in 0.5 mL of Opti-MEM reduced serum medium, mixed, incubated for 20 min

at room temperature, and then added to the cell culture for stable transfection. After 4 hours of incubation, the medium was refreshed and the cells were incubated for an additional 24 hrs. The transfected cells were selected by conditional incubation in the presence of 800 μg /mL G-418 (Gibco) for 5 days. The selected cells were then maintained in the medium containing 220 μg /mL of G-418.

3.2.1.6 Cell harvesting and membrane preparation

Highly confluent culture plates were placed on ice prior to harvesting. The plates were rinsed twice with phosphate-buffered saline (PBS). Then the cells were collected by scraping and centrifuged at 500 x g for 5 min at 4°C. The cell pellets were resuspended in 5 mL of membrane preparation buffer (50 mM Tris–HCl pH 7.4, 5 mM $MgCl_2$, 2.5 mM EGTA and 200 mM sucrose) and homogenized with a Polytron PT1600E Homogenizer (Kinematica, Littau-Lucerne, Switzerland). The lysed cells were centrifuged at 68,000 g for 5 min at 4 °C and the supernatant was collected. The remaining pellets were resuspended with membrane buffer and centrifuged three times. All supernatants were combined and centrifuged at 13,000 x g for 90 min at 4 °C. Pellets were then collected and re-suspended in membrane preparation buffer for competition binding assays.

3.2.1.7 Western Blot Analysis

Cells were lysed in Radio- immunoprecipitation assay buffer (RIPA) composed of 25 mM Tris-HCl, 150 mM NaCl, 1% NP-40, 1% sodium deoxycholate, 0.1% SDS (Thermo, NP 89901) and protease inhibitory cocktail (Thermo Scientific, P1861281), and centrifuged at 13,000 x *g* for 15 min at 4 °C. Supernatants were collected and protein concentrations were determined using the bicinchoninic acid protein assay kit (Pierce, Rockford, IL). Each sample (25 μg each) was

solubilized in SDS-sample buffer, separated on a 10% SDS–PAGE gel and transferred onto polyvinylidene difluoride membranes (PVDF). The membrane then was blocked with 0.1% Tween 20 in PBS (PBS-T) containing 5% non-fat dried milk for 1 hour and incubated in a solution of primary antibody diluted 250-fold (goat polyclonal antibody; Thermo Scientific, PA5-18428) for 1 hour at room temperature. After 3 washes with PBS-T for 10 min, the membrane was incubated in horseradish peroxidase-labeled secondary antibody solution (Santa Cruz Biotechnology, Santa Cruz, CA, and 2000 x dilute) for 1 hour at room temperature. Following 3 additional washes with PBS-T, the membrane was developed with using ECL Western Blotting Detection Reagents (Super Signal West Femto, Thermo Scientific).

3.2.1.8 Competition binding assay

The protein concentration was measured using Pierce BCA Protein Assay (Rockford, IL). Three structurally distinct, representative cannabinoid ligands were used (**Figure** 3-3) in this study. CP-55,940 (CB agonist) and SR144528 (inverse agonist) were obtained from RTI International (Research Triangle Park, NC) and XIE95-26 (inverse agonist) was synthesized recently in our lab [269]. The ligand binding was performed as previously described [305]. Briefly, non-radioactive (or cold) ligands were diluted in binding buffer (50 mM Tris-HCl, 5 mM $MgCl_2$, 2.5 mM EGTA, 0.1% (w/v) fatty acid free BSA, pH 7.4), supplemented with 10% dimethyl sulfoxide and 0.4% methyl cellulose. Each assay plate well contained a total of 200 μL of reaction mixture of 5 μg of membrane protein, 3 nM of labeled [^{3}H]-CP-55,940 (RTI International Research Triangle Park, NC) and concentrations of unlabeled 3 ligands described above. Plates were incubated at 30 ^{o}C for 1 hour with gentle shaking. The reaction was terminated by rapid filtration through Unifilter GF/C filter plates using a Unifilter Cell Harvester (PerkinElmer, NL). After the plate was allowed to dry

overnight, 30 μL of MicroScint-0 cocktail (PerkinElmer) was added to each well and the radioactivity was counted using PerkinElmer TopCounter. All assays were performed triplicate in duplicate wells and data are represented as the mean ± S.E.M. Bound radioactivity data was analyzed for K_i values using non-linear regression analysis via GraphPad Prism 5.0 software.

3.2.1.9 cAMP assay

A LANCE® cAMP 384 kit (PerkinElmer) was used to detect cAMP as previously described [264]. Briefly, the assay is based on competition between a Europium-labeled cAMP trace complex and sample cAMP for binding sites on cAMP-specific antibodies labeled with a fluorescent dye. The energy emitted from the Eu-chelate is transferred to the dye on the antibodies, which in turn generates a time-resolved fluorescent resonant energy transfer (TR-FRET) signal at 665 nm. The fluorescence at 665 nm will decrease in the presence of cAMP from test sample. CB2 WT and mutant transfected CHO cells were seeded in a 384-well white ProxiPlate (Perkin Elmer, Bridgeville, USA) at a density of 2500 cells per well in 5 μL of RPMI-1640 medium containing 1% dialyzed FBS, 100 μg/mL penicillin, 100 U/mL streptomycin and 200 μg/mL of G-418. After culture overnight, 2.5 μL of cAMP antibody and RO20-1724 (phosphodiesteras inhibitor) (50 μM final concentration) in stimulation buffer (DPBS 1x, containing 0.1% BSA) was added to each well, followed by addition of 2.5 μL CP-55,940 (various concentration) in 5 μM forskolin stimulation buffer for agonist-inhibited AC activity assay. After incubation for 45 min at room temperature, 10 μL of detection reagent was added to each well and incubated for 1 hr at room temperature. The fluorescence was detected with a Synergy H1 hybrid reader (BioTek) at 340nm excitation/665nm emission. Each cAMP determination was averaged from at least three independent experiments, each in triplicate. EC_{50} values were calculated by nonlinear regression,

dose–response curves (GraphPad Prism 5).

3.2.1.10 Constitutive activation of the wild type CB2 receptors

We also evaluated the ability of inverse agonists SR144528 and Xie-95-26 to inhibit the stimulated cAMP in the absence of a cannabinoid agonist. Comparatively, we evaluated the agonist CP55,940 on decreasing the forskolin stimulated AC activity. The study design was briefly, different concentrations of forskolin (10-10^5 nM) incubated with wild type receptor with and without ligands (0.3 μM final concentration). The folds of cAMP accumulation were measured using LANCE cAMP kit. The cell preparation and procedure are the same as previously described in the agonist-induced inhibition of cAMP production. The constitutive activation has been investigated in previous studies [284, 288].

3.2.2 Results

3.2.2.1 Homology modeling and molecular docking

A 3D homology model of CB2 was derived with the I-TASSER protein structure prediction server. As shown in (**Figure** 3-4 **A**) and **(Figure** 6-4 in **appendix A)** , a putative binding pocket of the minimized CB2 model was found among residues pertaining to helices II, III, V, VI and VII. CP-55,940, SR144528 and XIE95-26 compounds were docked into the binding pocket using the Surflex-Dock module [302]. **(Figure** 3-4 **B, C and D**) shows molecular docking results for CP-55,940, SR144528 and XIE95-26, respectively. Several important interactions were observed for each ligand. For example: Asn188 and Ser285 are predicted to participate in H-bonding with CP-55,940 and XIE95-26 respectively and Leu192, Leu201 and Val 261 exhibit a hydrophobic interactions with ligands. We also compared the binding modes between agonist and antagonists.

Hydrophilic interactions between the CB2 model and agonist (CP-55,940) were found in the top of the binding pocket, while hydrophilic interactions between CB2 and antagonists were found in the bottom (or middle) of the binding pocket (**Figure** 6-4 **and Figure** 6-5 in **appendix A)**. His95 and Asn188 formed hydrogen bonds with CP-55,940, while these two residues only formed hydrophobic interactions with antagonists, including SR-144528 and our in-house compound XIE95-26. Moreover, Ser285 formed hydrogen bonds both with SR144528 (3.5~4.7 Å) and XIE95-26 (within 3 Å). However, only hydrophobic interactions were observed between Ser285 and CP-55,940. In addition, we found that XIE95-26 had closer interactions with Trp258 than SR144528.

In second approach utilizing MOLCAD 3D models implemented in SYBYL-X 1.3, we provided the second potential orthostatic ligand-binding pocket and residues involved in the binding pocket of CB2 as shown in (**Figure 3-5 A**) and (**Figure** 6-5 in **appendix A**). Consistent with the I-TASSER models and residues previously reported in the literature, the CB2 receptor pocket is located between helices III, V, VI, and VII Figure 3-5 B. Beside the orthosteric ligand-binding pocket, we found a small binding pocket, which was close to the orthosteric one. Moreover, a channel connecting these two pockets together can be observed in our model, as shown in (**Figure** 3-6). This allosteric pocket was formed by conserved residues including Asn51, Val54, Leu76, Ala77, Ala79, Asp80, Ser120, Leu124, Trp258, Asn291, Ser292, Asn295, Asn296,Tyr299 present in A_{2A}A receptor [306] and the δ-opioid receptor [75] . this pocket using highlighted some residue including Phe87, Phe91, Phe94, Asp101, Phe106, Lys109, Ile110, Val113, Phe117, Glu181, Leu182, Phe183, Trp194, Phe197, Trp258, Val261, Met265, Lys278, Lys279, Phe281, and Ser285.

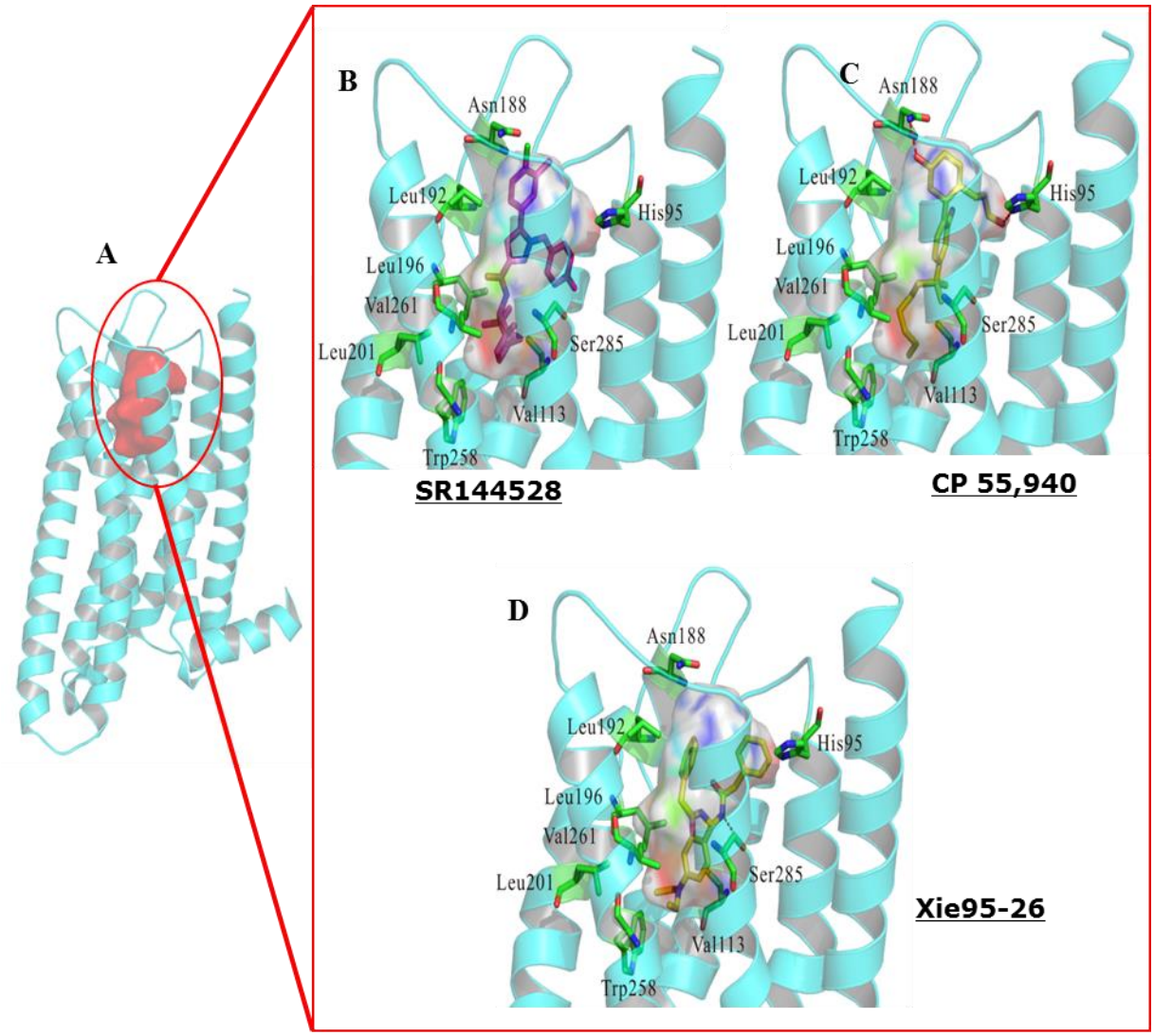

Figure 3-4. Molecular docking of CB2 ligands into putative CB2 binding site using I-TASSER protein structure prediction.

A 3D homology model of the CB2 seven transmembrane helices showing an amphipathic-binding cavity. B-D Interactions between each ligand and the receptor Magnified views of the predicted binding pocket, which show hydrophobic residues such as L201, V261, V113, L192 predicted to interact with CP-55,940, SR144528 and XIE95-26. In addition, N188 is predicted to form H-bonds with both CP-55,940 and SR144528.

A.

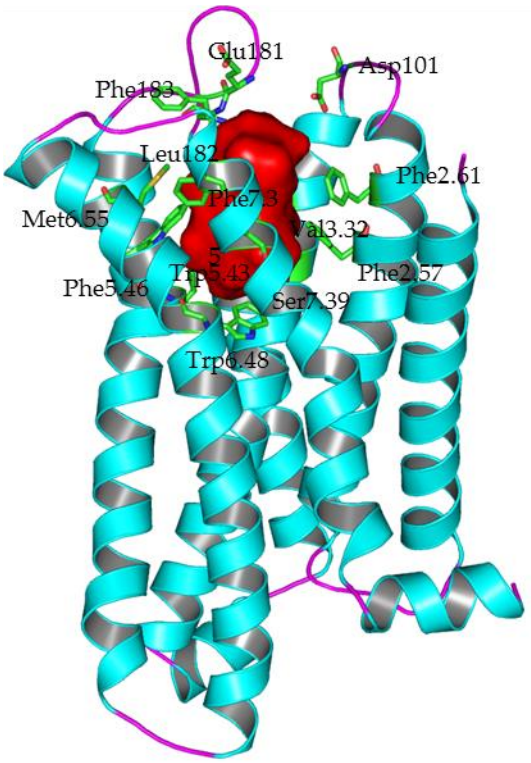

B.

Residues predicted in both models			
I-TASSER server		10 know co-crystal structure	
Ser90	Phe91	Phe87	Phe91
Phe106	Leu108	Phe94	Asp101
ILe110	Ser112*	Phe106	Lys109*
Val113	Met115	ILe110	Val113
Phe117*	Pro168	Phe117*	Glu181
Leu169	Trp172*	Phe183	Trp194*
Leu182	Asn188	Phe197*	Trp258*
Leu192	Trp194*	Val261*	Met265*
Phe197*	Trp258*	Phe281	Ser285*
Val261*	Leu262*		
Met265*	Ser268		
Phe281	Ser285*		
Leu296			

- Residues subjected to mutation in our study
- Residues common in both models
- * previously studied residues [272, 273]

Figure 3-5. Potential binding pocked and residues involved in the binding pocket of CB2 based on ten known crystal structures of GPCRs.

A. The potential binding pocket was highlighted in red, which was mainly formed by helices III, V, VI, and VII, but also can extend into helix IV. Important residues involved in the binding pocket were highlighted in green sticks, which included: Phe87$^{2.57}$, Phe91$^{2.61}$, Phe94$^{2.64}$ (not shown), Asp101 (ECL1), Phe106$^{3.25}$ (not shown), Lys109$^{3.28}$ (not shown), Ile110$^{3.29}$, Val113$^{3.32}$, Phe117$^{3.36}$ (not shown), Glu181 (ECL2), Leu182 (ECL2), Phe183 (ECL2), Trp194$^{5.43}$, Phe197$^{5.46}$, Trp258$^{6.48}$, Val261$^{6.51}$ (not shown), Met265$^{6.55}$, Phe281$^{7.35}$, and Ser285$^{7.39}$.

B. The common residues predicted in both models some of which have been conformed from previous studies [272,273].

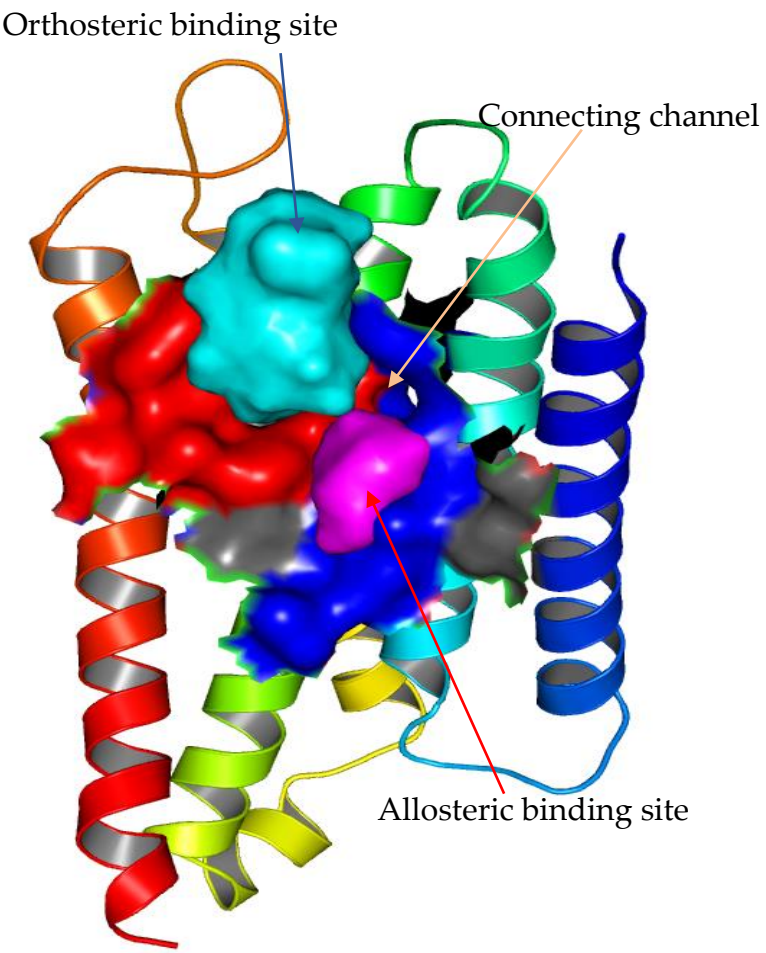

Figure 3-6. Potential allosteric binding pocket in CB2 model.

The orthosteric ligand-binding pocket (highlighted in cyan) and the allosteric pocket (highlighted in magenta), which was formed by Asn51$^{1.50}$, Val54$^{1.53}$, Leu76$^{2.46}$, Ala77$^{2.47}$, Ala79$^{2.49}$, Asp80$^{2.50}$, Ser120$^{3.39}$, Leu124$^{3.43}$, Trp258$^{6.48}$, Asn291$^{7.45}$, Ser292$^{7.46}$, Asn295$^{7.49}$, Asn296$^{7.50}$, and Tyr299$^{7.53}$

3.2.2.2 Expression of recombinant human wild type and mutant CB2 in CHO cells

The expression of wild-type human CB2 and V113E/L, L192S/A and F183V mutants in stably transfected polyclonal Chinese hamster ovary (CHO) cell lines was analyzed and confirmed by western blot (**Figure** 3-7). The CB2 receptor is shown as the band corresponding to 41 kDa.

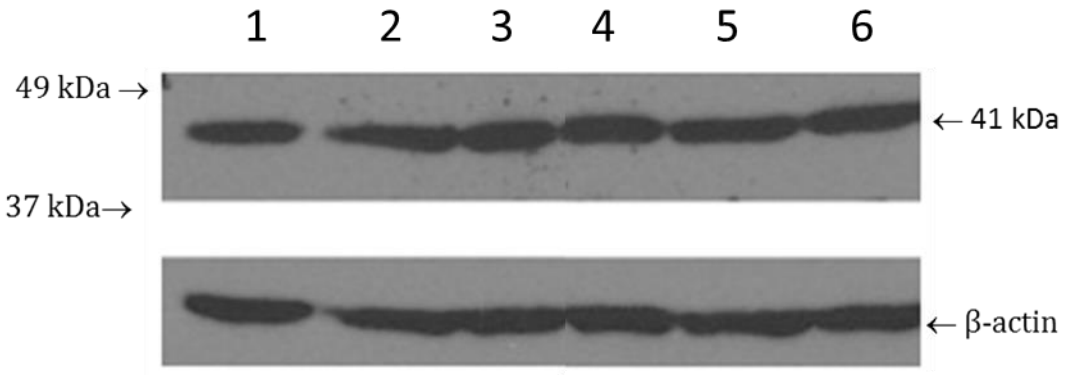

Figure 3-7. Western Blot analysis of wild type and mutant h-CB2 receptor isoforms in transfected CHO cells.

Western blot analysis of expression level of WT and mutants Hu-CB2 receptors in transfected CHO cells. From left to right: 1-CB2 WT (wild type), 2- V113E, 3-V113L, 4-F183V, 5- L192S, and 6- L192A.

3.2.2.3 Ligand binding of wild type and mutant CB2 receptors

The ligand binding affinity of wild-type and mutant CB2 receptors were determined by competitive binding assays using radioactive [^{3}H]-CP-55,940 and three non-radioactive ligands: CP-55,940 (agonist), SR144528 (inverse agonist) and XIE95-26 (inverse agonist). Binding data (**Figure 3-8**, summarized in **Table 4**) indicated that the L192A substitution had no effect on the

affinity of CB2 for CP-55,940; whereas the binding affinities of SR144528 and XIE95-26 were slightly reduced compared to the wild-type. Similarly, the V113L substitution resulted in a slight reduction in CB2 affinity for SR144528, yet no significant effect was observed for CP-55,940 or XIE95-26 binding. Substitutions at V113E, F183V/Q, L192S and F281K independently resulted in the complete loss of binding affinity for each of the three ligands used (**Table 4)**.

Receptors	SR144528	CP55940	Xie95-26
CB2 WT	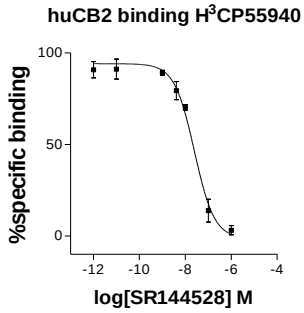	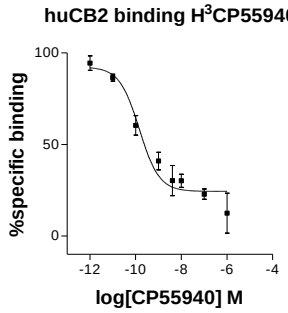	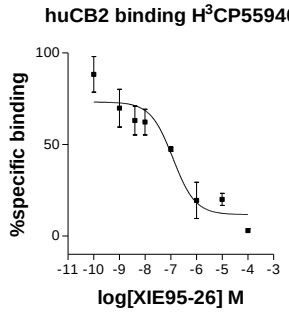
V113L	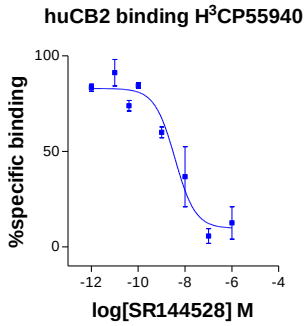	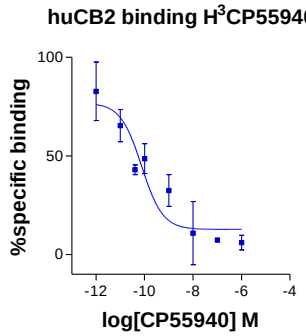	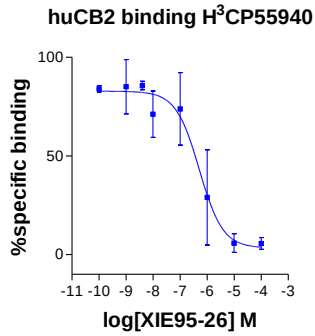
L192A	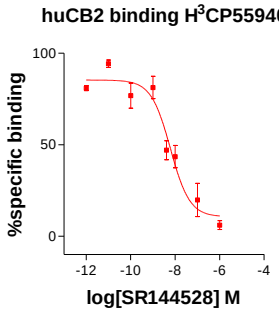	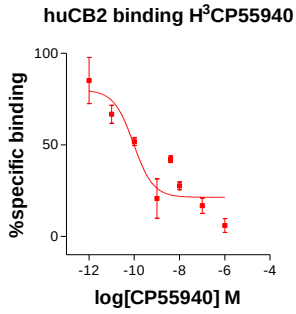	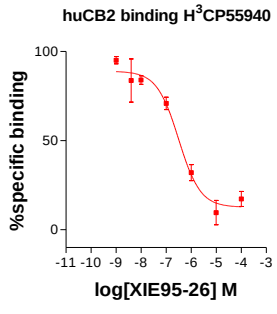

Figure 3-8. Competitive ligand displacement assay for mutant CB2 for agonist and inverse agonist.

Binding profile of (A) for CP55940; (B) for SR144528; and (C) Xie95-26 for WT, V113L and L192A. The dynamic range of the binding is show in **Table 4**. Competitive displacement of the [^{3}H] CP55940 was obtained by using an increased amount of unlabelled ligands. Assay was performed in duplicate (n = 2). Data represented as mean ± SEM.

Table 4. Cannabinoid receptor ligands binding affinity of wild type (WT) and mutant CB2 receptors stably expressed in CHO cells (K_i, nM)*

	SR144528		CP55940		Xie95-26	
Receptors	Binding affinity	Relative CPM	Binding affinity	Relative CPM	Binding affinity	Relative CPM
CB2 WT	19 (10-74)	837-2217	0.1 (0.05-0.4)	474-1085	96 (25-362)	752-1246
V113E	ND	975-1027	ND	897-927	ND	888-977
V113L	2.9 (1.2-8.5)	960-1481	0.7 (0.02-3)	680-1100	411 (105-972)	914-1799
F183Q	ND	988-1007	ND	756-840	NT	-
F183V	ND	527-578	ND	527-582	NT	-
L192A	4.8 (2.9-12.5)	1018-1374	2.8 (0.7-7.1)	739-1170	252 (109-580)	762-1101
L192S	ND	888-915	ND	817-1031	ND	756-780
F281K	ND	954-1159	ND	988-1038	NT	-

* Data are the means and corresponding 95% confidence intervals of two independent experiments each performed in duplicate. ND: binding not detected, NT not tested.

3.2.2.4 Agonist-induced inhibition of cAMP production

A LANCE cAMP time-resolved fluorescence resonance energy transfer (TR-FRET) immunoassay was used to detect the signal from CHO cells stably expressing wild type CB2 and four mutant receptors. CP-55,940 was used as an agonist to induce inhibition of cAMP production in the presence of 5 μM forskolin and the phosphodiesterase inhibitor RO20-1724 (50 μM). When the agonist concentration was increased, the inhibition on the forskolin-induced cAMP production also increased, resulting in an enhancement of the LANCE signal, which is inversely proportional to the concentration of cAMP. These results were congruent with the ligand-receptor binding affinity data. EC_{50} values were 32 nM, 9.7 nM and 0.14 nM for wild-CB2, V113L and L192A, respectively. Further, V113E and L192S substitutions resulted in a complete loss of signal transduction (**Figure 3-9**).

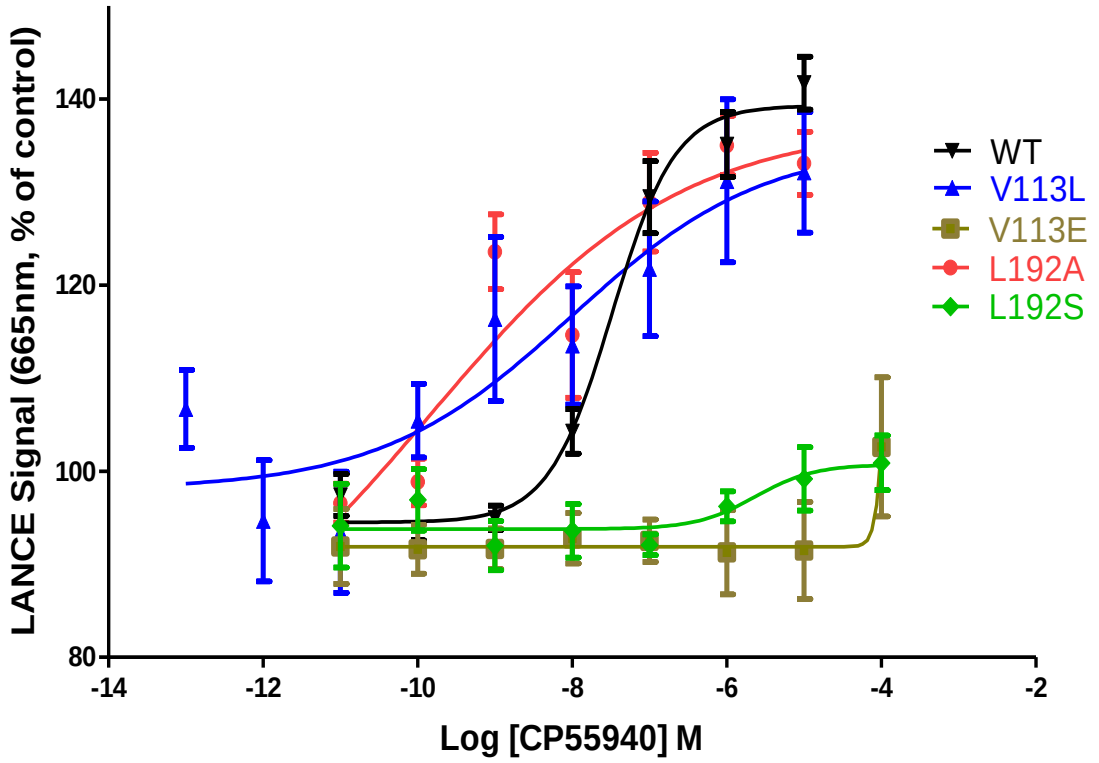

Reading/Receptor	WT	V113L	V113E	L192S	L192A
Cells (FK+CP55940)	141.7 to 97.4	132.12-106.7	102.6-91.9	100.9 - 94.1	133.1-96.5

*** The base cAMP was measured in the present of forskolin.**

Figure 3-9. Agonist-induced inhibition of forskolin-stimulated cAMP accumulation.

Agonist-induced inhibition of forskolin-stimulated cAMP accumulation of CB2 WT and all mutants' receptors. (▼) WT- CB2, (▲) V113L, (■) V113E (●) L192A and (◆) L192S. All receptors were stably expressed in CHO cells. Data are mean ± S.E.M. of at least two independent experiments in triplicate.

3.2.2.5 FSK-stimulated

The effects of the agonist and inverse agonist (SR144528 and Xie95-26) have been tested on the FSK-stimulated of the CB2 receptor (wild type). This effect was assessed by decreasing or increasing the levels of forskolin-stimulated cAMP accumulation (shifting on the EC_{50} value) before and after incubation of the cells with 0.3 μM of ligands. In the absent of the ligands the forskolin will stimulate the adenylyl cyclase leads to stimulate the cAMP levels. Treatment of the CHO cells stably expressing human CB2 WT receptor with CB2 inverse agonists (0.3 μM) led to a reduction of the EC_{50} to 0.2 (0.16–0.25) μM and to 0.18 (0.14-2.4) μM for SR144528 and Xie95-26 respectively. Whereas treatment with 0.3 μM of CP55940 decreased the forskolin stimulated AC activity, with a higher EC_{50}=13.4 (8.5-15.1) μM compared to the no cannabinoid ligand treated control (forskolin alone) with EC_{50}=1.38 (1.0–1.8) μM as shown in (**Figure** 3-10**)** and **Table 5**. The constitutive activation effects were not tested for the mutation receptors.

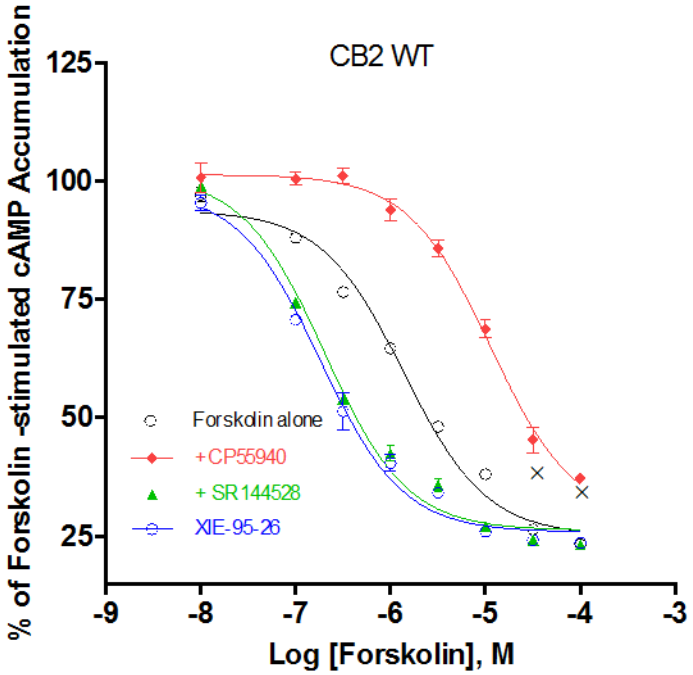

Table 5. Effects of CB2 inverse agonists SR144528, Xie95-26 and agonist CP55,940 on constitutive activation of CB2 WT. (EC_{50}, µM).

Receptor	Forskoline alone	+ SR144528	+ Xie95-26	+ CP55,940
Wild Type	1.38 (1.0-1.8)	0.2 (0.16-0.25)	0.18 (0.14-2.4)	13.4 (8.5-15.1)

Figure 3-10. The FSK-stimulated of the wild type CB2 receptor.

CHO cells expressing CB2 wild type receptor were assayed for cAMP accumulation in the presence of a gradient concentration forskolin (10–10^5 nM) with or without the presence of 0.3 µM ligands (CP55940, SR144528 and Xie95-26). The results were expressed as percentage of the LANCE signal representing forskolin- stimulation cAMP accumulation. The base cAMP accumulation was measured in the absence of forskolin. Data shown represent the means and corresponding 95% confidence intervals of three independent experiments performed in triplicate.

3.2.3 Discussion

In this study, molecular modeling and mutagenesis experiments were applied to gain valuable insights into the effect of certain CB2 residues on receptor binding with agonists and antagonists. A 3D homology model of CB2 was first constructed and then further minimized using a conjugate gradient method. The minimized model served as the basis for molecular docking studies (see Materials and Methods). A putative binding pocket was first predicted via the MOLCAD analysis, which suggested the importance of several residues such as SER112, TRP172, TYR190, TRP194, PHE197, TRP258, and SER285 that have previously been validated experimentally [261-268]. As shown in (**Figure 3-4 and Figure 3-5**), the putative binding pocket was amphipathic and composed of hydrophilic and electrically charged residues, such as Asn188 and His95 near the upper part of the pocket facing the extracellular loop 2 (ECL-2) and hydrophobic residues such as Val113, Leu201, Val261 and Trp258 near the bottom of the pocket. These results were found to be congruent with previously reported studies, which also suggested a hydrophobic binding pocket [307, 308]. Receptor chimera studies by Shire *et al* [279] showed that ECL2 is important for the binding of CP55940 to CB2. Replacing ECL2 of CB2 with ECL2 of CB1 resulted in a loss of binding of CP55940. A prior report affirmed that this loop dipped down toward the binding site of SR144528 to make a π-sulfur interaction with the Cys17 [283]. Therefore, we investigated the effect of the aromatic side chain of Phe183 in ECL2 for SR144528 binding. Mutation of Phe183 *in silico*, indicated that CB2 did not form strong hydrophobic interactions with SR144528 and CP55940. Mutation of Phe183 to the polar uncharged amino acid such as glutamine (F183Q) or to a hydrophobic side chain such as valine (F183V) abolished the binding of SR144528 to CB2 and CP55940 binding affinity to Phe183 mutated CB2 were also tested, and the similar results can be

found in **Table 4**. Phe183 did not form a π−π interaction with CP55940 and maybe did not form a hydrophobic interaction (or a very weak hydrophobic interaction), but the mutations of Phe183 showed a significant effect for CP55940 binding. We therefore suggested that the mutations of Phe183 significantly affected both SR144528 and CP55940 binding affinity. Moreover, some residues in ECL2 may have similar effects, including Glu181 (ECL2) and Leu182 (ECL2) [279].

In addition, Phe281 formed a strong π−π interaction with SR144528, but it formed a hydrophobic interaction with CP55940. We therefore mutated it to a charged chain such as lysine (F281K) to study its influence on CB2 ligand binding. As shown in **Table 4**, our results showed that this kind of mutation led to the complete loss of CB2 ligand binding. Phe281 also had an important role in the binding of SR144528 and CP55940 to CB2 through a π−π interaction or a hydrophobic interaction. In our model, we found that Phe183 in ECL2, Met265, and Phe281 formed a strong hydrophobic pocket in the extracellular side of CB2. Mutations of F183Q and F281K will change the charge environment, while the mutation of F183V will affect the hydrophobic pocket. We suggest that these three mutations will reduce the affinities of ligands on CB2. Further, results of molecular docking with the CP-55,940, SR144528 and XIE95-26 ligands are shown in (**Figure 3-4 B, C and D**), revealing other important ligand-receptor interactions for each ligand. Specifically, five hydrophobic residues were found to be in close contact with all three ligands during docking simulations: Val113, Leu192, Leu201, Val261 and Trp258. Indeed, Leu201, Val261 and Trp258 have previously been implicated in the formation of the ligand-binding pocket [267, 283]. A prior report affirms that residue 3.32 is occupied by a negatively charged amino acid in biogenic amine receptors (D2 Dopamine, ß2 Adrenergic and m3 Muscarinic) and that it is essential for recognition and binding of endogenous amines [309] [310].

In an attempt to resemble the functionality of this residue in amine receptors, Jiang *et al*. substituted endogenous V83 (position 3.32) with aspartic acid (D) in the A2a adenosine receptor. The V83D mutant A2a was unable to bind to any ligand tested. Interestingly, substitution of the same valine residue with leucine (V83L) did not significantly affect biding with any ligand with respect to the wild-type A2a. Using a similar approach, in the present study with the CB2, the V113E substitution led to the complete loss of binding for CB2 ligands and the elimination of receptor downstream signaling activities. Whereas, the V113L isoform displayed specific binding activity that was comparable to wild-type CB2. Molecular docking analyses showed that V113 maintains hydrophobic interactions with the alkyl chain of CP-55,940, the fenchyl (bulky) group of SR144528 and an aromatic ring of XIE95-26 at distances of 3.27 Å, 3.33 Å and 3.04 Å, respectively. Similarly, Leu192 interacted hydrophobically with CP-55,940, SR144528 and XIE95-26. In order to validate the modeling studies, these two residues were subjected to mutagenesis experiments. Mutation of Val113 to Glu and Leu192 to Ser interrupted the hydrophobic interactions with all three ligands leading to loss the binding affinity **(Table 4).** However, the hydrophobic feature of L192A and V113L mutants restored the binding with minimal effect on binding for CP-55,940, SR144528 and XIE95-26 compared to the CB2 receptor. In fact, L192A and V113L mutants showed only 5-fold and 6-fold reduction for SR144528 binding and almost no significant change for CP-55,940 and XIE95-26 binding (**Table 4**). These results confirmed that our predicted residues play an important role in CB2 ligand binding.

The following functional experiment further proved the importance of the predicted residues: V113 and L192. In a cell-based cyclase assay, an agonist will activate CB2 receptor, cause the dissociation of Gαi and inhibit forskolin-induced AC activity, [311] resulting in a decreased cAMP and an increased LANCE signal. As shown in (**Figure 3-9**), there is no inhibition of cAMP

accumulation mediated by CP-55,940 in the V113E and L192S mutant cells. However, mutating to different hydrophobic residues restored the functionality of the receptor as shown by the mutants V113L and L192A. The EC50 values of CP-55,940 on the WT, V113L and L192A were 32 nM, 9.7 nM and 0.14 nM, respectively. These results indicated that hydrophobic residues at positions 3.32 (V113) and 5.41 (L192) are important for both ligand-receptor interaction and function of the receptor. For the testing the constitutive activation effect of the ligands on the CB2 receptor (WT), we conducted the assay to measure the change in EC50 value of the CB2 receptor with or without the ligands. The results showed significant inhibitory effects ($p < 0.05$, two-tailed t-test) for the agonist on the EC_{50} (increase) comparing to the enhancement effect of SR144528 and Xie95-26 which represented as decreased in the EC_{50} as illustrated in (**Figure 3-10 and Table 5)**. These changes in FSK-stimulated for both agonist and invers agonists were comparing to the cells that treated with forskolin alone as shown in **(Figure 3-10)**. The EC_{50} values of WT CB2 receptor stimulated by forskolin alone was 1.3 µM for CP-55,940 was 11.3 µM and for SR144528 and Xie95-26 were 0.2 µM and 0.18 µM. Other CB2 mutant receptors have not tested for the constitutive activation.

3.2.4 Conclusion

In this study, molecular modeling studies were first performed to derive a homology model of CB2 receptor and predict a putative binding site for CB2 ligands. During molecular docking simulations consisting of three different CB2 ligands (CP-55,940, SR144528 and XIE95-26) and the CB2 model, several important ligand-receptor interactions were observed. To validate our in silico findings, we performed site-directed mutagenesis experiments and functional assays for four residues, namely V3.32 (V113), F183, L5.41 (L192), and F7.35 (F281) that had hydrophobic and

π–π interaction with all ligands during the simulation. Mutating such hydrophobic residues to non-hydrophobic residues such as V113E, F183Q/V, L192S and F281K eliminated the binding for all ligands as well as the functional activity of the CB2 receptor. However, mutating to different hydrophobic residues such as V113L and L192A had minimal effect the binding of CB2 ligands and functional activity of the receptor. To the best of our knowledge, these four residues have not previously been reported and our findings provide the first insights into the importance of these residues for the binding of CB2 ligands as well as the functional activity of the CB2 receptor.

4.0 GENERATION AND CHARACTERIZATION OF CONSTRUCTS OF CANNABINOID RECEPTOR CB2 FOR STRUCTURAL STUDIES USING AN INSECT CELL SYSTEM

4.1 INTRODUCTION

With the exception of rhodopsin, which has been crystalized without modification, different strategies for expression, purification and crystallization of chimeric GPCRs have been performed. These approaches include the combination of a variety of modification steps including: 1: Refolding proteins from *E.coli*, 2: Detergent solubilization and stabilization with different ligands in different crystal forms. 3: Increasing the protein expression by using different thermostabilization point mutations, 4: Removing the glycosylation position and truncating the N- and/or C-terminals, and 5-: Insertion of a fusion counterpart or antibodies in the N-terminal, second or third intracellular loops.

Understanding the residuals interaction involved in the activation mechanisms of GPCRs during binding and downstream signaling events is crucial for solving the structure of common GPCRs. Locking in conformational states and removing unstructured regions are essential for producing proteins suitable for co-crystallization [51]. In addition, combinations of the baculovirus expression system and epitope-tagged proteins have allowed for facilitating GPCRs purification. Previous studies provided guidance in two methods of fusion protein insertion [51][17]. The first study used highly stable soluble proteins to replace the structurally variable third intracellular loop region of either ICL2 or ICL3. This conformed to the lattice-forming contacts needed for crystallization. For example, in β2-adrenergic receptors (β2AR), various constructs with the T4L fusion protein were generated in order to determine the optimal length and position of fusion proteins for crystallization studies [43]. Truncation of both β2AR N- and C-terminus were also essential to remove the glycosylation sites. In an additional set of receptor stabilization constructs, monoclonal antibody Fab fragments were used against a synthetic polypeptide mimicking the N-

and C-terminal domains [43]. This is a second study demonstrated fusion of the T4L protein into the N-terminus of β2AR was also suitable for crystallization studies. The T4L C-terminus was fused to the first amino acid of the β2AR transmembrane helix 1. Subsequently, the flexible region of the β2AR C-terminus was removed to generate a rigid interaction. These data indicated insertion of alanine-like and mutations in the extracellular loops (M for receptors highly homologous to the CB2 receptor, M96T and M98T) were essential to improve GPCRs expression levels. Additionally, residues of the third intracellular loop were deleted to prevent proteolysis during purification [312].

Overall, the GPCR co-crystal structures published to-date have experienced rigorous optimization including chimeric receptor truncation, introduction of thermostabilization point mutations, selecting the proper fusion proteins for insertion, cell culture optimization, and determination of ideal conditions for X-ray diffraction, and structure determination.

CB1 and CB2 belong to the rhodopsin family of GPCRs. Only 44% of the amino acid sequence of CB2 is homologous to the CB1 receptor, though the percentage increases to 68% in the transmembrane domains [250]. Upon ligand binding and activation of the cannabinoid receptor, the third intracellular loop and C-terminus couples to G_i, leading to inhibition of adenylyl cyclase (a reduction in cAMP levels), activation of the MAPK cascade, and inhibition of PKA phosphorylation. Each of these cascade steps is critical in maintaining cell function integrity [259, 313].

CB1 is generally expressed in CNS and is less abundant in peripheral organs and tissues, such as the heart and lungs [171, 250]. In contrast, CB2 is expressed throughout the peripheral immune system, including the spleen, lymph nodes, tonsils, thymus, and immune cells (T cells, B cells, macrophages, and monocytes)[250]. The tissue distribution pattern of CB2 implies the

receptor plays a crucial role in the immune system and thus, may be a target in the treatment of autoimmune and immunological disorders similar to multiple sclerosis [314]. Additionally, research supporting modulation of CB2 signaling has demonstrated potential for the treatment of various cancers such as lung, bladder [255], pancreas [256], breast [257] and prostate [230]. The CB2 agonist HU-910/308 has been shown to attenuate oxidative stress markers, inflammation, and cell death following hepatic ischemia reperfusion injury in mouse models [217, 218]. Therapeutic intervention through targeting the CB2 receptor is a feasible proposal. However, specific details of receptor structure, as well as molecular-level interactions among ligands and G-proteins, have not yet been confirmed to design effective CB2-specific therapies.

CB2 has shown to be expressed in insect cells [315, 316]. The heterologous expressed receptor was purified as tagged or untagged protein. Both the N-terminus Flag tagged and C-terminus 6xHis tagged CB2 constructs revealed high binding affinities when compared to other constructs. Western blot analysis indicated acceptable levels of the receptor as well, the glycosylated region of the receptor was removed due to the presence of the double-tag. This was shown by anti-His and anti-CB2 antibodies. Mass spectroscopic analysis indicated adequate protein expression levels. [316]. Functional expression of the wild type and mutant cannabinoid receptor was evaluated in sf9 cells. In this study, the irreversible affinity properties of AM-841, as well as the use of ligand-assisted protein structure (LAPS), allow for the study of residual and direct identification by mass spectrometry (MS). Cysteine at TMH 6 (257) in hCB2R has shown an important role of the binding and function of the receptor.

To begin to study these ideas for expression and purification of functional CB2 constructs in insect cells, we have collaborated with Dr. Kobilka and his colleagues. We will insert fusion protein T4 Lysozyme or apocytochrome b562RIL (BRIL) into the third intracellular loop and N-

terminus and evaluate the changes on the structured integrity of the cannabinoid receptor CB2. Previously, it has been shown that the distance between the N- and C-terminus of the fusion protein needs to be within 6-14 Å [51]. Therefore, we have designed our constructs to fulfill this requirement. In collaboration with the Kobilka lab, a variety of constructs of CB2 expressed in Sf9 cells using the Bac-to-Bac system (Invitrogen, Carlsbad, CA), were constructed. These constructs feature dual Flag and His-6 tags at the N- and C-termini, respectively. One area of concern is the precise placement of the T4L either at the N termini or between helices V and VI.

Therefore, the position of the T4L was adjusted by a determinate number of residues in order guarantee adequate stability during protein expression and lattice-forming contacts in pre-crystallization trials. Moreover, receptor truncations, de-glycosylation and proteolytic cleavage were also considered during construct design and purification to create a stabilized receptor that also retains complete functional activity. Among the many constructs assessed, few revealed sufficient expression levels and binding activity in small-scale purifications.

The goal of this study is to screen and understand the effects of chimeric receptor modifications in order to provide the best constructs for large-scale purification. This will be further discussed in chapter (5).

4.2 MATERIAL AND METHODS

4.2.1 Insect cells expression system and reagents

The insect cells and *E. coli* (strain DH10) BAC to BAC baculovirus expression system was purchased from Invitrogen (Carlsbad, CA). Bac-to-Bac contains site-specific transpositioning of Tn7 to generate recombinant bacmid DNA. DH10Bac™ *E. coli* was utilized to host the pFastBac™ constructs which contain a shuttle vector (bacmid) and a helper plasmid. All restriction and DNA modifying enzymes were purchased from New England Biolabs (Ipswich, MA). The sf900 II SFM was purchased from Life Technology (Pittsburgh, PA) and the fetal bovine serum from Thermo Scientific (Pittsburgh, PA). ^{3}H-CP55,940 (specific activity: 88.3 Ci/mmol), CP55,940 and SR144,528 were obtained from RTI International (Research Triangle Park, NC). Xie 2-64 was synthesized as described previously [317]. Protease inhibitor cocktail was purchased from Sigma (St. Louis, MO). Dodecyl- β-D-maltoside (DDM), n-tetradecylphosphocholine **(**FC14), Lauryl Maltose Neopentyl Glycol (MNG) and cholesteryl hemisuccinate (CHS) were purchased from Affymetrix (Alabaster, AL). CHAPS detergent and other chemicals, unless otherwise mentioned, were obtained from Fisher Scientific (Pittsburgh, PA).

4.2.2 Vector design of various CB2 constructs

Nineteen different recombinant CB2 constructs expression were generated in vector of pFastBac dual form BAC to BAC (California, LA). Truncation of these constructs at N and/or C terminal were obtained to remove the amino acids not involved in binding and could hamper crystal formation. Moreover, two different fusion proteins used for the insertion namely:

thermostabilized apocytochrome b562RIL:

*(*ADLEDNWETLNDNLKVIEKADNAAQVKDALTKMRAAALDAQKATPPKLEDKSPDSPE MKDFRHGFDILVGQIDDALKLANEGKVKEAQAAAEQLKTTRNAYIQKYL) [51] . T4 lysozyme have been amplified from DNA obtained from Addgene (Cambridge, MA) and used for ligation into either N or C terminal of the CB2 constructs.

(NIFEMLRIDEGLRLKIYKDTEGYYTIGIGHLLTKSPSLNAAKSELDKAIGRNTNGVITKDE AEKLFNQDVDAAVRGILRNAKLKPVYDSLDAVRRAALINMVFQMGETGVAGFTNSLR MLQQKRWDEAAVNLAKSRWYNQTPNRAKRVITTFRTGTWDAY) [51] .

Wild CB2 was amplified from pcDNA3.1 + 3X – HA-hCB2, obtained from Missouri S&T cDNA Resources Center and was designed to separate the N-terminal of CB2 from the Flag epitope (DYKKDDDDK) and HA signal peptide (MKTIIALSYIFCLVFA) by Tobacco Etch Virus (TEV) at the enzymatic cleavage site. TEV was also used to separate the C-terminal of CB2 from the 6 X His, as shown in (**Figure 4-1).** The receptor design was adapted from [318]. Similar modifications were previously used for the β 2 adrenergic receptor expressed in insect cell membranes and were shown to have no effect on the ligand binding profile. We used the overlapping gene segments by PCR in which we used template DNA for another PCR to create a full-length gene of the receptor [319] as following condition for all of the CB2 constructs.

3 step PCR Method for 30 cycles

98°C	for	10 sec.
55°C	for	10 sec.
72°C	for	1 minute /kb

Recombinant CB2 DNAs were subcloned into the pFastBac vector between the 5′ BamHI or EcoRI cloning sites and the 3′ HindIII cloning site.

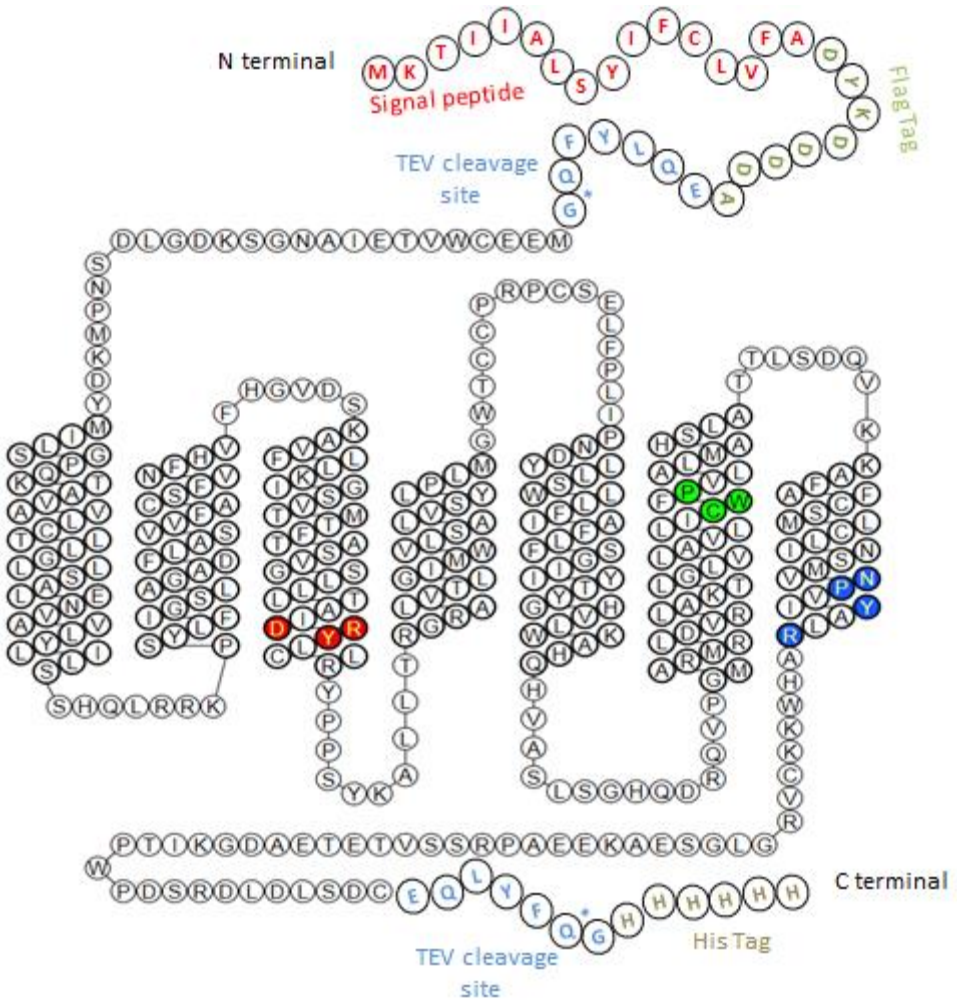

Figure 4-1. Two-dimensional structure of the wild type cannabinoid receptor CB2.

The wild type CB2 receptor design showing Flag at N-terminal and 6X His at C-terminal to facilitate the purification. TEV cleavage sites designed to separate the CB2 protein from tags in the last step.

4.2.3 Receptor truncation

To ligate the HA signaling peptide, Flag tag and TEV protease cleavage site to the N terminal regions of cannabinoid receptor (wild type), we have used the primers as shown in **Table 6**. Moreover, we ligate the TEV protease cleavage site and 6XHis to different positions at the carboxylic terminus of cannabinoid receptor using the primers as shown in **Table 6**. Finlay, we have used high fidelity PrimeSTAR HS DNA polymerase for all processes of the PCR, including the overlapping PRC and sub-cloning process (Takara Clontech). To verify insertion into the vector, we carried out double digestion of the parent gene with HindIII and BamHI or EcoRI to release the CB2 gene fragment. The released product was gel purified and sequence verified as CB2 receptor cDNA. All sequences were verified by automated DNA sequencing at the University of Pittsburgh Genomics core facility.

Table 6. Primers used for truncation and tags ligation for both N and C terminals.

Position of insertion/truncation	Sequence of insertion and position at CB2	Primer used
Position 1 amino acid (Met) of CB2 (N –terminal)	MKTIIALSYIFCLVFADYKD DDDAENLYFQG--------- CB2 start at (MEEEC……)	5’ - ATC GAA GAA TTC AAG ACG ATC ATC GCC CTG AGC TAC ATC TTC TGC CTG GTG TTC GCC ATG GAT TAC AAG GAT GAC GAT GAC AAG GAG AAC CTG TAC TTC CAG GGT ATG GAG GAA TGC TGG GTG ACA GAG –’3 .
Position 18 amino acid (Asp) of CB2 (N –terminal)	MKTIIALSYIFCLVFADYKD DDDAENLYFQG--------- CB2 start at (DSNPM……)	5’ - ATC GAA AAG ACG ATC ATC GCC CTG AGC TAC ATC TTC TGC CTG GTG TTC GCC ATG GAT TAC AAG GAT GAC GAT GAC AAG GAG AAC CTG TAC TTC CAG GGT GAT TCC AAC CCT ATG AAG GAT –’3
Position 26 amino acid (Met) of CB2 (N –terminal)	MKTIIALSYIFCLVFADYKD DDDAENLYFQG--------- CB2 start at (MILSG……)	5’ – ATC GAA TTC AAG ACG ATC ATC GCC CTG AGC TAC ATC TTC TGC CTG GTG TTC GCC ATG GAT TAC AAG GAT GAC GAT GAC AAG GAG AAC CTG TAC TTC CAG GGT ATG ATC CTG AGT GGT CCC CAG –’3
Position 360 amino acid (Cys) of CB2 (C –terminal)	CB2 end at (DLSDC)------- ENLYFQGHHHHHH	5’ – C AAG CTT CTA TTA ATG GTG ATG GTG ATG GTG ACC CTG GAA GTA CAG GTT CTC GCA ATC AGA GAG GTC TAG TC –’3.
Position 340 amino acid (Thr) of CB2 (C –terminal)	CB2 end at (SVTET)------- ENLYFQGHHHHHH	5’ – C AAG CTT CTA TTA ATG GTG ATG GTG ATG GTG ACC CTG GAA GTA CAG GTT CTC TGT CTC GGT GAC TGA GGA TCT –’3.
Position 322 amino acid (Gly) of CB2 (C –terminal)	CB2 end at (KCVRG)------- ENLYFQGHHHHHH	5’ – GAA TTC CTA ATG GTG ATG GTG ATG GTG ACC CTG GAA GTA CAG GTT GCC CCT CAC ACA CTT CTT CCA GTG –’3.

4.2.4 The fusion insertion position

Two different fusion partners (T4L and apocytochrome b562RIL) and two attachment sites (the N- and third intracellular loop) were used in our study.

4.2.4.1 N- Terminal fusion insertion

We used T4L and apocytochrome b562RIL as fusion proteins at the N-terminal of the CB2 receptor. Two constructs were generated based on previously published data on β2-adrenoceptor [312]. The first construct was generated and annotated by pFastBac: HA -Flag-TEV-APO (N-terminal) CB2 ΔICL3 (220-234) (340 C-terminal). In this construct, we removed CB2's N terminals and replaced it by a TEV cleavage site followed by apocytochrome b562RIL. In addition, a portion of the third intracellular loop was removed between amino acids 220 and 234 to diminish the flexibility. The C-termini also truncated and ligated to TEV cleavage site followed by 6XHis to facilitate the purification. The second construct generated was annotated by pFastBac: HA-Flag-TEV-AA-T4 (N-terminal) CB2 ΔICL3 (220-234) (340 C terminal). Similar modifications were introduced, however, one difference, the fusion protein (T4 lysozyme) was inserted after two alanine to facilitate the protease cleavage. The multiple primers used in this study are presented in **Table 7.**

Table 7. Primers used for N-terminal fusion protein insertion.

Insertion at N-terminal	Information of motifs	Amino acid sequences of the motifs	Primers used
N-terminal apocytochrome b562RIL	HA-Flag-TEV-apocytochrome b562RIL	MKTIIALSYIFCLVFADYKDD DDAENLYFQGADLEDNWET LNDNLKVIEKADNAAQVKD ALTKMRAAALDAQKATPPK LEDKSPDSPEMKDFRHGFDI LVGQIDDALKLANEGKVKE AQAAAEQLKTTRNAYIQKY L	5' – ATC GAA GAA TTC AAG ACG ATC ATC GCC CTG AGC TAC ATC TTC TGC CTG GTG TTC GCC ATG GAT TAC AAG GAT GAC GAT GAC AAG GAG AAC CTG TAC TTC CAG GGT GCT GAT CTG GAA GAC AAT TGG G –'3
	Truncated N-terminal	MKTIIALSYIFCLVFADYKDD DDAENLYFQGADLEDNWET LNDNLKVIEKADNAAQVKD ALTKMRAAALDAQKATPPK LEDKSPDSPEMKDFRHGFDI LVGQIDDALKLANEGKVKE AQAAAEQLKTTRNAYIQKY L CB2 start at 18 (DSNPM……)	5' – GGA ATG CAT ACA 5' – GGA ATG CAT ACA TTC AGA AGT ACC TGA TGA TCC TGA GTG GTC CCC AGA AG –'3 5' – CTT CTG GGG ACC ACT CAG GAT CAT CAG GTA CTT CTG AAT GTA TGC ATT CC –'3
	Truncated C-terminal	CB2 end at 340 (SVTET)------ ENLYFQGHHHHHH	5' – C AAG CTT CTA TTA ATG GTG ATG GTG ATG GTG ACC CTG GAA GTA CAG GTT CTC TGT CTC GGT GAC TGA GGA TCT – '3
N-terminals T4Lysosyme	HA-Flag-TEV-T4 lysozyme	MKTIIALSYIFCLVFADYKDD DDAENLYFQGNIFEMLRIDE GLRLKIYKDTEGYYTIGIGHL LTKSPSLNAAKSELDKAIGR NTNGVITKDEAEKLFNQDVD AAVRGILRNAKLKPVYDSLD AVRRAALINMVFQMGETGV AGFTNSLRMLQQKRWDEAA VNLAKSRWYNQTPNRAKRV ITTFRTGTWDAYAA	5' – ATC GAA GAA TTC AAG ACG ATC ATC GCC CTG AGC TAC ATC TTC TGC CTG GTG TTC GCC ATG GAT TAC AAG GAT GAC GAT GAC AAG GAG AAC CTG TAC TTC CAG GGT ATT ATA TTT GAA ATG TTA CGT ATA –'3
	Truncated N-terminal	MKTIIALSYIFCLVFADYKDD DDAENLYFQGNIFEMLRIDE GLRLKIYKDTEGYYTIGIGHL LTKSPSLNAAKSELDKAIGR NTNGVITKDEAEKLFNQDVD AAVRGILRNAKLKPVYDSLD AVRRAALINMVFQMGETGV AGFTNSLRMLQQKRWDEAA VNLAKSRWYNQTPNRAKRV ITTFRTGTWAYAA CB2 start at 18 (DSNPM……)	5' – ACT GGC ACT TGG GAC GCG TAT GCG GCG TAC ATG ATC CTG AGT GGT CCC –'3 5' – GGG ACC ACT CAG GAT CAT GAT CGC CGC ATA CGC GTC CCA AGT GCC AGT –'3.

	Truncated C-terminal	CB2 start at 340 (SVTET) ENLYFQGHHHHHH	5’ – C AAG CTT CTA TTA ATG GTG ATG GTG ATG GTG ACC CTG GAA GTA CAG GTT CTC TGT CTC GGT GAC TGA GGA TCT – ’3
N-terminal apocytochrome b562RIL and T4Lysosyme	3ICL truncation in both constructs between (220-234)	CB2 ΔICL3 (V220 to A235)	5’ – CTC TGG AAG GCC CAT CAG CAT GTG GCC CGA ATG AGG CTG GAT GTG AAG-’3 and 5’ – CCT CAC ATC CAG CCT CAT TCG GGC CAC ATG CTG ATG GGC CTT CCA GAG -’3 5’ – C AAG CTT CTA TTA ATG GTG ATG GTG ATG GTG ACC CTG GAA GTA CAG GTT CTC TGT CTC GGT GAC TGA GGA TCT – ’3.

4.2.4.2 3ICL fusion insertion

For the third extracellular loop, we considered fusion insertion based on the previously successful co-crystal structure fusion location. We selected the sequences of CB2 (UniProtID: P34972) and other GPCRs belongs to same rhodopsin family. These receptors are beta-2 adrenergic receptor (UniProtID: P07550), adenosine receptor A2a (UniProtID: P29274), C-X-C chemokine receptor type 4 (UniProtID: P61073), D3 dopamine receptor (UniProtID: P35462), muscarinic acetylcholine receptor M2 sphingosine 1-phosphate receptor 1 (UniProtID: P08172), and HRH1 (UniProtID: P35367) to carry out the sequence alignments on UniProt online server (http://www.uniprot.org) based on their sequence identities and using the Clustalo program. Default parameters are as follows: The default transition matrix is Gonnet, gap opening penalty is 6 bits, and gap extension is 1 bit. Clustal-Omega uses the HHalign algorithm, and its default settings were the core alignment engine. The algorithm is described in [320]. Moreover, we have used different primers for insertion– either T4L or apocytochrome b562RIL–in 3ILC, combined with or without N- and/or C-terminal truncations as listed in **Table 17** of **Appendix B**.

4.2.5 Optimization of the wild type and truncated receptor production

4.2.5.1 Culturing of *Spodoptera frugiperda* for virus and protein production

Healthy Sf9 cells of less than 25 generations were grown in Sf-900 II SFM (Serum-Free Media) in both forms–a monolayer attached to the bottom of the plates or as suspension culture in a vented flask. 2% of serum is added to the culture at the time of shaking to reduce the shared forces and aggregation of the cells in .Usually, the cell double within 24-30 hours when cultured at 27 °C.

The culture media and LB agar plates were supplemented with antibiotics: 50 µg/ml kanamycin, 7 µg/ml gentamicin, 10 µg/ml tetracycline, and 10 µg/ml gentamicin.

4.2.5.2 Producing the Virus

All CB2 constructs go through the same process of producing the virus. Briefly, 1-5 µl of recombinant pFastBac DNA was transform used to DH10Bac *E. coli* and cells were incubated on ice for 30 minutes. The competent cells were heat-shocked for 45 seconds at 42°C. The cells then chilled on ice for 5 minutes. In order to increase transformation efficiency, 0.5 ml of S.O.C. medium was added to the competent cells and cultures were shaken at 250 rpm in 37°C for 4 hours. Serials dilutions of the media were added to LB agar plates that contained 50 µg/ml kanamycin, 7 µg/ml gentamicin, 10 µg/ml tetracycline, 100 µg/ml Bluo-gal, and 40 µg/ml IPTG. The plates were incubated for 48 hours at 37°C or until white and blue colonies appeared. Colonies were picked up and re-streaked on fresh LB agar plates containing 50 µg/ml kanamycin, 7 µg/ml gentamicin, 10 µg/ml tetracycline, 100 µg/ml Bluo-gal, and 40 µg/ml IPTG and incubated for 24 hours at 37°C. The process was done twice to insure that the colonies were well isolated. These colonies were used for producing the recombinant bacmid DNA using PureLink™ HiPure Plasmid kit. Bacmids were prepared according to manufacturer's protocols. All DNA was stored in -20°C until further use. Moreover, to ensure insertion and transposition of the DNA into the bacmid had been successful, we did a PCR analysis using pUC/M13 primers:

pUC/M13 forward 5' -CCCAGTCACGACGTTGTAAAACG-3' and

pUC/M13 reverse 5' -AGCGGATAACAATTTCACACAGG-3'.

The PCR conditions are described in **Table 18** of **Appendix B**. Based on the concentration of the bacmid, transfection took place using Cellfectin II reagent (Invitrogen). Different

concentrations of the bacmid and Cellfectin were used to transfect 6-well (35 mm) plates according to the Bac-to-Bac expression system manual. Briefly, a mixture of DNA and Cellfectin in Grace's Insect Medium, Un-supplemented (Invitrogen) were added to the cells and incubated at 27°C for four hours. After four hours, the transfection media was exchanged for 2ml of fresh Sf-900 II (2%FBS) medium and incubated again in a humidified environment at 27°C. After 5-7 days, the media was collected and spun down at 500 x g for 5 minutes to remove dead cells and large debris. The supernatant is considered P1 virus stock that was either stored at 4°C for the short term or at -20°C for long-term storage. In addition, 2% FBS was added to the virus stock as substrate for proteases.

4.2.5.3 Amplification of the virus (P2)

Using first generation virus (P1 stock), 0.4 to 0.5 ml was added to 20 ml of the Sf9 cells at 2.5 x 10^6 cells/ml in a vented flask for 4 days. The virus was collected by centrifugation of the cells at speed 500x g for 10 minutes in a JA 30,50 rotor in the Beckman Avanti J-30I centrifuge. The viral supernatant (P2) was either stored at 4°C for short term or at -20°C for long term in 2% FBS. In order to determine the titer of viral stock to be used in the infection, we used the viral plaque assay to measure the plaque forming units, pfu/ml for P1.

We seeded 2 ml of sf9 cell suspension containing 5×10^5 cells/mL into six-well plates followed by one-hour incubation in an incubator to allow the cells to settle on the bottom. The medium was then replaced with 1 ml that contained an 8-logs of serial dilution (10^{-1} to 10^{-8}) of baculoviral stock, and one well of the plate was used as control where the medium contained no virus. The cells were incubated with virus for 1 hour at room temperature. The medium was removed, replaced with 2 mL of plaque medium (30 mL of Sf-900 II (1.3X) and 10 mL of melted 4% agarose

gel) and incubated for one hour at room temperature. The plate was then incubated at 27°C in a humidified incubator for 7-10 days until plaques were visible and ready to count. The final step was to visualize the plaques using tetrasodium thiazolal blue bromide (MTT). Two milliliters of 0.1 mg/mL MTT solution in 1x PBS was overlaid on the agarose medium, and the plates were kept at room temperature in the dark for 3-5 hours. The yellowish medium turns purple color due to the reduction of MTT formazan, and the number of plaque formed are counted. To calculate the viral titer, we counted the number of plaques present at each dilution and used the following equation:

$$\text{Titer (pfu/ml)} = \text{number of plaques} \times \text{dilution factor} \times \frac{1}{ml\ of\ inoculum/well}$$

4.2.6 Preparation of insect cell membrane fractions

The viral stock, P2, was then used to infect the Sf9 cells. Different ratios of the virus: cells were used to determine the best time and ratio for cell harvesting. Pellets from 1.5 x 10^6 to 2.5 x 10^6 cells/ml were harvested and pelleted down by centrifugation at 6000× g for 5 minutes. The pellets were then washed twice with 0.1 M Tris-HCI pH 8.0 buffer and re-suspended in lysis buffer: (40mM Tris-HCl pH 7.8, 1mM EDTA, and protease inhibitors (400X, 64mg/ml benzamidine and 1mg/ml leupeptin). The suspended pellet was incubated on ice and homogenized using a glass dounce homogenizer stroked for approximately 20 times. The supernatant was subjected to centrifugation (500× g, 10 minutes) at 4°C using an Eppendorf centrifuge 5702 R. The obtained membrane pellet was washed in 10 mM HEPES, pH 7.4, three times and homogenized using a using a glass dounce homogenizer stroked for approximately 20 times followed by centrifugation at 100,000 × g for 30 minutes. The washed membrane pellets were then re-suspended in the storage

buffer: (20 mM HEPES + 150 mM NaCl + 20% glycerol). Then aliquots were stored at -80°C for subsequent use. The protein concentration was estimated using the Bio-Rad Bradford or BCA assays.

4.2.7 Western blotting

Western blotting analysis for the expression of parental and truncated CB2 was done using protein obtained from membrane preparations or from small samples of cells that were lysed with 400 µl of 1X SDS-PAGE buffer (62.5 mM Tris-HCl, pH 6.8, 2% SDS). The supernatant was isolated from the cell debris by centrifugation at 13,000x g for 10 min at 4°C. Each sample (25 µg protein each) mixed with 3X sample buffer before the load into the SDS page well. The sample separated by electrophoresis on a 12% SDS–PAGE gel and transferred onto polyvinylidene difluoride membranes (PVDF) using 130 volts. PVDF membranes were incubated at blotted 1:1000 with either with anti-Flag M2 (Cell Signaling) or anti-His, cannabinoid receptor CB2 (Santa cruze) in 0.1% Tween 20 in PBS (PBS-T) containing 5% non-fat dried milk. The PVDF membranes were washed three time with PBS-T for 10 min followed by incubation with secondary antibodies 1:2000. Following three rinses the bands on the membrane were detected using ECL detection kit (Super Signal West Femto, Thermo Scientific).

4.2.8 ^{3}H-Radioactive saturation and binding assay

Membrane proteins obtained from infected Sf9 cells were evaluated in displacement binding and saturation binding assays. Saturation and binding experiments were used to characterize the CB2 receptor by measuring the total and non-specific binding at various concentrations of

radiolabeled ligand. Two values were derived, K_d (equilibrium dissociation constant) and B_{max} (receptor density). Briefly, the previously prepared membrane fractions (20 μg) were incubated with increasing concentrations of [^{3}H]-CP55,940 (0.01–5 nM) in 96-well plates at 30°C with gentle shaking for 1 hr. The incubation buffer was composed of 50 mM Tris–HCl (pH 7.4), 5 mM MgCl2, 2.5 mM EGTA, and 0.1% (w/v) fatty acid free BSA. The radiolabel ligand was diluted in incubation buffer supplemented with 10% dimethyl sulfoxide (less than 1% per each well) and 0.4% methylcellulose. Non-specific binding determined in the presence of unlabeled CP55,940 (5000 nM) in excess. The reaction was terminated by rapid filtration through Unifilter GF/C filter plates using a Unifilter Cell Harvester (PerkinElmer). The plate was left to dry overnight, then 35 μl of MicroScint-20 cocktail (PerkinElmer) was added to each well. The count per minute (CPM) were measured with a PerkinElmer Top Count instrument.

For the competitive displacement binding assay, ligand binding was performed as previously described [321]. Briefly, non-radioactive (or cold) ligands diluted in binding buffer (50 mM Tris-HCl, 5 mM MgCl2, 2.5 mM EGTA, 0.1% (w/v) fatty acid free BSA, pH 7.4), supplemented with 10% dimethyl sulfoxide and 0.4% methyl cellulose. Each well contained a total of 200 μL reaction mixture consisting of 10 μg membrane protein, 3 nM labeled [^{3}H]-CP-55,940 (RTI International Research Triangle Park, NC) and different concentrations of the unlabeled agonists. Plates were incubated at 30°C for 1 hour with gentle shaking. The reaction was terminated by rapid filtration through Unifilter GF/B filter plates using a Unifilter Cell Harvester (PerkinElmer). The plate was left to dry overnight, then 40 μL MicroScint-0 cocktail, (PerkinElmer) was added to each well and the (CPM) was counted by PerkinElmer TopCount instrument. All assays were performed in duplicate and data represented, as the mean ± S.E.M. Bound radioactivity data analyzed for K_i values using non-linear regression analysis via GraphPad Prism 5.0 software

4.3 RESULTS AND DISCUSSION

4.3.1 Expression of CB2 wild type and truncated variant of the receptor

It is noteworthy that the flexible portions of unstructured extracellular and/or intracellular domains of Class B, C, and F GPCRs participant in protein–protein interactions, ligand recognition, and signal transduction [7], [13]. However, these parts of these regions need to be deleted to facilitate the crystal formation. Thus, the truncation of the GPCRs needs to done in order to obtain less flexible receptors and maintain the overall receptor integrity and expression levels with no significant change in the GPCRs structure. **Figure 4-2** show the overall methodology involved in the expression and screening of best CB2-fusion constructs to select the best construct for the large scale purification from insect cell. In an attempt to achieve this structural engineering in the cannabinoid receptor CB2, 3 different constructs and wild type CB2 receptors were generated. First truncated at the (Threonine) located at 340 of the CB2 amino acid sequence in the C terminal (construct #3). This position has been tested previously in beta 2 adrenergic GPCRs. The result shows that the expression was comparable to the parental type of the CB2 receptor as shown in (**Figure 4-3)**.

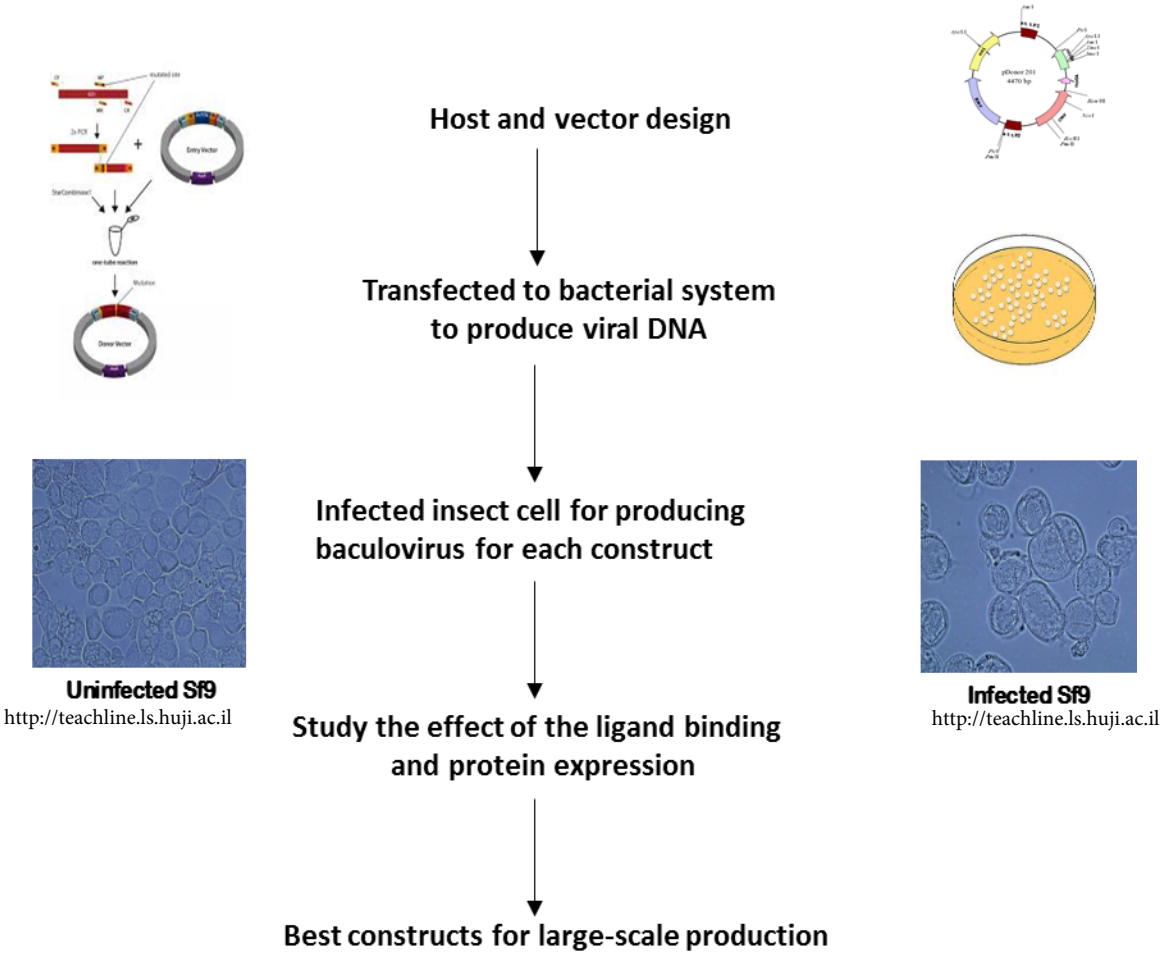

Figure 4-2. Flowchart of the cannabinoid receptor CB2 chimeric construction screening.

Second, we generated two different N terminal truncation constructs that were more cautious because the N-terminus and second extracellular loop of CB2 receptor were previously shown in report to be involved in the ligand binding site recognition [322]. These truncations were based on the S1P1 receptor crystal structure [65]. In the first (construct#11), seventeen amino acids removed before aspartic acid. Notably this removal of 17 amino acids did not affect the receptor expression and incorporate one of the N- linked glycosylation positions. Generally, the presence of the glycosylation is required for expression and folding of some GPCRs. However, the deglycosylation facilitates crystal formation. Further, there are some examples of glycosylated GPCRs that have been crystalized including rhodopsin, SMO [155], mGlu5 [154] and A2A [306] receptors. In our case, deglycosylation of CB2 at position 11 does not seem to affect expression levels and also produces functional receptor (will discuss later). We also made other constructs (#6) to remove both glycosylation positions (at 11 and 20). The N -Terminus completely removed to the first amino acid of the TMH (Methionine). The results indicate that removal of all N-terminus completely reduces expression levels, decrease binding affinity and disrupts in the overall receptor function (**Figure** 4-3**)**.

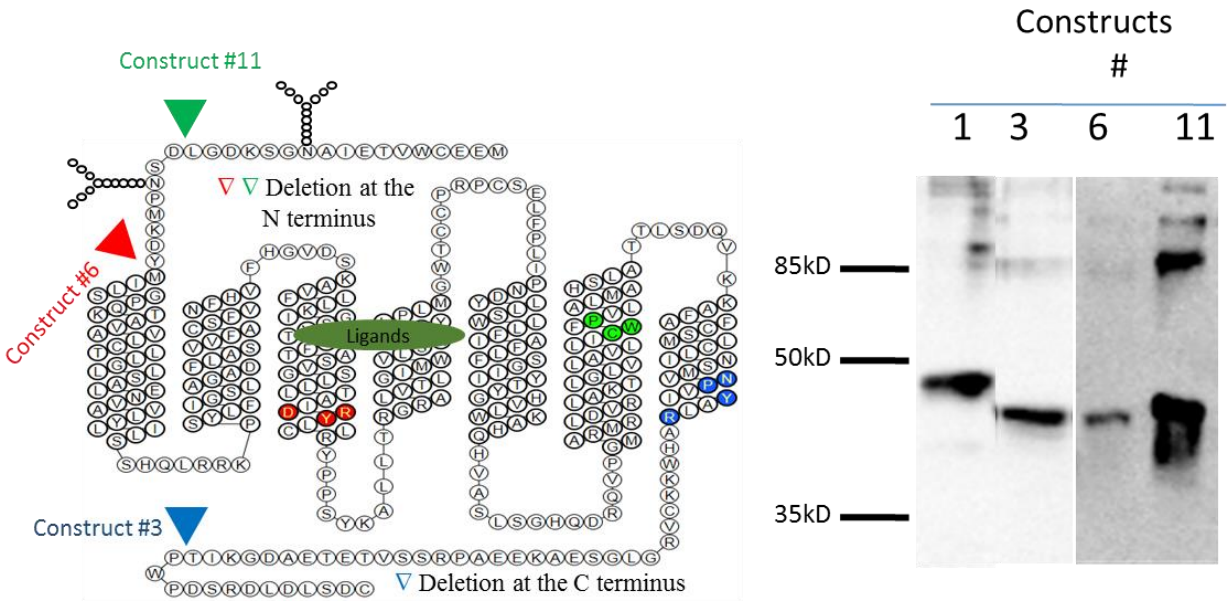

Construction No	Starting	Ending	T4 fusion position	EXPRESSION LEVEL	Note
1	Met1	Cys360	No T4L	+++	Wild type CB2 receptor
3	Met1	Thr340	No T4L	+++	Similar C-terminus truncation position in B2AR
6	Met26	Cys360	No T4L	+	Similar N-terminus truncation position in B2AR
11	Asp18	Cys360	No T4L	+++	Similar N-terminus truncation position in S1P1R

Figure 4-3. Diagram of modification and truncation position and expression levels.

2 diminution diagram for the truncation modification of CB2 receptor showing the position for the amino acids deletion. Construct #1 (wild type), #3 (C – terminus truncated CB2 receptor), and #6, 11 (N–terminus truncated CB2 receptor) expressed in Sf9 and detected by anti-Flag antibody western blot. (adapted from Dr. Kobilka's lab).

4.3.2 Expression of CB2 with fusion partner

There are different advantages of utilizing soluble fusion protein partners which tend to be insert into the GPCRs. For example it helps to solve the lack of hydrophilic surface needed for crystallization and also to lend receptor rigidity to solve the flexibility problems that are inherent in GPCRs [63]. Thus, extensive screening must be done in order to find positions for insertion of the fusion proteins within the GPCRs. There are different characteristics required for successful protein insertion into the chimeric receptor including: 1- The ligand binding affinities of the GPCRs after insertion are similar or close to wild type receptor; 2) The expression levels of chimeric receptors are close or comparable to wild type; 3) The protein is functional after purification; and 4) the Chimeric receptor needs to be stable in the presence of all detergents, ligands, and lipid material. Thus, two approaches were considered in our protein engineering for fusion insertion: The N-terminal and 3ICL fusion insertion.

4.3.2.1 N-terminal fusion protein expression

An N-terminal fusion insertion has been successfully implemented to obtain many GPCRs co-crystal structures. For example, using T4L in β2-adrenoceptor, Zou, Y et al., made extensive modifications to the β2-adrenoceptor at different position in the N-terminus, 3ICL and C-terminus. Not only did this modification enable them to obtain receptor crystals but also the downstream signaling was maintained similar to the wild type. Inserting the fusion protein at the N-terminus of the GPCRs causing no disruption of the downstream signaling [312]. Thus, the receptor maintained the coupling to the G protein at intracellular site .This is considered one of the major advantages of using the N-terminus fusion protein over the 3ICL insertion approach. On the other hand, the receptor chimeric modifications including 3ICL modifications (deletion or

fusion insertion) and /or C-terminal truncation leads to disrupt the coupling of the GPCRs with intracellular effector proteins in most cases [312]. Utilizing a T4L insertion at the N-terminal, the Rasmussen group was able to produce a crystal structure for the β2-adrenoceptor binding to Gs protein. This structure was the first and unique example demonstrating G-protein coupling to the receptor [60]. The β2-adrenergic receptor has also been crystalized in complexes with agonist and antibody [323, 324]. Apocytochrome BRIL has also been used previously as an N-terminal fusion protein for the determination of GPCR crystal structures, including, nociceptin/orphanin FQ, glucagon, smoothened receptor, metabotropic glutamate receptor 1 and human δ receptors [51, 75, 153, 155].

Two different fusion proteins were used in our study to generate two CB2 constructs. Briefly, we considered similar approaches to the β2-adrenoceptor [312]. For the T4L protein, the N-terminus of the cannabinoid receptor was truncated at the first amino acid in the TMH and replaced with T4 lysozyme. Part of 3ICL was also removed between V220 (5.69) and A235 (6.25) since this removal was necessary for the case of β2-adrenoceptor to reduce the flexibility of the third loop and to reduce proteolysis [62]. In addition, part of the C terminal (last 20 amino acids) was removed based on our preliminary data of the truncation effect (section 4.3.1). The plasmid for this construct annotated by PfastBac: (HA tag-Flag-TEV-T4L A-A N terminal) CB2 ΔICL3 (220-234) (340 C-terminal). The second fusion protein insertion used apocytochrome b562RIL that been generated the same way as T4L but missing the Ala linker. The plasmid for this construct was annotated by PfastBac: (HA tag-Flag-TEV-Apo N- terminal) CB2 ΔICL3 (220-234) (340 C-terminal). The expression levels results show that both constructs are significantly reduced and the function of the receptor was also disrupted (**Figure 4-4)** and (Section 4.3.2.3). Although this approach has been successfully used for the β2-adrenergic receptor, the removal of the N terminus

of CB2 and replacement with a fusion partner did not work for either expression or functional activity.

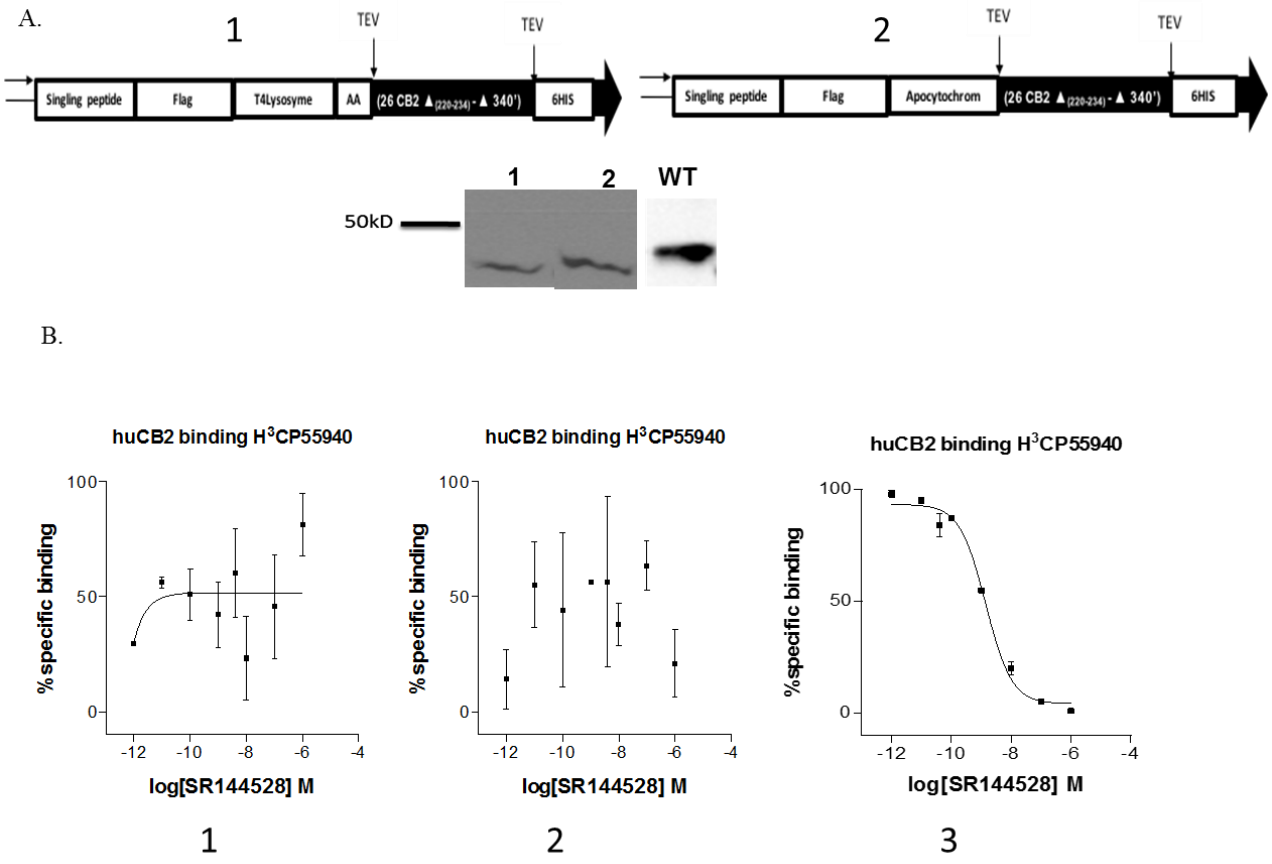

Figure 4-4. Expression and function of both N-terminal constructs.

A. Schematic diagram of human CB2 fusion protein inserted at N-terminus and western blot analysis showing the expression levels comparing to WT CB2 receptor.

B. The competitive binding assay for the corresponding construct (1 and 2) and for the wild type (3). The relative CPMs are shown in **Table 9**. The binding was only the detected for the wild type. the competitive displacement of the ^{3}H-CP55,940 was obtained by using an increased amount of cold ligands of SR 144528 and assay was performed in duplicate (n = 2). Data represented as mean ± S EM.

4.3.2.2 Intracellular loop (3ICL) fusion protein expression

Unlike the N-terminus approach, insertion the fusion protein partner into third intracellular (IC3) loop of GPCRs is the best chose to provide most common GPCRs co-crystals up to date. It has been shown previously for the purpose of crystallization that removal of this region in receptors is generally preferable to control the relative motion of surrounding helices. In addition, the removal provides a hydrophilic core for forming crystal lattice contacts [62]. However, the overall structural integrity needs to be maintained during the fusion protein insertion and not affect protein topology [51]. Generally, there is no criteria established yet for determining the best position to insert of fusion protein in GPCRs [51]. In an attempt to gain insight into some positions to begint with for the CB2 receptor, we and our collaborator (Dr. Brian Kobilka) performed multiple amino acids sequence alignments with 7 crystal structures of GPCRs as shown in (**Figure** 4-5**)** and **Table 8**. The result of the multiple sequence alignment analysis of these GPCRs revealed about 40% TM similarity between CB2 and other GPCRs, but overall the sequence identities are far less similar due to the diversity observed within the extracellular and transmembrane-intracellular (TM-IC) regions. However, the results of the alignment revealed potential truncation sites, highlighted in (**Figure** 4-5**)** based on the nature of the amino acids. For example, an insertion between postion 5.69 and 6.25 is considered to be the most popular postion for T4L insertion based on the previous studies of the β2AR. In addition, the CB2 N-terminus truncation at Asp18 and the C-terminus truncation at Thr340 are similar to S1P1R and β2AR, respectively. Thirteen different constructs shown in (**Figure 4-6)** and **Table 9** have been generated based on this sequence homology analysis **(Figure** 4-5**)** as well as the effects of truncations that have been mentioned previously. The receptor expression levels and the ligands binding affinity profiles of the protein each constructs for fusion insertions with or without truncations were assessed (**Figure** 4-6**)** and **Table 9**. The results showed

that different constructs were shown to be comparable to the wild type. Modifications in three of these constructs significantly reduced either receptor expression or radio-ligand binding affinity for constructs 12 and 15, 19 respectively. In construct #12 the receptor was subjected to the maximum truncation in both the N – and C- terminus which potentially accounts for the decrease in receptor expression as well as the loss of binding affinity. In contrast, constructs 15 and 19, the effect of the truncation modifications to the receptor was not in receptor expression levels. Rather, the effect of the fusion insertion was loss of structural integrity and radio-ligand binding affinity (**Figure** 4-6**)** and **Table 9**.

A.

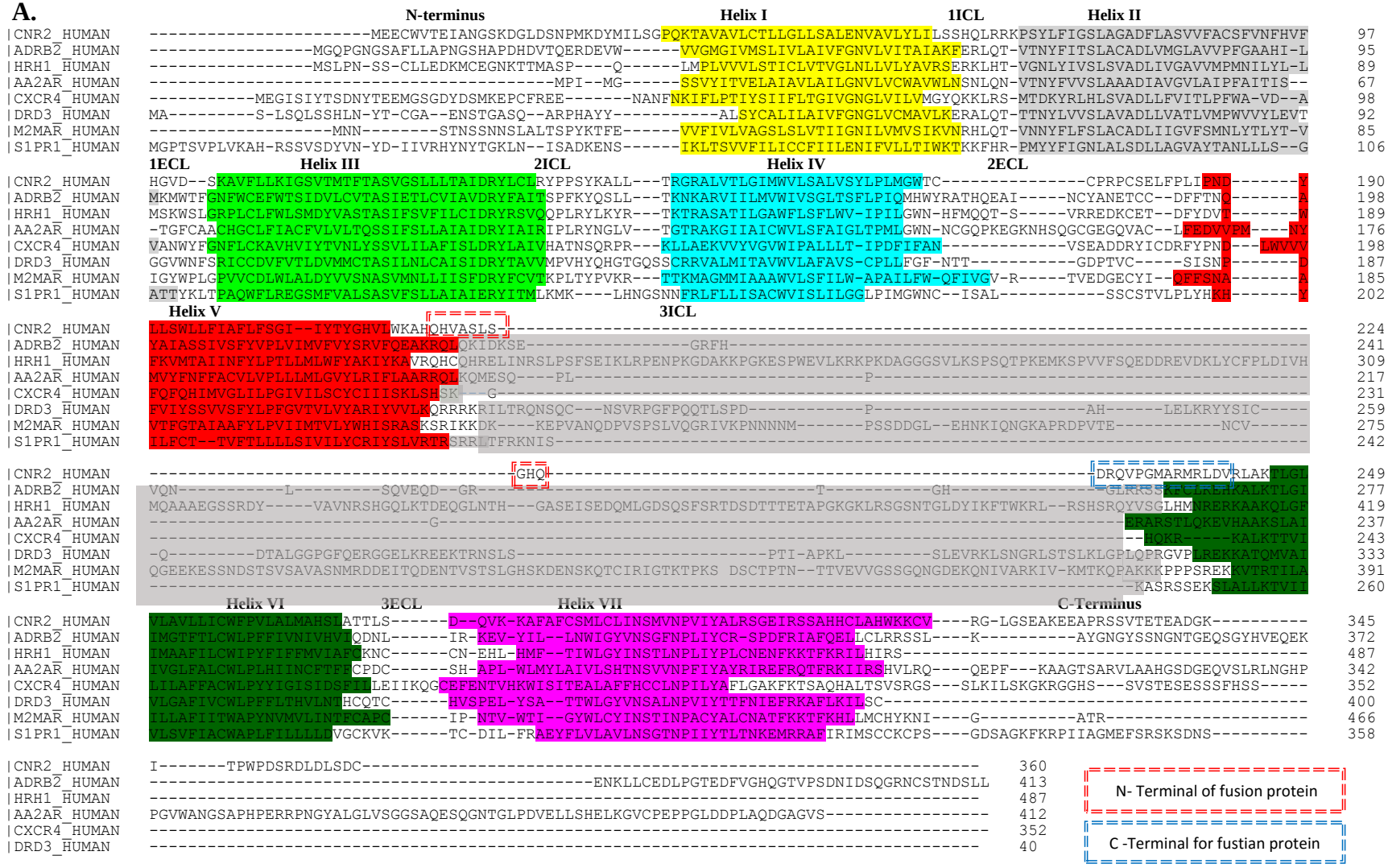
N-terminus
Helix I
1ICL
Helix II
1ECL
Helix III
2ICL
Helix IV
2ECL
Helix V
3ICL
Helix VI
3ECL
Helix VII
C-Terminus
|CNR2_HUMAN
|ADRB2_HUMAN
|HRH1_HUMAN
|AA2AR_HUMAN
|CXCR4_HUMAN
|DRD3_HUMAN
|M2MAR_HUMAN
|S1PR1_HUMAN
N- Terminal of fusion protein
C -Terminal for fustian protein

B.

Table 8. Comparison table between CB2 and other GPCRs.

	CXCR4	M2MAR	DRD3	ADRB2	AA2AR2	HRH1	S1PR1
PDB entry	3OEO	3UON	3PBL	2RH1	3EML	3RZE	3V2W
Resolution (Å)	2.9	3	2.9	2.4	2.6	3.1	3.3
CB2 to GPCR whole sequence identity (%)	17.1	13.1	15.5	18.6	18.8	12.8	22.2
CB2 to GPCR sequence identity in TM (%)	19	25	26	26	27	28	32
CB2 to GPCR sequence similarity in TM (%)	38	43	43	47	44	49	50
Deletion of amino acid for fusion insertion	S229-K230	K218-K375	R222-R319	I233-L266	Q210-A221	Q222-G404	Q222-G404

Figure 4-5. Multiple sequence alignment and homology study of CB2 and eight GPCRs.

A. Sequence alignment of CB2 receptor with most recently revealed GPCR crystal structures. Colored regions represent the helices and deletion regions of intercellular loops for T4L or APO fusion insertion by UniProt analysis.

B. Comparison of seven GPCRs with CB2 sequences in terms of identity, similarity for whole sequence, and within TM by UniProt analysis. CXCR4: chemokine (C-X-C motif) receptor 4; M2MAR: muscarinic acetylcholine receptor M2; DRD3: D (3) dopamine receptor; ADRB2: beta-2 adrenergic receptor; AA2AR2: adenosine receptor A2a; HRH1: histamine H1 receptor; OPRD: delta-type opioid receptor; S1PR1: sphingosine 1-phosphate receptor.

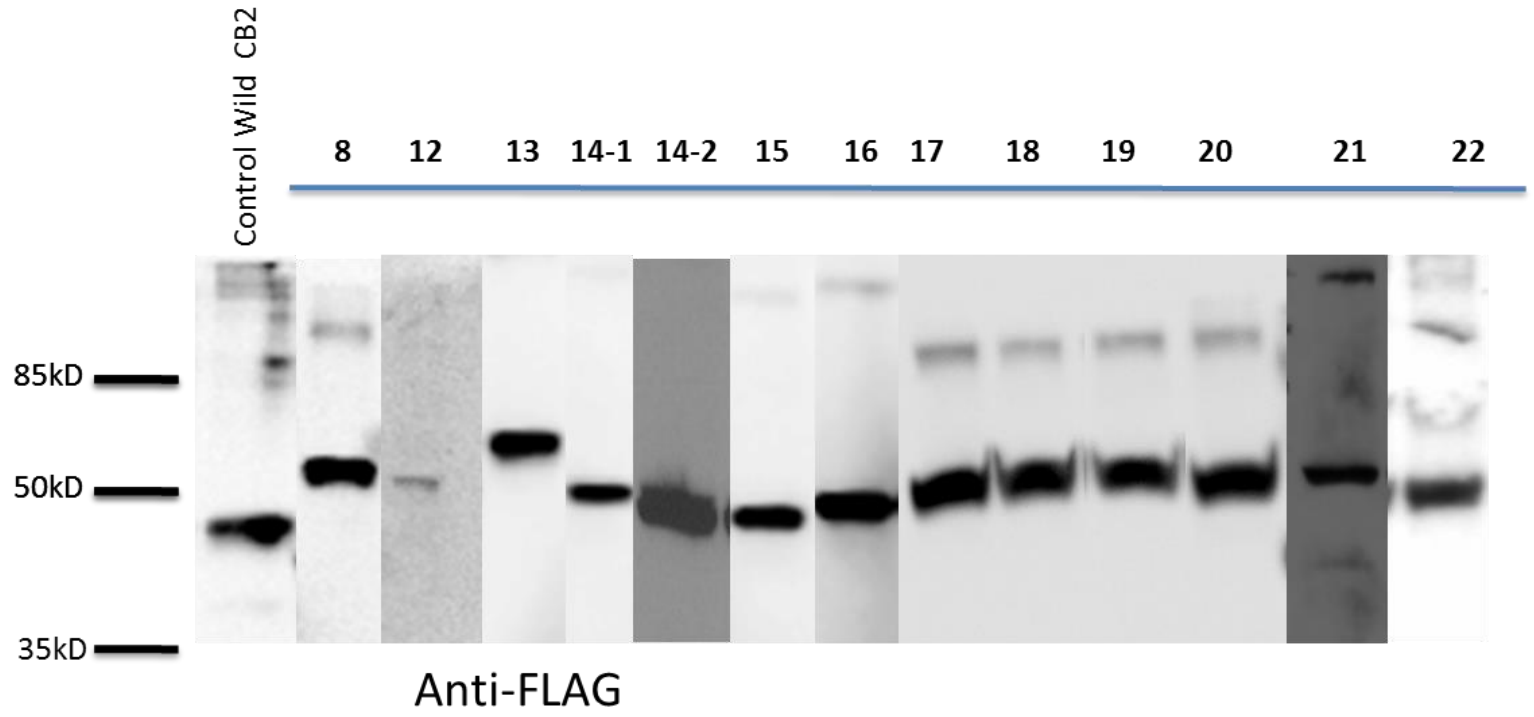

Figure 4-6. Expression levels of CB2 constructs (3ICL fusion insertion).

Thirteen different construct and wild type CB2 receptor expressed in sf9 and tested for expression levels using western blot probed against (anti Flag antibodies). All WB results for expression were adapted from (Dr. Brian Kobilka lab) with exception of construct 14-2 and 21.

Table 9. Expression and binding affinity results of cannabinoid receptor CB2 constructs (3ICL fusion insertion).

Construction No.	Starting	Ending	Fusion position	Binding affinity (nM)	Dynamic range of the binding (CPM)	Expression levels	Notes
3ICL fusion insertion							
1	1	360	No fusion	1	259 to 2285	+++	Wild type CB2 receptor
3	Met1	Thr340	No T4L	1.4	235 to 1930	+++	Similar C-terminus with B2AR
5	Met1	Arg322	No T4L	1.9	480 to 824	++	
6	Met26	Cys360	No T4L	NB	301 to 345	+	
8	Met1	Cys360	V220(5.69)-T4L-A235(6.25)	1	206 to 1060	+++	Most popular T4L fusion positions
11	Asp18	Cys360	No T4L	2	281 to 2033	+++	Similar N-terminus with S1P1R
12	Met26	Gly322	G210(5.59)-T4L-L239(6.29)	NB	352 to 447	+	Most truncated constructs
13	Met1	Thr340	V220(5.69)-T4L-A235(6.25)	5.7	355 to 932	+++	
14-1	Asp18	Thr340	V220(5.69)-T4L-A235(6.25)	6.3	309 to719	+++	Most popular inserted position
14-2	Asp18	Thr340	V220(5.69)-APO-A235(6.25)	2.9	489 to 1227	+++	Most popular inserted position
15	Asp18	Thr340	Q218 (5.67) –T4L-M237(6.27)	NB	332 to 403	+++	
16	Asp18	Thr340	S222 (5.71)-T4L-A235 (6.25)	2.8	206 to 860	+++	
17	Met1	Cys360	M234 (6.24)-T4L-A235(6.25)	7.5	1051 to 2381	+++	
18	Met1	Cys360	Q227(5.76)-T4L-D228(5.78)	8.5	963 to 2097	+++	
19	Met1	Cys360	V220 (5.69)-T4L-A221(5.67)	NB	909 to 1095	+++	
20	Met1	Cys360	S224(5.73)-T4L-V231(6.21)	7.5	1191 to 5410	+++	
21	Met1	Thr340	S224(5.73)-T4L-V231(6.21)	4.6	230 to 1697	+++	
22	Asp18	Thr340	S224(5.73)-T4L-V231(6.21)	0.4	605 to 2538	+++	
N-terminus fusion insertion							
23	T4L-AA-Met26	Thr340	V(5.69)-A(6.25)	NB	506-432	+	
24	APO-Met26	Thr340	V(5.69)-A(6.25)	NB	499-560	+	

Constructs with loss of protein expression relative to WT – 5, 6, 12, 23 and 24. Constructs with diminished binding activity relative to WT – 5, 6, 12, 13, 14-1, 14-2, 15, 16, 17, 18, 19, 20, 21 & 22.

4.3.2.1 Competitive ligand binding assay for measuring CB2 structural integrity

As we assessed the effect of the receptor modification on the expression levels, the binding affinity was tested. Ligand binding at the active site confirms the native structure of the receptor. We performed competitive ligand displacement binding assays to ensure that proper folding occurred and expression and to verify that fusion protein insertion did not compromise the structural integrity of the receptor. In these assays, different ligands including SR144528 as inverse agonist (unlabeled) were used to displace a radioactively ligand. In this case, there is no ambiguity of the unlabeled ligand occupying a different site other than the radiolabeled ligand. We have tested wild type (construct # 1) and truncated variants of CB2 (construct # 3, 6 and 11) for ligand binding capability. All receptors were expressed in Sf9 and the membrane fraction was used for the binding assay. The results indicated that the modifications (i.e., N- and C-terminus truncations) led to diminished binding activity relative to WT – in constructs 5, 6, 12, 13, 14-1, 14-2, 15, 16 , 17, 18, 19, 20, 21 & 22 as illustrated in **(Figure** 4-3**)** and (**Figure** 4-7**)** . In construct 6, we have completely removed the N-terminal of cannabinoid receptor and the loos of the binding affinity was consistent with the decrease the expression levels (**Figure** 4-6**)**. The fusion proteins junction position also has been tested for their ability to maintain the structure of the receptor after insertion. Unfortunately, none of the N-terminus fusion insertion constructs have maintained comparable competitive ligand binding activity compared to wild type. These results are consistence with the receptor expression levels as shown in **(Figure** 4-3**)**. However, the 3ILC fusion protein constructs have shown promising results. All Thirteen constructs were tested for the binding and some of them for the saturation-binding assay as well and showed positive for binding. Only three constructs out of thirteen exhibited no binding after the insertion positions or due to the decrease

in expression levels (12, 15 and 19). Despite the fact that the truncations have shown a diminished in binding profile with the WT, relative CPM counting (CPM of total, specific, and non-specific binding) for the binding of ^{3}H-labeled ligands is significantly lower in some truncation. However in construct # 20, we notice the CPM is higher comparing to other constructs as shown in (**Figure** 4-7**)** and **Table 9**. The non-specific background CPM's window was only 5-fold instead of 10-fold as in WT. This fact suggests that further optimization may be needed to improve the expression level and stability of the recombinant expressed receptor [51].

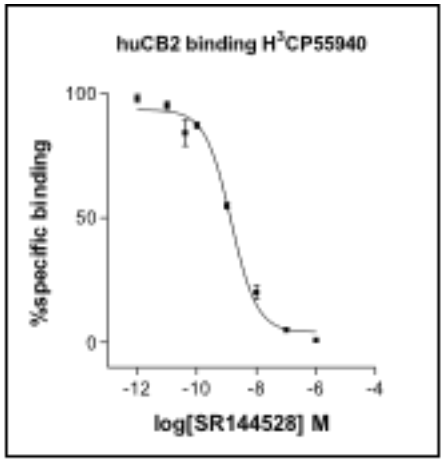

#1	Met1	Cyc360	No fusion
Ki=1.0 nM			

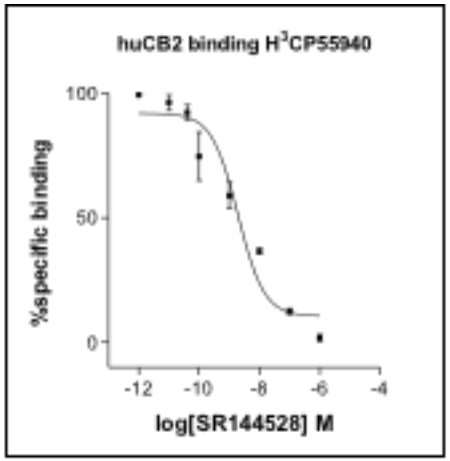

#3	Met1	Cyc340	No fusion
Ki=1.4 nM			

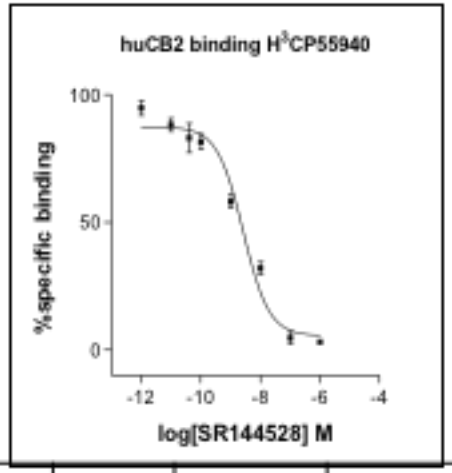

#5	Met1	Gly322	No fusion
Ki=1.9 nM			

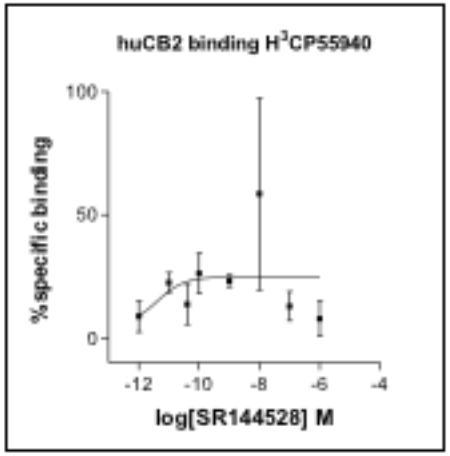

#6	Met26	Cyc360	No fusion
Ki=NB			

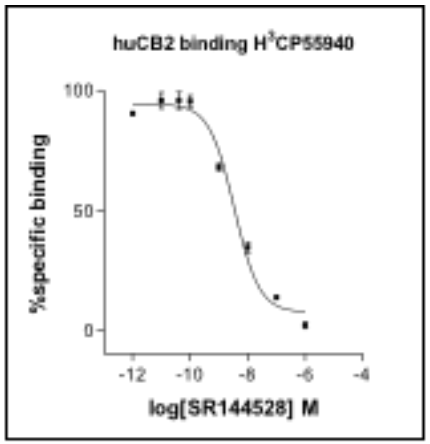

#11	Asp18	Cyc360	No fusion
Ki=2.5 nM			

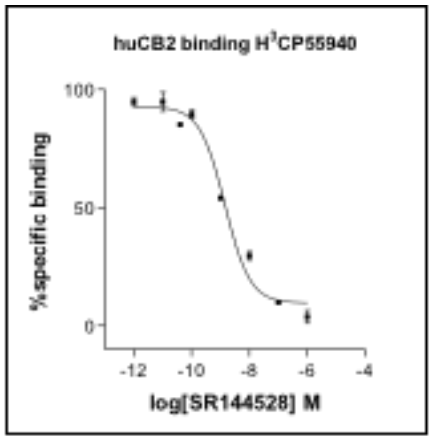

#8	Met1	Thr360	V220(5.69)T4L-A235 (6.25)
Ki=1.0 nM			

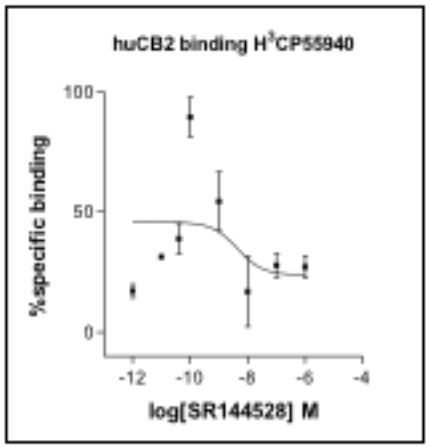

#12	Met26	Gly322	G210(5.59)T4L-L239 (6.29)
Ki=NB			

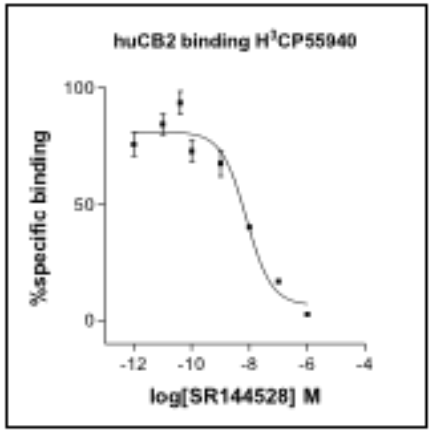

#13	Met1	Thr340	V220(5.69)T4L-A235 (6.25)
Ki=5.7 nM			

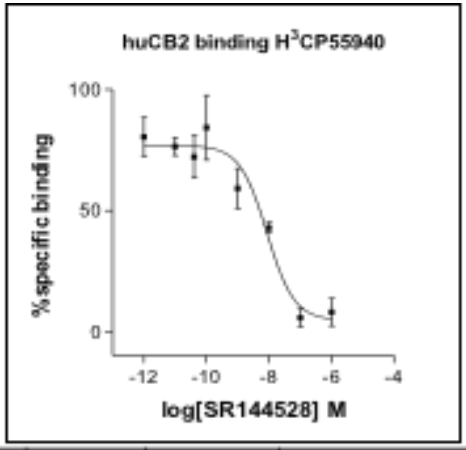

#14-1	Asp18	Thr340	V220(5.69)T4L-A235 (6.25)
Ki=6.3 nM			

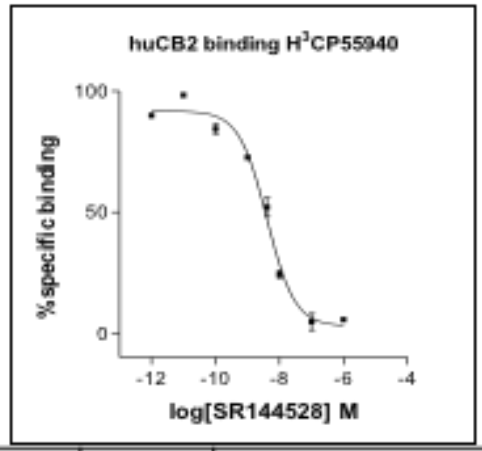

#14-2	Asp18	Thr340	V220(5.69)APO-A235 (6.25)
Ki=2.9 nM			

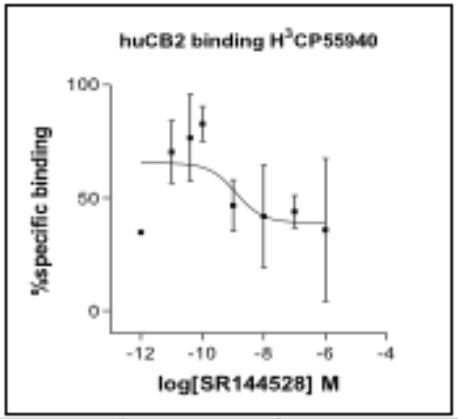

#15	Asp18	Thr340	Q218(5.67)T4L-M237 (6.27)
Ki=NB			

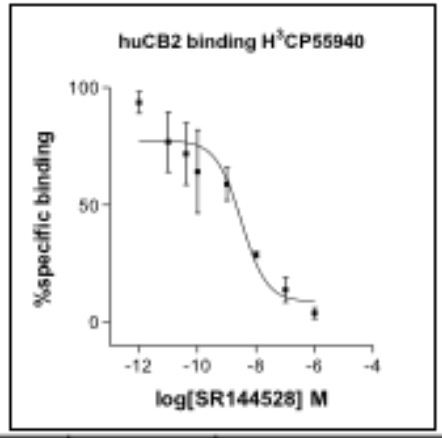

#16	Asp18	Thr340	S222(5.71)T4L-A235 (6.25)
Ki=2.2 nM			

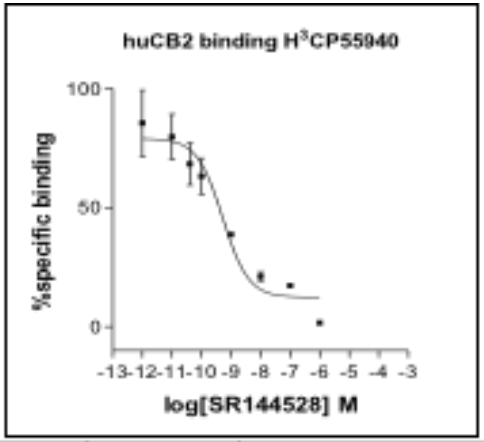

#21	Met1	Cys340	S222(5.73)T4L-A231(6.21)
Ki=4.6 nM			

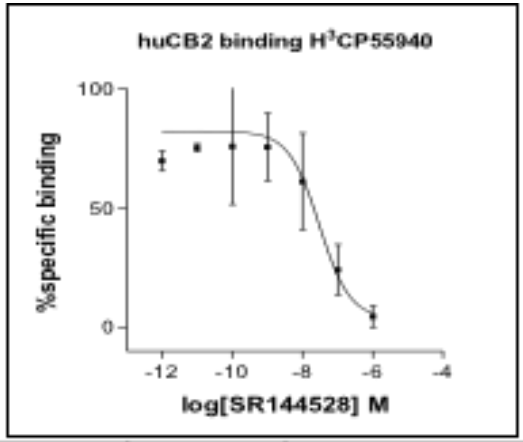

#22	Asp340	Thr340	S222(5.73)T4L-A231(6.21)
Ki=0.4 nM			

Figure 4-7. Competitive binding assay of SR144528 for all CB2 construction.

Competitive binding experiments were performed on membrane proteins harvested from sf9 cells expressing CB2 receptors of various constructs. Competitive displacement of [^{3}H]-CP55, 940 was obtained by using an increased amount of SR144528. Constructs #1, 3, 6 and 11 represent the wild type and N- and or C- terminals truncation receptor binding affinity. All other receptor constructs have fusion protein, with or without truncation. The position for insertion is indicated in the table below each binding. Assay was performed in triplicate (n = 2). Data is represented as mean ± SEM. The dynamic rage of the binding showed in **Table 9**.

4.4 CONCLUSION

Overall, the cannabinoid receptor CB2 appears to be amenable to the fusion protein insertion, similar to the family A class of GPCRs for both expression and ligands binding properties. In the first approach using N-terminal fusion protein -CB2, we were not able to produce large amounts of the protein as well as the receptor integrity was disrupted, which was confirmed by ligand binding assay. However, if we wanted to study the effect of the N-terminal fusion strategies in more detail, a few steps could be explored. For example, determining which N-terminus junction positions is suitable for protein insertion, also how many amino acids need to be removed for both 3ICL and C-terminus. We have demonstrated that the truncated receptors at Asp 18 have no effect on the binding and expression of the receptor. Despite our observation that the N-terminus is not suitable for the fusion protein insertion, the CB2 receptor has showed some tolerance for fusion protein insertion at the 3ICL sites. In this study, we observed the effect of two fusion partners in several constructs. Some of these constructs # (14-B, 20 and 21) could be tested for large-scale purification in Chapter 5.

5.0 PURIFICATION OF FUNCTIONAL CHARACTERIZATION CANNABINOID RECEPTOR CB2 AND BIOPHYSICAL ANALYSIS

5.1 INTRODUCTION

5.1.1 Fusion protein for the functional expression and purification of GPCRs

High-affinity tags are considered efficient tools for expression and purification of proteins. This method is now widespread in biological, structural, and functional proteomics research [325-327]. Variability in heterologous expression, solubility, stability, and functionality of GPCRs, presents a great challenge in purification of large functional quantitates of the protein. The presence of tags is essential for the expression and purification of GPCRs. Tags are divided into two categories, affinity tags, which aid in purification, and solubility tags, which enhance the function and solubility of the protein as shown in **Table 10** [326, 327]. Generally, a combination of these tags are present in most GPCR gene constructs, especially when they are expressed as heterologous proteins in *E. coli* [94]. However, the presence of some of these tags in the proteins after purification may affect the protein conformation, potentially altering the function of the receptor and becoming toxic to the host cell. Native proteins need to be removed by inserting protease susceptible peptide sequences that are amenable to removal of the tag from the protein. Examples of these proteases are shown in **Table 11 .** HA signaling peptides and other helpers, such as β-galactosidase in the N-terminal, are essential for the inner membrane targeting of β2-adrenoceptor in mammalian cell [108]. The presence of maltose-binding protein (MBP) and thioredoxin A (TRX) at both N- and C-terminals, respectively, contribute to an enhanced 40-fold increase of expression and purification of neurotensin NTS1 [48, 113] and CB2 receptors [110]. In addition, MBP is also used as an N-terminal fusion partner for the A2A receptor [112].

To ensure greater implementation of the inner membrane of mammalian or sf9 cell lines, studies of fusion-related methodologies on extensive receptor modification and truncation need to

be performed [94]. A biotin–protein ligase recognition site (BRS) has been used as support in receptor detection and purification. This has previously been implemented the functional expression and purification of CB2 in *E. coli* [328]. BRS was introduced into the C-terminus, upstream of deca-histidine and in the N-terminus. The ligand-binding affinity of these constructs was fully retained, and they were able to generate approximately 1mg of CB2 protein per liter. These methodologies, not only helped in the purification of the protein, but also provided homogeneous support in immobilization. Likewise, Rho-tag at the C-terminal of the CB2/1D4 antibody system has been utilized for functional production, purification, and analysis of the receptor using surface plasmon resonance (SPR). This study was the first to demonstrate the use of a Rho-tag in producing GPCRs in *E. coli*. [328]. The tag was sufficient for immobilization and characterization of the CB2 on a 1D4-coated SPR sensor surface [329].

In our lab, we have previously demonstrated that Mistic and TarCF, as novel fusion partners, have successfully enabled us to express and produce a functional CB2 receptor [110]. Mistic was derived from *B. subtilis* integral membrane protein [330], and TarCF is the carboxylic terminal fragment of a chemotactic response transducer [331]. Our study is the first study to elucidate the effects of introducing both partners in the production of GPCRs. More importantly, the combination Mistic and TarCF fusion proteins led to localization of the receptor in the inner bacterial membrane, which assists in maintaining the function of the receptor. Different cannabinoid ligands were tested, such as CP55, 940, SR144528, WIN 55212-2.

Table 10. All current recombinant affinity and solubility tags.

Adapted [326, 327].

A. Affinity Tag			
Tag Name	Size (aa)	Comments	Reference
Flag	8 aa	Can be used for the purification of either Ca^{2+}-dependent (M1) or Ca^{2+}-independent (M2) and mAB protein. It is introduced in C- or N-terminals.	[332]
Strep tag II	8 aa	Can be used for streptavidin-modified protein, eluted with biotin analog.	[333]
Poly His	6 up to 12 aa	Most commonly used tag for N- and C-terminal, native and denatured protein purification.	[334]
HA tag	9 aa	For hemagglutinin, antibody-based purification. Can be tagged both for N- and C-terminal of the protein.	[326]
T7 Tag	11-16 aa	The purification is antibody based. This tag can be used in N-terminal and internal tagging.	[335]
S tag	15 aa	N- or C-terminal purification using s resin.	[336]
c-myc tag	10 aa	N- or C-terminal tagging; purification is mAb-based purification.	[327]
Chitin-binding domain	51 aa	Bound to chitin. Used for tagging the protein at N- and C-terminal.	[327]
Calmodulin-binding peptide	26 aa	Used for both N- and C-terminal tagged protein and can be eluted by A or EGTA with 1 M NaCl.	[337]
Cellulose-binding domain	27-129 aa	Can be tagged in different positions, at N- or C-terminal, or internally. The protein can be eluted by guanidine HCl or urea > 4 M or ethylene glycol.	[338]
DHFR	25 kda	Can be used as N-terminal fusion protein.	[327]
Poly Arg	5-6 aa	Can be used for C-terminal tagged protein. The protein can be eluted by linear gradient from NaCl.	[339]

B. Solubility Tags			
Tag Name	Size (aa)	Comment	Reference
Thioredoxin	109 aa	It has been used for many GPCR crystal structures to enhance solubility.	[48, 113]
MBP	396 aa	Can be introduced at both N- and C-terminals. It has a role in both enhancing purification and solubility.	[340]
GST	201 aa	Used previously in many GPCR protein solubilities from E.coli such as CB2. Usually tagged at N-terminal of protein.	[110, 117]
NusA	459 aa	It is fused to the N-terminal of the protein. It is needed for solubility and proper folding of the protein.	[341]
SUMO	100 aa	A small ubiquitin-modifying protein. It has been used for N-terminal protein fusion to increase folding and increase solubility. The fusion protein can be removed by using a specific protease.	[342]
Xylanase 10A	163 aa	It has been used to increase the solubility of human β (2)-adrenergic and human A (2A) adenosine receptors for crystallization trials.	[51]
T4 Lysozyme (wild and mutant)	160 aa	Most used fusion protein for solubilization of GPCR junction to N-terminal and internal portion of the protein for the purpose of crystallization.	[51]
apocytochrome b562RIL	106 aa		

Table 11. Proteases commonly used for tagging and fusion removal.

Adapted from [18] and [326, 327].

Name of protease	Cleavage site	Comment	Reference
TEV protease	EQLYFQ*__G__	It is highly specific and suitable for low temperatures.	[343]
Thrombin	LVPR*__GS__	It performs some non-specific cleavage due to impurities. It is less sensitive to detergent compared to other proteases.	[344]
Factor Xa	IDGR*	Factor Xa has two disulfide links, which may be sensitive for reduction in the buffer.	[345, 346]
Enterokinase	DDDDK*	Cleavage efficiency is 61 - 88%. May have unintended cleavage site.	[345]
SUMO	SUMO proteases S. cerevisiae Ulp1	It is preferable in wide pH ranges and temperatures; a good choice in inclusion body purification.	[347]
PreScission	LEVLFQ*__GP__	The advantage over others is maintenance of optimal activity at 4°C for cleaving many fusion proteins.	[348, 349]
3C protease	ETLFQ*__GP__		
Aminopeptidase M	Exopeptidase	Cleaves N-terminal, does not cleave X-P.	[350, 351]
DAPase (TAGZyme)	Exo(di)peptidase	It used for cleaving His tag at N-terminal with 75–90% cleavage recovery.	[352]
Granzyme B	D*X, N*X, M*N, S*X	Serine proteases show highly specific and efficient processing.	[353]
Sortase A	LPET*__G__	Recognizes and cleaves the Thr–Gly bond in LPXTG sequence in presence of Ca^{2+} and/or triglycine.	[354]
Carboxypeptidase A	Exopeptidase	Cleaves C-terminal. No cleavage at X-R, P.	[350, 351]
Carboxypeptidase B	Exopeptidase	Cleaves C-terminal R, K.	[350, 351]
Intein	Self-cleavable	Self-splicing catalyzation by post-translational process.	[355]
Aeromonas aminopeptidase	Exopeptidase	Cleaves N-terminal, effective on M, L. Requires Zn.	[351]

5.1.2 Current methodologies for purification of GPCRs and cannabinoid receptor CB2

The native environment where a membrane protein is inserted and expressed is altered after the extraction and purification of the protein. The thermal stability of GPCRs is significantly lower after solubilization and cell disruption [94], [356]. Therefore, exaggerated and overheated forces should be avoided during the entire purification process. The process of membrane protein purification begins with lysing or breaking the cell membrane. There is considerable variability in cell membrane composition of different host cells, and bacterial membranes are considered rigid and not easy to break [94]. Consequently, alternative lysis agents, such as lysozymes are added. Conversely, mammalian and insect cell biological membranes are susceptible to easy breakage. Each method requires a different buffer be used for cell disruption before solubilization. In mammalian and insect cells, a hypotonic buffer (low salt) flow to a hypertonic buffer (up to 1.0 M NaCl) in a freeze-thaw or mechanical process (e.g. dounce homogenization), is the most common way to achieve cell disruption and remove cytoplasmic proteins [357]. Notably, the entire process requires ice and protease inhibitors (e.g. PMSF, benzamidine, leupeptin or protease cocktails) to minimize proteolytic degradation. Several studies have been performed to identify a family of structurally related detergents for GPCR extraction from mammalian cells [358]. It has been shown that many GPCRs are not stable in certain types of detergents due to their inherent structural flexibility [48]. These detergents are used alone or in combination for testing the extraction of the membrane proteins after cell lysis. **Table 12** provides the most commonly used detergents for crystallography. In order to remove the N- and C-termini tags after purification, the detergents must be compatible with protease cleavage. In addition, the thiol group of the cysteine residues within the receptor need to be blocked to reduce the aggregation. This is commonly achieved by

incorporation of either an alkylating agent, such as iodoacetamide, or a reducing agent, such as tris2-carboxyethylphosphine (TCEP) or dithiothreitol (DTT). Although the extent of detergent solubilization varies from receptor to receptor, the purpose behind the use of detergent is a key selection criteria. For example, different studies have shown that mixtures of NG, HPTO, HTG, DDM, LDAO and OG have been successful in solubilizing the bovine Rhodopsin [140, 359-362]. However, from the crystallization standpoint for other GPCRs there are other preferable detergents. DDM and DM at concentrations of (0.5–1.0%, w/v) and (1.5–2% w/v) respectively are the most common detergents [356]. Compared to the widely used conventional detergents such as *n*-dodecyl β-D-maltoside (DDM) and tetradecylphosphocholine (FC14), certain kinds of maltose-neopentyl glycol (MGN) detergents have been successfully used to solubilize many GPCRs [60, 363]. In some cases, the use of MGN rather than DDM was necessary to obtain high-resolution GPCR crystal structures [363]. A mixture of sodium cholate with digitonin or LMNG or DDM have also been used at (0.2-0.35%) to determine the structure of the human M2 muscarinic receptor, human protease-activated receptor 1, human OX2 orexin and δ-opioid receptor [66, 67, 69, 151]. The addition of a cholesterol derivative to the solubilization process at concentrations in the range (0.1–0.3%) w/v was necessary [356]. Cholesterol is known to stabilize GPCR structures while maintaining their activity. It has been co-crystallized with several GPCRs catalogued in the PDB [364].

Table 12. List of detergents with corresponding CMC values tested for GPCR extraction from mammalian cells and insect cells.

	Detergents	CMC (mM)	Ref
1	n-octyl-b-D-glucopyranoside	23.4	[365]
2	n-decyl-b-D-maltoside	1.8	[366]
3	n-dodecyl-b-D-maltoside (DDM)	0.17	[367]
4	Cyclohexyl-butyl-b-D-maltoside (Cymal-4)	4.76	[368]
5	Cyclohexyl-pentyl-b-D-maltoside (Cymal-5)	2.4	[368]
6	Cyclohexyl-hexyl-b-D-maltoside (Cymal-6)	0.56	[368]
7	Cholic Acid, Sodium Salt	9.5-14	[369]
8	Cyclohexyl-heptyl-b-D-maltoside (Cymal-7)	0.19	[368]
9	n-octylphosphocholine (Fos-choline-8)	114	[370]
10	n-decylphosphocholine (Fos-choline-10)	11	[371]
11	3[(3cholamidopropyl)dimethylammonio]-1-propanesulfonate hydrate (CHAPS)	8	[372]
12	Diheptanoyl-phosphocholine (DHPC)	1.4	[373]
13	n-tetradecylphosphocholine (Fos-Choline-14)	0.12	[374]
14	Lauryl Maltose Neopentyl Glycol (MNG)	0.01	[363]

The solubilization of the CB2 receptor from bacterial membranes has been evaluated. At least 40 detergents from different classes were screened for solubilization. It was evident that only a few detergents were able to maintain receptor binding during the solubilization [375]. Mixtures of relatively high concentrations of dodecyl maltoside (DDM) (1% w/v) and CHAPS (0.5% w/v), in combination with cholesterol was among the more efficient detergents identified [375]. Similarly, the combination of DDM, CHAPS and CHS for the stabilization of GPCRs was also reported for the neurotensin receptor with an efficiency of 85% [50]. These high concentrations of detergents are only required for the solubilization process. After the solubilization process, the subsequent amount of the detergents in the purification buffer can be reduced 10-30 times according to the critical micelle concentration (CMC). This decrease in detergents allows the protein to remain in the folded, soluble, functional form [364] . In the case of CB2 receptor, the detergent was reduced to 0.1%, 0.5% and 0.1% for DDM, CHAPS and CHS respectively [375].

In chapter 4.0 we discussed a couple of CB2 candidate constructs for large-scale purification. We evaluated the fusion protein junction position for the various CB2 constructs. Construct # 20 was the most ideal in regards to the expression, and binding of the receptor.

Throughout this chapter, we assessed the stability profiles of membrane proteins within different detergents in the presence and absence of ligands before executing the entire process of purification. Multistep purifications that were conducted using immobilized metal affinity chromatography (IMAC), M2 Flag, and other separation techniques were performed. During the purification process, optimization of various conditions of additives, buffer components, and cleavage processes were assessed in an attempt to maintain the structural and functional integrity of expressed CB2 proteins. The purified protein obtained from this this study will be tested in pre-crystallization trials in the future.

5.2 MATERIAL AND METHODS

5.2.1 Optimized large scale productionCB2 pellets for detergent extraction and purification

Pellets of CB2–fusion constructs #20, 21 and 22 in **Table 9** were produced by infecting the P2 of the corresponding virus at ration of 1:50 to 3 L of Sf9 at 2.5 x 10^6 cells/ml. The cells were grown and maintained in sf 900 II SFM (life technology) throughout the process. We have determined the viral titer for all construct using plaque assay as mention in 4.2.5.3 .The MOI was 0.75. The cells were kept in the shaker for 50 hours at 27°C. Cell pellets were collected by centrifugation the cell at 4500 RPM for 15 minutes in JA 10 rotor using The Beckman Avanti J-30I centrifuge. The pellet was washed using sf900 media and centrifuged again. Cell pellets stored at -20°C until further use.

5.2.2 Detergent extraction analysis to carry out purifications

To optimize detergent solubilization, we tested the solubility of constructs # 20 and 14 in three different detergents namely (n-dodecyl-b-D-maltoside (DDM), n-tetradecylphosphocholine (Fos-Choline-14) and Lauryl Maltose Neopentyl Glycol (MNG) with or without 0.2% of sodium cholate. All detergents were purchased from Anatrace (Maumee, OH). The membrane fractions from sf9 expressing the CB2- fusion proteins were lysed in 10mM Tris (pH 7.6), 1 mM EDTA (pH 8.0), 2mg/ml of iodoacetamide and protease inhibitors in the presence of the inverse agonist (SR144528 10mM) and stirred at 4°C for 30 minutes. Then, resulting mixture was centrifugation at 18,000 RPM for 15 minutes. All CB2 containing pellets were re-suspended in basic buffer then

split into ten parts in to which corresponding detergents were added. The concentrations of detergents used was 1% and 0.5% for DDM and CHAPS respectively. The buffer containing detergents and membrane protein homogenized 20 times in the dounce homogenizer and incubated at 4°C and stirred for four hours. Samples were collected after four hours by centrifugation at 20,000 RPM for 90 minutes and both the soluble fraction and pellet were evaluated by western blotting (more details in **Table 19** in **Appendix B**).

5.2.3 Large-scale preparatory purification of pFastBac-Flag-TEV-1-CB (T4L 224-231) 340-TEV-6His

5.2.3.1 Immobilized metal affinity purification

Insect cell membranes were disrupted by thawing frozen cell pellets in lysis buffer containing 10 mM Tris (pH 7.6), 1mM EDTA (pH 8.0), 2mg/ml IA powder,10 mM SR144528, and protease inhibitor cocktail (Roche) with brief dounce homogenization 30 times. The insoluble materials resulting from centrifugation of the pellets (18,000 rpm for 15 minutes at 4°C) were solubilized in buffer containing 1% DDM, 0.3% CHS, 0.5% CHAPS, 30mM HEPES (pH 7.8), 750 mM NaCl, 30% glycerol, 2mg/ml IA powder, 2uM mM SR144528, and protease inhibitor cocktail (Roche). After four hours of stirring in solubilization buffer at 4°C, the supernatant was isolated by centrifugation at 20,000 rpm for 90 minutes. The supernatant was then loaded into an IMAC column (GE Healthcare His trap HP), which had been pre-equilibrated with column buffer. The pre-equilibration buffer consisted of 0.1% DDM, 0.1% CHS, 0.5% CHAPS, 30 mM HEPES (pH 7.8), 750 mM NaCl, 30% glycerol, 2uM SR144528, and 40 mM imidazole to removal of non-specifically bound proteins. The column was then washed with the same buffer, but the imidazole

concentration was raised to 70 mM. The protein was eluted with four column volumes of 0.1% DDM, 0.1% CHS, 0.5% CHAPS, 30 mM HEPES (pH 7.8), 750 mM NaCl, 30% glycerol, and 2 uM SR14528 supplemented with 400 mM imidazole. The eluted protein was concentrated using an Amicon concentrator (Millipore, MWCO-~30 kDa), and the protein concentration of the solution was determined using the Bradford assay. We added 5 mM (1mg/ml) IA before the final concentration was stored at -80°C. The protein purity and expression was evaluated in 12% SDS-page gels.

5.2.3.2 Flag purification

Typically, the appearance of purified CB2 protein (IMAC) on Coomassie brilliant blue gel determines the need for Flag purification. Briefly, Flag resin (A2220, sigma), 3 ml/L of pellet, was used for more purifying steps of CB2 protein. The beads had been equilibrated in advance with Flag wash buffer (0.1% DDM, 0.1% CHS, 0.5% CHAPS, 30 mM HEPES, 500 mM NaCl, 2 uM SR144528) before used. The beads were then mixed with CB2 elution samples (IMAC elution from previous steps) and incubated at 4°C and stirred for four hours. The beads were then washed twice (~15 ml each) with buffer contains 10 -fold reduced in detergents (0.05% DDM, 0.01% CHS, 0.05% CHAPS, 30 mM HEPES, 500 mM NaCl, 2 uM SR144528. Then the CB2 eluted from the beads using 10 ml of buffer (0.05% DDM, 0.01% CHS, 0.05% CHAPS, 30 mM HEPES, 500 mM NaCl, 2 uM SR144528) containing 100 μL of Flag peptide (final conc. ~200 uM, 0.2 mg/ml) and 200 μL of EDTA (0.25 M). The Flag eluents was tested for the amount of the protein and concentrated to small volume of 0.4 ml using a 10 kDa molecular weight cut off concentrator.

5.2.3.3 Cleavage and deglycosylation

It has been shown previously that non-glycosylated and glycosylated versions of CB2 receptor can form specifically when using His-tag at the C-terminus [316]. Thus, it may be necessary to treat the purified receptor with glycosylation. The concentrated CB2 protein was deglycosylated by incubation with N-glycosidase F (PNGase F) overnight at 4°C. To remove the Flag and 6x His tags from the deglycosylated protein, incubation samples with TEV protease was carried out for three hours at 30°C then overnight at 4°C to ensure cleavage efficiency. The cleaved, purified protein was then subjected to size exclusion chromatography (SEC).

5.2.3.4 Size exclusion chromatography

Size exclusion chromatography (SEC) purification was conducted on a column (Superdex 200 10/300 GL) equilibrated with SEC washing buffer (0.1% DDM, 0.1% CHS, 0.5% CHAPS, 30 mM HEPES, 500 mM NaCl, 2 uM SR144528) for three column volume. Then, each of the eluents loaded into the column at a rate of 0.5 ml/min. The proteins elations were monitored by UV absorbance using an AKTA purifier machine. The eluted proteins fractionations by volume were analyzed using SDS-PAGE.

5.2.4 Protein titration assay for the ligand binding

The eluted CB2 proteins were tested for their ability to bind radioactive ligands. In order to use the protein efficiently and determine the amount of proteins required for the saturation binding assay, we performed a protein titration assay by fixing the amount of radioactive ligands (^{3}H-SR144528 and ^{3}H -CP44,940) to be 2 nM per well. The total reaction volume was 200 µL/well.

Each well was filled with 50 mM Tris-HCl (pH 7.4), 5 mM $MgCl_2$, 2.5 mM EGTA, and 0.1% (w/v) fatty acid-free BSA and supplemented with 10% dimethyl sulfoxide and 0.4% methylcellulose. The protein concentration varied between 0.1 and 10 μg. We also mimicked the purification buffer by adding 0.1 to 1% DDM to the reaction buffer. Assays were performed in duplicate and data points were analyzed in (Prism 5, GraphPad). We used the Unifilter GF/C filter plates to harvest and terminate the reaction. MicroScint-20 Scintillators (PerkinElmer) were used to detect CPMs using the TopCount NXT machine.

5.2.5 ^{3}H-CP55940 saturation and binding assay for purified protein

The competitive radiolabeled ligand binding assays for CB2 receptors after purification were performed using a Perkin Elmer 96-well Top Counter to determine the cannabinoid receptor binding affinity (K_i) for CB2 inverse agonist by displacing [^{3}H]-CP55,940 (specific activity: 88.3 Ci/mmol) [376]. In short, the inverse agonist (SR144528) was diluted in binding buffer (50 mM Tris-HCl (pH 7.4), 5 mM $MgCl_2$, 2.5 mM EGTA, and 0.1% (w/v) fatty acid-free BSA) and supplemented with 1% dimethyl sulfoxide and 0.4% methylcellulose. We also included the detergents and lipid to mimic the elution buffer and maintain structure. Each assay plate well contained a total of 200 μL of reaction mixture comprising 5 μg of purified CB2, labeled [^{3}H]-CP55,940 at a final concentration of 3 nM, with the unlabeled ligand at varying dilutions. Plates were incubated at 30°C for one hour with gentle shaking. The reaction was terminated by rapid filtration through Unifilter GF/B filter plates using a UniFilter cell harvester (PerkinElmer). After the plate was allowed to dry overnight, 40 μL of MicroScint-0 cocktail (PerkinElmer) was added to each well, and radioactivity was counted with a PerkinElmer TopCount. All assays were

performed in duplicate and data points were represented as mean ± range. The K_i was calculated using nonlinear regression analysis (Cheng-Prusoff equation).

Saturation binding experiments were performed in order to characterize receptor expression and the quality of the receptor after purification. The experiments were carried out as previously described [376]. The method measures the total and non-specific binding at various concentrations of the radioligand. Two values are calculated from data: K_d (equilibrium dissociation constant) and B_{max} (receptor density). Briefly, the purified receptor (10 μg) was incubated with increasing concentrations of [^{3}H] (CP55,940) (0.01–5nM) in 96-well plates at 30°C with slow shaking for one hour. The incubation buffer was composed of 50 mM Tris–HCl (pH 7.4), 5 mM $MgCl_2$, 2.5 mM EGTA, and 0.1% (w/v) fatty acid-free BSA and supplemented with detergents and lipid. Radiolabeled ligand was diluted in incubation buffer and supplemented with 10% dimethyl sulfoxide and 0.4% methylcellulose. Non-specific binding was determined in the presence of 1:1000 unlabeled SR144528 (5000 nM) in excess. The reaction was terminated by rapid filtration through Unifilter GF/C filter plates using a Unifilter Cell Harvester (PerkinElmer). After the plate was allowed to dry overnight, 40μL of MicroScint-20 cocktail (PerkinElmer) was added to each well, and radioactivity was counted using a PerkinElmer TopCount.

5.2.6 In gel trypsin digestion

The gel trypsin digestion method was carried out as previously described [377]. Excised gel bands were washed with HPLC water and destained with 50% acetonitrile (ACN)/25mM ammonium bicarbonate until there was no visible staining. Gel pieces were dehydrated with 100% ACN, reduced with 10mM dithiothreitol (DTT) at 56°C for 1 hour, followed by alkylation with 55mM iodoacetamide (IAA) at room temperature for 45min in the dark. Gel pieces were then again

dehydrated with 100% ACN to remove excess DTT and IAA, and rehydrated with 20ng/µl trypsin/25mM ammonium bicarbonate and digested overnight at 37°C. The resultant tryptic peptides were extracted with 70% CAN 5% / formic acid, vacuum dried and re-constituted in 18µl 0.1% formic acid.

5.2.7 Tandem mass spectrometry

Proteolytic peptides from in gel trypsin digestion were analyzed by a nanoflow reverse-phased liquid chromatography tandem mass spectrometry (LC-MS/MS). Tryptic peptides were loaded onto a C18 column (PicoChip™column packed with 10.5cm Reprosil C18 3µm120Å chromatography media with a 75µm ID column and a 15µm tip, New Objective, Inc., Woburn, MA) using a Dionex HPLC system (Dionex Ultimate 3000, ThermoFisher Scientific, San Jose, CA) operated with a double-split system (Personal communication with Dr. Steve Gygi from Department of Cell Biology, Harvard Medical School) to provide an in-column nano-flow rate (~300nl/min). Mobile phases used were 0.1% formic acid for A and 0.1% formic acid in acetonitrile. Peptides were eluted off the column using a 52 minute gradient (2-40% in 42 min, 40-95% in 1min, 95% for 1 min, 2% for 8 min) and injected into a linear ion trap MS (LTQ-XL, Thermo Fisher Scientific) through electrospray.

The LTQ XL was operated in a date-dependent MS/MS mode in which each full MS spectrum [acquired at 30000 automatic gain control (AGC) target, 50 ms maximum ion accumulation time, precursor ion selection range of m/z 300 to 1800] was followed by MS/MS scans of the 5 most abundant molecular ions determined from full MS scan (acquired based on the setting of 1000 signal threshold, 10000 AGC target, 100ms maximum accumulation time, 2.0 Da isolation width,

30 ms activation time and 35% normalized collision energy). Dynamic exclusion was enabled to minimize redundant selection of peptides previously selected for CID.

5.2.8 Peptide identification by database search

MS/MS spectra were searched using MASCOT search engine (Version 2.4.0, Matrix Science Ltd) against the UniProt human proteome database. The following modifications were used: static modification of cysteine (carboxyamidomethylation, +57.05 Da), variable modification of methionine (oxidation, +15.99Da). The mass tolerance was set at 1.4 Da for the precursor ions and 0.8 Da for the fragment ions. Peptide identifications were filtered using PeptideProphet™ and ProteinProphet® algorithms with a protein threshold cutoff of 99% and peptide threshold cutoff of 90% implemented in Scaffold™ (Proteome Software, Portland, Oregon, USA).

5.2.9 Circular dichroism spectroscopy

Circular dichroism spectra were recorded on the CD (Spectroscopy JASCO J-810) at 20 °C in a path length 1 mm quartz over the wavelength range of 190nm to 300 nm with average time of 5 seconds. Spectrum for purified CB2-T4L monomers (construct #21) were blanked to CD buffer (30mM phosphate buffer (pH7.8), 0.1% DDM, 150 mM NaCl and 10% glycerol). After baseline (buffer) subtraction, the mean residue molar ellipticity was calculated to all ranges and it is present in Θ MRM (deg X cm2 X dmol-1). The percentage of α-helix was calculated using the following equation: (-[θ222] + 3000)/39000 [378]. Moreover, we used K2D2 software to conform the result of the secondary structure of the purified receptor CB2-T4L and SOPMA calculations to predict the wild type α and β strand percentage content [379].

5.3 RESULTS AND DISCUSSION

5.3.1 Detergent screening

In an effort to determine the class of detergents that can effectively solubilize the CB2 – fusion from the extracted membrane fraction, numerous detergents were screened. These detergents were considered mild enough to not degrade protein structure and functionality. We used a set of three detergents known for having the highest solubility in GPCRs [60, 363], supplemented in buffers to identify the detergent with the highest membrane protein solubilizing capability. DDM and CHS have been widely utilized, among other detergents for pursuing lipid cubic phase (LCP) [356]. Cholesterol was required to support the receptor during extraction and to reduce conformational changes [356]. Since solubilization of GPCRs is dependent upon the formation of micelles in solution, it is important to increase the detergent concentration at this specific step to facilitate the membrane protein extraction for cell membrane [94]. The critical micelle concentration (CMC) for each detergent is the key factor for efficient solubilization. It is vital to keep the detergent at least 2-3 times higher than the CMC. Lowering this concentration may cause the protein to dissociate from the micelles and lead to aggregation. DDM, Fos-Choline-14, and MNG are known for their lower CMCs. Thus, in our lab and our collaborator's lab, we compared the solubilization and extraction effect in the presence of 0.2% sodium cholate as shown in (**Figure 5-1)**. The results clearly demonstrate that all three detergents in both concentrations, 1% and 0.5%, were efficient at extracting the protein with almost identical efficiency. Crystallization using LCP is a common method, thus, we decided to use a concentration of 1% and 0.5% from DDM for solubilization and immobilized metal affinity purification, respectively.

Figure 5-1 B also clearly shows that the pellets were extracted completely from the receptor for all three detergents which were analyzed by the western blot.

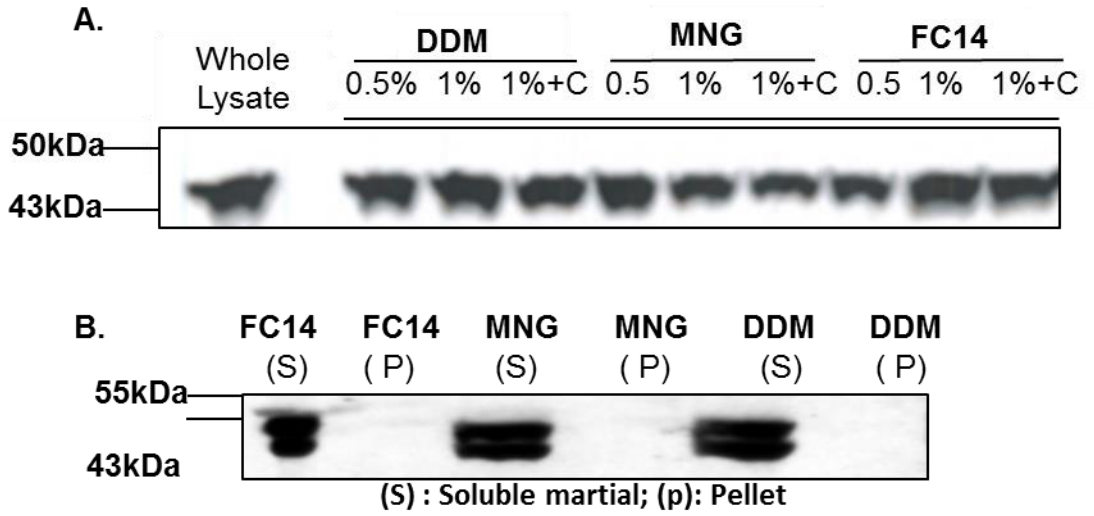

Figure 5-1. CB2- fusion protein detergents screening analysis by western blot.

A. Construct #8 carries T4 lysozyme expressed in Sf9 lysate, subjected to three different detergents in different concentrations, with or without 0.2% sodium cholate. All detergents can extract CB2 receptor efficiently. The receptor was detected by anti-Flag antibody (provided by our collaborator).

B. Construct #14-2 carries different fusion protein (apocytochrome b526), also tested with the same detergents. Equal protein amounts of soluble fractions and pellets were analyzed. The western blot shows complete extraction of the receptor and no trace in pellet. The receptor was detected by anti-Flag antibody.

5.3.2 Purification the CB-fusion pFastBAC: CB2 1 – T4 (224-231) Δ C terminal

Fifteen grams of cell pellets infected with third-generation recombinant virus for 50 hours (construct#21) was used as the starting material for the purification. Pellets were lysed and the receptor extracted in the presence of 1%, 0.5%, and 0.3% DDM, CHS, and CHAPS, respectively. Although CHAPS is not necessary in the purification of many other GPCRs, using a zwitterionic detergent, such as CHAPS, for cannabinoid receptor CB2 purification was necessary for both solubilization and maintaining the function of CB2 in micelles [380]. Moreover, CHAPS is also required to increase solubility of cholesterol in aqueous media. The presence of CHS and the inverse agonist, SR144528, maintain the receptor in its correctly folded state and mimics the receptor's natural state. **Figure 5-2** illustrates a schematic diagram of the overall steps involved in the extraction and purification of CB2 receptor from infected insect cells. In the first step of purification, a simple imidazole IMAC chromatography was conducted as presented in **(Figure 5-3 A)**. Briefly, CB2 1 – T4 (224-231) Δ C terminal was eluted from the IMAC column at pH 8, with 400 mM imidazole as a double band, ~57 kDa. Noticeably, contaminating proteins were less than ~30 kDa as determined by SDS PAGE CBB staining (**Figure 5-3 B**). Meanwhile, the N-terminal of the cannabinoid receptor CB2 has two positions of asparagine, making it susceptible to glycosylation. Although we have used PNGase F to eliminate glycosylation in non-denaturing conditions, a small trace of the glycosylated protein is still present. The double band typically represents the glycosylated version of the receptor. In addition, the amount of protein extracted from the pellet was significantly lower, indicating that increased time and solubilizing buffer are required. Due to the presence of the Flag tag at the N-terminal of the CB2-fusion protein, further purification was conducted using Flag resin to rectify the protein impurities.

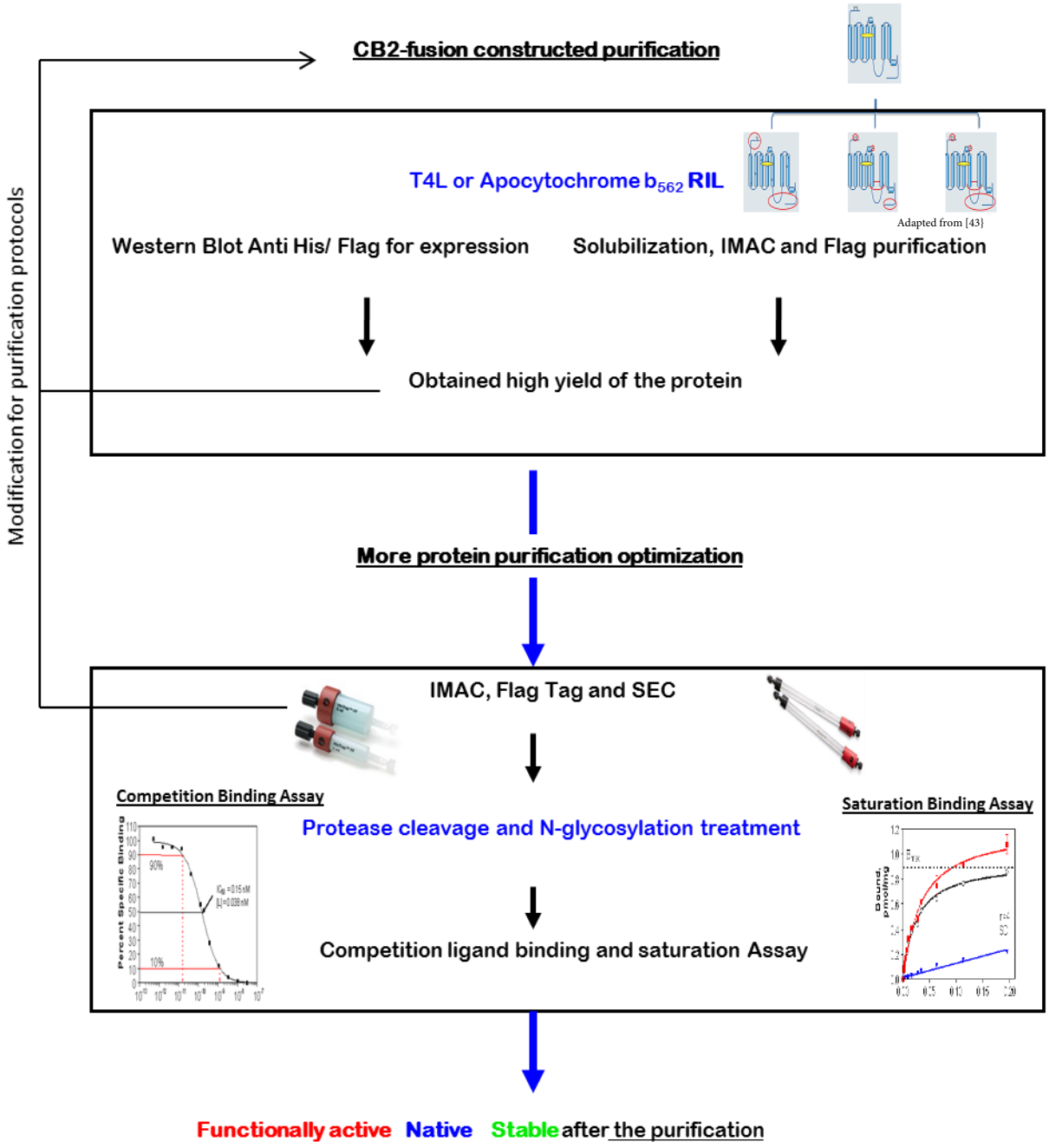

Figure 5-2. Schematic flow diagram for the processes required for the purification of chimeric receptor CB2 from sf9.

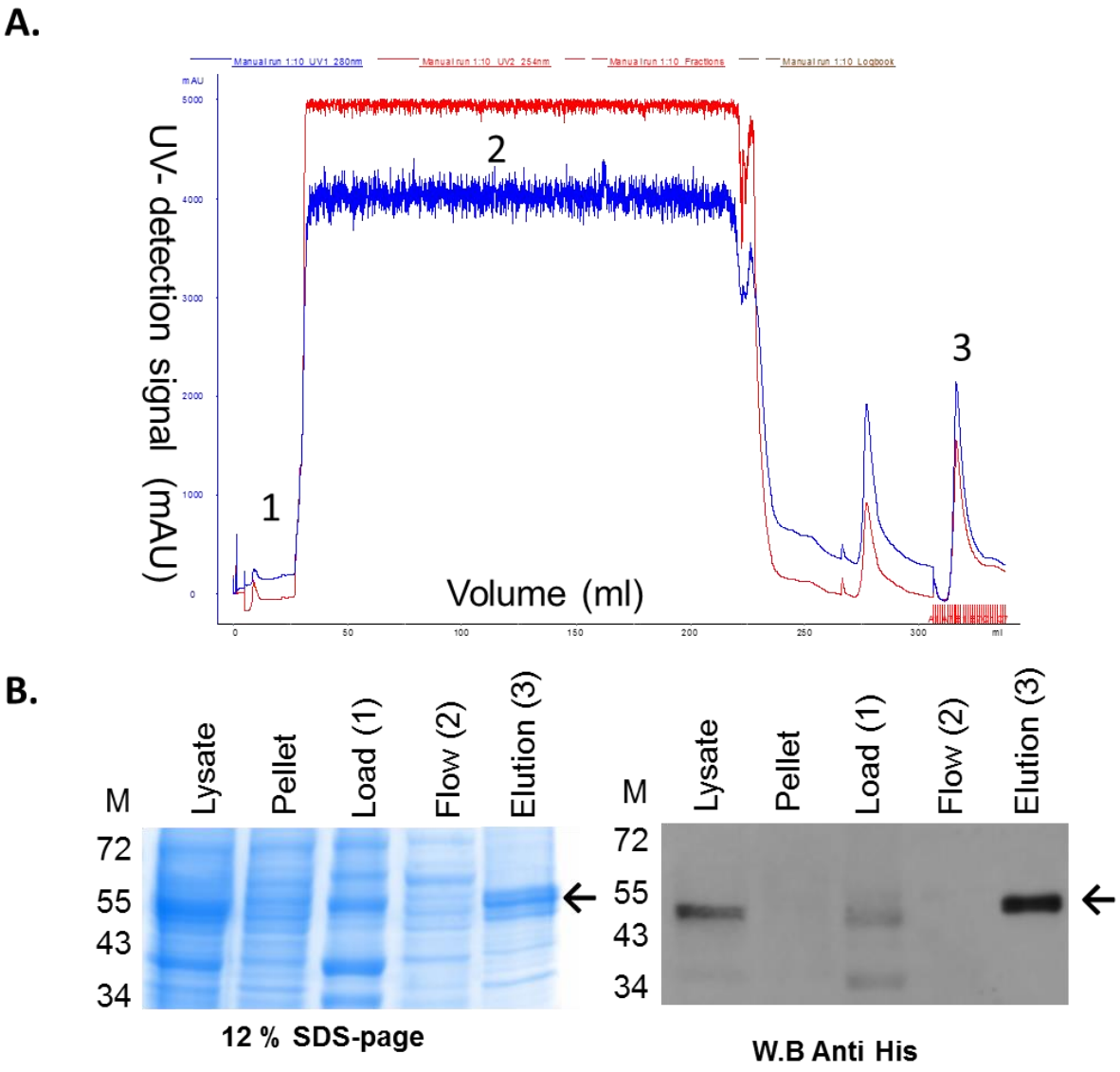

Figure 5-3. Scaled–up purification steps for CB2 1 – T4 (224-231) Δ C-terminal.

A. Multi-step purification on-column chromatography process using Äkta purifier. Two peaks appear in the washing and elution steps.

B. SDS-page and WB for CB2 1 – T4 (224-231) Δ C-terminal extracted by detergents DDM, CHS and CHAPS and purified by affinity chromatography (Ni^{2+}) column.

The IMAC eluent was incubated with Flag resin and eluted using the conventional method (i.e. Flag peptide and EDTA to chelate Ca^{+2} required for Flag–protein binding). Afterwards, CB2-fusion flag eluent protein was subjected to size exclusion chromatography using a Superdex column (10/300 GL GE Healthcare) to improve protein purity (**Figure 5-4 A)**. Moreover, SEC was used to separate the monomeric protein from other polymeric proteins that tend to aggregate at high molecular weights. As illustrated in (**Figure 5-4 B)**, the concentrated eluent of protein was loaded onto the SEC column and produced two separate peaks. The first peak is the monomeric peak, while the second one represents the flag peptide in the elution buffer. The amount of protein was considerably low for SDS-PAGE determination. All protein analyses were confirmed and tracked using western blotting.

In conclusion, we carried out the purification of CB2 by subjecting construct #21 to anti-Flag and 6 histidine (His6) tags and analyzed SR144528 as an inverse agonist. The protein was purified by a Ni-column followed by anti-Flag resins as shown in (**Figure 5-3)** and (**Figure 5-4)**. We were able to successfully purify ~0.6 mg CB2-T4L of fusion protein (construct # 21) from each liter of Sf9 cells, which was sufficient for proceeding with more biophysical studies. We also performed the complete purification analysis total protein, specific binding activity, and percent yield–after each step of the purification. This data allowed us to directly compare and evaluate the expression and purification strategies as presented in (**Figure 5-4 C)** and **Table 13**. We observed that specific activity is significantly increased 4-fold from 2039 CPM/10 µg of protein at the first step of solubilization to 8706 CPM/ 10 µg of protein at the last step.

A.

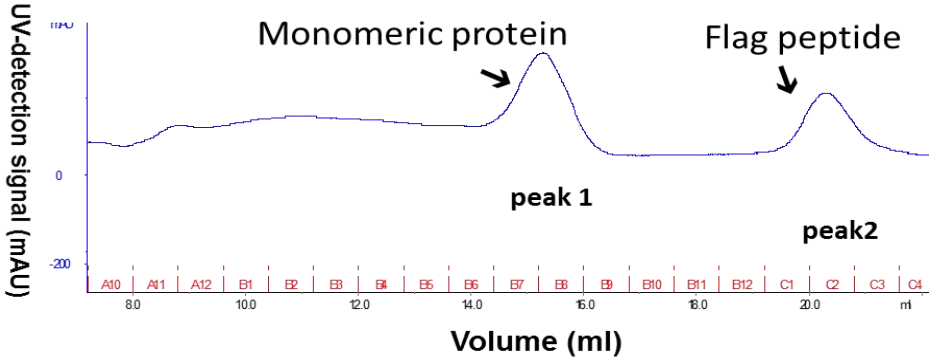

B.

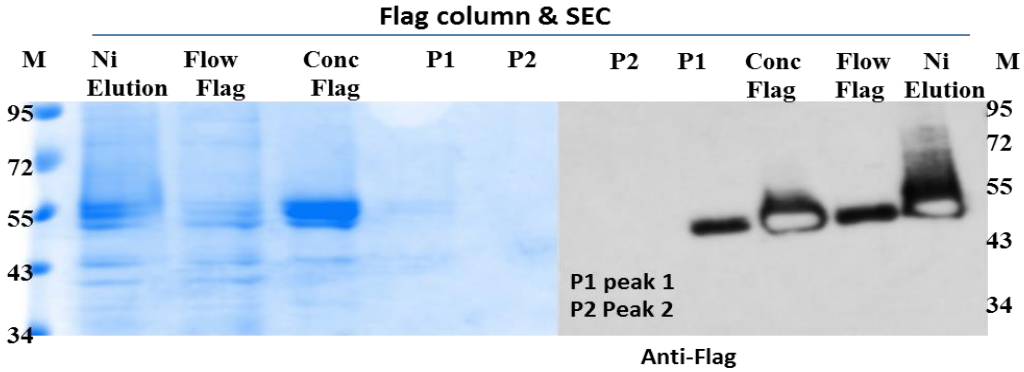

Table 13. C. Protein analysis throughout the construct #21 purification.

		Protein concentration (mg/ml)	Volume (ml)	Total protein (mg)	Yield %	Specific activity
	Whole lysate	2.25	150	337.5	100	B_{max} = 2039 CPM/10 µg K_D : 11.68 nM K_i =6.3 nM
In column	Soluble material	1.3	145	188.5	55.8	-
	Flow through	0.545	145	79.025	23.4	-
	Wash (non-specific peak)	0.4	15	6	1.7	-
	Elution	0.6	12	7.2	2.1	B_{max} =8706 CPM/10 µg K_D : 12.68 nM K_i =30 nM

Figure 5-4. Flag purification and gel filtration for 1 – T4 (224-231) Δ C-terminal.

A. The chromatography step of the Flag eluent for construct #21

B. SDS page and western blot for Flag and SEC purification

C. Analysis table for purification.

5.3.3 Purification of CB2-fusion CB2 18 – T4 (224-231) Δ C-terminal

To avoid the glycosylation removal step, which was not efficient in previous purifications, we selected a construct with a truncated amino acid 18. Construct #22 is similar to #20 with the exception of the N-terminus truncation. To remain consistent and eliminate variability in the purification, we have performed the same conditions for expression, receptor extraction, and purification. Throughout previous purifications, solubilization was not optimal (**Figure 5-3)**. Thus, increased the time for solubilization up to six hours at 4°C. Approximately nine grams of supernatant were collected from one liter and solubilized to CB2 protein. Treatment with DNA breaking enzymes (Pierce Universal Nuclease) was added at a concentration of 10U/L of culture. This incubation step was carried out at 4°C for half an hour. The sample was subsequently centrifuged for 1.5 hours at 29,000 rpm at 4°C. Following elution from the IMAC column, the eluted fractions were tested for purity, and total protein yield is depicted in (**Figure 5-5)**.

The protein analysis results demonstrate that the majority of CB2 protein was solubilized and the pellet was clear of any traces of protein. In addition, the purity of the protein appears higher with no evidence of double bands. In addition, the contaminant is smaller in this purification, ~30 kDa (**Figure 5-5 B)**. The amount of imidazole was 70 mM, enough to remove most of the non-specific contaminating proteins. We also used up to 100 mM of imidazole in the washing step, which did not affect the yield of the protein (data not shown). The final protein concentration determined by the Bradford assay was also comparable to previous purifications.

A.

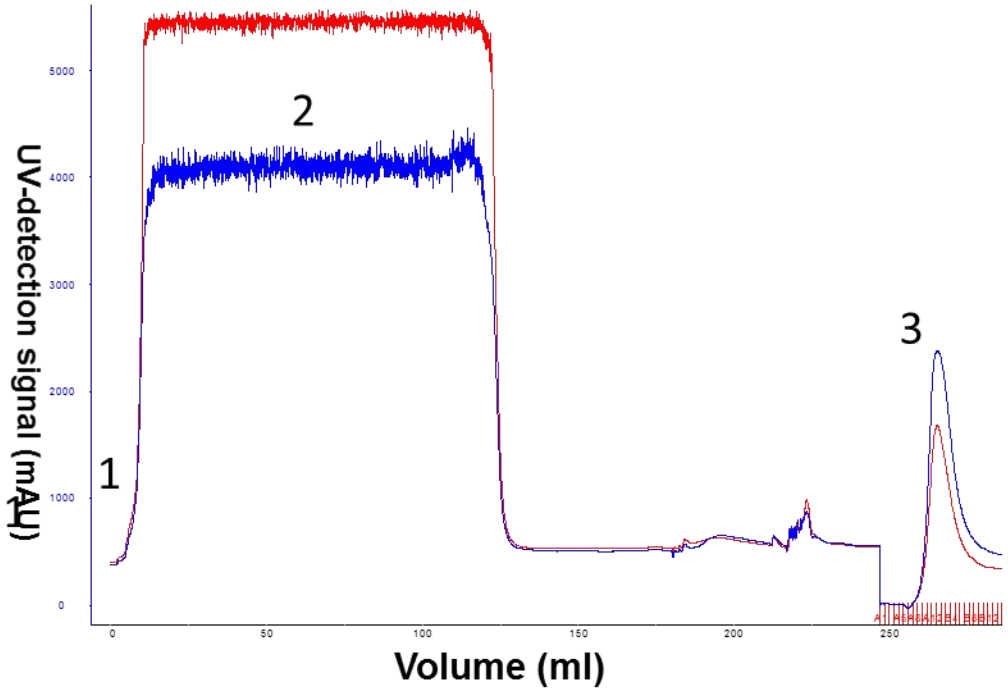
UV-detection signal (mAU)
Volume (ml)
1
2
3
0
1000
2000
3000
4000
5000
0
50
100
150
200
250

B.

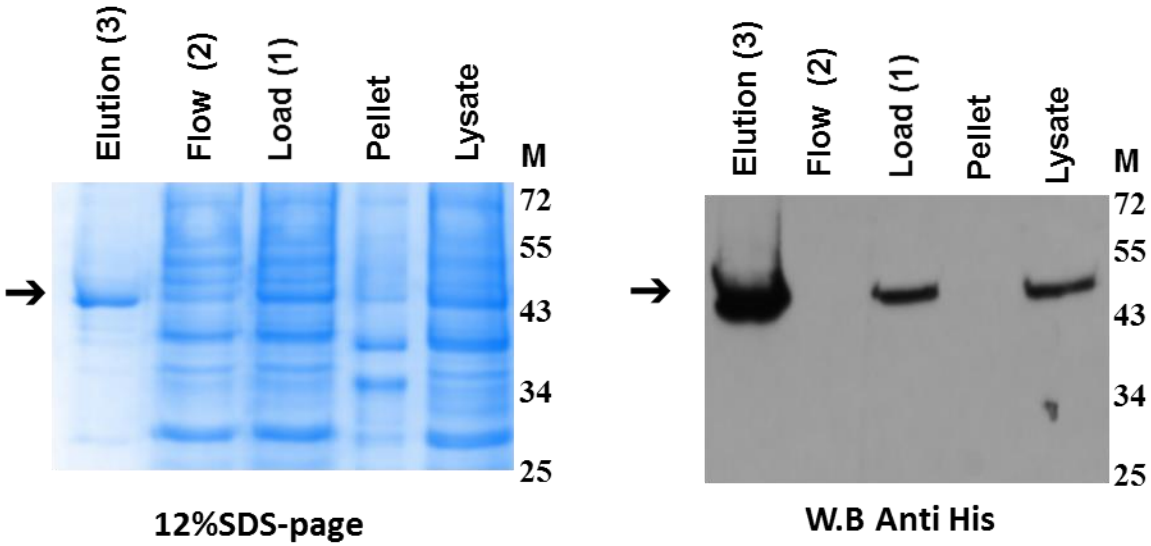
Elution (3)
Flow (2)
Load (1)
Pellet
Lysate
M
72
55
43
34
25
12%SDS-page
Elution (3)
Flow (2)
Load (1)
Pellet
Lysate
M
72
55
43
34
25
W.B Anti His

C.

Table 14. Protein analysis for construct # 22.

	Protein concentration (mg/ml)	Volume (ml)	Total protein (mg)	Yield%	Specific activity binding and inhibition constants
Whole lysate	3.23	120	387.6	100	B_{max} = 3083 CPM /10 µg K_D = 7.9 nM K_i = 0.19 nM
Soluble material	1.8	115	207	53.4	-
Flow through	1.3	110	143	36.9	-
Elution	1.09	11	11.9	3	B_{max} = 11400 CPM/10 µg K_D = 14.4 nM K_i = 3.4 nM

Figure 5-5 . Comparison purification process for CB2 18 – T4 (224-231) Δ C-terminal.

A. Chromatography profile for IMAC purification (load, flow though, wash1 and elution.

B. SDS-page and western blot analysis for entire purification process.

C. Comparison table for the percentage yield of the protein and specific activity throughout entire process.

Moreover, we performed the protein titration assay to assess the binding activity of the receptor, as well as, to gain an estimation of protein amount needed for the displacement, saturation and binding assays as shown in (**Figure 5-6)**. We have used a concentration of 2 mM/well of the radioactive ligands, CP55940 (CB2 agonist) and SR144528 (inverse agonist). The protein saturated reading was at 5 µg/µl (**Figure 5-7**) and **Table 14.**

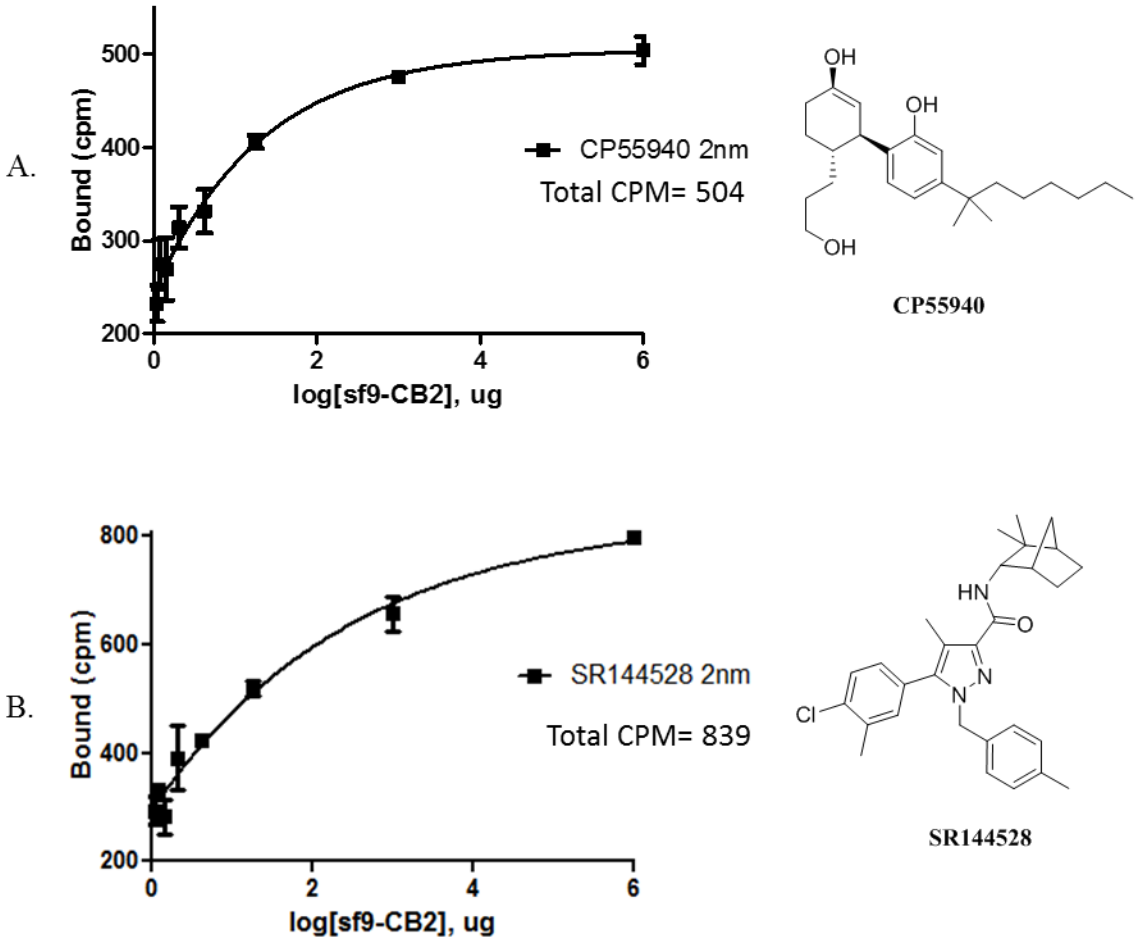

Figure 5-6. Protein-ligand titration assay for CB-fusion protein.

In this assay, we fixed the amount of the radioactive ligand (2 nM) in each well and titrated the protein amount. Two different, known ligands were used: CP55940 (agonist) and SR144528 (inverse agonist).

The maximum binding CPM has increased significantly from 3083 CPM to 11400 CPM, indicative of maintenance of binding activity. The competition-binding assay also preserved binding activity of the receptor as shown in **(Figure 5-7)**. Moreover, we used the SEC (Superdex 10/300 GL) to separate monomeric protein. In this construct, we observed CB2 protein elution at a high molecular weight (8 ml fraction) and trace amounts of protein eluted at 15 ml, which is representative of the monomeric version of the receptor as illustrated in (**Figure 5-8 A)**. In order to investigate the binding affinity pattern of a high molecular weight protein, we subjected the protein to titration, saturation, and binding assays. Interestingly, the protein provided, to some extent, binding activity as shown in (**Figure 5-8 B).** This variation in the elution pattern is due to the effect of the detergent on the receptor complex in the gel filtration column. We speculate that the cause is instability of the protein in the detergent, or misfolding/unfolding of the protein. This phenomena has been observed in human mu opioid receptor [379]. To study the detergent's effect, we desalted the IMAC elution using a zipa column and replaced the buffer with 500mM NaCl, 20mM KCl, 10mM MgCl2, 50mM HEPES (pH 7.5), 5% glycerol, 25mM imidazole, 0.05% (w/v) DDM, and 0.01% (w/v) CH, supplemented with SR144528. This buffer lacked the CHAPS detergent. Next, this was loaded onto a new IMAC column, 1 ml equilibrated with 500mM NaCl, 20mM KCl, 50 mM HEPES (pH 7.5), 10% (v/v) glycerol, 50 mM imidazole, 0.025% (w/v) DDM, and 0.005% (w/v) CHS. The column was then washed with 10 CV of 500mM NaCl, 20mM KCl, 50mM HEPES (pH 7.5), 10% (v/v) glycerol, 50 mM imidazole, 0.025% (w/v) DDM, and 0.005% (w/v) CHS. Finally, the column was eluted with 500mM NaCl, 20mM KCl, 50mM HEPES (pH 7.5), 10% (v/v) glycerol, 400 mM imidazole, 0.025% (w/v) DDM, 0.005% (w/v) CHS, and SR144528 (**Figure 5-9**) . Fractions corresponding to the elution protein were concentrated and loaded to Superdex 200 at a rate of 0.5 ml/min. The buffer was used at 500mM NaCl, 20mM KCl,

50mM HEPES (pH 7.5), 10% (v/v) glycerol, 0.025% (w/v) DDM, 0.005% (w/v) CHS, and SR144528) to run the gel filtration. We elucidated that the majority of the protein was eluted as a monomer phase (**Figure 5-9**).

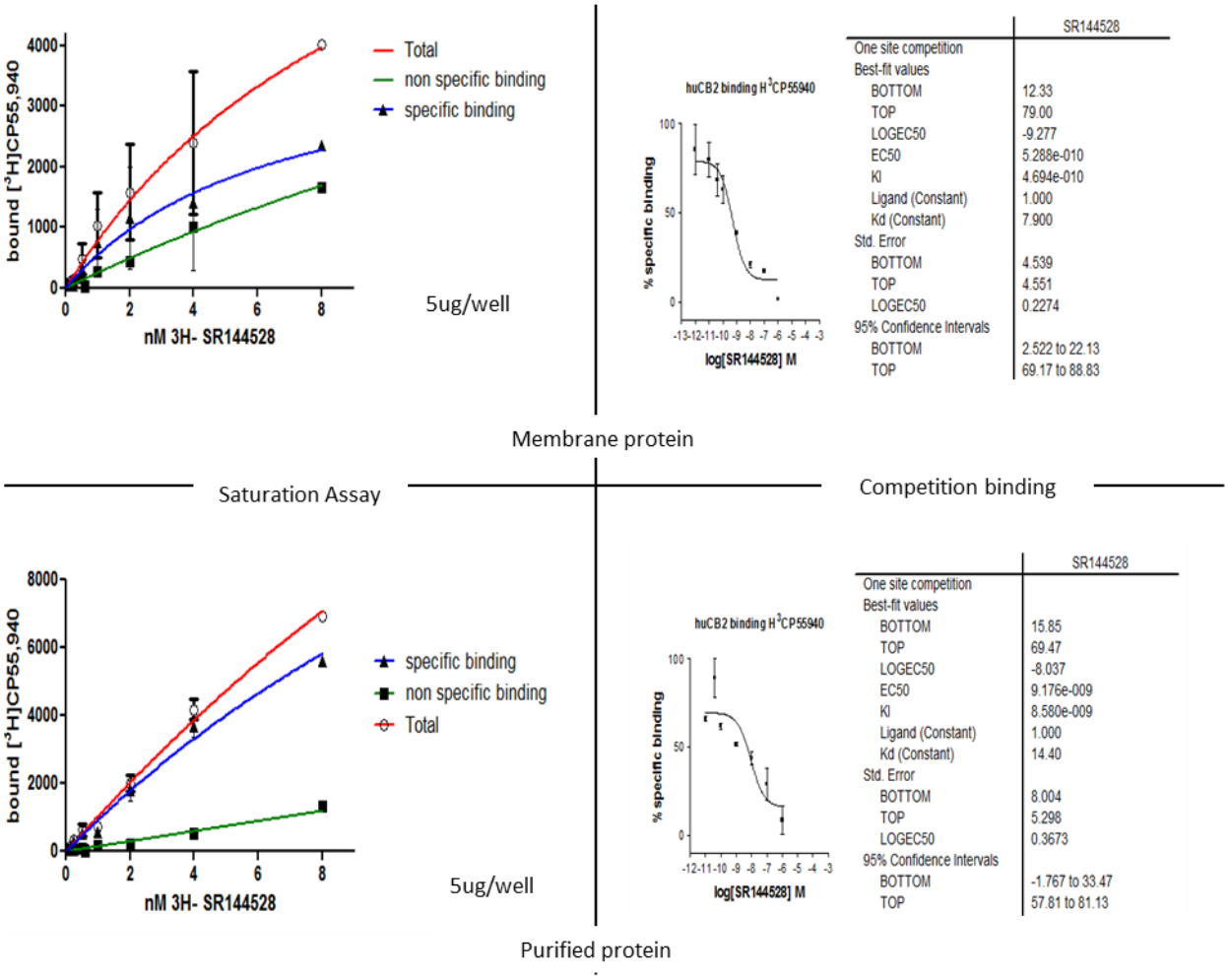

Figure 5-7 . Displacement and saturation binding assay for CB2-fusion.

In these assay, both membrane protein and purified protein expressing construct #22 test for the binding and saturation assays. *CPM's*, K_d, and K_i for the membrane protein are 3083 CPM's/10 µg protein, 7.9 nM, and 0.19 nm, respectively. Additionally, *CPM's*, K_d, and K_i for the purified protein are 11400 CPM's/10 µg protein, 14.4 nM, and 3.4 nm, respectively.

A.

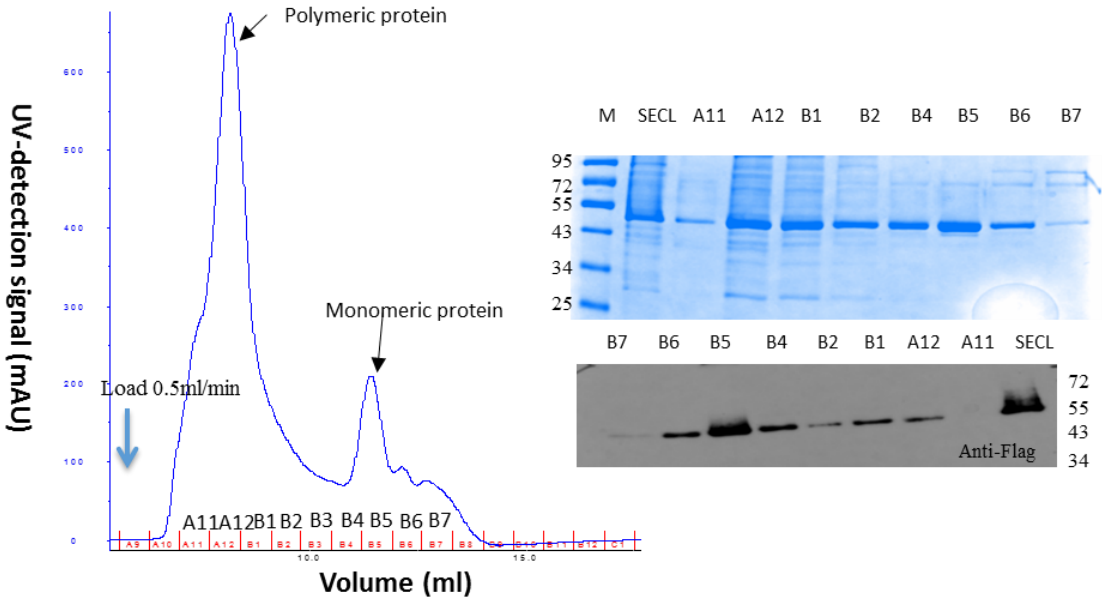

B.

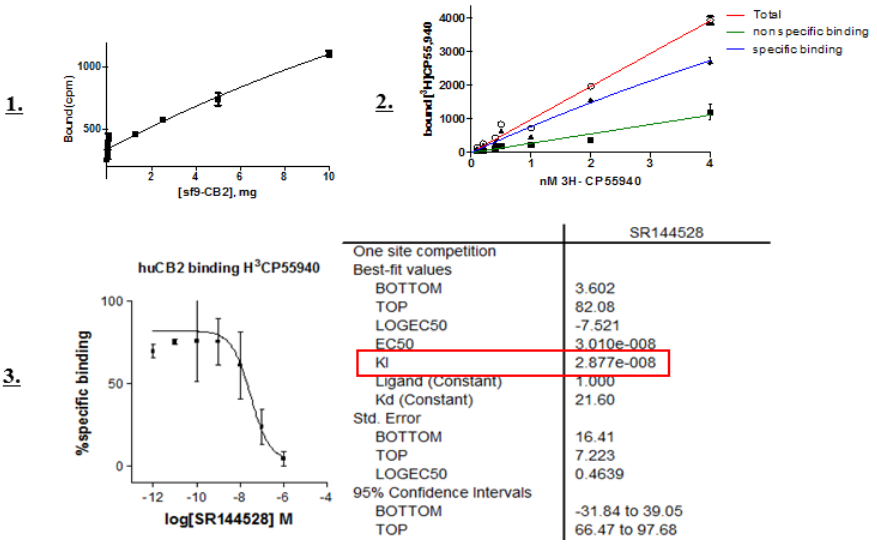

	SR144528
One site competition	
Best-fit values	
BOTTOM	3.602
TOP	82.08
LOGEC50	-7.521
EC50	3.010e-008
KI	2.877e-008
Ligand (Constant)	1.000
Kd (Constant)	21.60
Std. Error	
BOTTOM	16.41
TOP	7.223
LOGEC50	0.4639
95% Confidence Intervals	
BOTTOM	-31.84 to 39.05
TOP	66.47 to 97.68

Figure 5-8. Gel filtration for pFastBAC: CB2 1 – T4 (224-231) 340 C-terminal.

A. Chromatography profile for the gel filtration of CB2-fusion protein showing two major peaks. SDS-page and western blot for each corresponding fraction. CB-fusion was pure in the B5 fraction, which represent the monomeric peak.

B. Binding activity of the higher molecular weight protein; 1. Protein titration; 2. Saturation binding assay CPM's= 17561 CPM, K_d = 21.61nM and K_i = 28 nM.

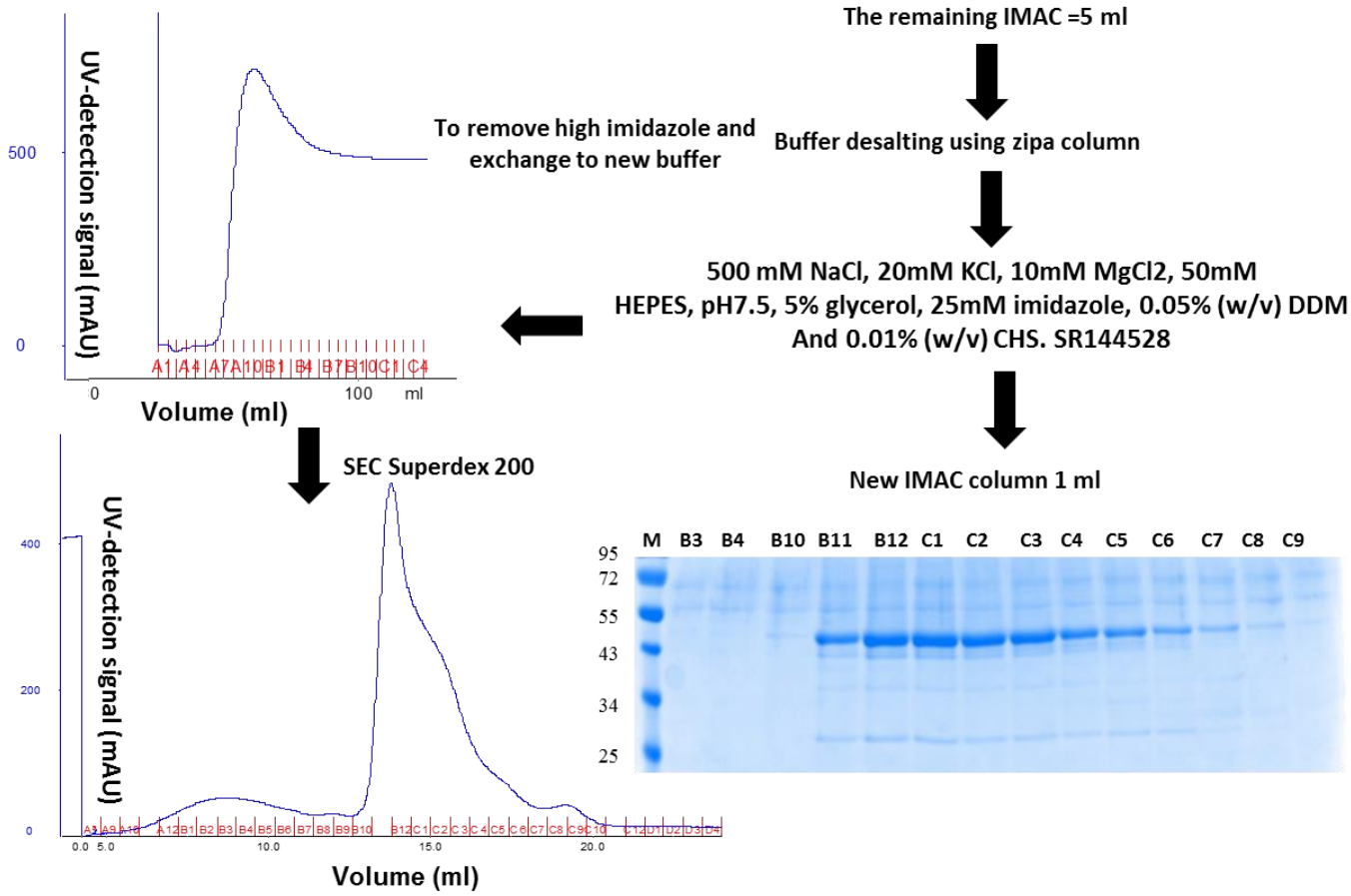

Figure 5-9. Gel filtration optimization for the nickel column.

The Nickle elution from previous purification was subjected to buffer exchange and new IMAC column purification. All fractions obtained were then loaded onto SEC and analyses done using SDS-page for each corresponding fraction.

To examine the effect of using different ligands in the purification and SEC profile of pFastBAC: CB2 18 – T4 (224-231) 340 C- terminus, we have added other inverse agonists throughout the purification process. Unlike previous purification in which we used SR144528, the new purification process included different in-house inverse agonists, Xie2-64 and a triaryl sulfonamide derivative, throughout the entire purification [381]. Xie2-64 has shown selectivity to CB2, with a K_i = 0.5 nM, which is increased over CB1 [381]. Similarly, pellets obtained from pFastBAC: CB2 18 – T4 (224-231) 340 C-terminal (construct #22) was purified using previous methods mentioned in **5.3.2** and **5.3.3**. Total protein yield and the purity of the final elution protein was comparable to previous purifications, as presented in chromatography profile **(Figure 5-10 A)**. Moreover, the monomeric separation of the protein on the size exclusion chromatograph was obtained (**Figure 5-10 B)**.

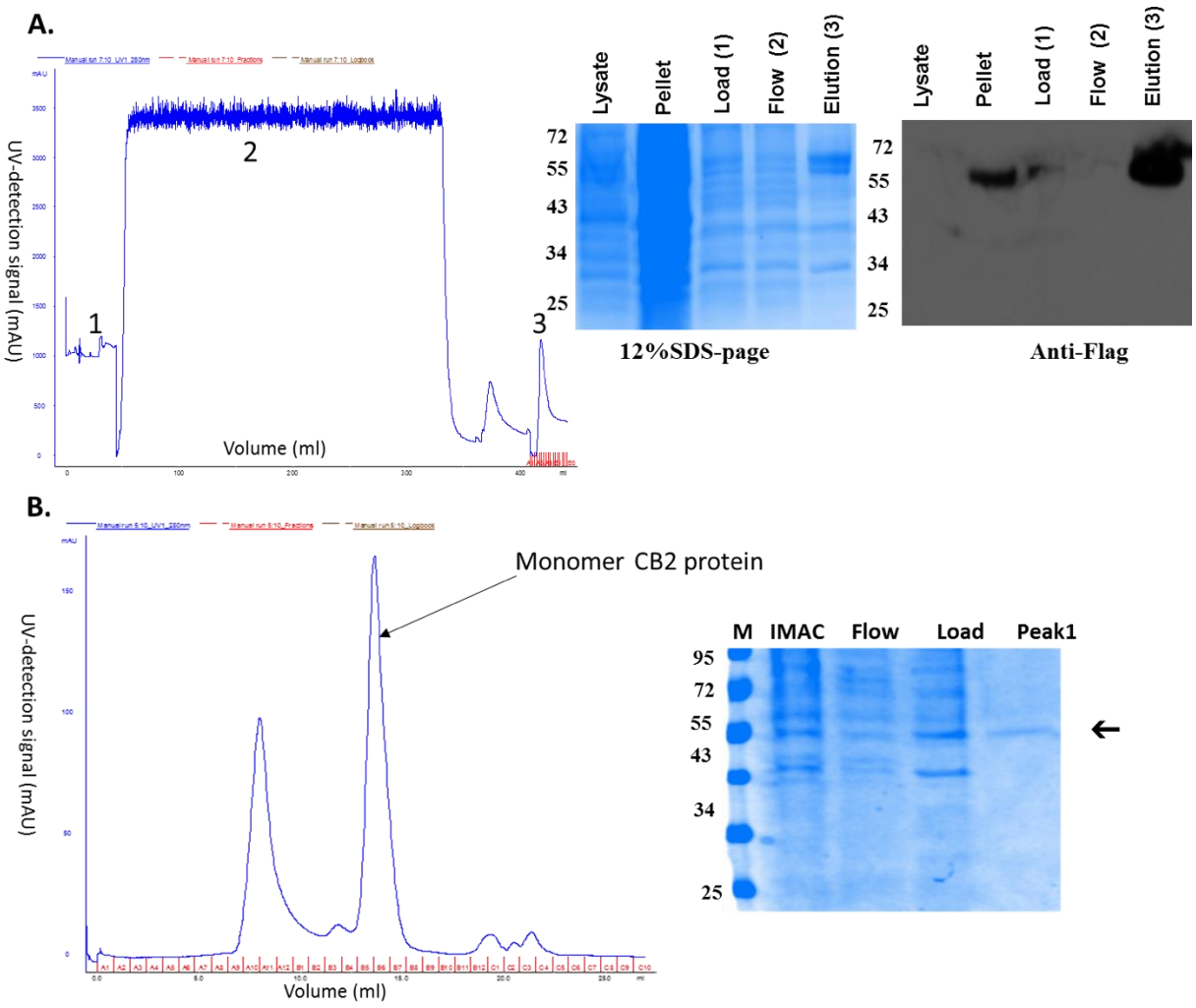

Figure 5-10. CB2 purification using different ligands, Xie2-64.

A. Chromatography profile, SDS-page and western blot for IMAC of CB2-fusion protein for construct #21 using different inverse agonist (Xie2-64).

B. Chromatography profile and SDS-page for Flag and SEC purification of CB2-fusion protein showing highly molecular weight CB2 and second peak for monomer CB2 protein.

We extended the experiment further to study the effect of using different fusion proteins. To examine this, we replaced T4L with apocytochrome b562RIL. This fusion protein was used previously for the successful GPCRs co-crystal structure determination in both 3ICL and N-terminal insertion [51, 75, 153, 155]. We used construct #22, harboring apocytochrome b562RIL at a position between amino acid 224 and 231 in the third intracellular loop. **Figure 5-11** clearly displays the expression levels comparable to those in previous T4L-fusion protein. It also demonstrates that purity was maintained throughout the purification. However, a significant portion of the protein was eluted at a high molecular weight, indicating aggregation, which proposes a challenge for crystallization set-up.

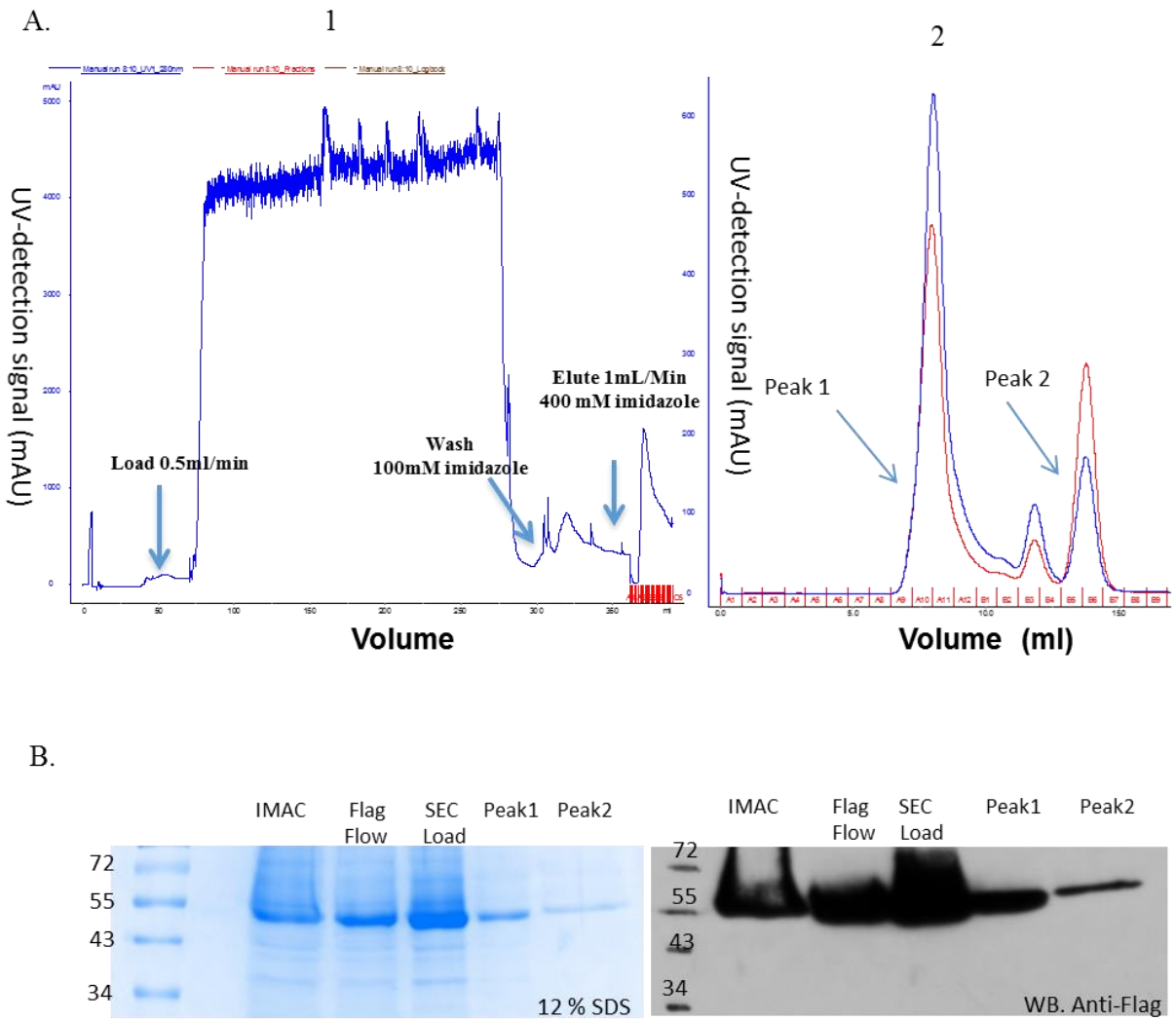

Figure 5-11. Scaled–up purification steps for the DDM - solubilized apocytochrome b562RIL -CB2 fusion construct.

A. Step-wise purification process for construct # 22 using Ni^{+2} column attached to AKTA purified (1). Flag and Gel filtration purification chromatography (2).

B. Purification analysis using SDS-page and western blot for the each IMAC, Flag and SEC corresponding step.

5.3.4 Protease cleavage for CB2-fusion protein

The eluted protein for CB2-fusion protein construct #21 and was concentrated using 30 kDa molecular weight cut-offs (MWCO) to increase the protein concentration and remove contaminants and salts of lower molecular weights. We performed the cleavage process using pro TEV plus obtained from Promega (1000IU) before the SEC. Multiple conditions were analyzed for cleavage according to the manufacturer's protocol. The protein was incubated with TEV protease at a concentration of 10 units per 20 μg total protein in non-denaturing conditions. The mixtures were incubated for 1, 5 hours and overnight at 4 C°. The cleavage efficiency was measured and analyzed using western blot. The data provide evidence that with increasing incubation time and protease units 100% cleavage efficiency for both tags (His and Flag) was achieved **(Figure 5-12)**. The western blot signals were clearly diminished after 1 hour, 5 hours and overnight when the protein samples were probed against anti-Flag and anti-His antibodies. This was not the case against anti-CB2 antibodies, indicating that the tags were no longer attached to the construct. The presence of the CB2 receptor was detected using a polyclonal antibody against CB2 Goat primary antibody (ThermoFisher).

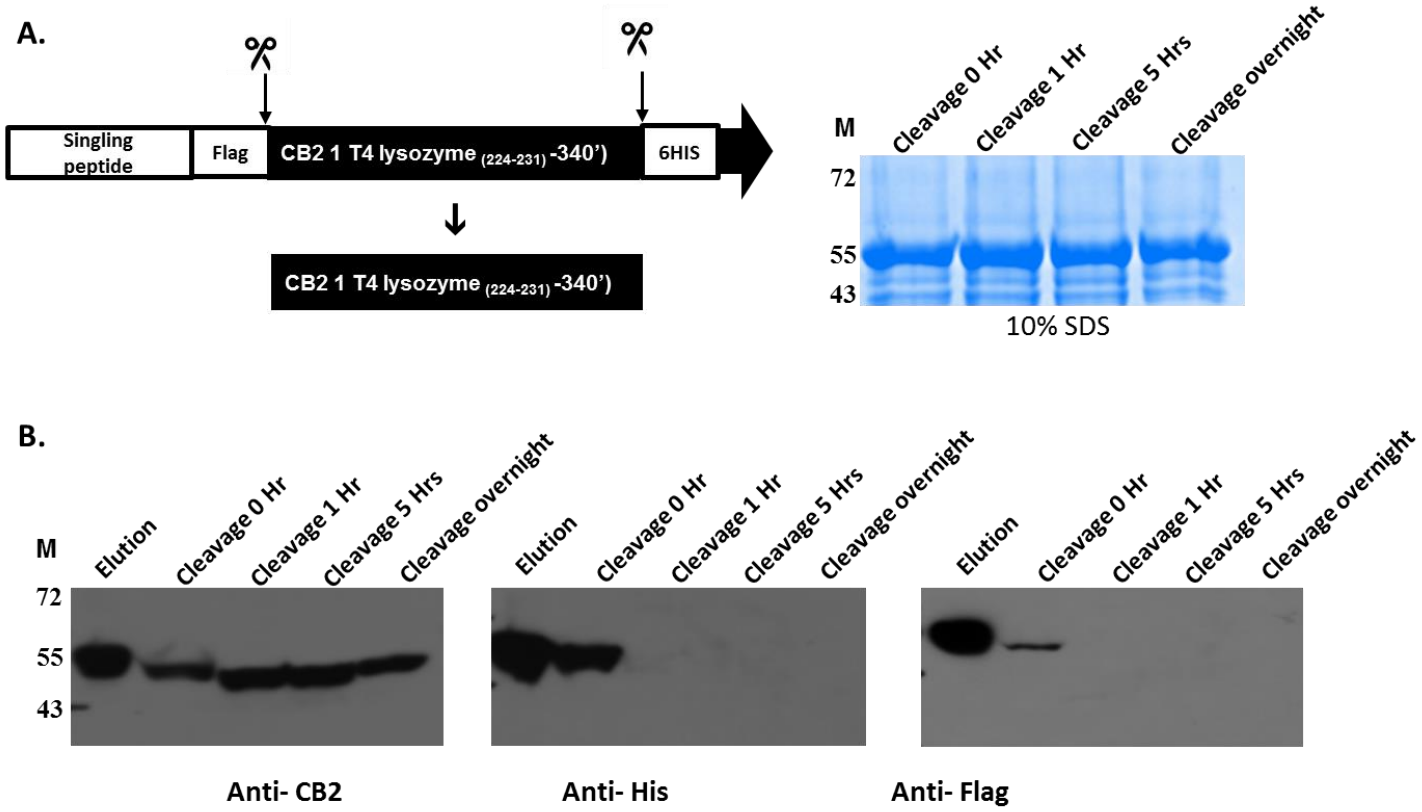

Figure 5-12. TEV protease cleavage of CB2-fusion protein.

Time point for cleavage efficiency of His, Flag tags attached to CB2 receptors. Increase contact time of the TEV protease to CB2 protein lead to cleave more tag form the construct. The TEV protease were add to all samples. Products yielded after the cleavage were verified by western blotting and was probed against Anti-Histidine, Anti-CB2 and Anti-CB2 antibodies. **A**. showed the loaded of the protein for each time point. **B**. represent the western blot for the cleavage efficiency for each time point.

5.4 SAMPLES ANALYSIS AND STUCTURAL CHARICTRIZATION

5.4.1 Proteomic analysis of SDS-Page samples and description of identified proteins

Concentrated protein samples were prepared for proteomic analysis by digestion of the gel bands for the SDS-Page with trypsin (**Figure 5-13 A)**. Digested samples were and analyzed by nano-LC-MS/MS and individual peptides were identified from the collision-induced dissociation (CID) spectra and are then queried against proteome database. The obtained list of identified peptides was correlated to identify specific proteins using MASCOT search engine. Using the Scaffold program, six unique peptide sequences corresponding to human cannabinoid receptor CB2 were identified, representing 21% total coverage of the protein (**Figure 5-13 B)** and **(Figure 6-6)** in **Appendix B.**

A.

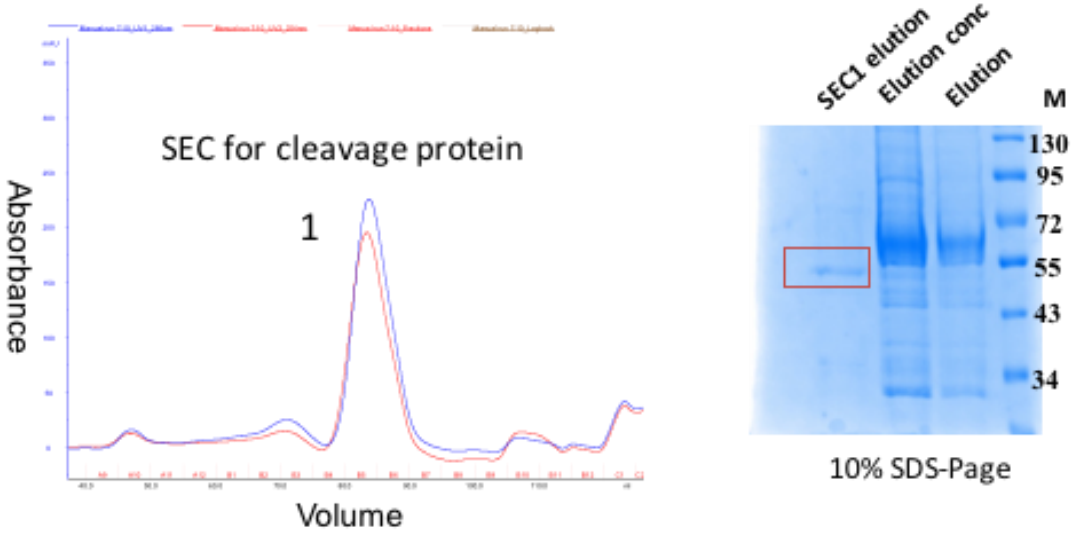

B.

Identified peptide sequence	Amino acid position
DGLDSNPMK	15-23
DGLDSNPMKDYMILSGPQK	15-33
DYMILSGPQK	24-33
IGSVTMTFTASVGSLLLTAIDR	110-131
AFAFCSMLCLINSMVNPVIYALR	280-302
GLGSEAKEEAPR	323-334

Figure 5-13. Sample purification for mass spectroscopy analysis.

A. Cleaved monomeric purified protein using for the MS/MS analysis

B. List of human-cannabinoid receptor CB2 peptides identified by MS/MS

5.4.2 Characterization of secondary structure of CB2 fusion protein

Receptor of construct #21 was purified in buffer contains (0.1% of DDM and 0.1%CHS) and were separated by SEC (Superdex 200) that equilibrated by buffer lacking the cholesterol **(Figure 5-14**). The monomer CB2 protein used for the performing circular dichroism studies.

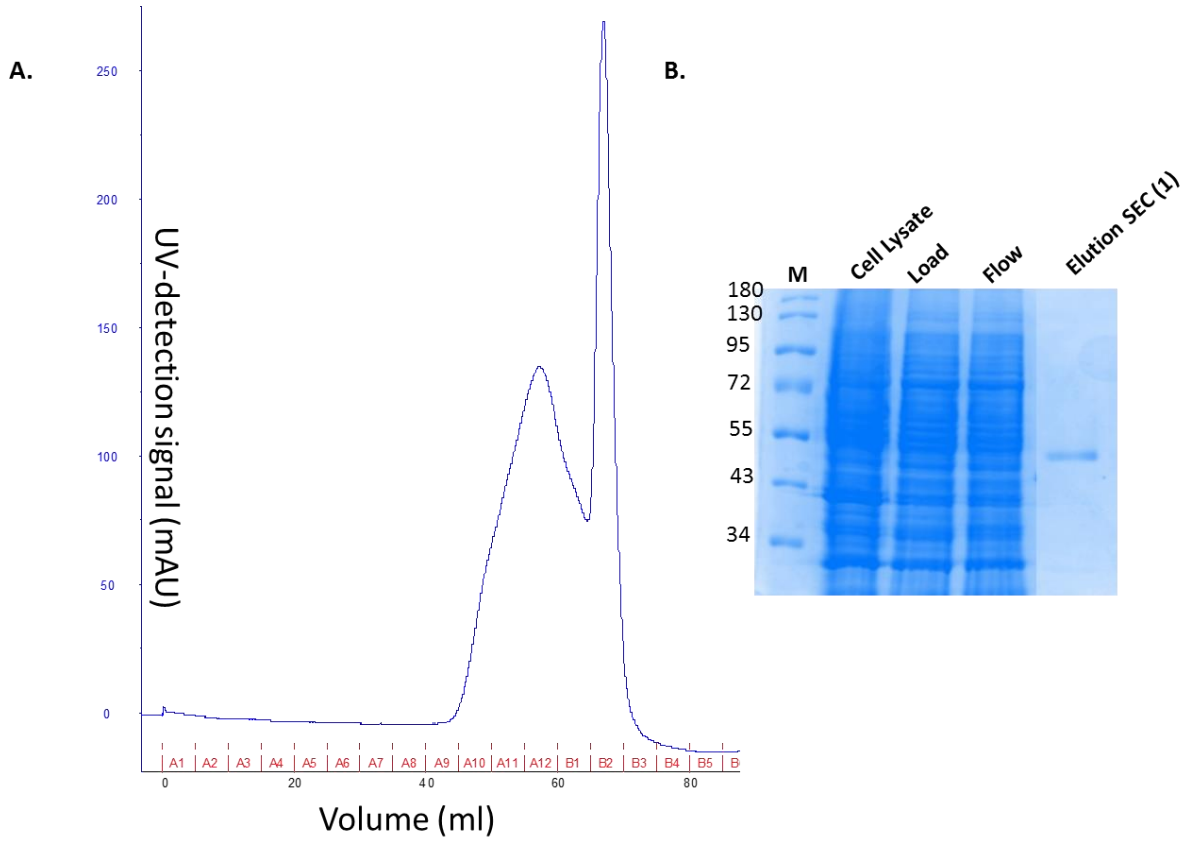

Figure 5-14. Purification of CB2-T4L for Circular dichroism.

A. SEC for the purified cleaved receptor (construct#21)

B. Corresponding SDS-page analysis for the protein purification

We performed the circular dichroism for the protein (0.1 mg/ml) in 30mM phosphate buffer (pH7.8), 0.1% DDM, 150 mM NaCl and 10% glycerol. As shown **(Figure 5-15 A)** the result shows double minima in the spectrum at about 208 and 222 nm characteristic for α-helical proteins. The helical content derived from the mean residue molar ellipticity was 45.9% using the equation:

$$\alpha\text{-helical \%} = (-[\theta 222] + 3000)/39000).$$

In addition, the K2D2 results (web server to estimate the α helix and β strand content of a protein from its circular dichroism spectrum) was slightly larger in helical percentage with 48.5% and 9.74% for β strand as shown in (**Figure 5-15 B)**. Moreover, by comparing the CD spectrum result for the fusion-CB2 with the wild type receptor CD spectrum obtained from previous literature report [382], the result for wild type receptor show comparable result about 49% alpha helix and our result was 48.5%.

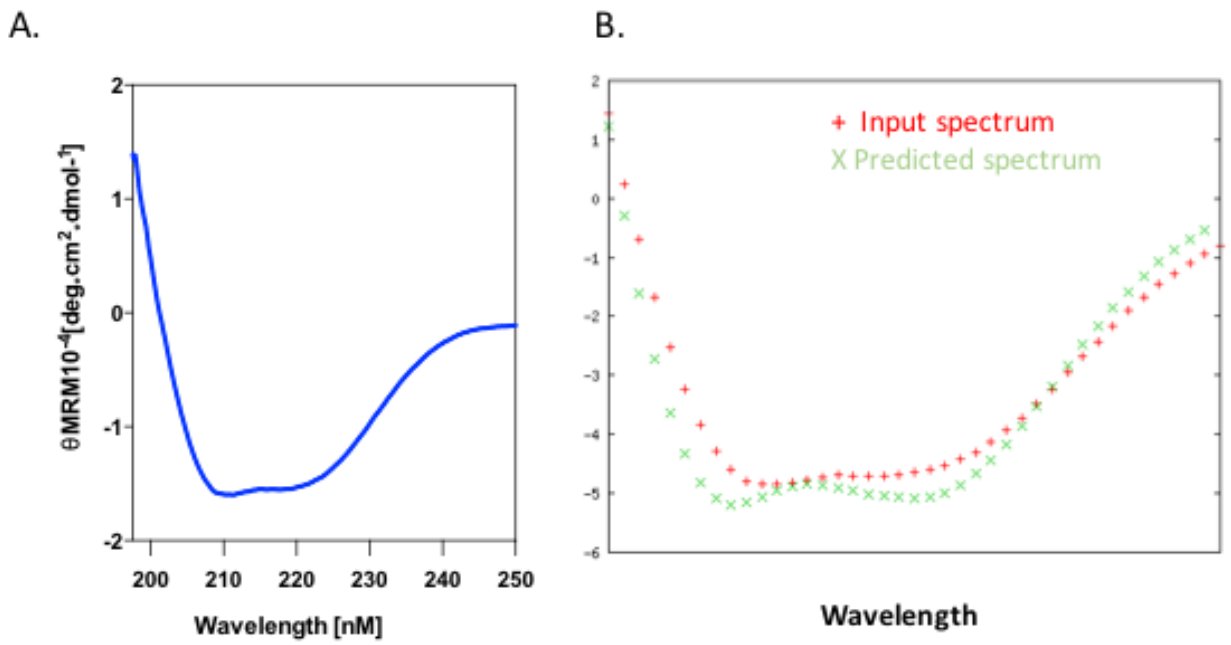

Figure 5-15. Circular dichroism spectra for purified CB2 - T4L monomer.

A. Mean residue ellipticity for each spectrum shown is the average of 5 replicate scans at 25 °C. The spectrum shows typical a-helical profile switch minima at 208 nm and 222 nm. The helical contents for CB2-T4L is 45.9%.

B. Predicted and fusion -CB2 CD result spectra using K2D2 software show 48.5% and and 9.74% for α helix and β strand respectively. These results suggest that CB2-T4L and folded correctly. Θ MRM (deg X cm2 X dmol-1). The spectrum generated by prism graphpad.

5.5 SCREENING CB2 CONSTRUCTS TOWARD CRYSTALLIZATION TRIALS

Similar to pervious GPCR purifications, our data demonstrated that purification of CB2 can also be obtained by using detergents including 1% DDM and 0.5% CHAPS and CHS [383, 384]. We have started an extensive screening for the optimal combination of ligands and constructs to produce large quantities of the functional monomeric fusion CB2 receptor. We used CP55,940 (agonist), SR144528, and Xie2-62 (inverse agonists). Constructs # 8, 13, 16, 18, 20, and 21 were subjected to IMAC, Flag purification, and SEC. As shown in (**Figure 5-16 A),** the SEC for the wild type CB2 receptor, using two ligands (CP55940 and SR144528), demonstrated that the agonist was able to stabilize the CB2 receptor in a monomeric form. Thus, we have screened the fusion CB2 receptor in combination with ligands. When evaluating constructs # 8, 13, and 16, construct #16 had a small amount of the receptor in monomeric phase, using CP55940 (agonist) in the presence of iodoacetamide as an alkylating reagent used to block reduced cysteine residues (**Figure 5-16 A)**. Constructs # 20 and 18 showed significant improvement in producing the monomeric peak in the presence of an agonist **(Figure 5-16 B)**. Moreover, constructs # 20 and 21 were the only ones that produced the expected monomeric peak using an inverse agonist (SR144528). Thus, we attempted a change to a different inverse agonist (Xie2-64). In a previous study, with a refolded CB2 receptor from an inclusion body using DMPC, Xie2-64 displayed advantages over other ligands in high affinity binding with the CB2 receptor (data not published). **Figure 5-16 C** indicates that the protein was more stable and produced a significant amount in monomeric phase after complete purification using IMAC, Flag, and size-exclusion chromatography with Xie2-64. This protein was in enough quantity to move forward with monoolein LCP crystallization trials.

A.

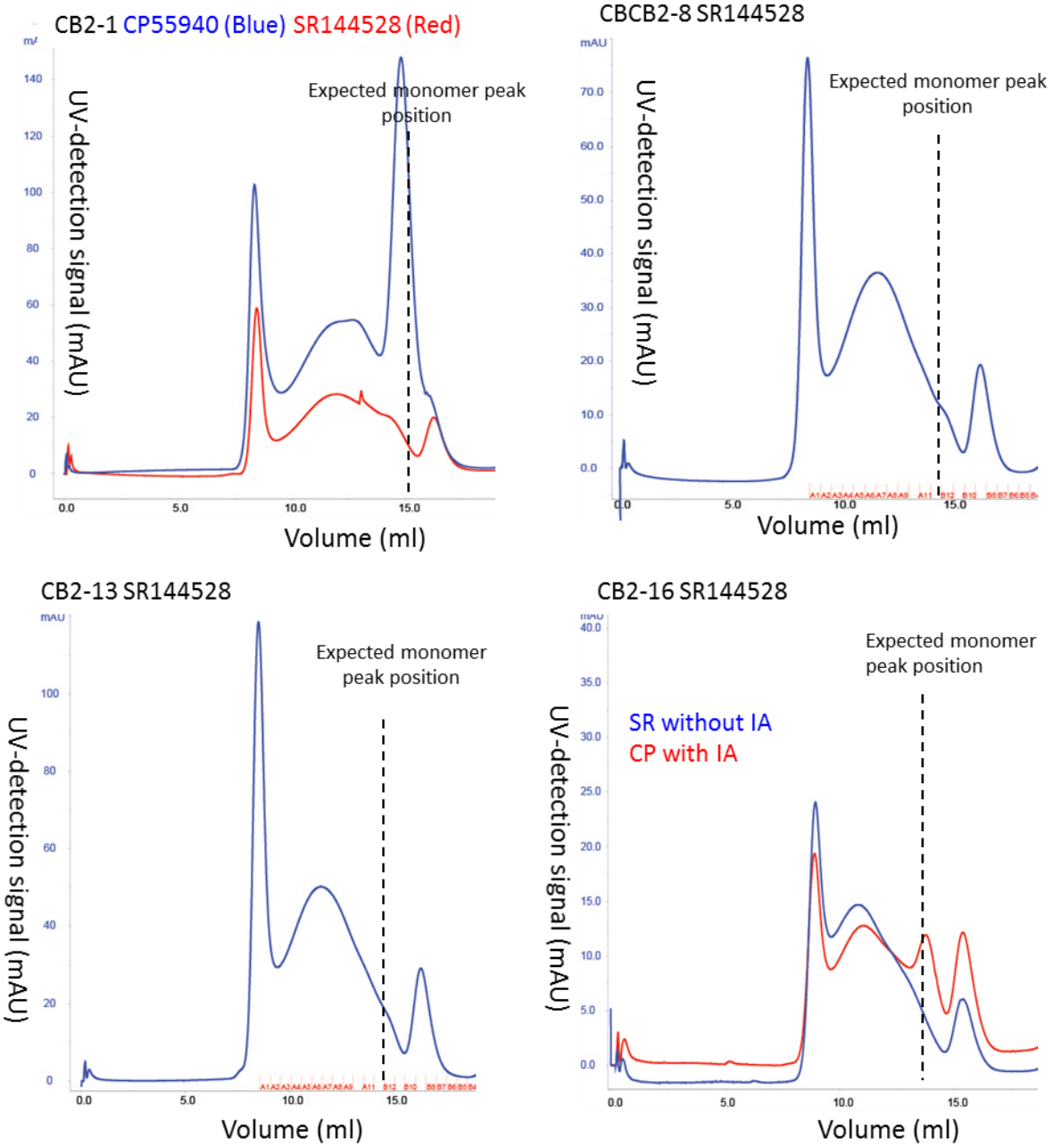
CB2-1 CP55940 (Blue) SR144528 (Red)
Expected monomer peak position
UV-detection signal (mAU)
Volume (ml)
CBCB2-8 SR144528
Expected monomer peak position
UV-detection signal (mAU)
Volume (ml)
CB2-13 SR144528
Expected monomer peak position
UV-detection signal (mAU)
Volume (ml)
CB2-16 SR144528
Expected monomer peak position
SR without IA
CP with IA
UV-detection signal (mAU)
Volume (ml)

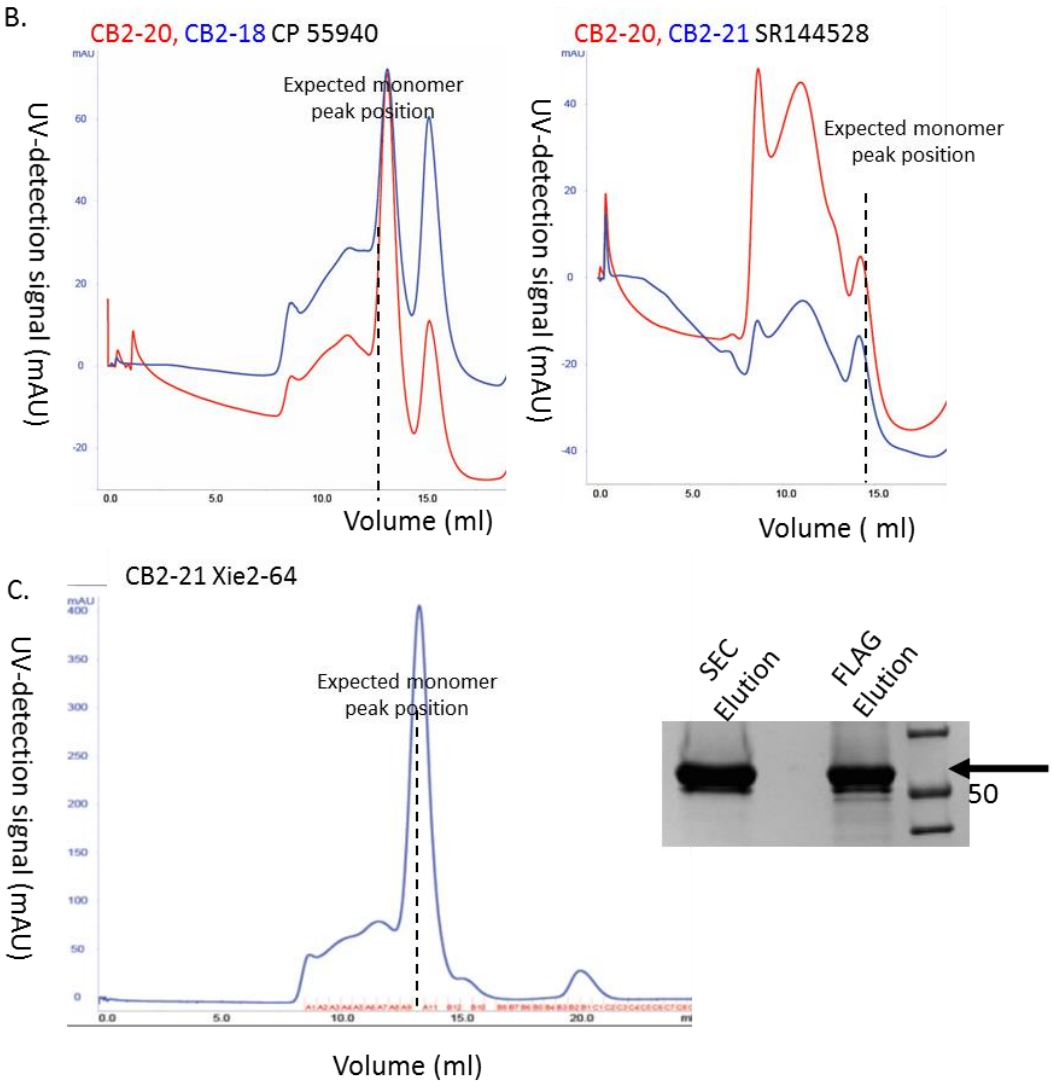

Figure 5-16. Ligand screening for production of monomeric protein.

SEC chromatography profiles for different constructs with different ligands. (**A**) Chromatogram for monomer CB2 protein for constructs WT, 8, 13 and 16 using either the inverse agonist SR144528 or the agonist CP55940. (**B**). Constructs #18, 20, and 21 were the only ones that produced monomeric protein more significantly with the agonist. Changing the inverse agonist to Xie2-64 led to higher amounts of the monomeric protein for construct #21, as shown in **C**. This figure provides by (Dr. B. Kobilka lab).

5.6 CONCLUSION

Studies involving GPCR structural biology often face significant technical obstacles. However, findings from these studies could contribute significantly to innovation in the field. Nevertheless, we anticipated that the successive rounds of affinity purification would maximize protein purity. Utilizing the Flag and 6xHis tags at the two termini of the recombinant protein would ensure that highly purified recombinant CB2 proteins could be isolated. Size eclusion chromatography (SEC) is the key step for determining the construct for crystallization. Due to variability in ligand structure, detergent characterization, and different candidate insertion positions for the fusion protein in CB2, screening different CB2 constructs was necessary to confirm that the binding of the receptor was preserved (chapter 4). Moreover, the conformation stability and using the best ligands and constructs to produce more monomer CB2 protein was our goal. Development of a good diffraction quality, membrane protein crystal presents a formidable challenge, and trial-and-error optimization may be necessary to achieve success. Optimization may involve altering phase composition, time, or temperature.

In our portion of experiments, we were able to overcome some of these challenges. We began by using the most optimal construct with highest binding activity and screened for the best combination of detergents for solubilization. We also tested the effects of structural modifications that assisted in reducing conformation changes, such as N- and C-terminal truncations in the overall production of active protein. Moreover, the position of the fusion insertion was also validated by using different fusion proteins (apocytochrome b562RIL), confirming the best construct to carry over to crystallization trials. Notably, the conformational changes of the CB2 receptor were monitored using saturation binding throughout the purification process.

6.0 SUMMARY AND FUTURE DIRECETION

6.1 PROCESS CONCLUSIONS

The study of the CB2 receptor structure, like other GPCRs, has recently increased. Due to structural instability, low expression profile, and optimal purification conditions the use of insect cells and bacterial systems is ideal for many scientists. The results presented in this dissertation provide insights and open multiple avenues for future studies relating to CB2 structure for the purpose of drug design.

Throughout the initial portion of this research, we mainly focused on the structural and functional requirements for binding and function of the CB2 receptor. This type of work will need to be advanced over several years however, in the interim, homology modeling is a powerful tool and a new strategy for generating models of GPCRs for drug discovery and functional studies. When provided an experimental crystal structure of GPCR (template), models can be generated for a homologous sequence (target) that possesses sequence similarity or identity. Models built with over 50% sequence identities are accurate enough for drug discovery. The models built between 25% and 50% sequence identities can be used for designing mutagenesis experiments and assess target potential [385]. Homology and pharmacophore models based on previous GPCR crystal structures have been successfully used for drug discovery in the past decade. Evers *et al*. [386] described homology modeling of the alpha 1A adrenergic receptor based on the X-ray structure of bovine rhodopsin and successfully found antagonists using virtual screening [140]. Likewise, Chin *et al*. generated a homology model of the human M1 muscarinic acetylcholine receptor (mAChR) based on the crystal structure of an M3 mAChR [142]. Virtual screening

experiments show that refined models can efficiently differentiate agonists from decoy molecules, with the TM5-modified models also providing good agonist/antagonist selectivity [387]. Homology models have proven to be an invaluable resource to rationalize SAR data and predict binding modes of experimental compounds for the cannabinoid receptor 2 [40], the human adenosine A2A receptor, and the alpha-1-adrenoreceptors [388]. Several repositories like Modbase (http://modbase.compbio.ucsf.edu), I-TASSER (http://zhanglab.ccmb.med.umich.edu/I-TASSER/), Protein Model Portal (http://proteinmodelportal.org), and SWISS-MODEL (http://swissmodel.expasy.org/SWISS-MODEL.html) contain protein models generated using various automated methods.

Our group also built homology and pharmacophore model for CB2 and screened for a new ligands (agonist, inverse agonists) based on their 3D CB2 homology structure and pharmacophore models [291] [40]. These models led to the discovery of a selective inverse agonists used as osteoclast inhibitors [317, 381]. Moreover, we reported on comprehensive studies of amino acids required for ligand binding and recognition. We have tested mutations of amino acids and their effects in the binding pockets of the CB2 receptor by utilizing the homology modeling of the CB2 receptor. Unlike other GPCRs, which have hydrophilic endogenous ligands, cannabinoid receptors are known for their neutral and highly lipophilic endogenous ligands [181]. Thus, we believe that some hydrophobic residues are involved in the ligand-binding pocket. Disruption of these interactions by mutations to polar or charged side chain amino acid residues leads to loss of the binding and downstream signaling [291]. These studies also highlighted the importance of the 2EL for ligand recognition, especially for inverse agonist binding. Although, homology and pharmacophore modeling provides a cost-effective alternative in the absence of experimental structures, generating models with sufficient accuracy remains a large challenge.

Throughout the second part of this research, our lab had previously investigated the expression purification and refolding process for fusion CB2 protein from *E. coli* to produce a fully functional protein (unpublished data). We attempted multiple different strategies, such as Mistic-CB2-TarCF, TrpΔLE-CB2-His6, and GST-CB2-His6 constructs for producing the binding receptors. However, among these constructs, only GST-CB2-His6 showed the sufficient results for binding (unpublished data). The need for refolding the CB2 receptor and insufficient amounts of protein for crystallography of the CB2 receptor was a limitation. To overcome this, we decided to pursue a different system that is known for maintaining post-translational modification. Likewise, in other GPCRs, the CB2 receptor was subjected to chimeric modification (i.e. truncation, fusion protein, and tags insertion), leading to different constructs. All constructs were tested for expression and conformed in a binding assay. This intensive work ultimately leads to fewer optimal CB2 constructs susceptible for large-scale purification.

In the final section of this dissertation, we tested various purification conditions, time courses for expression, titers of virus, and detergent solubilization. Purification tags in the receptor for the subsequent purification process were largely used. In spite of the hydrophobicity of the receptor causing impurities, the multi-step purification produced a highly purified protein. The protein also required cleavage by a protease that was highly efficient. We also tested the effect of different fusion proteins, ligands in expression, and obtaining high amounts of pure protein in monomeric phase. These steps are integral for producing active proteins that can be amenable to the lipidic cubic phase (LCP). In parallel, our collaborator analyzed multiple crystallization trials. Further studies will need to be performed to increase the success of crystallization. Overall, we have provided robust and dependable methods for the functional expression and purification of other

GPCRs that share structural homology to CB2, such as cannabinoid receptor (CB1) from insect cells.

6.2 LIMITATIONS AND FUTURE DIRECTION

The scope of CB2 functional expression is enormous and involves many levels of expertise in various areas, such as protein pharmacology, protein chemistry, molecular biology, and structural function determination. However, due to the cost of expression, purification, crystallization, and data inconsistency, tremendous effort must be made in order to provide scant amounts of the functional protein. In the future, we will need to improve the protein expression levels in order to reduce cost. Increased insertion position optimization and different fusion proteins need to be investigated to improve homogeneity of the receptor during the purification process. This challenge may lead to large decreases in quantity as they will appear as aggregated or non-functional protein for binding. We may also use a different protease that is known for its stability in many detergents as well as introduce a linker to increase cleavage efficiency. Thus, we provided construction modification to the current working construct (#21). Construct #21 was the best in terms of homogeneity before the crystallization trials (**Figure 5-16).** In addition, we included 19 amino acid drivers from β2AR in the N-terminus of the CB2 receptor followed by a linker, Flag tag peptide sequences, and C3 protease and linker as shown in (**Figure 6-1 B and C)**. Including the first nineteen amino acids of β2AR shown previously in our collaborator's lab, it boosted the expression for many GPCRs. Moreover, we introduced two linkers at both sites just before the C3 cleavage site to expose the C3 cleavage sequence and increased cleavage efficiency.

The preliminary data proved encouraging results regarding receptor over-expression. Moreover, as shown in **(Figure 6-2)**, we have tested construct # 21 and a new construct in a side by side comparison for their expression and binding. The binding capacity for the new construct was increased significantly using the same amount of protein for testing. The nineteen amino acids drivers from β2AR and the linker that attached to the CB2 N- terminus maintained structural integrity of the CB2 receptor and did not influence the expression and binding. We are currently in the process of purifying large-scale pellets for new constructs to obtain insight into its behavior for crystallization as well as cleavage efficiency. Functional CB2 receptor obtained in these steps will be used for also LCP crystallization trials with the assistance of our collaborator.

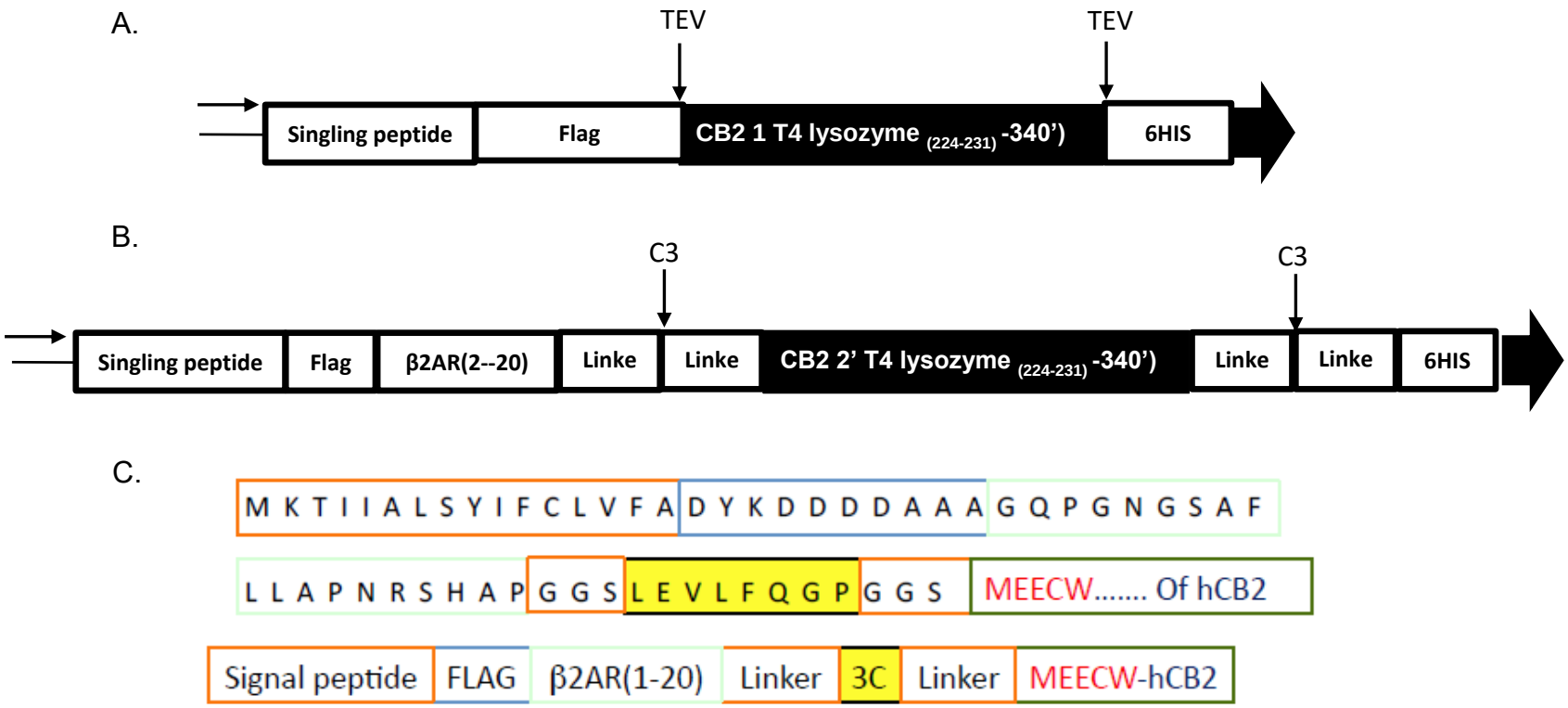

Figure 6-1. Schematic diagram of human CB2 fusion protein for constructs 21 and future work.

All expression plasmid vectors were constructed on the pFastBac vector backbone under the control of the polyhedrin (PH) promoter. **A**) Current working plasmid (construct # 21). HA signaling peptide and Flag tags in the N-terminal and His, C-terminal fusion tag were separated from the CB2 receptor by the TEV sequence. **B**) Nineteen amino acids of β2AR were inserted after HA and Flag tags in the N-terminal to boost expression. Here, we replaced TEV by a C3 cleavage sequence which was separated by two linkers at both termini to increase cleavage efficiency. **C**) Details of amino acid sequence explaining the new insertion.

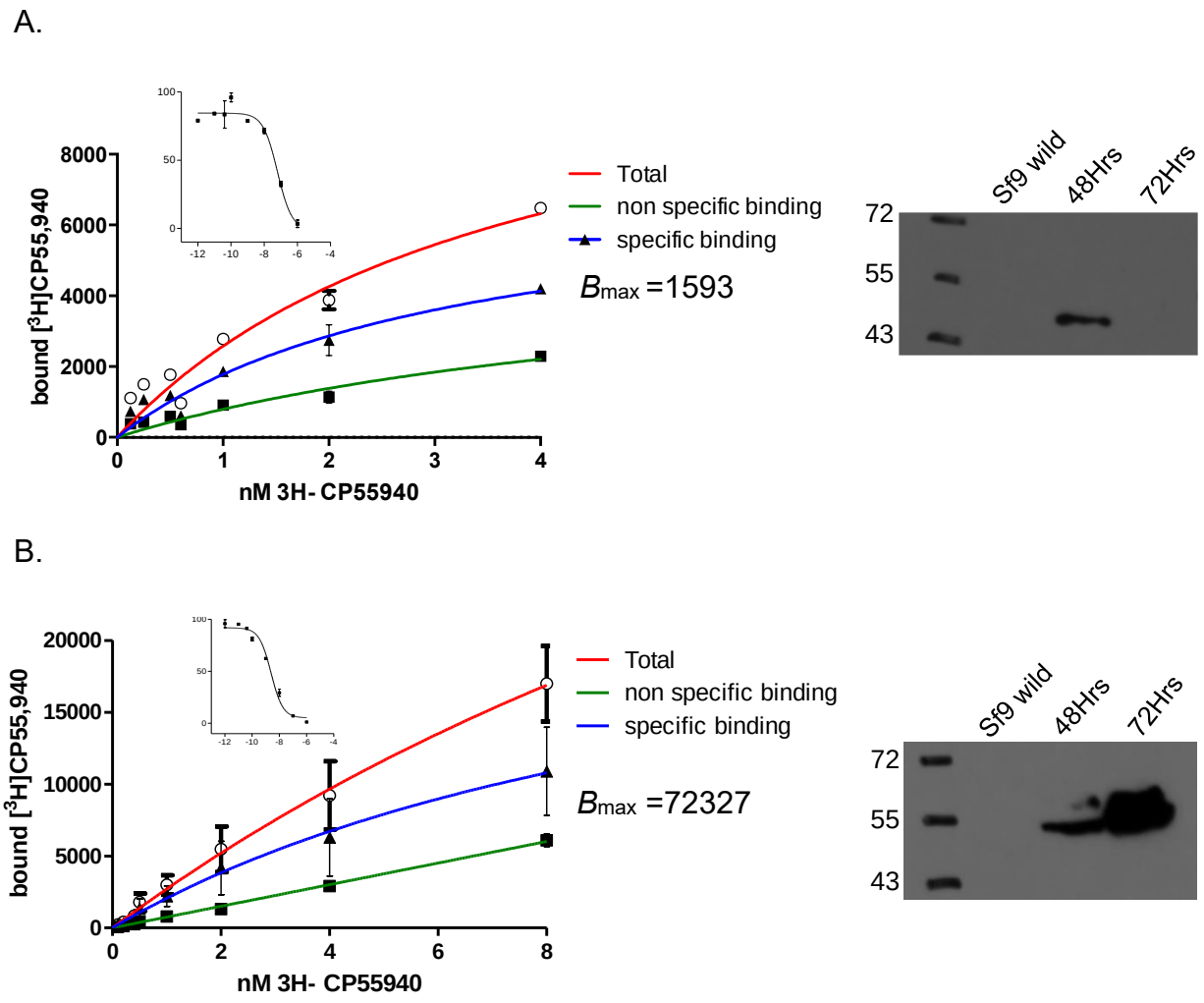

Figure 6-2. Comparison of the binding profiles between construct #21 and the future suggested construct.

A. Saturation and binding assay and expression profile of construct # 21. B_{max} = 1539 CPM.

B. Saturation binding assay and expression profile for newly suggested construct showing significant increase in B_{max} to 72327 CPM and receptor expression levels.

Assay was performed in duplicate (n = 2). Data represented as mean. We used 10 µg total protein for the saturation assay and 5 µg total protein for the binding assay.

Lastly, optimization will be performed during the entire purification process with different detergents other than DDM, such as amphiphiles, mainly lauryl maltose neopentyl glycol (MNG). Multiple examples in previous GPCR purifications demonstrated dependable and native-like environments after refolding using amphipols, such as in cannabinoid receptor CB1, serotonin receptors, and vasopressin [389]. Our small-scale purification and preliminary data obtained showed encouraging results. As evidenced in (**Figure 6-3 A)**, protein was eluted with high purity results and highlighted the glycosylation pattern. Moreover, the functionality assay was performed on the purified protein obtained from the SEC.

In conclusion, purifying CB2-fusion protein in homogenous form with large amounts will provide a platform for crystallization trails. Such trials can ultimately provide, for the first time, the first co-crystal structure of the endocannabinoid family.

A.

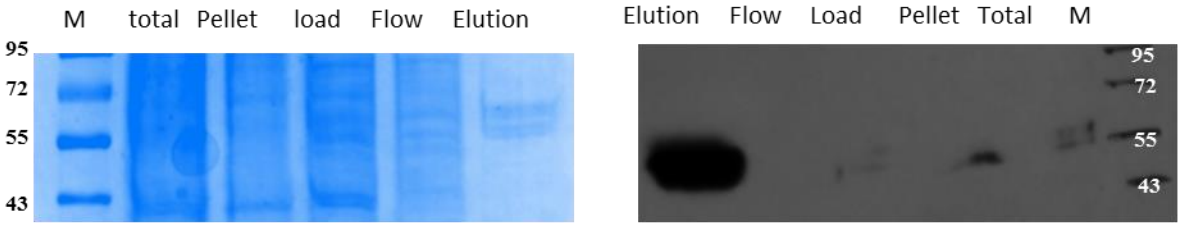

B.

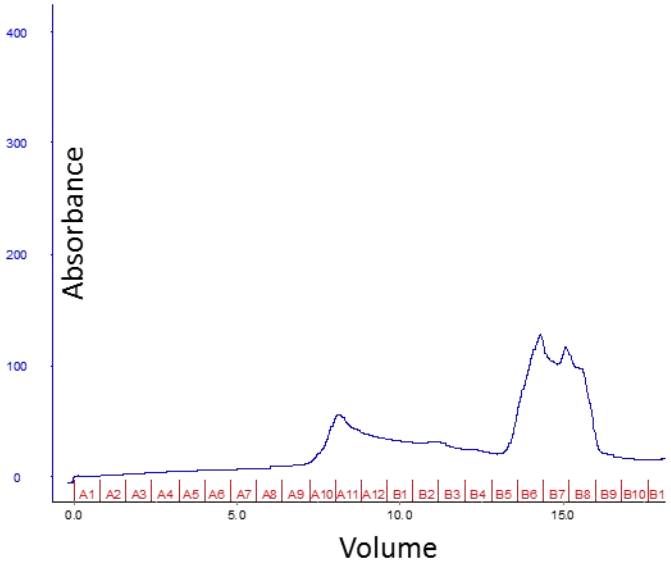

Figure 6-3. Purification of the CB2 fusion protein using MNG instead of DDM.

Half liter used for the purification of construct #21.

A. Represents the overall purification process in each step. Notably, the elution showed high protein purity.

B. Size exclusion chromatography for the protein, showing low aggregation and two peaks representing glycosylated CB2 protein.

APPENDIX A

License Number	3753290217659
License date	Nov 20, 2015
Licensed content publisher	Elsevier
Licensed content publication	Biochemical and Biophysical Research Communications
Licensed content title	Examining the critical roles of human CB2 receptor residues Valine 3.32 (113) and Leucine 5.41 (192) in ligand recognition and downstream signaling activities
Licensed content author	Mohammed Alqarni,Kyaw Zeyar Myint,Qin Tong,Peng Yang,Patrick Bartlow,Lirong Wang,Rentian Feng,Xiang-Qun Xie
Licensed content date	26 September 2014
Licensed content volume number	452
Licensed content issue number	3
Number of pages	6
Type of Use	reuse in a thesis/dissertation
Portion	full article
Format	both print and electronic
Are you the author of this Elsevier article?	Yes
Will you be translating?	No
Title of your thesis/dissertation	DESIGN, EXPRESSION AND PURIFICATION OF FUNCTIONAL HUMAN CANNABINOID RECEPTOR 2
Expected completion date	Apr 2016
Estimated size (number of pages)	220
Elsevier VAT number	GB 494 6272 12
Permissions price	0.00 USD
VAT/Local Sales Tax	0.00 USD / 0.00 GBP
Total	0.00 USD

Permission for using content of article in the thesis

AM

Alqarni, Mohammed Hamed

To: Alqarni, Mohammed Hamed;

Mon 3/7/2016 11:28 PM

DH

Darla Henderson <D_Henderson@acs.org>

To: Alqarni, Mohammed Hamed;

Reply all

Sun 11/22/2015 7:50 PM

> You forwarded this message on 3/7/2016 11:28 PM

Dear Mohammed Alqami,

Thank you for your outreach. I confirm you may reuse content from the article you co-authored here http://pubs.acs.org/doi/pdf/10.1021/ci5002718 in the thesis you are writing to complete the degree-granting requirements of your university. ACS asks that you:

- Cite the *Journal of Chemical Information and Modeling* article as the source of the segments you reuse;
- Note any modifications you make from the original article; and
- Include in your thesis a direct link to the *JCIM* article, direct link here: http://pubs.acs.org/doi/pdf/10.1021/ci5002718

Wishing you the best of luck with your dissertation.
With kind regards,
Darla

Darla Henderson, PhD
Asst Director, Open Access Progams
American Chemical Society

License Number	3823990530750
License date	Mar 07, 2016
Licensed content publisher	Elsevier
Licensed content publication	International Immunopharmacology
Licensed content title	Mutagenesis and computer modeling studies of a GPCR conserved residue W5.43(194) in ligand recognition and signal transduction for CB2 receptor
Licensed content author	Yuxun Zhang,Zhaojun Xie,Lirong Wang,Brielle Schreiter,John S. Lazo,Jurg Gertsch,Xiang-Qun Xie
Licensed content date	September 2011
Licensed content volume number	11
Licensed content issue number	9
Number of pages	8
Type of Use	reuse in a thesis/dissertation
Portion	excerpt
Number of excerpts	15
Format	both print and electronic
Are you the author of this Elsevier article?	No
Will you be translating?	No
Title of your thesis/dissertation	DESIGN, EXPRESSION AND PURIFICATION OF FUNCTIONAL HUMAN CANNABINOID RECEPTOR 2
Expected completion date	Apr 2016
Estimated size (number of pages)	220
Elsevier VAT number	GB 494 6272 12
Permissions price	0.00 USD
VAT/Local Sales Tax	0.00 USD / 0.00 GBP
Total	0.00 USD

Table 15. List of the primers used for the site directed mutagenesis.

Amino acids	Mutated amino acid	Primers used
Val113	V113L	5'- GCT GAA GAT TGG CAG CTT GAC TAT GAC CTT CAC -3' '3- GTG AAG GTC ATA GTC AAG CTG CCA ATC TTC AGC -'5
Val113	V113E	5'- GCT GAA GAG AAG CAG CGA AAC TAT GAC CTT CAC -3' '3- GTG AAG GTC ATA GTT TCG CTG CTT CTC TTC AGC -'5
Phe183	F183Q	5'- GGC CCT GCT CTG AGC TTC AGC CAC TGA TCC CCA ATG A-3' '3-T CAT TGG GGA TCA GTG GCT GAA GCT CAG AGC AGG GCC -'5
Phe183	F183V	5'- GCC CCT GCT CTG AGC TTG TCC CAC TGA TCC CCA ATG A -3' '3- T CAT TGG GGA TCA GTG GGA CAA GCT CAG AGC AGG GGC -'5
Leu192	L192A	5'- CCC AAT GAC TAC CTG GCG AGC TGG CTC CTG TT-3' '3-AA CAG GAG CCA GCT CGC CAG GTA GTC ATT GGG -'5
Leu192	L192S	5'- CCC AAT GAC TAC CTG TCG AGC TGG CTC CTG TT-3' '3-AA CAG GAG CCA GCT CGA CAG GTA GTC ATT GGG -'5
Phe281	F281K	5'- ACC AGG TCA AGA AGG CCA AGG CTT TCT GCT CCA TGC T -3' '3- A GCA TGG AGC AGA AAG CCT TGG CCT TCT TGA CCT GGT -'5

Table 16. Information of 10 crystal structures of GPCRs used in the present work**.**

	SMO	Bovine Rhodopsin	CXCR4	M2MAR	D3R	β2AR	$A_{2A}AR$	H1R	S1PR	β1AR
PDB entry	4JKV	1F88	3ODU	3UON	3PBL	2RH1	2YDO	3RZE	3V2W	2Y00
Resolution (Å)	2.45	2.40	2.50	3.00	2.89	2.40	3.00	3.10	3.35	2.50
Whole sequence identity (±2%)	14.4	17.4	19.1	20.9	23.5	24.4	25.1	25.2	28.5	28.5
Sequence identity in TM (±2%)	18	25	21	27	28	28	29	30	34	35
proSA-web Z-score	-2.80	-2.82	-3.54	-3.24	-2.72	-4.21	-4.87	-3.36	-3.49	-4.33
Reference	[16]	[27]	[57]	[66]	[30]	[63]	[63]	[64]	[65]	[246]

*We listed the information of 10 GPCRs used in the present work, including PDB entry, resolution, sequence identity to CB2 and the related references.

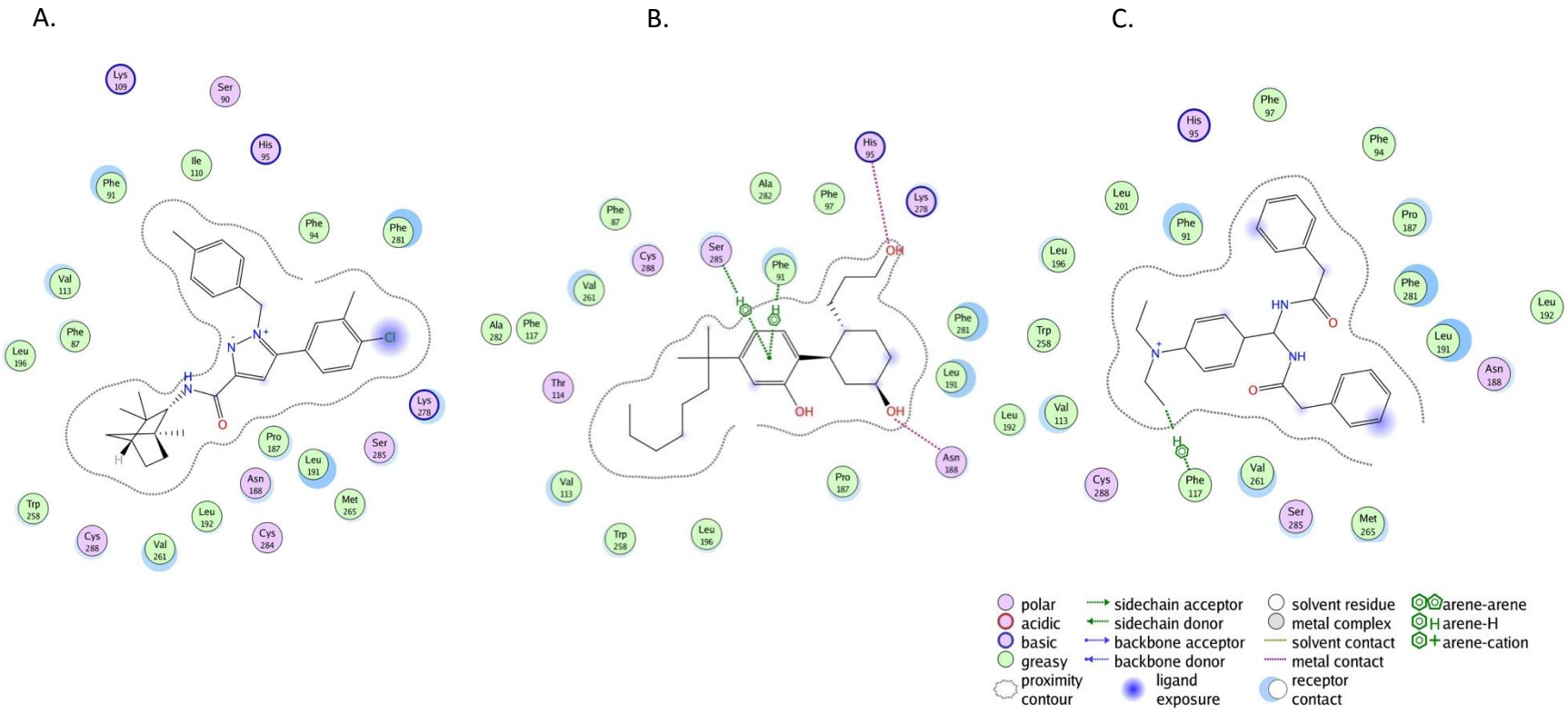

Figure 6-4 . Residuals interaction details between cannabinoid ligands and CB2 receptor model (I-TASSER).

Figures A and C represent the CB2 receptor- inverse agonist (SR144528 and Xie95-26 respectively) interaction with residues in the binding pocket. B interaction with agonist (CP55, 940). All details residuals mapping performed in models obtained from (I-TASSER).

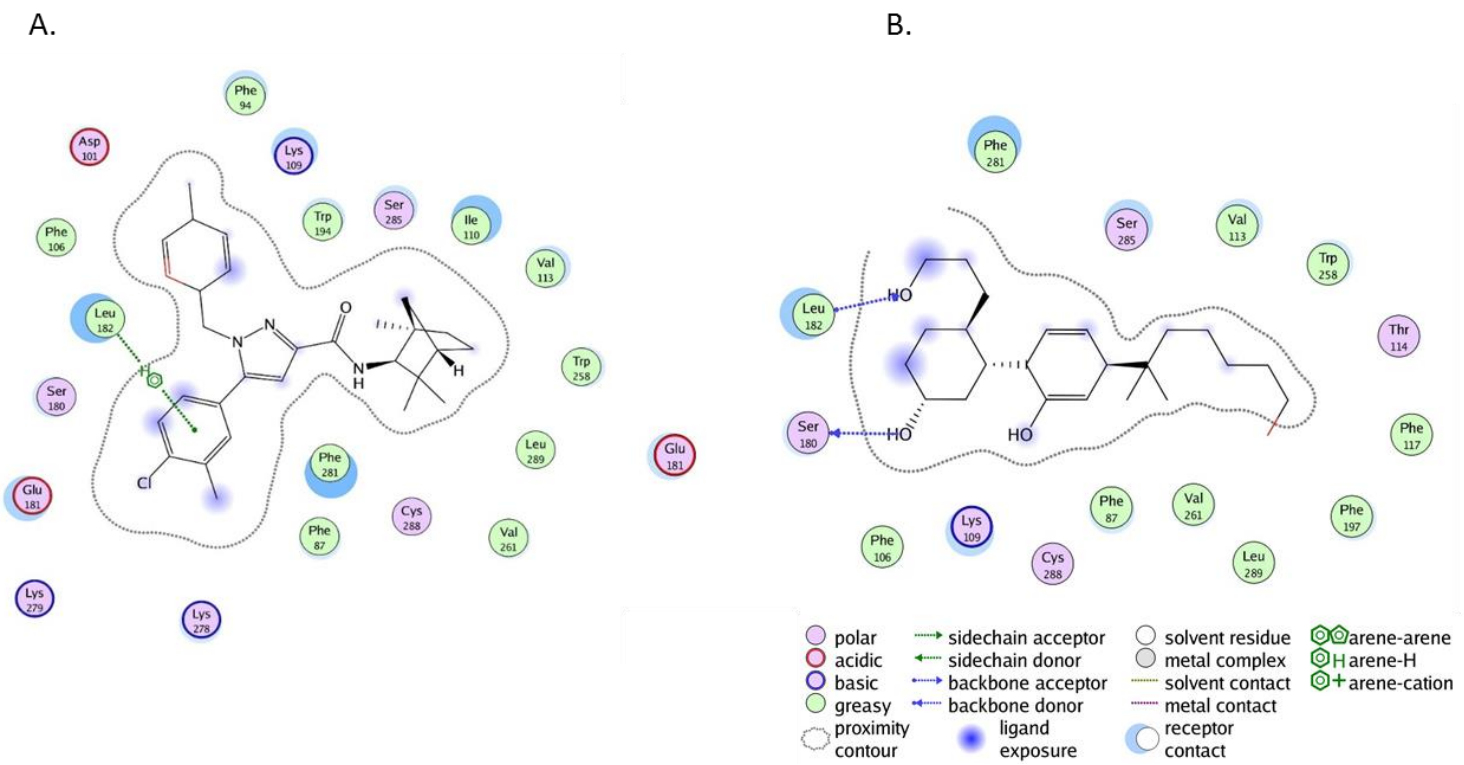

Figure 6-5. Residuals interaction details between cannabinoid ligands and CB2 receptor model. (ten known crystal structures of GPCRs).

Figures **A** represent the CB2 receptor- inverse agonist SR144528 interaction with residues in the binding pocket. **B**. Interaction with agonist (CP55, 940). All details residuals mapping performed in models obtained from (alignment with previous 10 co-crystals).

APPENDIX B

Table 17. List for the CB2 constructs and the primers used for 3ICL fusion partner's insertion.

Construct #	Fusion protein	Location of the 3ICL fusion insertion	Primers used
8	T4L	V220(5.69)-T4L-A235(6.25)	5' – TGG AAG GCC CAT CAG CAT GTG AAT AAT TTT GAA ATG TTA CGT –'3 , 5' – ACG TAA CAT TTC AAA TAT ATT CAC ATG CTG ATG GGC CTT CCA –'3, 5' – ACT GGC ACT TGG GAC GCG TAT GCC CGA ATG AGG CTG GAT GTT–'3 and 5' – CAC ATC CAG CCT CAT TCG GGC ATA CGC GTC CCA AGT GCC AGT –'3 .
12	T4L	G210(5.59)-T4L-L239(6.29)	5' – TTC CGG AAT CAT CAT CAC CTA TGG GAA TAT ATT TGA AAT GTT ACG TAT AGA TG –'3, 5' –CAT CTA TAC GTA ACA TTT CAA ATA TAT TCC CAT AGG TGT AGA TGA TTC CGG AA –'3, 5' – GTT TAG AAC TGG CAC TTG GGA CGC GTA TCT GGA TGT GAG GTT GGC CAA GAC –'3 and 5' – GTC TTG GCC AAC CTC ACA TCC AGA TAC GCG TCC CAA GTG CCA GTT CTA AAC –'3.
15	T4L	Q218 (5.67) –T4L-M237(6.27)	5' – GTT CTC TGG AAG GCC CAT CAG AAT ATA TTT GAA ATG TTA CGT ATA G –'3, 5' –CTA TAC GTA ACA TTT CAA ATA TAT TCT GAT GGG CCT TCC AGA

			GAA –’3, 5’ –GAA CTG GCA CTT GGG ACG CGT ATA TGA GGC TGG ATG TGA GGT TG –’3 and 5’ – CAA CCT CAC ATC CAG CCT CAT ATA CGC GTC CCA AGT GCC AGT TC–’3
16	T4L	S222 (5.71)-T4L-A235 (6.25)	5’ –GCC CAT CAG CAT GTG GCC AGC AAT ATA TTT GAA ATG TTA CGT ATA–’3, 5’ – CTA TAC GTA ACA TTT CAA ATA TAT TGC TGG CCA CAT GCT GAT GGG –’3, 5’ – ACT GGC ACT TGG GAC GCG TAT GCC CGA ATG AGG CTG GAT GTT–’3 and 5’ – CAC ATC CAG CCT CAT TCG GGC ATA CGC GTC CCA AGT GCC AGT –’3 .
18	T4L	Q227(5.76)-T4L-D228(5.78)	5’ –GCC AGC TTG TCT GGC CAC CAG AAT ATA TTT GAA ATG TTA CGT ATA –’3 ,5’ – TAT ACG TAA CAT TTC AAA TAT ATT CTG GTG GCC AGA CAA GCT GGC –’3 ,5’ – ACT GGC ACT TGG GAC GCG TAT GAC AAG CAG GTG CCA GGA ATG –’3 and 5’ –CAT TCC TGG CAC CTG CCT GTC ATA CGC GTC CCA AGT GCC AGT –’3
19	T4L	V220 (5.69)-T4L-A221(5.67)	5’ – TGG AAG GCC CAT CAG CAT GTG AAT AAT TTT GAA ATG TTA CGT –’3 , 5’ – ACG TAA CAT TTC AAA TAT ATT CAC ATG CTG ATG GGC CTT CCA –’3, ,5’ –ACT GGC ACT TGG GAC GCG TAT GCC AGC TTG TCT GGC CAC CAG –’3 and 5’ – CTG GTG GCC AGA CAA GCT GGC ATA CGC GTC CCA AGT GCC AGT–’3 and 5’ –

20-1	T4L	S224(5.73)-T4L-V231(6.21)	5’ – CAG CAT GTG GCC AGC TTG TCT AAT ATA TTT GAA ATG TTA CGT ATA–’3 , 5’ – TAT ACG TAA CAT TTC AAA TAT ATT AGA CAA GCT GGC CAC ATG CTG –’3, ,5’ – ACT GGC ACT TGG GAC GCG TAT GTG CCA GGA ATG GCC CGA ATG –’3 and 5’ –CAT TCG GGC CAT TCC TGG CAC ATA CGC GTC CCA AGT GCC AGT –’3.
14-1	apoRIL	V220(5.69)-APO-A235(6.25)	5’ – TCT CTG GAA GGC CCA TCA GCA TGC TGA TCT GGA AGA CAA TTG GG –’3 ,5’ – CCC AAT TGT CTT CCA GAT CAG CAT GCT GAT GGG CCT TCC AGA GA–’3, 5’ –TGC ATA CAT TCA GAA GTA CCT GCG AAT GAG GCT GGA TGT GAG GTT GG –’3 and 5’ –CCA ACC TCA CAT CCA GCC TCA TTC GCA GGT ACT TCT GAA TGT ATG C –’3
20-2	apoRIL	S224(5.73)-APO-V231(6.21)	5’ –CAT CAG CAT GTG GCC AGC TTG TCT GCT GAT CTG GAA GAA AAT TGG GAA –’3 ,5’ – TTC CCA ATT GTC TTC CAG ATC AGC AGA CAA GCT GGC CAC ATG CTG ATG–’3 ,5’ – AAT GCA TAC ATT CAG AAG TAC CTG GTG CCA GGA ATG GCC CGA ATG AGG–’3 and 5’ – CCT CAT TCG GGC CAT TCC TGG CAC CAG GTA GTT CTG AAT GTA TGC ATT –’3

Table 18. The PCR condition to conform the recombinant protein insertion.

Recombinant bacmid DNA	100 ng
10X PCR Buffer (thermoPol)	2.5 µl
10 mM dNTP Mix	0.5 µl
PCR Primers	0.5 µl each 10 M stock
Taq polymerase thermoPol	0.125 µl
Sterile Water	Add to 25 µl

Using the following condition:

3 step PCR Method for 30 cycles:

Initial denaturing

95C for 30 sec

30 cycles:

95°C	15-30 sec.
55°C	45 sec.
68°C	1min/kb
68°C	5 min

Table 19. Details procedure protocol for the detergent solubilization of membrane protein.

Take pellet out of -80C and let it be thawing

Prepare the Lysis buffer

Lysis buffer 100ml:

Stock buffer	Volume	Final concentration
1M Tris pH 7.6	1ml	10mM
0.25M EDTA pH 8.0	0.4ml	1mM
*IA powder	0.2g	2mg/ml
*400X Protease inhibitors	0.25ml	1X
*SR144528 or 10mM	2ul	200nM

Add water to 50ml

*Add freshly right before use

Transfer the half thawed pellet into Lysis buffer. Stir at 4C for 30mins. Split them into 9 parts with equal amount.

Spin down at 18,000 rpm for 15mins. Discard the supernatant.

Prepare solubilization buffers.

First make a basic composition without detergent and CHS.

Solubilization buffer Basic 100 ml:

Stock buffer	Volume	Final concentration
1M HEPES pH 7.8	3ml	30mM
5M NaCl	15ml	750mM
50%Glycerol	60ml	30%
*IA powder	0.2g	2mg/ml
*400X Protease inhibitors	0.25ml	1X
*SR144528 10mM	2ul	200nM

Add water to 100ml.

*Add freshly right before use

Split them into 10 parts with 10 ml each.

Then add detergent and CHS in.

Solubilization buffer (DDM-0.5) 10 ml:

Stock buffer	Volume	Final concentration
DDM powder	0.05g	0.5%
CHS powder	0.003g	0.03%

Solubilization buffer (DDM-1) 10 ml:

Stock buffer	Volume	Final concentration
DDM powder	0.1g	1%
CHS powder	0.003g	0.03%

Solubilization buffer (DDM-1+NaCholate 0.2) 10 ml:

Stock buffer	Volume	Final concentration
DDM powder	0.1g	1%
NaCholate powder	0.02g	0.2%
CHS powder	0.003g	0.03%

Solubilization buffer (MNG-0.5) 10 ml:

Stock buffer	Volume	Final concentration
MNG powder	0.05g	0.5%
CHS powder	0.003g	0.03%

Solubilization buffer (MNG-1) 10 ml:

Stock buffer	Volume	Final concentration
MNG powder	0.1g	1%
CHS powder	0.003g	0.03%

Solubilization buffer (MNG-1+NaCholate 0.2) 10 ml:

Stock buffer	Volume	Final concentration
DDM powder	0.1g	1%
NaCholate powder	0.02g	0.2%
CHS powder	0.003g	0.03%

Solubilization buffer (FC14-0.5) 10 ml:

Stock buffer	Volume	Final concentration
FC14 powder	0.05g	0.5%
CHS powder	0.003g	0.03%

Solubilization buffer (FC14-1) 10 ml:

Stock buffer	Volume	Final concentration
FC14 powder	0.1g	1%
CHS powder	0.003g	0.03%

Solubilization buffer (FC14-1+NaCholate 0.2) 10 ml:

Stock buffer	Volume	Final concentration
FC14 powder	0.1g	1%
NaCholate powder	0.02g	0.2%
CHS powder	0.003g	0.03%

Dissolve them by vortexing and mix under room temperature.

Add each of the 10ml solubilization buffer to each membranes and dounce for 20-30 times. (Take 20ul out from each sample for western)

Then mixing them for 2 hours at 4 degrees.

Centrifuge at 18,000 rpm (or maximum speed) at 4 degree for 30 minutes.

Take out 20ul out from each sample for western. Western Blot: add 20ul protein loading buffer into 10ul sample. Mix at room temperature for 5min before loading onto SDS-PAGE. 30ul samples each.

A.

P34972 (100%), 39,682.0 Da
CNR2_HUMAN Cannabinoid receptor 2 OS=Homo sapiens GN=CNR2 PE=1 SV=1
6 exclusive unique peptides, 13 exclusive unique spectra, 41 total spectra, 76/360 amino acids (21% coverage)

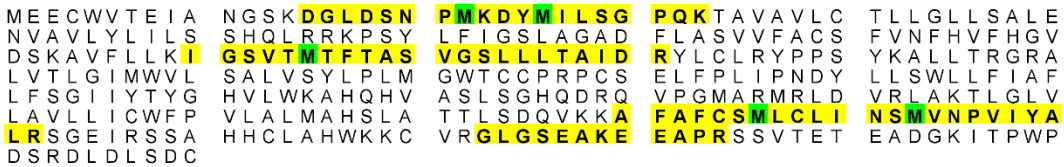

B.

Valid	...	Sequence	Prob	Masco...	Mascot Identity score	Mascot D...	NTT	Modifications	Observed	Actual Mass	Charge	Delta ...	Delta ...	Rete...	Intensity	TIC	Start	Stop	# Ot...	Other Prot...	Spectrum ID
☑	✓	(K)DGLDSNPMK(D)	99%	56.7	41.4	29.8	2	Oxidation (+16)	496.88	991.75	2	0.32	320	514		0.0000	15	23	0		File:P069483.mzX...
☑	✓	(K)DGLDSNPMK(D)	98%	54.5	41.6	22.1	2	Oxidation (+16)	496.76	991.51	2	0.077	78	451		0.0000	15	23	0		File:P069483.mzX...
☑	✓	(K)DGLDSNPMK(D)	98%	53.4	41.9	26.3	2	Oxidation (+16)	497.20	992.39	2	0.96	-46	544		0.0000	15	23	0		File:P069483.mzX...
☑	✓	(K)DGLDSNPMK(D)	98%	53.1	41.7	24.2	2		488.87	975.73	2	0.29	300	1610		0.0000	15	23	0		File:P069483.mzX...
☑	✓	(K)DGLDSNPMK(D)	97%	50.7	42.3	26.1	2		489.21	976.41	2	0.97	-32	1490		0.0000	15	23	0		File:P069483.mzX...
☑	✓	(K)DGLDSNPMK(D)	97%	49.1	42.4	19.6	2		489.12	976.23	2	0.79	-220	1520		0.0000	15	23	0		File:P069483.mzX...
☑	✓	(K)DGLDSNPMK(D)	96%	48.5	40.7	17.9	2	Oxidation (+16)	497.29	992.57	2	1.1	140	421		0.0000	15	23	0		File:P069483.mzX...
☑	✓	(K)DGLDSNPMK(D)	95%	46.6	40.9	25.0	2	Oxidation (+16)	496.86	991.71	2	0.28	280	483		0.0000	15	23	0		File:P069483.mzX...
☑	✓	(K)DGLDSNPMK(D)	91%	42.3	42.4	14.1	2		489.11	976.21	2	0.77	-240	1550		0.0000	15	23	0		File:P069483.mzX...
☑	✓	(K)DGLDSNPMK(D)	90%	41.8	42.1	15.7	2	Oxidation (+16)	496.66	991.31	2	-0.12	-120	384		0.0000	15	23	0		File:P069483.mzX...
☑	✓	(K)DGLDSNPMKDYMILSGPQK(T)	100%	66.9	40.0	54.3	2		1,055.38	2,108.75	2	0.75	-120	3270		0.0000	15	33	0		File:P069483.mzX...
☑	✓	(K)DGLDSNPMKDYMILSGPQK(T)	100%	54.5	40.3	34.8	2	Oxidation (+16), ...	714.91	2,141.71	3	1.7	-130	2640		0.0000	15	33	0		File:P069483.mzX...
☑	✓	(K)DGLDSNPMKDYMILSGPQK(T)	99%	54.3	40.5	36.1	2	Oxidation (+16), ...	715.17	2,142.49	3	2.5	230	2520		0.0000	15	33	0		File:P069483.mzX...
☑	✓	(K)DGLDSNPMKDYMILSGPQK(T)	99%	52.5	39.3	12.8	2	Oxidation (+16)	709.65	2,125.93	3	1.9	-30	3040		0.0000	15	33	0		File:P069483.mzX...
☑	✓	(K)DGLDSNPMKDYMILSGPQK(T)	98%	48.2	39.5	16.5	2	Oxidation (+16)	709.66	2,125.96	3	2.0	-16	2750		0.0000	15	33	0		File:P069483.mzX...
☑	✓	(K)DGLDSNPMKDYMILSGPQK(T)	98%	47.3	39.4	29.4	2	Oxidation (+16), ...	714.99	2,141.95	3	2.0	-19	2550		0.0000	15	33	0		File:P069483.mzX...
☑	✓	(K)DGLDSNPMKDYMILSGPQK(T)	98%	46.9	39.7	15.6	2	Oxidation (+16)	709.34	2,125.00	3	1.0	3.7	3010		0.0000	15	33	0		File:P069483.mzX...
☑	✓	(K)DGLDSNPMKDYMILSGPQK(T)	97%	49.0	39.2	37.6	2		1,055.44	2,108.87	2	0.87	-62	3300		0.0000	15	33	0		File:P069483.mzX...
☑	✓	(K)DGLDSNPMKDYMILSGPQK(T)	96%	44.0	40.6	26.0	2	Oxidation (+16), ...	714.82	2,141.44	3	1.5	210	2610		0.0000	15	33	0		File:P069483.mzX...
☑	✓	(K)DGLDSNPMKDYMILSGPQK(T)	91%	42.5	40.4	15.2	2	Oxidation (+16)	1,063.67	2,125.33	2	1.3	160	3020		0.0000	15	33	0		File:P069483.mzX...
☑	✓	(K)DGLDSNPMKDYMILSGPQK(T)	90%	39.0	40.5	22.7	2	Oxidation (+16), ...	714.73	2,141.17	3	1.2	85	2380		0.0000	15	33	0		File:P069483.mzX...
☑	✓	(K)DYMILSGPQK(T)	100%	67.4	41.2	45.6	2	Oxidation (+16)	584.66	1,167.31	2	0.74	-220	2090		0.0000	24	33	0		File:P069483.mzX...
☑	✓	(K)DYMILSGPQK(T)	99%	55.6	41.2	30.6	2	Oxidation (+16)	584.76	1,167.51	2	0.94	-53	2060		0.0000	24	33	0		File:P069483.mzX...
☑	✓	(K)DYMILSGPQK(T)	99%	54.5	41.3	28.5	2		576.72	1,151.43	2	0.86	-130	2430		0.0000	24	33	0		File:P069483.mzX...
☑	✓	(K)DYMILSGPQK(T)	98%	53.9	41.5	35.7	2		576.14	1,150.27	2	-0.30	-260	2400		0.0000	24	33	0		File:P069483.mzX...
☑	✓	(K)DYMILSGPQK(T)	97%	50.4	41.5	29.4	2		576.11	1,150.21	2	-0.36	-320	2550		0.0000	24	33	0		File:P069483.mzX...
☑	✓	(K)DYMILSGPQK(T)	96%	48.0	40.1	30.4	2	Oxidation (+16)	584.88	1,167.75	2	1.2	150	2190		0.0000	24	33	0		File:P069483.mzX...
☑	✓	(K)DYMILSGPQK(T)	94%	45.6	41.2	26.1	2	Oxidation (+16)	584.74	1,167.47	2	0.90	-87	2190		0.0000	24	33	0		File:P069483.mzX...
☑	✓	(K)DYMILSGPQK(T)	91%	42.3	41.2	18.2	2	Oxidation (+16)	584.70	1,167.39	2	0.82	-160	2140		0.0000	24	33	0		File:P069483.mzX...
☑	✓	(K)IGSVTMTFTASVGSLLLTAIDR(Y)	100%	54.6	39.4	38.5	2	Oxidation (+16)	757.73	2,270.17	3	2.0	-18	5050		0.0000	110	131	0		File:P069483.mzX...
☑	✓	(K)IGSVTMTFTASVGSLLLTAIDR(Y)	96%	48.3	40.0	36.8	2	Oxidation (+16)	1,136.43	2,270.85	2	2.6	-160	5020		0.0000	110	131	0		File:P069483.mzX...
☑	✓	(K)IGSVTMTFTASVGSLLLTAIDR(Y)	93%	44.1	40.1	34.6	2	Oxidation (+16)	1,135.28	2,268.55	2	0.34	150	5020		0.0000	110	131	0		File:P069483.mzX...
☑	✓	(K)AFAFCSMLCLINSMVNPVIYALR(S)	100%	75.4	39.5	61.9	2	Carbamidomethyl...	908.35	2,722.03	3	0.71	-110	4580		0.0000	280	302	0		File:P069483.mzX...
☑	✓	(K)AFAFCSMLCLINSMVNPVIYALR(S)	100%	70.2	38.8	36.0	2	Carbamidomethyl...	903.56	2,707.66	3	2.3	120	5350		0.0000	280	302	0		File:P069483.mzX...
☑	✓	(K)AFAFCSMLCLINSMVNPVIYALR(S)	98%	54.4	39.1	43.2	2	Carbamidomethyl...	1,362.89	2,723.77	2	2.5	160	4570		0.0000	280	302	0		File:P069483.mzX...
☑	✓	(K)AFAFCSMLCLINSMVNPVIYALR(S)	97%	45.7	39.5	15.8	2	Carbamidomethyl...	903.09	2,706.25	3	0.93	-28	5320		0.0000	280	302	0		File:P069483.mzX...
☑	✓	(K)AFAFCSMLCLINSMVNPVIYALR(S)	97%	44.3	39.5	16.1	2	Carbamidomethyl...	903.65	2,707.93	3	2.6	-150	5190		0.0000	280	302	0		File:P069483.mzX...
☑	✓	(K)AFAFCSMLCLINSMVNPVIYALR(S)	96%	43.7	39.5	22.5	2	Carbamidomethyl...	908.33	2,721.97	3	0.65	-130	4550		0.0000	280	302	0		File:P069483.mzX...
☑	✓	(R)GLGSEAKEEAPR(S)	100%	62.2	41.5	35.3	2		622.35	1,242.69	2	0.065	52	1240		0.0000	323	334	0		File:P069483.mzX...
☑	✓	(R)GLGSEAKEEAPR(S)	99%	55.1	41.1	30.8	2		622.40	1,242.79	2	0.16	130	1210		0.0000	323	334	0		File:P069483.mzX...
☑	✓	(R)GLGSEAKEEAPR(S)	98%	46.0	40.4	24.4	2		415.63	1,243.87	3	1.2	200	1230		0.0000	323	334	0		File:P069483.mzX...

Figure 6-6. Details mass spectrometry of CB-T4L.

Sequence coverage of trypsin digested peptide fragments identified by MS/MS (A). Details information of spectrum of an identified peptide fragment (B).

BIBLIOGRAPHY

1. Oesterhelt, D. and J. Tittor, *Two pumps, one principle: light-driven ion transport in halobacteria.* Trends Biochem Sci, 1989. **14**(2): p. 57-61.
2. Bjarnadottir, T.K., et al., *Comprehensive repertoire and phylogenetic analysis of the G protein-coupled receptors in human and mouse.* Genomics, 2006. **88**(3): p. 263-73.
3. Ren, H., et al., *High-level production, solubilization and purification of synthetic human GPCR chemokine receptors CCR5, CCR3, CXCR4 and CX3CR1.* PLoS One, 2009. **4**(2): p. e4509.
4. Wise, A., K. Gearing, and S. Rees, *Target validation of G-protein coupled receptors.* Drug Discov Today, 2002. **7**(4): p. 235-46.
5. Yoshida, M., M. Miyazato, and K. Kangawa, *Orphan GPCRs and methods for identifying their ligands.* Methods Enzymol, 2012. **514**: p. 33-44.
6. Palczewski, K. and T. Orban, *From atomic structures to neuronal functions of g protein-coupled receptors.* Annu Rev Neurosci, 2013. **36**: p. 139-64.
7. Katritch, V., V. Cherezov, and R.C. Stevens, *Diversity and modularity of G protein-coupled receptor structures.* Trends Pharmacol Sci, 2012. **33**(1): p. 17-27.
8. Fredriksson, R., et al., *The G-protein-coupled receptors in the human genome form five main families. Phylogenetic analysis, paralogon groups, and fingerprints.* Mol Pharmacol, 2003. **63**(6): p. 1256-72.
9. Attwood, T.K. and J.B. Findlay, *Fingerprinting G-protein-coupled receptors.* Protein Eng, 1994. **7**(2): p. 195-203.
10. Lagerstrom, M.C. and H.B. Schioth, *Structural diversity of G protein-coupled receptors and significance for drug discovery.* Nat Rev Drug Discov, 2008. **7**(4): p. 339-57.
11. Ahren, B., *Islet G protein-coupled receptors as potential targets for treatment of type 2 diabetes.* Nat Rev Drug Discov, 2009. **8**(5): p. 369-85.
12. Bjarnadottir, T.K., R. Fredriksson, and H.B. Schioth, *The adhesion GPCRs: a unique family of G protein-coupled receptors with important roles in both central and peripheral tissues.* Cell Mol Life Sci, 2007. **64**(16): p. 2104-19.
13. Paavola, K.J. and R.A. Hall, *Adhesion G protein-coupled receptors: signaling, pharmacology, and mechanisms of activation.* Mol Pharmacol, 2012. **82**(5): p. 777-83.
14. Niswender, C.M. and P.J. Conn, *Metabotropic glutamate receptors: physiology, pharmacology, and disease.* Annu Rev Pharmacol Toxicol, 2010. **50**: p. 295-322.
15. Sheffler, D.J., et al., *Allosteric modulation of metabotropic glutamate receptors.* Adv Pharmacol, 2011. **62**: p. 37-77.
16. Wang, C., et al., *Structure of the human smoothened receptor bound to an antitumour agent.* Nature, 2013. **497**(7449): p. 338-43.
17. Schulte, G. and V. Bryja, *The Frizzled family of unconventional G-protein-coupled receptors.* Trends Pharmacol Sci, 2007. **28**(10): p. 518-25.
18. Hutchings, C.J., M. Koglin, and F.H. Marshall, *Therapeutic antibodies directed at G protein-coupled receptors.* MAbs, 2010. **2**(6): p. 594-606.
19. Bockaert, J. and J.P. Pin, *Molecular tinkering of G protein-coupled receptors: an evolutionary success.* EMBO J, 1999. **18**(7): p. 1723-9.

20. Kobilka, B.K., *G protein coupled receptor structure and activation.* Biochim Biophys Acta, 2007. **1768**(4): p. 794-807.
21. Kenakin, T., *Inverse, protean, and ligand-selective agonism: matters of receptor conformation.* FASEB J, 2001. **15**(3): p. 598-611.
22. Mobarec, J.C. and M. Filizola, *Advances in the Development and Application of Computational Methodologies for Structural Modeling of G-Protein Coupled Receptors.* Expert Opin Drug Discov, 2008. **3**(3): p. 343-355.
23. Kristiansen, K., *Molecular mechanisms of ligand binding, signaling, and regulation within the superfamily of G-protein-coupled receptors: molecular modeling and mutagenesis approaches to receptor structure and function.* Pharmacol Ther, 2004. **103**(1): p. 21-80.
24. Venkatakrishnan, A.J., et al., *Molecular signatures of G-protein-coupled receptors.* Nature, 2013. **494**(7436): p. 185-94.
25. Kobilka, B.K. and X. Deupi, *Conformational complexity of G-protein-coupled receptors.* Trends Pharmacol Sci, 2007. **28**(8): p. 397-406.
26. Xie, X.Q. and A. Chowdhury, *Advances in methods to characterize ligand-induced ionic lock and rotamer toggle molecular switch in G protein-coupled receptors.* Methods Enzymol, 2013. **520**: p. 153-74.
27. Palczewski, K., et al., *Crystal structure of rhodopsin: A G protein-coupled receptor.* Science, 2000. **289**(5480): p. 739-45.
28. Shim, J.Y., *Understanding functional residues of the cannabinoid CB1.* Curr Top Med Chem, 2010. **10**(8): p. 779-98.
29. Alewijnse, A.E., et al., *The effect of mutations in the DRY motif on the constitutive activity and structural instability of the histamine H(2) receptor.* Mol Pharmacol, 2000. **57**(5): p. 890-8.
30. Chien, E.Y., et al., *Structure of the human dopamine D3 receptor in complex with a D2/D3 selective antagonist.* Science, 2010. **330**(6007): p. 1091-5.
31. Trzaskowski, B., et al., *Action of molecular switches in GPCRs--theoretical and experimental studies.* Curr Med Chem, 2012. **19**(8): p. 1090-109.
32. Vilardaga, J.P., *Switching modes for G protein-coupled receptor activation.* Nat Chem Biol, 2006. **2**(8): p. 395-6.
33. Gether, U., et al., *Structural instability of a constitutively active G protein-coupled receptor. Agonist-independent activation due to conformational flexibility.* J Biol Chem, 1997. **272**(5): p. 2587-90.
34. Shi, L., et al., *Beta2 adrenergic receptor activation. Modulation of the proline kink in transmembrane 6 by a rotamer toggle switch.* J Biol Chem, 2002. **277**(43): p. 40989-96.
35. Jongejan, A., et al., *Linking agonist binding to histamine H1 receptor activation.* Nat Chem Biol, 2005. **1**(2): p. 98-103.
36. Van Arnam, E.B., H.A. Lester, and D.A. Dougherty, *Dissecting the functions of conserved prolines within transmembrane helices of the D2 dopamine receptor.* ACS Chem Biol, 2011. **6**(10): p. 1063-8.
37. Tan, E.S., et al., *Toward deciphering the code to aminergic G protein-coupled receptor drug design.* Chem Biol, 2008. **15**(4): p. 343-53.
38. McAllister, S.D., et al., *An aromatic microdomain at the cannabinoid CB(1) receptor constitutes an agonist/inverse agonist binding region.* J Med Chem, 2003. **46**(24): p. 5139-52.

39. McAllister, S.D., et al., *Structural mimicry in class A G protein-coupled receptor rotamer toggle switches: the importance of the F3.36(201)/W6.48(357) interaction in cannabinoid CB1 receptor activation.* J Biol Chem, 2004. **279**(46): p. 48024-37.
40. Feng, Z., et al., *Modeling, molecular dynamics simulation, and mutation validation for structure of cannabinoid receptor 2 based on known crystal structures of GPCRs.* J Chem Inf Model, 2014. **54**(9): p. 2483-99.
41. Rhee, M.H., et al., *Role of the highly conserved Asp-Arg-Tyr motif in signal transduction of the CB2 cannabinoid receptor.* FEBS Lett, 2000. **466**(2-3): p. 300-4.
42. Tuteja, N., *Signaling through G protein coupled receptors.* Plant Signal Behav, 2009. **4**(10): p. 942-7.
43. Rosenbaum, D.M., S.G. Rasmussen, and B.K. Kobilka, *The structure and function of G-protein-coupled receptors.* Nature, 2009. **459**(7245): p. 356-63.
44. Insel, P.A. and R.S. Ostrom, *Forskolin as a tool for examining adenylyl cyclase expression, regulation, and G protein signaling.* Cell Mol Neurobiol, 2003. **23**(3): p. 305-14.
45. Yao, X., et al., *Coupling ligand structure to specific conformational switches in the beta2-adrenoceptor.* Nat Chem Biol, 2006. **2**(8): p. 417-22.
46. Swaminath, G., et al., *Sequential binding of agonists to the beta2 adrenoceptor. Kinetic evidence for intermediate conformational states.* J Biol Chem, 2004. **279**(1): p. 686-91.
47. Katritch, V., V. Cherezov, and R.C. Stevens, *Structure-function of the G protein-coupled receptor superfamily.* Annu Rev Pharmacol Toxicol, 2013. **53**: p. 531-56.
48. Grisshammer, R., *Purification of recombinant G-protein-coupled receptors.* Methods Enzymol, 2009. **463**: p. 631-45.
49. Chiu, M.L., et al., *Over-expression, solubilization, and purification of G protein-coupled receptors for structural biology.* Comb Chem High Throughput Screen, 2008. **11**(6): p. 439-62.
50. Sarramegn, V., et al., *Recombinant G protein-coupled receptors from expression to renaturation: a challenge towards structure.* Cell Mol Life Sci, 2006. **63**(10): p. 1149-64.
51. Chun, E., et al., *Fusion partner toolchest for the stabilization and crystallization of G protein-coupled receptors.* Structure, 2012. **20**(6): p. 967-76.
52. Brueckner, F., et al., *Structure of beta-adrenergic receptors.* Methods Enzymol, 2013. **520**: p. 117-51.
53. Kobilka, B. and G.F. Schertler, *New G-protein-coupled receptor crystal structures: insights and limitations.* Trends Pharmacol Sci, 2008. **29**(2): p. 79-83.
54. Sharma, S. and S.C. Sharma, *An update on eicosanoids and inhibitors of cyclooxygenase enzyme systems.* Indian J Exp Biol, 1997. **35**(10): p. 1025-31.
55. Nie, J. and D.L. Lewis, *Structural domains of the CB1 cannabinoid receptor that contribute to constitutive activity and G-protein sequestration.* J Neurosci, 2001. **21**(22): p. 8758-64.
56. Shukla, A.K., J.P. Sun, and R.J. Lefkowitz, *Crystallizing thinking about the beta2-adrenergic receptor.* Mol Pharmacol, 2008. **73**(5): p. 1333-8.
57. Wu, B., et al., *Structures of the CXCR4 chemokine GPCR with small-molecule and cyclic peptide antagonists.* Science, 2010. **330**(6007): p. 1066-71.
58. Jaakola, V.P., et al., *The 2.6 angstrom crystal structure of a human A2A adenosine receptor bound to an antagonist.* Science, 2008. **322**(5905): p. 1211-7.
59. Milic, D. and D.B. Veprintsev, *Large-scale production and protein engineering of G protein-coupled receptors for structural studies.* Front Pharmacol, 2015. **6**: p. 66.

60. Rasmussen, S.G., et al., *Structure of a nanobody-stabilized active state of the beta(2) adrenoceptor.* Nature, 2011. **469**(7329): p. 175-80.
61. Hino, T., et al., *G-protein-coupled receptor inactivation by an allosteric inverse-agonist antibody.* Nature, 2012. **482**(7384): p. 237-40.
62. Rasmussen, S.G., et al., *Crystal structure of the human beta2 adrenergic G-protein-coupled receptor.* Nature, 2007. **450**(7168): p. 383-7.
63. Cherezov, V., et al., *High-resolution crystal structure of an engineered human beta2-adrenergic G protein-coupled receptor.* Science, 2007. **318**(5854): p. 1258-65.
64. Shimamura, T., et al., *Structure of the human histamine H1 receptor complex with doxepin.* Nature, 2011. **475**(7354): p. 65-70.
65. Hanson, M.A., et al., *Crystal structure of a lipid G protein-coupled receptor.* Science, 2012. **335**(6070): p. 851-5.
66. Haga, K., et al., *Structure of the human M2 muscarinic acetylcholine receptor bound to an antagonist.* Nature, 2012. **482**(7386): p. 547-51.
67. Granier, S., et al., *Structure of the delta-opioid receptor bound to naltrindole.* Nature, 2012. **485**(7398): p. 400-4.
68. White, J.F., et al., *Structure of the agonist-bound neurotensin receptor.* Nature, 2012. **490**(7421): p. 508-13.
69. Zhang, C., et al., *High-resolution crystal structure of human protease-activated receptor 1.* Nature, 2012. **492**(7429): p. 387-92.
70. Hollenstein, K., et al., *Structure of class B GPCR corticotropin-releasing factor receptor 1.* Nature, 2013. **499**(7459): p. 438-43.
71. Kruse, A.C., et al., *Structure and dynamics of the M3 muscarinic acetylcholine receptor.* Nature, 2012. **482**(7386): p. 552-6.
72. Manglik, A., et al., *Crystal structure of the micro-opioid receptor bound to a morphinan antagonist.* Nature, 2012. **485**(7398): p. 321-6.
73. Wacker, D., et al., *Structural features for functional selectivity at serotonin receptors.* Science, 2013. **340**(6132): p. 615-9.
74. Tan, Q., et al., *Structure of the CCR5 chemokine receptor-HIV entry inhibitor maraviroc complex.* Science, 2013. **341**(6152): p. 1387-90.
75. Fenalti, G., et al., *Molecular control of delta-opioid receptor signalling.* Nature, 2014. **506**(7487): p. 191-6.
76. Thompson, A.A., et al., *Structure of the nociceptin/orphanin FQ receptor in complex with a peptide mimetic.* Nature, 2012. **485**(7398): p. 395-9.
77. Wu, H., et al., *Structure of a class C GPCR metabotropic glutamate receptor 1 bound to an allosteric modulator.* Science, 2014. **344**(6179): p. 58-64.
78. Kruse, A.C., et al., *Activation and allosteric modulation of a muscarinic acetylcholine receptor.* Nature, 2013. **504**(7478): p. 101-6.
79. Egloff, P., et al., *Structure of signaling-competent neurotensin receptor 1 obtained by directed evolution in Escherichia coli.* Proc Natl Acad Sci U S A, 2014. **111**(6): p. E655-62.
80. Scott, D.J., et al., *Stabilizing membrane proteins through protein engineering.* Curr Opin Chem Biol, 2013. **17**(3): p. 427-35.
81. Tate, C.G., *A crystal clear solution for determining G-protein-coupled receptor structures.* Trends Biochem Sci, 2012. **37**(9): p. 343-52.

82. Reilander, H. and H.M. Weiss, *Production of G-protein-coupled receptors in yeast.* Curr Opin Biotechnol, 1998. **9**(5): p. 510-7.
83. Asada, H., et al., *Evaluation of the Pichia pastoris expression system for the production of GPCRs for structural analysis.* Microb Cell Fact, 2011. **10**: p. 24.
84. McCusker, E.C., et al., *Heterologous GPCR expression: a bottleneck to obtaining crystal structures.* Biotechnol Prog, 2007. **23**(3): p. 540-7.
85. Shiroishi, M., et al., *Production of the stable human histamine H(1) receptor in Pichia pastoris for structural determination.* Methods, 2011. **55**(4): p. 281-6.
86. David, N.E., et al., *Expression and purification of the Saccharomyces cerevisiae alpha-factor receptor (Ste2p), a 7-transmembrane-segment G protein-coupled receptor.* J Biol Chem, 1997. **272**(24): p. 15553-61.
87. Lundstrom, K., *Structural genomics of GPCRs.* Trends Biotechnol, 2005. **23**(2): p. 103-8.
88. Lu, Q., J.C. Bauer, and A. Greener, *Using Schizosaccharomyces pombe as a host for expression and purification of eukaryotic proteins.* Gene, 1997. **200**(1-2): p. 135-44.
89. Lundstrom, K.H. and M.L. Chiu, *G protein-coupled receptors in drug discovery*. Drug discovery series. 2006, Boca Raton: Taylor & Francis. 362 p.
90. Zhang, R., et al., *Biochemical and mass spectrometric characterization of the human CB2 cannabinoid receptor expressed in Pichia pastoris--importance of correct processing of the N-terminus.* Protein Expr Purif, 2007. **55**(2): p. 225-35.
91. Kim, T.K., et al., *Expression and characterization of human CB1 cannabinoid receptor in methylotrophic yeast Pichia pastoris.* Protein Expr Purif, 2005. **40**(1): p. 60-70.
92. Feng, W., et al., *Expression of CB2 cannabinoid receptor in Pichia pastoris.* Protein Expr Purif, 2002. **26**(3): p. 496-505.
93. Mathew, E., et al., *Functional fusions of T4 lysozyme in the third intracellular loop of a G protein-coupled receptor identified by a random screening approach in yeast.* Protein Eng Des Sel, 2013. **26**(1): p. 59-71.
94. Milic, D. and D.B. Veprintsev, *Large-Scale Production and Protein Engineering of G Protein-Coupled Receptors for Structural Studies.* Frontiers in Pharmacology, 2015. **6**.
95. Reckel, S., et al., *Solution NMR structure of proteorhodopsin.* Angew Chem Int Ed Engl, 2011. **50**(50): p. 11942-6.
96. Wada, T., et al., *Crystal structure of the eukaryotic light-driven proton-pumping rhodopsin, Acetabularia rhodopsin II, from marine alga.* J Mol Biol, 2011. **411**(5): p. 986-98.
97. Chakraborty, R., et al., *Expression of G protein-coupled receptors in Mammalian cells.* Methods Enzymol, 2015. **556**: p. 267-81.
98. Andrell, J. and C.G. Tate, *Overexpression of membrane proteins in mammalian cells for structural studies.* Mol Membr Biol, 2013. **30**(1): p. 52-63.
99. Shukla, A.K., et al., *Biochemical and pharmacological characterization of the human bradykinin subtype 2 receptor produced in mammalian cells using the Semliki Forest virus system.* Biol Chem, 2006. **387**(5): p. 569-76.
100. Sen, S., et al., *Functional expression and direct visualization of the human alpha 2B -adrenergic receptor and alpha 2B -AR-green fluorescent fusion protein in mammalian cell using Semliki Forest virus vectors.* Protein Expr Purif, 2003. **32**(2): p. 265-75.
101. Shukla, A.K., C. Reinhart, and H. Michel, *Comparative analysis of the human angiotensin II type 1a receptor heterologously produced in insect cells and mammalian cells.* Biochem Biophys Res Commun, 2006. **349**(1): p. 6-14.

102. Standfuss, J., et al., *Crystal structure of a thermally stable rhodopsin mutant.* J Mol Biol, 2007. **372**(5): p. 1179-88.
103. Kim, T.K. and J.H. Eberwine, *Mammalian cell transfection: the present and the future.* Anal Bioanal Chem, 2010. **397**(8): p. 3173-8.
104. Standfuss, J., et al., *The structural basis of agonist-induced activation in constitutively active rhodopsin.* Nature, 2011. **471**(7340): p. 656-60.
105. Deupi, X., et al., *Stabilized G protein binding site in the structure of constitutively active metarhodopsin-II.* Proc Natl Acad Sci U S A, 2012. **109**(1): p. 119-24.
106. Singhal, A., et al., *Insights into congenital stationary night blindness based on the structure of G90D rhodopsin.* EMBO Rep, 2013. **14**(6): p. 520-6.
107. Kaushal, S., K.D. Ridge, and H.G. Khorana, *Structure and function in rhodopsin: the role of asparagine-linked glycosylation.* Proc Natl Acad Sci U S A, 1994. **91**(9): p. 4024-8.
108. Rands, E., et al., *Mutational analysis of beta-adrenergic receptor glycosylation.* J Biol Chem, 1990. **265**(18): p. 10759-64.
109. Rens-Domiano, S. and T. Reisine, *Structural analysis and functional role of the carbohydrate component of somatostatin receptors.* J Biol Chem, 1991. **266**(30): p. 20094-102.
110. Chowdhury, A., et al., *Mistic and TarCF as fusion protein partners for functional expression of the cannabinoid receptor 2 in Escherichia coli.* Protein Expr Purif, 2012. **83**(2): p. 128-34.
111. Marullo, S., et al., *Human beta 2-adrenergic receptors expressed in Escherichia coli membranes retain their pharmacological properties.* Proc Natl Acad Sci U S A, 1988. **85**(20): p. 7551-5.
112. Weiss, H.M. and R. Grisshammer, *Purification and characterization of the human adenosine A(2a) receptor functionally expressed in Escherichia coli.* Eur J Biochem, 2002. **269**(1): p. 82-92.
113. Grisshammer, R., R. Duckworth, and R. Henderson, *Expression of a rat neurotensin receptor in Escherichia coli.* Biochem J, 1993. **295 (Pt 2)**: p. 571-6.
114. Bertin, B., et al., *Functional expression of the human serotonin 5-HT1A receptor in Escherichia coli. Ligand binding properties and interaction with recombinant G protein alpha-subunits.* J Biol Chem, 1992. **267**(12): p. 8200-6.
115. Hulme, E.C. and C.A. Curtis, *Purification of recombinant M1 muscarinic acetylcholine receptor.* Biochem Soc Trans, 1998. **26**(4): p. S361.
116. Furukawa, H. and T. Haga, *Expression of functional M2 muscarinic acetylcholine receptor in Escherichia coli.* J Biochem, 2000. **127**(1): p. 151-61.
117. Michalke, K., et al., *Mammalian G-protein-coupled receptor expression in Escherichia coli: I. High-throughput large-scale production as inclusion bodies.* Anal Biochem, 2009. **386**(2): p. 147-55.
118. Bane, S.E., J.E. Velasquez, and A.S. Robinson, *Expression and purification of milligram levels of inactive G-protein coupled receptors in E. coli.* Protein Expr Purif, 2007. **52**(2): p. 348-55.
119. McCusker, E. and A.S. Robinson, *Refolding of G protein alpha subunits from inclusion bodies expressed in Escherichia coli.* Protein Expr Purif, 2008. **58**(2): p. 342-55.
120. Vallejo, L.F. and U. Rinas, *Strategies for the recovery of active proteins through refolding of bacterial inclusion body proteins.* Microb Cell Fact, 2004. **3**(1): p. 11.

121. Kiefer, H., et al., *Expression of an olfactory receptor in Escherichia coli: purification, reconstitution, and ligand binding.* Biochemistry, 1996. **35**(50): p. 16077-84.
122. Baneres, J.L., et al., *Molecular characterization of a purified 5-HT4 receptor: a structural basis for drug efficacy.* J Biol Chem, 2005. **280**(21): p. 20253-60.
123. Arcemisbehere, L., et al., *Leukotriene BLT2 receptor monomers activate the G(i2) GTP-binding protein more efficiently than dimers.* J Biol Chem, 2010. **285**(9): p. 6337-47.
124. Michalke, K., et al., *Mammalian G protein-coupled receptor expression in Escherichia coli: II. Refolding and biophysical characterization of mouse cannabinoid receptor 1 and human parathyroid hormone receptor 1.* Anal Biochem, 2010. **401**(1): p. 74-80.
125. Derynck, R., et al., *Human transforming growth factor-alpha: precursor structure and expression in E. coli.* Cell, 1984. **38**(1): p. 287-97.
126. Xie, X.Q., J. Zhao, and H. Zheng, *Expression, purification, and isotope labeling of cannabinoid CB2 receptor fragment, CB2(180-233).* Protein Expr Purif, 2004. **38**(1): p. 61-8.
127. Zhang, Y. and X.Q. Xie, *Biosynthesis, purification, and characterization of a cannabinoid receptor 2 fragment (CB2(271-326)).* Protein Expr Purif, 2008. **59**(2): p. 249-57.
128. Zheng, H., et al., *A transmembrane helix-bundle from G-protein coupled receptor CB2: biosynthesis, purification, and NMR characterization.* Biopolymers, 2006. **83**(1): p. 46-61.
129. Zheng, H., et al., *Biosynthesis and purification of a hydrophobic peptide from transmembrane domains of G-protein-coupled CB2 receptor.* J Pept Res, 2005. **65**(4): p. 450-8.
130. Kost, T.A., J.P. Condreay, and D.L. Jarvis, *Baculovirus as versatile vectors for protein expression in insect and mammalian cells.* Nat Biotechnol, 2005. **23**(5): p. 567-75.
131. Kenneth, H.L., *Recombinant G Protein-Coupled Receptors for Drug Discovery*, in *G Protein-Coupled Receptors in Drug Discovery*. 2005, CRC Press. p. 143-158.
132. Warne, T., J. Chirnside, and G.F. Schertler, *Expression and purification of truncated, non-glycosylated turkey beta-adrenergic receptors for crystallization.* Biochim Biophys Acta, 2003. **1610**(1): p. 133-40.
133. Huang, J., et al., *Crystal structure of oligomeric beta1-adrenergic G protein-coupled receptors in ligand-free basal state.* Nat Struct Mol Biol, 2013. **20**(4): p. 419-25.
134. Miller-Gallacher, J.L., et al., *The 2.1 A resolution structure of cyanopindolol-bound beta1-adrenoceptor identifies an intramembrane Na+ ion that stabilises the ligand-free receptor.* PLoS One, 2014. **9**(3): p. e92727.
135. Lebon, G., et al., *Agonist-bound adenosine A2A receptor structures reveal common features of GPCR activation.* Nature, 2011. **474**(7352): p. 521-5.
136. Dong, X., et al., *A diverse family of GPCRs expressed in specific subsets of nociceptive sensory neurons.* Cell, 2001. **106**(5): p. 619-32.
137. Kleymann, G., et al., *Human beta 2-adrenergic receptor produced in stably transformed insect cells is functionally coupled via endogenous GTP-binding protein to adenylyl cyclase.* Eur J Biochem, 1993. **213**(2): p. 797-804.
138. Fisher, i.b.t., *Growth and Maintenance of Insect Cell Lines*. therom Fisher company, 1990.
139. Roy, A., et al., *Employing Rhodobacter sphaeroides to functionally express and purify human G protein-coupled receptors.* Biol Chem, 2008. **389**(1): p. 69-78.
140. Okada, T., K. Takeda, and T. Kouyama, *Highly selective separation of rhodopsin from bovine rod outer segment membranes using combination of divalent cation and alkyl(thio)glucoside.* Photochem Photobiol, 1998. **67**(5): p. 495-9.

141. Murakami, M. and T. Kouyama, *Crystal structure of squid rhodopsin.* Nature, 2008. **453**(7193): p. 363-7.
142. Okada, T., et al., *X-Ray diffraction analysis of three-dimensional crystals of bovine rhodopsin obtained from mixed micelles.* J Struct Biol, 2000. **130**(1): p. 73-80.
143. Salom, D., et al., *Heterologous expression of functional G-protein-coupled receptors in Caenorhabditis elegans.* FASEB J, 2012. **26**(2): p. 492-502.
144. Sarmiento, J., et al., *Adenovirus mediated expression "in vivo" of the chemokine receptor CXCR1.* J Struct Funct Genomics, 2009. **10**(1): p. 17-23.
145. Zhang, L., et al., *Expression of functional G protein-coupled receptors in photoreceptors of transgenic Xenopus laevis.* Biochemistry, 2005. **44**(44): p. 14509-18.
146. Park, S.H., et al., *Structure of the chemokine receptor CXCR1 in phospholipid bilayers.* Nature, 2012. **491**(7426): p. 779-83.
147. Warne, T., et al., *Structure of a beta1-adrenergic G-protein-coupled receptor.* Nature, 2008. **454**(7203): p. 486-91.
148. Wang, C., et al., *Structural basis for molecular recognition at serotonin receptors.* Science, 2013. **340**(6132): p. 610-4.
149. Wu, H., et al., *Structure of the human kappa-opioid receptor in complex with JDTic.* Nature, 2012. **485**(7398): p. 327-32.
150. Zhang, K., et al., *Structure of the human P2Y12 receptor in complex with an antithrombotic drug.* Nature, 2014. **509**(7498): p. 115-8.
151. Yin, J., et al., *Crystal structure of the human OX2 orexin receptor bound to the insomnia drug suvorexant.* Nature, 2015. **519**(7542): p. 247-50.
152. Srivastava, A., et al., *High-resolution structure of the human GPR40 receptor bound to allosteric agonist TAK-875.* Nature, 2014. **513**(7516): p. 124-7.
153. Siu, F.Y., et al., *Structure of the human glucagon class B G-protein-coupled receptor.* Nature, 2013. **499**(7459): p. 444-9.
154. Dore, A.S., et al., *Structure of class C GPCR metabotropic glutamate receptor 5 transmembrane domain.* Nature, 2014. **511**(7511): p. 557-62.
155. Wang, C., et al., *Structural basis for Smoothened receptor modulation and chemoresistance to anticancer drugs.* Nat Commun, 2014. **5**: p. 4355.
156. Pertwee, R.G., *The pharmacology of cannabinoid receptors and their ligands: an overview.* Int J Obes (Lond), 2006. **30 Suppl 1**: p. S13-8.
157. Cota, D., *CB1 receptors: emerging evidence for central and peripheral mechanisms that regulate energy balance, metabolism, and cardiovascular health.* Diabetes Metab Res Rev, 2007. **23**(7): p. 507-17.
158. Watkins, B.A. and J. Kim, *The endocannabinoid system: directing eating behavior and macronutrient metabolism.* Front Psychol, 2014. **5**: p. 1506.
159. Devane, W.A., et al., *Isolation and structure of a brain constituent that binds to the cannabinoid receptor.* Science, 1992. **258**(5090): p. 1946-9.
160. Cravatt, B.F., et al., *Molecular characterization of an enzyme that degrades neuromodulatory fatty-acid amides.* Nature, 1996. **384**(6604): p. 83-7.
161. Dinh, T.P., et al., *Brain monoglyceride lipase participating in endocannabinoid inactivation.* Proc Natl Acad Sci U S A, 2002. **99**(16): p. 10819-24.
162. Reggio, P.H. and H. Traore, *Conformational requirements for endocannabinoid interaction with the cannabinoid receptors, the anandamide transporter and fatty acid amidohydrolase.* Chem Phys Lipids, 2000. **108**(1-2): p. 15-35.

163. Grotenhermen, F., *Pharmacology of cannabinoids.* Neuro Endocrinol Lett, 2004. **25**(1-2): p. 14-23.
164. Hall, W. and N. Solowij, *Adverse effects of cannabis.* Lancet, 1998. **352**(9140): p. 1611-6.
165. Rice, A.S., *Cannabinoids and pain.* Curr Opin Investig Drugs, 2001. **2**(3): p. 399-414.
166. Xie, S., et al., *The endocannabinoid system and rimonabant: a new drug with a novel mechanism of action involving cannabinoid CB1 receptor antagonism--or inverse agonism--as potential obesity treatment and other therapeutic use.* J Clin Pharm Ther, 2007. **32**(3): p. 209-31.
167. Gaoni Y, M.R., *Isolation, structure, and partial synthesis of an active constituent of hashish.* J Am Chem Soc, 1964. **86**: p. 1646–1647.
168. Matsuda, L.A., et al., *Structure of a cannabinoid receptor and functional expression of the cloned cDNA.* Nature, 1990. **346**(6284): p. 561-4.
169. Gerard, C.M., et al., *Molecular cloning of a human cannabinoid receptor which is also expressed in testis.* Biochem J, 1991. **279 (Pt 1)**: p. 129-34.
170. Munro, S., K.L. Thomas, and M. Abu-Shaar, *Molecular characterization of a peripheral receptor for cannabinoids.* Nature, 1993. **365**(6441): p. 61-5.
171. Kaminski, N.E., et al., *Identification of a functionally relevant cannabinoid receptor on mouse spleen cells that is involved in cannabinoid-mediated immune modulation.* Mol Pharmacol, 1992. **42**(5): p. 736-42.
172. Moreira, F.A. and J.A. Crippa, *The psychiatric side-effects of rimonabant.* Rev Bras Psiquiatr, 2009. **31**(2): p. 145-53.
173. Wickman, K. and D.E. Clapham, *Ion channel regulation by G proteins.* Physiol Rev, 1995. **75**(4): p. 865-85.
174. Galiegue, S., et al., *Expression of central and peripheral cannabinoid receptors in human immune tissues and leukocyte subpopulations.* Eur J Biochem, 1995. **232**(1): p. 54-61.
175. Schatz, A.R., et al., *Cannabinoid receptors CB1 and CB2: a characterization of expression and adenylate cyclase modulation within the immune system.* Toxicol Appl Pharmacol, 1997. **142**(2): p. 278-87.
176. Pettit, D.A., et al., *Cannabinoid receptor expression in immune cells.* Adv Exp Med Biol, 1996. **402**: p. 119-29.
177. Pertwee, R.G., *Cannabinoids and multiple sclerosis.* Pharmacol Ther, 2002. **95**(2): p. 165-74.
178. McKallip, R.J., et al., *Targeting CB2 cannabinoid receptors as a novel therapy to treat malignant lymphoblastic disease.* Blood, 2002. **100**(2): p. 627-34.
179. Atwood, B.K. and K. Mackie, *CB2: a cannabinoid receptor with an identity crisis.* Br J Pharmacol, 2010. **160**(3): p. 467-79.
180. Sawzdargo, M., et al., *Identification and cloning of three novel human G protein-coupled receptor genes GPR52, PsiGPR53 and GPR55: GPR55 is extensively expressed in human brain.* Brain Res Mol Brain Res, 1999. **64**(2): p. 193-8.
181. Reggio, P.H., *Endocannabinoid binding to the cannabinoid receptors: what is known and what remains unknown.* Curr Med Chem, 2010. **17**(14): p. 1468-86.
182. Whyte, L.S., et al., *The putative cannabinoid receptor GPR55 affects osteoclast function in vitro and bone mass in vivo.* Proc Natl Acad Sci U S A, 2009. **106**(38): p. 16511-6.
183. Franklin, J.M., et al., *Cannabinoid 2 receptor- and beta Arrestin 2-dependent upregulation of serotonin 2A receptors.* Eur Neuropsychopharmacol, 2013. **23**(7): p. 760-7.

184. Glass, M. and C.C. Felder, *Concurrent stimulation of cannabinoid CB1 and dopamine D2 receptors augments cAMP accumulation in striatal neurons: evidence for a Gs linkage to the CB1 receptor.* J Neurosci, 1997. **17**(14): p. 5327-33.
185. Hermanson, D.J. and L.J. Marnett, *Cannabinoids, endocannabinoids, and cancer.* Cancer Metastasis Rev, 2011. **30**(3-4): p. 599-612.
186. Thon, L., et al., *Ceramide mediates caspase-independent programmed cell death.* FASEB J, 2005. **19**(14): p. 1945-56.
187. Velasco, G., et al., *Cannabinoids and ceramide: two lipids acting hand-by-hand.* Life Sci, 2005. **77**(14): p. 1723-31.
188. Pacher, P., S. Batkai, and G. Kunos, *The endocannabinoid system as an emerging target of pharmacotherapy.* Pharmacol Rev, 2006. **58**(3): p. 389-462.
189. Sanchez, C., et al., *The CB(1) cannabinoid receptor of astrocytes is coupled to sphingomyelin hydrolysis through the adaptor protein fan.* Mol Pharmacol, 2001. **59**(5): p. 955-9.
190. Carrier, E.J., et al., *Cultured rat microglial cells synthesize the endocannabinoid 2-arachidonylglycerol, which increases proliferation via a CB2 receptor-dependent mechanism.* Mol Pharmacol, 2004. **65**(4): p. 999-1007.
191. Bouaboula, M., et al., *Signaling pathway associated with stimulation of CB2 peripheral cannabinoid receptor. Involvement of both mitogen-activated protein kinase and induction of Krox-24 expression.* Eur J Biochem, 1996. **237**(3): p. 704-11.
192. Nackley, A.G., A. Makriyannis, and A.G. Hohmann, *Selective activation of cannabinoid CB(2) receptors suppresses spinal fos protein expression and pain behavior in a rat model of inflammation.* Neuroscience, 2003. **119**(3): p. 747-57.
193. Szabo, G.G., et al., *Presynaptic calcium channel inhibition underlies CB(1) cannabinoid receptor-mediated suppression of GABA release.* J Neurosci, 2014. **34**(23): p. 7958-63.
194. Mackie, K., W.A. Devane, and B. Hille, *Anandamide, an endogenous cannabinoid, inhibits calcium currents as a partial agonist in N18 neuroblastoma cells.* Mol Pharmacol, 1993. **44**(3): p. 498-503.
195. Mackie, K., et al., *Cannabinoids activate an inwardly rectifying potassium conductance and inhibit Q-type calcium currents in AtT20 cells transfected with rat brain cannabinoid receptor.* J Neurosci, 1995. **15**(10): p. 6552-61.
196. Sugiura, T., et al., *Inhibition by 2-arachidonoylglycerol, a novel type of possible neuromodulator, of the depolarization-induced increase in intracellular free calcium in neuroblastoma x glioma hybrid NG108-15 cells.* Biochem Biophys Res Commun, 1997. **233**(1): p. 207-10.
197. Sugiura, T., et al., *2-Arachidonoylglycerol, a putative endogenous cannabinoid receptor ligand, induces rapid, transient elevation of intracellular free Ca2+ in neuroblastoma x glioma hybrid NG108-15 cells.* Biochem Biophys Res Commun, 1996. **229**(1): p. 58-64.
198. Zoratti, C., et al., *Anandamide initiates Ca(2+) signaling via CB2 receptor linked to phospholipase C in calf pulmonary endothelial cells.* Br J Pharmacol, 2003. **140**(8): p. 1351-62.
199. Guzman, M., *Cannabinoids: potential anticancer agents.* Nat Rev Cancer, 2003. **3**(10): p. 745-55.
200. Fernandez-Lopez, D., et al., *Cannabinoids: well-suited candidates for the treatment of perinatal brain injury.* Brain Sci, 2013. **3**(3): p. 1043-59.

201. Fgli, S. and M. Cristina, *the molecular basis of cannabinoid action in cancer* Cancer Therapy, 2008. **6**(103): p. 103-116.
202. Todaro, B., *Cannabinoids in the treatment of chemotherapy-induced nausea and vomiting.* J Natl Compr Canc Netw, 2012. **10**(4): p. 487-92.
203. Pertwee, R.G., *Emerging strategies for exploiting cannabinoid receptor agonists as medicines.* Br J Pharmacol, 2009. **156**(3): p. 397-411.
204. Oreja-Guevara, C., *Clinical efficacy and effectiveness of Sativex, a combined cannabinoid medicine, in multiple sclerosis-related spasticity.* Expert Rev Neurother, 2012. **12**(4 Suppl): p. 3-8.
205. Vermersch, P., *Sativex((R)) (tetrahydrocannabinol + cannabidiol), an endocannabinoid system modulator: basic features and main clinical data.* Expert Rev Neurother, 2011. **11**(4 Suppl): p. 15-9.
206. Kaminski, N.E., *Inhibition of the cAMP signaling cascade via cannabinoid receptors: a putative mechanism of immune modulation by cannabinoid compounds.* Toxicol Lett, 1998. **102-103**: p. 59-63.
207. Ofek, O., et al., *Peripheral cannabinoid receptor, CB2, regulates bone mass.* Proc Natl Acad Sci U S A, 2006. **103**(3): p. 696-701.
208. Bab, I. and A. Zimmer, *Cannabinoid receptors and the regulation of bone mass.* Br J Pharmacol, 2008. **153**(2): p. 182-8.
209. Idris, A.I., et al., *Regulation of bone mass, bone loss and osteoclast activity by cannabinoid receptors.* Nat Med, 2005. **11**(7): p. 774-9.
210. Bab, I., A. Zimmer, and E. Melamed, *Cannabinoids and the skeleton: from marijuana to reversal of bone loss.* Ann Med, 2009. **41**(8): p. 560-7.
211. Sophocleous, A., et al., *The Type 2 Cannabinoid Receptor Regulates Bone Mass and Ovariectomy-Induced Bone Loss by Affecting Osteoblast Differentiation and Bone Formation.* Endocrinology, 2011.
212. Pandey, R., et al., *Endocannabinoids and immune regulation.* Pharmacol Res, 2009. **60**(2): p. 85-92.
213. Cabral, G.A. and L. Griffin-Thomas, *Emerging role of the cannabinoid receptor CB2 in immune regulation: therapeutic prospects for neuroinflammation.* Expert Rev Mol Med, 2009. **11**: p. e3.
214. Zuardi, A.W., et al., *Cannabidiol, a Cannabis sativa constituent, as an antipsychotic drug.* Braz J Med Biol Res, 2006. **39**(4): p. 421-9.
215. Kozela, E., et al., *Cannabidiol Inhibits Pathogenic T-Cells, Decreases Spinal Microglial Activation and Ameliorates Multiple Sclerosis-Like Disease in C57bl/6 Mice.* Br J Pharmacol, 2011.
216. Rivers, J.R. and J.C. Ashton, *The development of cannabinoid CBII receptor agonists for the treatment of central neuropathies.* Cent Nerv Syst Agents Med Chem, 2010. **10**(1): p. 47-64.
217. Horvath, B., et al., *A new cannabinoid 2 receptor agonist HU-910 attenuates oxidative stress, inflammation, and cell death associated with hepatic ischemia/reperfusion injury.* Br J Pharmacol, 2011.
218. Rajesh, M., et al., *Cannabinoid-2 receptor agonist HU-308 protects against hepatic ischemia/reperfusion injury by attenuating oxidative stress, inflammatory response, and apoptosis.* J Leukoc Biol, 2007. **82**(6): p. 1382-9.

219. Kasten, K.R., et al., *The cannabinoid 2 receptor as a potential therapeutic target for sepsis.* Endocr Metab Immune Disord Drug Targets, 2010. **10**(3): p. 224-34.
220. Valenzano, K.J., et al., *Pharmacological and pharmacokinetic characterization of the cannabinoid receptor 2 agonist, GW405833, utilizing rodent models of acute and chronic pain, anxiety, ataxia and catalepsy.* Neuropharmacology, 2005. **48**(5): p. 658-72.
221. Chakravarti, B., J. Ravi, and R.K. Ganju, *Cannabinoids as therapeutic agents in cancer: current status and future implications.* Oncotarget, 2014. **5**(15): p. 5852-72.
222. Khasabova, I.A., et al., *A decrease in anandamide signaling contributes to the maintenance of cutaneous mechanical hyperalgesia in a model of bone cancer pain.* J Neurosci, 2008. **28**(44): p. 11141-52.
223. Hald, A., et al., *Differential effects of repeated low dose treatment with the cannabinoid agonist WIN 55,212-2 in experimental models of bone cancer pain and neuropathic pain.* Pharmacol Biochem Behav, 2008. **91**(1): p. 38-46.
224. Munson, A.E., et al., *Antineoplastic activity of cannabinoids.* J Natl Cancer Inst, 1975. **55**(3): p. 597-602.
225. McKallip, R.J., et al., *Targeting CB2 cannabinoid receptors as a novel therapy to treat malignant lymphoblastic disease*. Vol. 100. 2002. 627-634.
226. Nomura, D.K., et al., *Monoacylglycerol lipase regulates a fatty acid network that promotes cancer pathogenesis.* Cell, 2010. **140**(1): p. 49-61.
227. Guindon, J. and A.G. Hohmann, *The endocannabinoid system and cancer: therapeutic implication.* Br J Pharmacol. **163**(7): p. 1447-63.
228. Sarfaraz, S., et al., *Cannabinoids for cancer treatment: progress and promise.* Cancer Res, 2008. **68**(2): p. 339-42.
229. Caffarel, M.M., et al., *Cannabinoids reduce ErbB2-driven breast cancer progression through Akt inhibition.* Mol Cancer, 2010. **9**: p. 196.
230. Melck, D., et al., *Suppression of nerve growth factor Trk receptors and prolactin receptors by endocannabinoids leads to inhibition of human breast and prostate cancer cell proliferation.* Endocrinology, 2000. **141**(1): p. 118-26.
231. Sanchez, M.G., et al., *Activation of phosphoinositide 3-kinase/PKB pathway by CB(1) and CB(2) cannabinoid receptors expressed in prostate PC-3 cells. Involvement in Raf-1 stimulation and NGF induction.* Cell Signal, 2003. **15**(9): p. 851-9.
232. Nithipatikom, K., et al., *2-arachidonoylglycerol: a novel inhibitor of androgen-independent prostate cancer cell invasion.* Cancer Res, 2004. **64**(24): p. 8826-30.
233. Sarfaraz, S., et al., *Cannabinoid Receptor as a Novel Target for the Treatment of Prostate Cancer.* Cancer Research, 2005. **65**(5).
234. Olea-Herrero, N., et al., *Inhibition of human tumour prostate PC-3 cell growth by cannabinoids R(+)-Methanandamide and JWH-015: involvement of CB2.* Br J Cancer, 2009. **101**(6): p. 940-50.
235. Tolon, R.M., et al., *The activation of cannabinoid CB2 receptors stimulates in situ and in vitro beta-amyloid removal by human macrophages.* Brain Res, 2009. **1283**: p. 148-54.
236. Aso, E. and I. Ferrer, *Cannabinoids for treatment of Alzheimer's disease: moving toward the clinic.* Front Pharmacol, 2014. **5**: p. 37.
237. Idris, A.I., et al., *Regulation of bone mass, osteoclast function, and ovariectomy-induced bone loss by the type 2 cannabinoid receptor.* Endocrinology, 2008. **149**(11): p. 5619-26.
238. Ashton, J.C., et al., *Cannabinoid CB1 and CB2 receptor ligand specificity and the development of CB2-selective agonists.* Curr Med Chem, 2008. **15**(14): p. 1428-43.

239. Marriott, K.S. and J.W. Huffman, *Recent advances in the development of selective ligands for the cannabinoid CB(2) receptor.* Curr Top Med Chem, 2008. **8**(3): p. 187-204.
240. Huffman, J.W., *CB2 receptor ligands.* Mini Rev Med Chem, 2005. **5**(7): p. 641-9.
241. Huffman, J.W., *The search for selective ligands for the CB2 receptor.* Curr Pharm Des, 2000. **6**(13): p. 1323-37.
242. Xu, F., et al., *Structure of an agonist-bound human A2A adenosine receptor.* Science, 2011. **332**(6027): p. 322-7.
243. Congreve, M. and F. Marshall, *The impact of GPCR structures on pharmacology and structure-based drug design.* Br J Pharmacol, 2010. **159**(5): p. 986-96.
244. de Graaf, C. and D. Rognan, *Selective structure-based virtual screening for full and partial agonists of the beta2 adrenergic receptor.* J Med Chem, 2008. **51**(16): p. 4978-85.
245. Katritch, V., et al., *Analysis of full and partial agonists binding to beta2-adrenergic receptor suggests a role of transmembrane helix V in agonist-specific conformational changes.* J Mol Recognit, 2009. **22**(4): p. 307-18.
246. Warne, T., et al., *The structural basis for agonist and partial agonist action on a beta(1)-adrenergic receptor.* Nature, 2011. **469**(7329): p. 241-4.
247. Heydenreich, F.M., et al., *Stabilization of G protein-coupled receptors by point mutations.* Front Pharmacol, 2015. **6**: p. 82.
248. Baldwin, J.M., *The probable arrangement of the helices in G protein-coupled receptors.* The EMBO Journal, 1993. **12**(4): p. 1693-1703.
249. Matsuda, L.A., et al., *Structure of a cannabinoid receptor and functional expression of the cloned cDNA.* Nature, 1990. **346**(6284): p. 561.
250. Munro, S., K.L. Thomas, and M. Abu-Shaar, *Molecular characterization of a peripheral receptor for cannabinoids.* Nature, 1993. **365**(6441): p. 61.
251. Howlett, A.C., et al., *International Union of Pharmacology. XXVII. Classification of cannabinoid receptors.* Pharmacol Rev, 2002. **54**(2): p. 161-202.
252. Racz, I., et al., *Crucial role of CB(2) cannabinoid receptor in the regulation of central immune responses during neuropathic pain.* J Neurosci, 2008. **28**(46): p. 12125-35.
253. Mbvundula, E.C., K.D. Rainsford, and R.A. Bunning, *Cannabinoids in pain and inflammation.* Inflammopharmacology, 2004. **12**(2): p. 99-114.
254. Karsak, M., et al., *Cannabinoid receptor type 2 gene is associated with human osteoporosis.* Hum Mol Genet, 2005. **14**(22): p. 3389-96.
255. Hart, S., O.M. Fischer, and A. Ullrich, *Cannabinoids induce cancer cell proliferation via tumor necrosis factor alpha-converting enzyme (TACE/ADAM17)-mediated transactivation of the epidermal growth factor receptor.* Cancer Res, 2004. **64**(6): p. 1943-50.
256. Blazquez, C., et al., *Cannabinoid receptors as novel targets for the treatment of melanoma.* FASEB J, 2006. **20**(14): p. 2633-5.
257. De Petrocellis, L., et al., *The endogenous cannabinoid anandamide inhibits human breast cancer cell proliferation.* Proc Natl Acad Sci U S A, 1998. **95**(14): p. 8375-80.
258. Milligan, G. and R.A. Bond, *Inverse agonism and the regulation of receptor number.* Trends Pharmacol Sci, 1997. **18**(12): p. 468-74.
259. Demuth, D.G. and A. Molleman, *Cannabinoid signalling.* Life Sci, 2006. **78**(6): p. 549-63.
260. Ortega-Gutierrez, S. and M.L. Lopez-Rodriguez, *CB1 and CB2 cannabinoid receptor binding studies based on modeling and mutagenesis approaches.* Mini Rev Med Chem, 2005. **5**(7): p. 651-8.

261. Tao, Q., et al., *Role of a conserved lysine residue in the peripheral cannabinoid receptor (CB2): evidence for subtype specificity.* Mol Pharmacol, 1999. **55**(3): p. 605-13.
262. Rhee, M.H., et al., *Functional role of tryptophan residues in the fourth transmembrane domain of the CB(2) cannabinoid receptor.* J Neurochem, 2000. **75**(6): p. 2485-91.
263. McAllister, S.D., et al., *A critical role for a tyrosine residue in the cannabinoid receptors for ligand recognition.* Biochem Pharmacol, 2002. **63**(12): p. 2121-36.
264. Zhang, Y., et al., *Mutagenesis and computer modeling studies of a GPCR conserved residue W5.43(194) in ligand recognition and signal transduction for CB2 receptor.* International Immunopharmacology, 2011. **11**(9): p. 1303-1310.
265. Song, Z.H., et al., *The difference between the CB(1) and CB(2) cannabinoid receptors at position 5.46 is crucial for the selectivity of WIN55212-2 for CB(2).* Mol Pharmacol, 1999. **56**(4): p. 834-40.
266. Tao, Q. and M.E. Abood, *Mutation of a highly conserved aspartate residue in the second transmembrane domain of the cannabinoid receptors, CB1 and CB2, disrupts G-protein coupling.* J Pharmacol Exp Ther, 1998. **285**(2): p. 651-8.
267. Nebane, N.M., et al., *Residues accessible in the binding-site crevice of transmembrane helix 6 of the CB2 cannabinoid receptor.* Biochemistry, 2008. **47**(52): p. 13811-21.
268. Rhee, M.H., *Functional role of serine residues of transmembrane dopamin VII in signal transduction of CB2 cannabinoid receptor.* J Vet Sci, 2002. **3**(3): p. 185-91.
269. Yang, P., et al., *Lead Discovery, Chemistry Optimization, and Biological Evaluation Studies of Novel Biamide Derivatives as CB(2) Receptor Inverse Agonists and Osteoclast Inhibitors.* J Med Chem, 2012.
270. Miller, J.L. and C.G. Tate, *Engineering an ultra-thermostable beta(1)-adrenoceptor.* J Mol Biol, 2011. **413**(3): p. 628-38.
271. Shire, D., et al., *Cannabinoid receptor interactions with the antagonists SR 141716A and SR 144528.* Life Sci, 1999. **65**(6-7): p. 627-35.
272. Poso, A. and J.W. Huffman, *Targeting the cannabinoid CB2 receptor: modelling and structural determinants of CB2 selective ligands.* British Journal of Pharmacology, 2008. **153**(2): p. 335.
273. Raitio, K.H., et al., *Targeting the cannabinoid CB2 receptor: mutations, modeling and development of CB2 selective ligands.* Current Medicinal Chemistry, 2005. **12**(10): p. 1217-37.
274. Zhang, R., et al., *Cysteine 2.59(89) in the second transmembrane domain of human CB2 receptor is accessible within the ligand binding crevice: evidence for possible CB2 deviation from a rhodopsin template.* Mol Pharmacol, 2005. **68**(1): p. 69-83.
275. Chin, C.N., et al., *The third transmembrane helix of the cannabinoid receptor plays a role in the selectivity of aminoalkylindoles for CB2, peripheral cannabinoid receptor.* J Pharmacol Exp Ther, 1999. **291**(2): p. 837-44.
276. Song, Z.H. and T.I. Bonner, *A lysine residue of the cannabinoid receptor is critical for receptor recognition by several agonists but not WIN55212-2.* Mol Pharmacol, 1996. **49**(5): p. 891-6.
277. Zhang, R., *Mutagenesis of aromatic microdomains at human CB2 cannabinoid receptor*, in *2004 Symposium on the Cannabinoids. 2004: Paestum, Italy.*

278. Feng, W. and Z.H. Song, *Effects of D3.49A, R3.50A, and A6.34E mutations on ligand binding and activation of the cannabinoid-2 (CB2) receptor.* Biochem Pharmacol, 2003. **65**(7): p. 1077-85.
279. Shire, D., et al., *Structural features of the central cannabinoid CB1 receptor involved in the binding of the specific CB1 antagonist SR 141716A.* J Biol Chem, 1996. **271**(12): p. 6941-6.
280. Probst, W.C., et al., *Sequence alignment of the G-protein coupled receptor superfamily.* DNA Cell Biol, 1992. **11**(1): p. 1-20.
281. Wess, J., et al., *Functional role of proline and tryptophan residues highly conserved among G protein-coupled receptors studied by mutational analysis of the m3 muscarinic receptor.* EMBO J, 1993. **12**(1): p. 331-8.
282. Suzuki, T., et al., *A highly conserved tryptophan residue in the fourth transmembrane domain of the A adenosine receptor is essential for ligand binding but not receptor homodimerization.* J Neurochem, 2009. **110**(4): p. 1352-62.
283. Gouldson, P., et al., *Mutational analysis and molecular modelling of the antagonist SR 144528 binding site on the human cannabinoid CB(2) receptor.* Eur J Pharmacol, 2000. **401**(1): p. 17-25.
284. Zhang, Y., et al., *Mutagenesis and computer modeling studies of a GPCR conserved residue W5.43(194) in ligand recognition and signal transduction for CB2 receptor.* Int Immunopharmacol, 2011. **11**(9): p. 1303-10.
285. Felder, C.C., et al., *Comparison of the pharmacology and signal transduction of the human cannabinoid CB1 and CB2 receptors.* Mol Pharmacol, 1995. **48**(3): p. 443-50.
286. Ballesteros, J.A. and H. Weinstein, *[19] Integrated methods for the construction of three-dimensional models and computational probing of structure-function relations in G protein-coupled receptors*, in *Methods in Neurosciences*, C.S. Stuart, Editor. 1995, Academic Press. p. 366-428.
287. Song, Z.H. and W. Feng, *Absence of a conserved proline and presence of a conserved tyrosine in the CB2 cannabinoid receptor are crucial for its function.* FEBS Lett, 2002. **531**(2): p. 290-4.
288. Nebane, N.M., B. Kellie, and Z.H. Song, *The effects of charge-neutralizing mutation D6.30N on the functions of CB1 and CB2 cannabinoid receptors.* FEBS Lett, 2006. **580**(22): p. 5392-8.
289. Horn, F., et al., *GPCRDB information system for G protein-coupled receptors.* Nucleic Acids Res, 2003. **31**(1): p. 294-7.
290. Isberg, V., et al., *GPCRdb: an information system for G protein-coupled receptors.* Nucleic Acids Res, 2016. **44**(D1): p. D356-64.
291. Alqarni, M., et al., *Examining the critical roles of human CB2 receptor residues Valine 3.32 (113) and Leucine 5.41 (192) in ligand recognition and downstream signaling activities.* Biochem Biophys Res Commun, 2014. **452**(3): p. 334-9.
292. Mercier, R.W., et al., *hCB2 ligand-interaction landscape: cysteine residues critical to biarylpyrazole antagonist binding motif and receptor modulation.* Chem Biol, 2010. **17**(10): p. 1132-42.
293. Feng, W. and Z.H. Song, *Functional roles of the tyrosine within the NP(X)(n)Y motif and the cysteines in the C-terminal juxtamembrane region of the CB2 cannabinoid receptor.* FEBS Lett, 2001. **501**(2-3): p. 166-70.

294. Jaakola, V.-P., et al., *The 2.6 Angstrom Crystal Structure of a Human A2A Adenosine Receptor Bound to an Antagonist.* Science, 2008. **322**(5905): p. 1211-1217.
295. Chien, E.Y.T., et al., *Structure of the Human Dopamine D3 Receptor in Complex with a D2/D3 Selective Antagonist.* Science, 2010. **330**(6007): p. 1091-1095.
296. Okada, T., et al., *Functional role of internal water molecules in rhodopsin revealed by x-ray crystallography.* Proceedings of the National Academy of Sciences, 2002. **99**(9): p. 5982-5987.
297. Palczewski, K., et al., *Crystal structure of rhodopsin: A G protein-coupled receptor.* Science, 2000. **289**(5480): p. 739-745.
298. Warne, T., et al., *The structural basis for agonist and partial agonist action on a [bgr]1-adrenergic receptor.* Nature, 2011. **469**(7329): p. 241-244.
299. Warne, T., et al., *Structure of a beta1-adrenergic G-protein-coupled receptor.* Nature, 2008. **454**(7203): p. 486.
300. Roy, A., A. Kucukural, and Y. Zhang, *I-TASSER: a unified platform for automated protein structure and function prediction.* Nat. Protocols, 2010. **5**(4): p. 725.
301. Zhang, Y., *Template-based modeling and free modeling by I-TASSER in CASP7.* Proteins: Structure, Function, and Bioinformatics, 2007. **69**(S8): p. 108.
302. *SYBYL-X 1.2*. 1699 South Hanley Rd., St. Louis, Missouri, 63144, USA; .
303. Chen, J.-Z., J. Wang, and X.-Q. Xie, *GPCR Structure-Based Virtual Screening Approach for CB2 Antagonist Search.* Journal of Chemical Information and Modeling, 2007. **47**(4): p. 1626-1637.
304. Bramblett, R.D., et al., *Construction of a 3D model of the cannabinoid CB1 receptor: determination of helix ends and helix orientation.* Life Sciences, 1995. **56**(23/24): p. 1971-1982.
305. Lunn, C.A., et al., *A novel cannabinoid peripheral cannabinoid receptor-selective inverse agonist blocks leukocyte recruitment in vivo.* Journal of Pharmacology and Experimental Therapeutics, 2006. **316**(2): p. 780-788.
306. Liu, W., et al., *Structural basis for allosteric regulation of GPCRs by sodium ions.* Science, 2012. **337**(6091): p. 232-6.
307. Chen, J.Z., J. Wang, and X.Q. Xie, *GPCR structure-based virtual screening approach for CB2 antagonist search.* J Chem Inf Model, 2007. **47**(4): p. 1626-37.
308. Xie, X.Q., J.Z. Chen, and E.M. Billings, *3D structural model of the G-protein-coupled cannabinoid CB2 receptor.* Proteins, 2003. **53**(2): p. 307-19.
309. van Rhee, A.M. and K.A. Jacobson, *Molecular Architecture of G Protein-Coupled Receptors.* Drug Dev Res, 1996. **37**(1): p. 1-38.
310. Jiang, Q., et al., *Mutagenesis reveals structure-activity parallels between human A2A adenosine receptors and biogenic amine G protein-coupled receptors.* J Med Chem, 1997. **40**(16): p. 2588-95.
311. Rhee, M.H., et al., *Cannabinoid receptor activation differentially regulates the various adenylyl cyclase isozymes.* J Neurochem, 1998. **71**(4): p. 1525-34.
312. Zou, Y., W.I. Weis, and B.K. Kobilka, *N-terminal T4 lysozyme fusion facilitates crystallization of a G protein coupled receptor.* PLoS One, 2012. **7**(10): p. e46039.
313. Glass, M. and J.K. Northup, *Agonist selective regulation of G proteins by cannabinoid CB(1) and CB(2) receptors.* Mol Pharmacol, 1999. **56**(6): p. 1362-9.
314. Docagne, F., et al., *Therapeutic potential of CB2 targeting in multiple sclerosis.* Expert Opin Ther Targets, 2008. **12**(2): p. 185-95.

315. Zvonok, N., et al., *Comprehensive proteomic mass spectrometric characterization of human cannabinoid CB2 receptor.* J Proteome Res, 2007. **6**(6): p. 2068-79.
316. Filppula, S., et al., *Purification and mass spectroscopic analysis of human CB2 cannabinoid receptor expressed in the baculovirus system.* J Pept Res, 2004. **64**(6): p. 225-36.
317. Yang, P., et al., *Lead discovery, chemistry optimization, and biological evaluation studies of novel biamide derivatives as CB2 receptor inverse agonists and osteoclast inhibitors.* J Med Chem, 2012. **55**(22): p. 9973-87.
318. Kobilka, B.K., *Amino and carboxyl terminal modifications to facilitate the production and purification of a G protein-coupled receptor.* Anal Biochem, 1995. **231**(1): p. 269-71.
319. Heckman, K.L. and L.R. Pease, *Gene splicing and mutagenesis by PCR-driven overlap extension.* Nat Protoc, 2007. **2**(4): p. 924-32.
320. Soding, J., *Protein homology detection by HMM-HMM comparison.* Bioinformatics, 2005. **21**(7): p. 951-60.
321. Lunn, C.A., et al., *A novel cannabinoid peripheral cannabinoid receptor-selective inverse agonist blocks leukocyte recruitment in vivo.* J Pharmacol Exp Ther, 2006. **316**(2): p. 780-8.
322. Pei, Y., et al., *Ligand-binding architecture of human CB2 cannabinoid receptor: evidence for receptor subtype-specific binding motif and modeling GPCR activation.* Chem Biol, 2008. **15**(11): p. 1207-19.
323. Ring, A.M., et al., *Adrenaline-activated structure of beta2-adrenoceptor stabilized by an engineered nanobody.* Nature, 2013. **502**(7472): p. 575-9.
324. Weichert, D., et al., *Covalent agonists for studying G protein-coupled receptor activation.* Proc Natl Acad Sci U S A, 2014. **111**(29): p. 10744-8.
325. Structural Genomics, C., et al., *Protein production and purification.* Nat Methods, 2008. **5**(2): p. 135-46.
326. Arnau, J., et al., *Current strategies for the use of affinity tags and tag removal for the purification of recombinant proteins.* Protein Expr Purif, 2006. **48**(1): p. 1-13.
327. Terpe, K., *Overview of tag protein fusions: from molecular and biochemical fundamentals to commercial systems.* Appl Microbiol Biotechnol, 2003. **60**(5): p. 523-33.
328. Krepkiy, D., et al., *Bacterial expression of functional, biotinylated peripheral cannabinoid receptor CB2.* Protein Expr Purif, 2006. **49**(1): p. 60-70.
329. Locatelli-Hoops, S.C., et al., *Expression, surface immobilization, and characterization of functional recombinant cannabinoid receptor CB2.* Biochim Biophys Acta, 2013. **1834**(10): p. 2045-56.
330. Roosild, T.P., et al., *NMR structure of Mistic, a membrane-integrating protein for membrane protein expression.* Science, 2005. **307**(5713): p. 1317-21.
331. Krikos, A., et al., *Chimeric chemosensory transducers of Escherichia coli.* Proc Natl Acad Sci U S A, 1985. **82**(5): p. 1326-30.
332. Einhauer, A. and A. Jungbauer, *The FLAG peptide, a versatile fusion tag for the purification of recombinant proteins.* J Biochem Biophys Methods, 2001. **49**(1-3): p. 455-65.
333. Cass, B., et al., *Purification of recombinant proteins from mammalian cell culture using a generic double-affinity chromatography scheme.* Protein Expr Purif, 2005. **40**(1): p. 77-85.

334. Chaga, G., et al., *Natural poly-histidine affinity tag for purification of recombinant proteins on cobalt(II)-carboxymethylaspartate crosslinked agarose.* J Chromatogr A, 1999. **864**(2): p. 247-56.
335. Chatterjee, D.K. and D. Esposito, *Enhanced soluble protein expression using two new fusion tags.* Protein Expr Purif, 2006. **46**(1): p. 122-9.
336. Raines, R.T., et al., *The S.Tag fusion system for protein purification.* Methods Enzymol, 2000. **326**: p. 362-76.
337. Vaillancourt, P., et al., *Affinity purification of recombinant proteins fused to calmodulin or to calmodulin-binding peptides.* Methods Enzymol, 2000. **326**: p. 340-62.
338. Xu, M.Q., H. Paulus, and S. Chong, *Fusions to self-splicing inteins for protein purification.* Methods Enzymol, 2000. **326**: p. 376-418.
339. Sassenfeld, H.M. and S.J. Brewer, *A Polypeptide Fusion Designed for the Purification of Recombinant Proteins.* Nat Biotech, 1984. **2**(1): p. 76-81.
340. Smyth, D.R., et al., *Crystal structures of fusion proteins with large-affinity tags.* Protein Sci, 2003. **12**(7): p. 1313-22.
341. Nallamsetty, S. and D.S. Waugh, *Solubility-enhancing proteins MBP and NusA play a passive role in the folding of their fusion partners.* Protein Expr Purif, 2006. **45**(1): p. 175-82.
342. Butt, T.R., et al., *SUMO fusion technology for difficult-to-express proteins.* Protein Expr Purif, 2005. **43**(1): p. 1-9.
343. Parks, T.D., et al., *Release of proteins and peptides from fusion proteins using a recombinant plant virus proteinase.* Anal Biochem, 1994. **216**(2): p. 413-7.
344. Vergis, J.M. and M.C. Wiener, *The variable detergent sensitivity of proteases that are utilized for recombinant protein affinity tag removal.* Protein Expr Purif, 2011. **78**(2): p. 139-42.
345. Young, C.L., Z.T. Britton, and A.S. Robinson, *Recombinant protein expression and purification: a comprehensive review of affinity tags and microbial applications.* Biotechnol J, 2012. **7**(5): p. 620-34.
346. Jenny, R.J., K.G. Mann, and R.L. Lundblad, *A critical review of the methods for cleavage of fusion proteins with thrombin and factor Xa.* Protein Expr Purif, 2003. **31**(1): p. 1-11.
347. Malakhov, M.P., et al., *SUMO fusions and SUMO-specific protease for efficient expression and purification of proteins.* J Struct Funct Genomics, 2004. **5**(1-2): p. 75-86.
348. Cordingley, M.G., et al., *Substrate requirements of human rhinovirus 3C protease for peptide cleavage in vitro.* J Biol Chem, 1990. **265**(16): p. 9062-5.
349. Lichty, J.J., et al., *Comparison of affinity tags for protein purification.* Protein Expr Purif, 2005. **41**(1): p. 98-105.
350. Kenig, M., et al., *Influence of the protein oligomericity on final yield after affinity tag removal in purification of recombinant proteins.* J Chromatogr A, 2006. **1101**(1-2): p. 293-306.
351. Arnau, J., et al., *Reprint of: Current strategies for the use of affinity tags and tag removal for the purification of recombinant proteins.* Protein Expr Purif, 2011.
352. Pedersen, J., et al., *Removal of N-terminal polyhistidine tags from recombinant proteins using engineered aminopeptidases.* Protein Expr Purif, 1999. **15**(3): p. 389-400.
353. Lorentsen, R.H., et al., *Expression, refolding, and purification of recombinant human granzyme B.* Protein Expr Purif, 2005. **39**(1): p. 18-26.

354. Mao, H., *A self-cleavable sortase fusion for one-step purification of free recombinant proteins.* Protein Expr Purif, 2004. **37**(1): p. 253-63.
355. Liu, X.Q., *Protein-splicing intein: Genetic mobility, origin, and evolution.* Annu Rev Genet, 2000. **34**: p. 61-76.
356. Ghosh, E., et al., *Methodological advances: the unsung heroes of the GPCR structural revolution.* Nat Rev Mol Cell Biol, 2015. **16**(2): p. 69-81.
357. Thompson, A.A., et al., *GPCR stabilization using the bicelle-like architecture of mixed sterol-detergent micelles.* Methods, 2011. **55**(4): p. 310-7.
358. Corin, K., et al., *Structure and function analyses of the purified GPCR human vomeronasal type 1 receptor 1.* Sci Rep, 2011. **1**: p. 172.
359. Park, J.H., et al., *Crystal structure of the ligand-free G-protein-coupled receptor opsin.* Nature, 2008. **454**(7201): p. 183-7.
360. Okada, T., et al., *The retinal conformation and its environment in rhodopsin in light of a new 2.2 A crystal structure.* J Mol Biol, 2004. **342**(2): p. 571-83.
361. Edwards, P.C., et al., *Crystals of native and modified bovine rhodopsins and their heavy atom derivatives.* J Mol Biol, 2004. **343**(5): p. 1439-50.
362. Choe, H.W., et al., *Crystal structure of metarhodopsin II.* Nature, 2011. **471**(7340): p. 651-5.
363. Chae, P.S., et al., *Maltose-neopentyl glycol (MNG) amphiphiles for solubilization, stabilization and crystallization of membrane proteins.* Nat Methods, 2010. **7**(12): p. 1003-8.
364. Hanson, M.A., et al., *A specific cholesterol binding site is established by the 2.8 A structure of the human beta2-adrenergic receptor.* Structure, 2008. **16**(6): p. 897-905.
365. De Pinto, V., R. Benz, and F. Palmieri, *Interaction of non-classical detergents with the mitochondrial porin. A new purification procedure and characterization of the pore-forming unit.* Eur J Biochem, 1989. **183**(1): p. 179-87.
366. Meetani, M.A. and K.J. Voorhees, *MALDI mass spectrometry analysis of high molecular weight proteins from whole bacterial cells: pretreatment of samples with surfactants.* J Am Soc Mass Spectrom, 2005. **16**(9): p. 1422-6.
367. VanAken, T., et al., *Alkyl glycoside detergents: synthesis and applications to the study of membrane proteins.* Methods Enzymol, 1986. **125**: p. 27-35.
368. Gray, D.N., *Extraction of proteins from naturally occurring membranes*. 1997, Google Patents.
369. Womack, M.D., D.A. Kendall, and R.C. MacDonald, *Detergent effects on enzyme activity and solubilization of lipid bilayer membranes.* Biochim Biophys Acta, 1983. **733**(2): p. 210-5.
370. Vinogradova, O., F. Sonnichsen, and C.R. Sanders, 2nd, *On choosing a detergent for solution NMR studies of membrane proteins.* J Biomol NMR, 1998. **11**(4): p. 381-6.
371. Cortes, D.M. and E. Perozo, *Structural dynamics of the Streptomyces lividans K+ channel (SKC1): oligomeric stoichiometry and stability.* Biochemistry, 1997. **36**(33): p. 10343-52.
372. Neugebauer, J., *A Guide to the Properties and Uses of Detergents in Biology and Biochemistry*. 1994.
373. Hauser, H., *Short-chain phospholipids as detergents.* Biochim Biophys Acta, 2000. **1508**(1-2): p. 164-81.
374. Gobl, C., et al., *Influence of phosphocholine alkyl chain length on peptide-micelle interactions and micellar size and shape.* J Phys Chem B, 2010. **114**(13): p. 4717-24.

375. Yeliseev, A.A., *Methods for recombinant expression and functional characterization of human cannabinoid receptor CB2.* Comput Struct Biotechnol J, 2013. **6**: p. e201303011.
376. Leifert, W.R., et al., *Radioligand binding assays: application of [(125)I]angiotensin II receptor binding.* Methods Mol Biol, 2009. **552**: p. 131-41.
377. Shevchenko, A., et al., *In-gel digestion for mass spectrometric characterization of proteins and proteomes.* Nat Protoc, 2006. **1**(6): p. 2856-60.
378. Morrow, J.A., et al., *Differences in stability among the human apolipoprotein E isoforms determined by the amino-terminal domain.* Biochemistry, 2000. **39**(38): p. 11657-66.
379. Ma, Y., J. Kubicek, and J. Labahn, *Expression and purification of functional human mu opioid receptor from E.coli.* PLoS One, 2013. **8**(2): p. e56500.
380. Vukoti, K., et al., *Stabilization of functional recombinant cannabinoid receptor CB(2) in detergent micelles and lipid bilayers.* PLoS One, 2012. **7**(10): p. e46290.
381. Yang, P., et al., *Novel triaryl sulfonamide derivatives as selective cannabinoid receptor 2 inverse agonists and osteoclast inhibitors: discovery, optimization, and biological evaluation.* J Med Chem, 2013. **56**(5): p. 2045-58.
382. Krepkiy, D., K. Gawrisch, and A. Yeliseev, *Expression and purification of CB2 for NMR studies in micellar solution.* Protein Pept Lett, 2007. **14**(10): p. 1031-7.
383. Proverbio, D., et al., *Functional properties of cell-free expressed human endothelin A and endothelin B receptors in artificial membrane environments.* Biochimica et Biophysica Acta (BBA) - Biomembranes, 2013. **1828**(9): p. 2182-2192.
384. Ishihara, G., et al., *Expression of G protein coupled receptors in a cell-free translational system using detergents and thioredoxin-fusion vectors.* Protein Expr Purif, 2005. **41**(1): p. 27-37.
385. Cavasotto, C.N. and S.S. Phatak, *Homology modeling in drug discovery: current trends and applications.* Drug Discov Today, 2009. **14**(13-14): p. 676-83.
386. Evers, A. and T. Klabunde, *Structure-based drug discovery using GPCR homology modeling: successful virtual screening for antagonists of the alpha1A adrenergic receptor.* J Med Chem, 2005. **48**(4): p. 1088-97.
387. Chin, S.P., et al., *Toward activated homology models of the human M1 muscarinic acetylcholine receptor.* J Mol Graph Model, 2014. **49**: p. 91-8.
388. Li, M., et al., *Computational studies of the binding site of alpha1A-adrenoceptor antagonists.* J Mol Model, 2008. **14**(10): p. 957-66.
389. Baneres, J.L., J.L. Popot, and B. Mouillac, *New advances in production and functional folding of G-protein-coupled receptors.* Trends Biotechnol, 2011. **29**(7): p. 314-22.